THE UNIVERSITY
of EDINBURGH

Reconstruction of coarse sediment recycling in rivers using cosmogenic nuclides in the Great Plains, USA

Zui Tao

THE UNIVERSITY
of EDINBURGH

Thesis submitted in fulfilment of
the requirements for the degree of
Doctor of Philosophy
to the
University of Edinburgh — 2019

Declaration

I declare that this thesis has been composed solely by myself and that it has not been submitted, either in whole or in part, in any previous application for a degree. Except where otherwise acknowledged, the work presented is entirely my own.

Zui Tao
August 2019

Abstract

Fluvial systems are regarded as a critical component of earth surface processes because they link the sediment source and the basin. The characteristics of fluvial sediments are influenced by tectonic and climatic processes. Thus, sediment grains, as the basic element of fluvial sediments, are often used to reconstruct changing tectonic and climatic conditions. One common observation of fluvial sediments is a tendency for the bedload to become finer downstream. In many studies, large pebbles located far away from the sources have been interpreted to be caused by tectonic or climatic influences. In the Great Plains, USA, large pebbles can be found more than 1400 km away from the sources. In this area, it has been demonstrated that slow subsidence resulted in multiple cycles of fluvial incision and aggradation. A hypothesis can then be proposed that large pebbles downstream came from the recycling of the paleosediments. To test this hypothesis, three main geological tools were applied: grain sizes analysis, cosmogenic nuclides analysis and numerical modelling of cosmogenic ^{21}Ne.

In the grain sizes analysis, downstream fining curves were generated, and similarity statistics were done. Based on the result, three locations of probable lateral sediment input from recycled paleo-channel deposits were recognised. For each of these locations, grain size distributions with and without lateral sediment input were generated by combining the grain size fitting curves and the similarity distributions. From the comparison between the grain size distributions with and without lateral sediment input, it can be concluded that almost all the pebbles collected from these three locations are from recycling of palesediments.

Cosmogenic nuclides accumulated when the sediments were exposed, so that they can provide information about the exposure and burial history of fluvial sediments. In this thesis, we analysed eighty-two samples (in total) for cosmogenic ^{21}Ne and five samples for ^{10}Be. A "steady-state" model and a "simplified migration" model were built to estimate the maximum concentration of cosmogenic ^{21}Ne accumulated from the source to the target location (Keystone) with a constant migration rate. From the comparison between this maximum concentration of cosmogenic ^{21}Ne and the concentrations of cosmogenic ^{21}Ne measured from the pebbles, it can be concluded that most pebbles collected from Keystone have experienced a long time of storage. This provides support for the existence of

recycling in the Great Plains. Next, based on the Ne/Be ratio, the oldest age of recycled sediments in the Great Plains was defined as at least Miocene in age.

The result of cosmogenic nuclides analysis introduced an interesting apparent conflict that cosmogenic ^{21}Ne concentrations contained within the samples collected from upstream are higher than those from downstream. To resolve this conflict, numerical models were built to test the controls of cosmogenic ^{21}Ne accumulated during recycling. Two geological parameters, elevation and age of paleosediments, were tested in these models. As suggested from the results, elevation plays a dominant role in the accumulation of cosmogenic ^{21}Ne during recycling. And, the paleosediments of Pliocene/Miocene are the main sources of the recycled pebbles in the Great Plains, but the portion of them plays a minor role in the distributions of cosmogenic ^{21}Ne contained within the pebbles collected along the North Platte River. For the influence of grain size, the data show no relationship between the grain size and the concentration of cosmogenic ^{21}Ne. Lastly, a previous study which used grain size to reconstruct paleo-river profile was tested to evaluate the impact of introducing recycling on the previous interpretations. As the result shows, regional grain size fining rate cannot be used directly to reconstruct the gradient of the whole channels, when recycling is dominant.

To conclude, I have shown that in the Great Plains, recycling is the main reason for the existence of pebbles 1400 km away from the sources, and recycling happened in modern time can affect the paleosediments as old as Miocene in age. Besides, it was concluded that elevation is the main factor that influences the concentration of ^{21}Ne accumulated during recycling, and the paleosediments of Miocene/Pliocene are the main sources of recycling. In the end, it was recommended that recycling should be taken into consideration in geological studies.

Acknowledgements

First and foremost, I want to thank my three supervisors, Hugh Sinclair, Simon Mudd, and Fin Stuart. With special thanks to Hugh Sinclair. It has been an honour to be one of his PhD students. I appreciate all his contributions of time and ideas to make my PhD life productive and stimulating.

My gratitude is without measure to my girlfriend Lixia Wang. I appreciate all her time, her patience and the most important, her warmth. She is the shiniest light in the darkest time of my life. May she have a life full of love and joy.

The members of the LSD group have contributed a lot to my study at the University of Edinburgh. The group has been a source of friendships as well as useful advice and collaboration. I am especially grateful for the help from Lizzie, Fiona and Boris. For the laboratory work, I'm grateful for the help of Andy and Elaine on samples preparation,acid etching and crushing, in the School of GeoSciences, I'm also feeling grateful to Marta, and other kinds of stuff working in SUERC, they gave me much help when I was working there.

Ziying Wang, guided me out of confusion and gave me a lot of help; Arthur, as my first roommate and my best friend in Edinburgh. We shared much memory all around Scotland. Hanning Mai, as my second roommate, taught me a lot. My time at Edinburgh was made enjoyable in large part due to the friends and groups here. Many thanks to them, they made me feel home in this foreign city.

I gratefully acknowledge CSC and The University of Edinburgh, the funding sources of my PhD. Many thanks to them, they gave me a chance living in this beautiful country, getting a higher level on Geology, and having an unforgettable journey. My work was also supported by BSG. Many thanks to this group.

Lastly, I would like to thank my family for all their love. I'm now making them feel proud.

Zui Tao, University of Edinburgh, August 2019

Contents

List of Tables

List of Figures

Chapter 1

Introduction

1.1 Motivation

There exists a precise relationship between the textual parameters of sedimentary deposits and the transport processes that deliver them to their sites of accumulation. For a long time, this relationship has been noticed by geologists. Grains, as the fundamental element of deposits, their amount, sizes and distributions are controlled by climatic changes, source area lithologies, hillslope processes, sediment transport processes dynamics and tectonic processes of subsidence and uplift. Grain-size analysis, therefore, has a wide application for assessing sedimentary signals (Passega, 1964; Visher, 1969) and reconstructing the history of fluvial transport in continental settings (Dawson, 1988; Heller and Paola, 1992).

A widely used feature of grains in fluvial systems is that the sizes of fluvial sediments tend to become finer downstream. This feature was thought to have a significant impact on the observed hydraulic behaviour of rivers downstream (Knighton, 1980; Dawson, 1988; Ferguson and Ashworth, 1991; Heller and Paola, 1992). Several studies have revealed that there are two sets of processes that mainly contribute to this downstream fining trend in fluvial system: abrasion and sorting through selective process (Knighton, 1980; Dawson, 1988; Ferguson and Ashworth, 1991).

The typical downstream fining of sediment grains follows an exponential trend against the distance (Heller and Paola, 1992; Paola et al., 1992; Fedele and Paola, 2007; Whittaker et al., 2011):

$$D_x = D_0 e^{-ax} \tag{1.1}$$

Where D_0 is the grain size at the start point in the upland catchment (flowing distance = 0), a is the fining exponent, and x is the flowing distance from the start point.

Some studies have suggested that for fluvial sediments, it often takes tens of kilometres for a reduction in grain size of one phi (–phi scale, grain size in mm can be transformed into –phi scale using 2^{-phi}). This situation is easy to be recognised in gravel rivers. A considerable amount of literature has found that there is a place or an area where the gravel bedload changes into sand bedload, this area is always named "gravel front" or 'gravel-sand transition' (Sambrook Smith and Ferguson, 1995; Parker and Cui, 1998). As suggested by the previous studies, the location of the gravel front is often kilometres to hundreds of kilometres from the sources (Table 1.1).

Table 1.1: Distances of "pebble front" from their sources for some rivers in the world (Sambrook Smith and Ferguson, 1995)

Author	**River**	**Country**	**Median Grain Size Before/After (mm)**	**Distance Downstream Before/After (km)**
Ichim and Radoane (1990)	Siret	Romania	5.0/0.3	566/578
Knighton (1980)	Bollin	England	7.4/1.1	26/35
McLean and Church (1986)	Lower Fraser	Canada	42.0/0.4	84/125
Pickup (1984) , Parker (1991)	Ok Tedl-Fly	Papua New Guinea	31.0/0.2	140/150
Shaw and Kellerhals (1982)	Milk	Canada	123./0.3	214/273
	North Saskatchewan		7.2/0.3	888/909
	South Saskatvhewan		7.9/0.2	940/965
	Red Deer		37.4/0.3	524/549
Yatsu (1955)	Kinu	Japan	17.0/0.9	53/58
	Nagara		25.0/1.1	14/16
	Sho		27.0/1.8	19/24
	Kiso		37.0/0.6	19/20
	Watarase		28.0/0.7	20/22
Smith and Ferguson (1995)	Allt Dubbalg	Scotland	14.6/0.5	2.6/2.8
	Endrick		6.6/0.6	34/35
	Tulla		13.9/0.6	14.5/14.9
	Sunwapta	Canada	8.2/0.3	21/22
	Beauty Creek		6.0/0.3	7.7/8.0

As the grain sizes are strongly influenced by the transport processes, it has been

suggested that using the grain size data of the paleosediments to reconstruct the depositional characteristics of these paleochannels. Paola and Mohrig (1996) developed an equation to describe the relationship between the grain size and the channel gradient for gravelly channels, building a reliable basis for the reconstruction of the gradients of paleochannels with grain sizes.

On the other hand, despite these findings on the downstream fining, several studies have revealed that this fining trend in grain sizes along the channel is often irregular (Ballantyne, 1978; Menting et al., 2015), previous literature and journals have been published to explain the causes of the irregular downstream fining (Seal et al., 1997; Rice, 1999; Menting et al., 2015). As suggested by the results of these studies, the causes of the irregular downstream fining can be divided into two groups: the autocyclic mechanisms and the allocyclic mechanisms. The former are the mechanisms resulted from the influences within the sedimentary system, while the later are the mechanisms resulted from the external influences (Heller and Paola, 1992). The autocyclic mechanisms include lithological composition, sorting and abrasion, and the allocyclic mechanisms include the changes in geological setting and climate (Seal et al., 1997; Rice, 1999; Menting et al., 2015).

The North Platte River is located in the northwest United States. It flows from the Rockies and across the Great Plains. In the central Great Plain, along the North Platte River, large pebbles (r=2^2 to 2^3 mm) can be collected more than 1400 km from the sources (illustrated in Figure 1.1). As described on the previous page, "gravel fronts" are always hundreds of kilometres away from the sources in maximum. The existence of pebbles at least 1400 km from the source of the river indicates that the location of the "gravel front" of the North Platte River is relatively unusual.

Previous studies suggested that large pebbles located far away from the sources could be interpreted as the result of tectonic activities or climatic changes (Paola et al., 1992). In the Great Plains, it has been demonstrated that slow subsidence resulted in alternating periods of fluvial incision and aggradation, which contributed to multiple episodes of erosion forming unconformities in the Tertiary stratigraphy (illustrated in Figure 1.2). There have been several investigations into the causes of the development of the stratigraphy of the Great Plains. The range of processes that have been used to partly explain the unusual extent of the conglomerates across the Great Plains include regional tectonic tilting (McMillan et al., 2002; Duller et al., 2012), rifting and volcanism (Duller et al., 2012), dynamic uplift (McMillan et al., 2002; Leonard, 2002), and northern hemispheric climate shifts with the onset of glaciation (Pelletier, 2009; Duller et al., 2012).

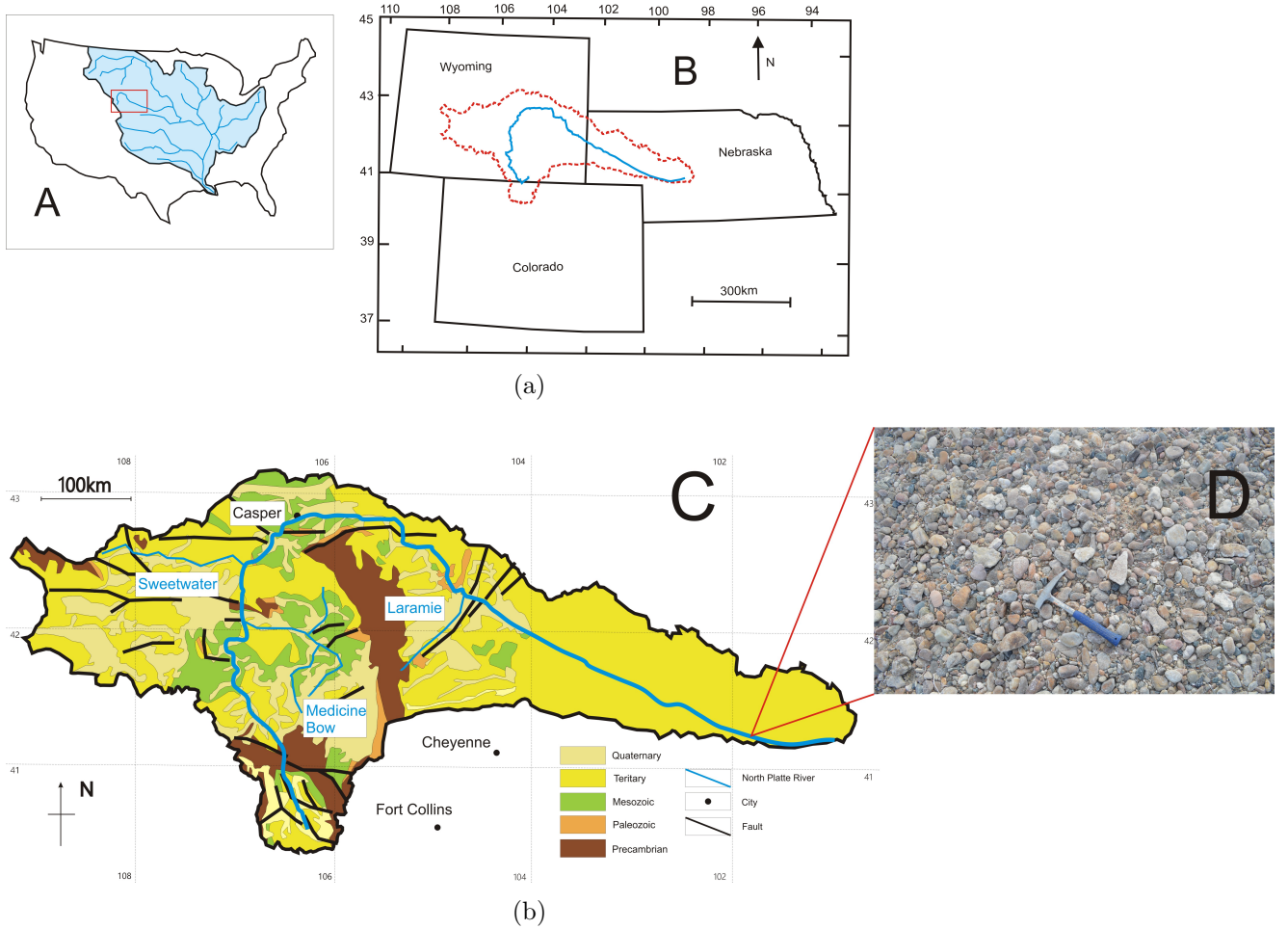

Figure 1.1: Maps showing location of North Platte River in context of the Mississippi River system (A), its location in context of central USA (B), and its geological context (sorted from USGS). D is a photo of pebbles taken near Keystone, NE, USA, which is about 1400 km downstream along the North Platte River from the sources, WY, USA.

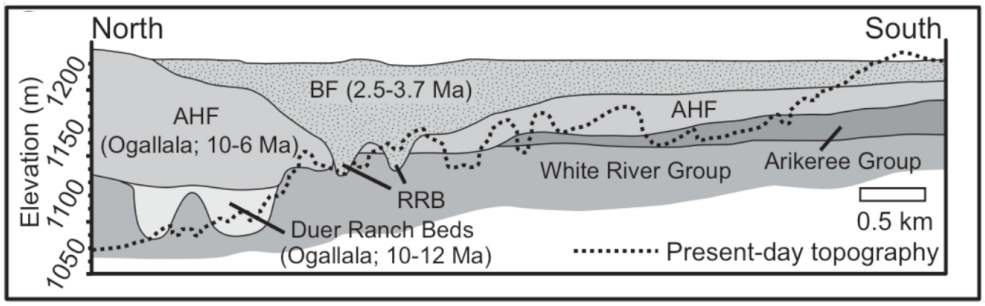

Figure 1.2: North-South strike cross-section of Tertiary stratigraphy. AHF-Ash Hollow Formation, BF-Broadwater Formation, RRB-Remsburg Ranch Beds (Duller et al., 2012).

As indicated above, the unconformities throughout the succession (McMillan et al., 2002; Pelletier, 2009; Duller et al., 2012) indicate that this area has undergone a long history of late Cenozoic aggradation and stream incision. A hypothesis can then be proposed that large pebbles downstream in the modern river system came from the recycling of the paleosediments rather than carrying directly from the sources of mountain area (shown in Figure 1.2, recycling process through incision is simplified as Figure 1.3). However, until recently, there has been little interest in recycling. The reason for this situation might be that there has never been a technique to measure recycling. More recently, literature has emerged that apply cosmogenic nuclides to solve geological problems, representing a potential breakthrough in our ability to "read" the recycling processes. This method has widespread application in geomorphology, but has not been testable to measure recycling processes. In this study cosmogenic nuclides are used to quantify recycling due to its ability to record the duration of the exposure of the sediments before being buried by further sediment accumulation (Libarkin et al., 2002; Codilean et al., 2008).

In 1934 A.V Grosse (1934) found that when cosmic rays reached the Earth's surface and interacted with the minerals on the surface (or within several meters under the surface), radioactive nuclides were produced. During the 1970s, the theory of the accumulation of this kind of nuclides was clear, and it was applied to date the exposure time of sediments (Lal and Peters, 1967). In the early 1980s, with the appearance of Accelerator Mass Spectrometer (AMS) and highly sensitive noble gas mass spectrometry, the enormous potential of terrestrial cosmogenic nuclides (TCN) once again got the attention of geologists (Gosse and Phillips, 2001). Nowadays, cosmogenic nuclides play an increasingly important role, being used widely on dating geological events, and on quantifying the deposition and erosion processes.

The galactic cosmic radiation which can produce cosmogenic nuclides is mostly consisting of high-energy particles (1 to 10^{10} GeV), mainly protons. When these high-energy particles reach the upper atmosphere, they cause nuclear reactions,

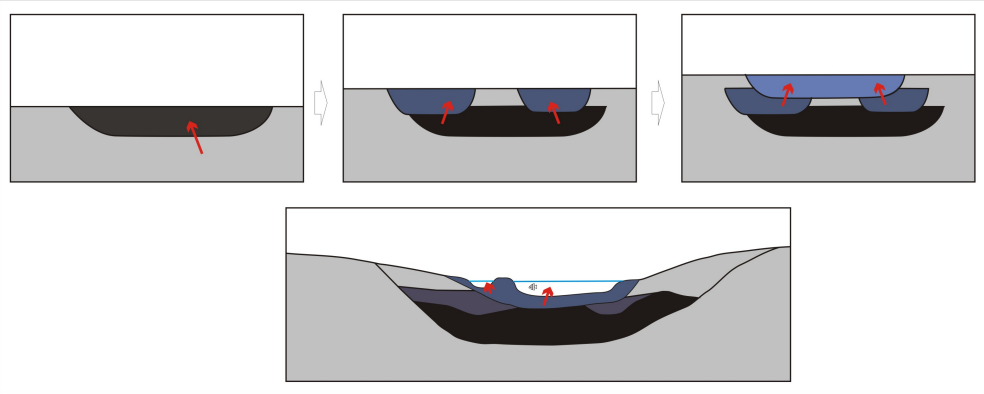

Figure 1.3: A schematic representation showing the recycling through incision (cross-section), the red arrows represent the path of recycling through multi-period of incision.

and their energy decreases. After this, the secondary cosmic rays, which are mainly neutrons and muons of MeV energy, are produced. Then these secondary cosmic rays reach the Earth's surface, they interact with the minerals in situ and produce terrestrial cosmogenic nuclides (TCN, shown in Figure 1.4).

The cosmogenic nuclides produced are controlled by the details of the arriving cosmic ray particles, including their types and their energy, and the details of the interacted minerals. The production rates of these nuclides are dependent on two factors, elevation and latitude (Codilean et al., 2008). Because of the attenuation process, they can only be produced within a limited depth scale (Von Blanckenburg, 2006). Thus it is possible to determine the time the minerals spend at the Earth's surface and the amount of pre-detachment cosmogenic nuclides they acquire. That's the basic idea to use cosmogenic nuclides to assess bedrock erosion rates and any changes in surface elevation. The longer the grains are exposed to the cosmic rays, the more cosmogenic nuclides become accumulated in the grains. As Figure 1.5 shows, grains with different moving paths would obtain different number of cosmogenic nuclides. The pebbles which were deposited on the plain and recycled into modern rivers could accumulate more cosmogenic nuclides than those of the pebbles carried from the source directly, because of the longer duration of storage. There would be, therefore, a reasonable assumption that the concentration of cosmogenic nuclides can act as a tool to quantify recycling.

To understand whether recycling played a significant role in the accumulation of conglomerates and modern gravels in the Great Plain, several questions need to be answered:

1. Where would recycling take place in the catchments?

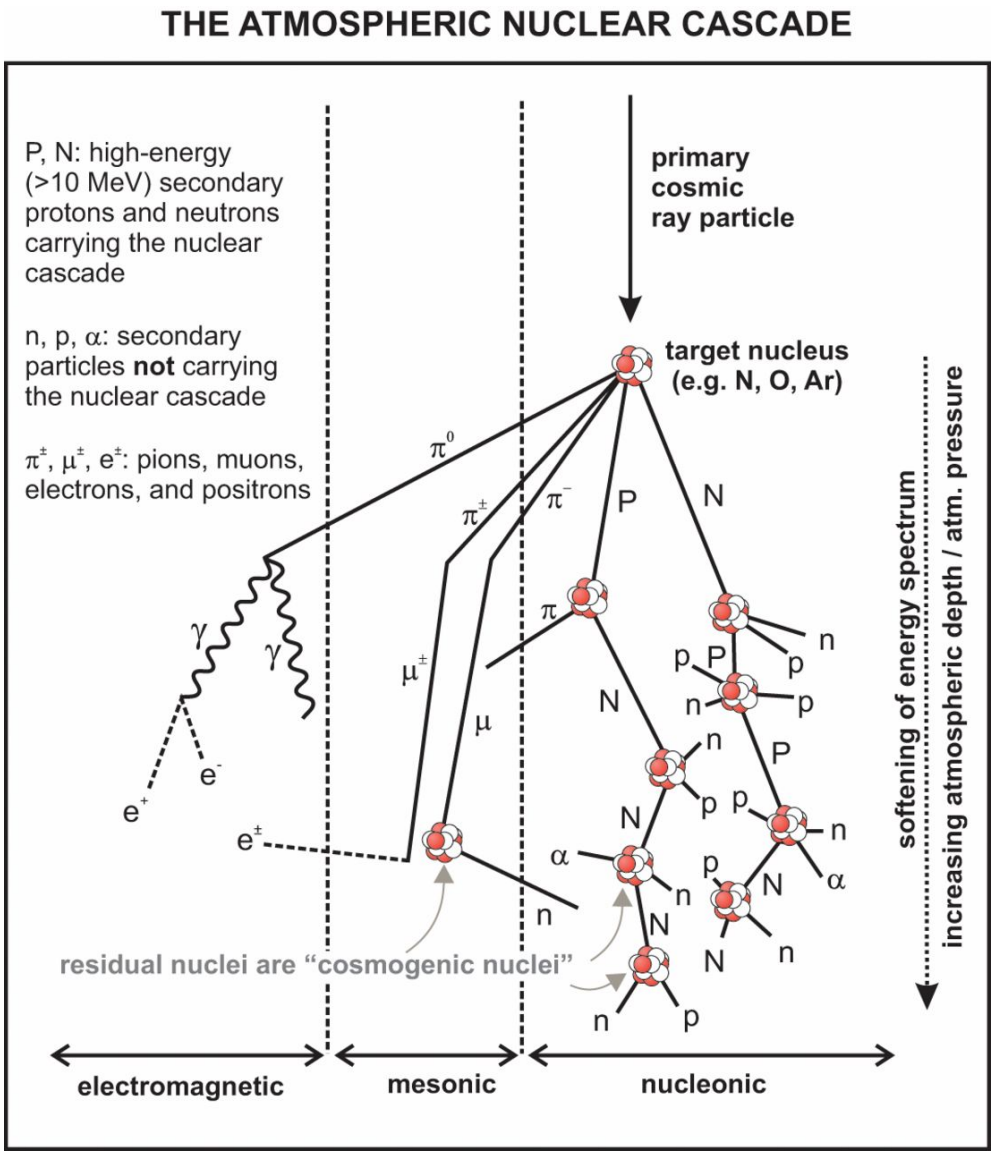

Figure 1.4: A schematic representation showing the secondary particle production in atmosphere and rock (Dunai and Lifton, 2014).

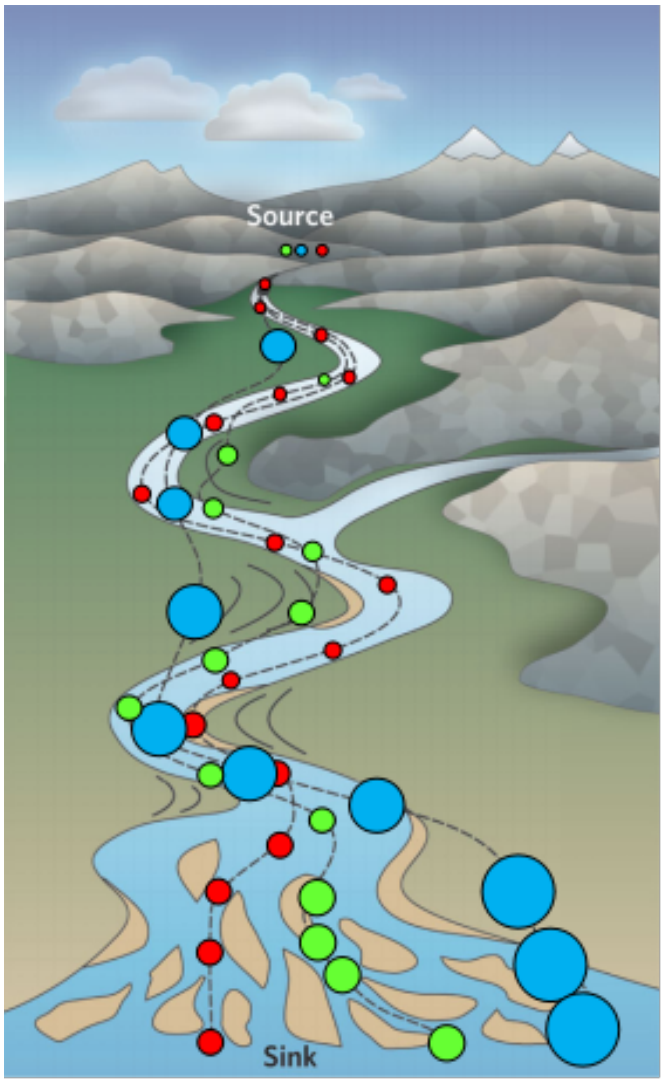

Figure 1.5: A schematic representation showing the basic idea to measure recycling using cosmogenic nuclides. The dashed lines, with circles of different colours, represent the accumulation of cosmogenic nuclides in different transport paths; the circles represent the concentration of cosmogenic nuclides, the larger the circle, the more the cosmogenic nuclides contained within the grain.

2. What is the age of the paleosediments that could be recycled, and hence how long might they have been preserved in the basin prior to recycling?

3. What are the main physical controls of recycling?

4. What is the impact of introducing recycling on the previous grain-based geological studies?

1.2 Aims

This PhD project aims to characterise the recycling process for the sediments of Miocene to present times in the Great Plains. There will be four branches of research methodology for this project. The first part is grain size analysis. We have collected samples and taken photographs along the North Platte River, with which we will obtain the sedimentological information carried with these grains. Abnormal downstream change of grain sizes will be used to explore the signals of recycling. The grain size data were used to reconstruct the detailed distributions of the grain sizes within several sites along the North Platte River. The second part of this research is cosmogenic nuclides (^{21}Ne and ^{10}Be) analysis. Quartzite pebbles within the modern North Platte River and the older Miocene and Pliocene paleochannels were collected. With the concentrations of cosmogenic nuclides contained within these samples, the exposure and burial histories can be developed for the pebbles collected along the North Platte River. The third part is numerical modelling. In the cosmogenic nuclides analysis, models were built to assess the maximum concentration of cosmogenic nuclides accumulated in the pebbles without storage. This model is used to support the existence of recycling in the Great Plains. Some other models were also built to test the controls on the cosmogenic ^{21}Ne accumulated during recycling. Lastly, a previous study which used grain size to reconstruct paleo-river profile was tested to evaluate the impact of introducing recycling on the previous studies. These lines of research will come together in a broader context to understand the role of recycling in the transport and deposition of gravels and cobbles across the Great Plains.

1.3 Research Background

1.3.1 Study Area

The Great Plains (sometimes termed “the Plains”) is a broad and low gradient region located in the central western North America (Figure 1.6 and Figure 1.7). It covers most of the area between the Mississippi River and the Rocky Mountains. Our research area is a part of the central Great Plains, limited within south-eastern Wyoming, western Nebraska and eastern Colorado (Figure 1.6). The place is mainly the catchment area of the Platte River. There are two parts of

the Platte River, the North Platte River and the South Platte River. The North Platte River is mainly sourced from Jackson County, Colorado, surrounded by Rock Mountain. For the South Platte River, its source is located in Colorado, which covers most of the eastern side of the Rocky Mountains. These two rivers meet near North Platte City, Nebraska. The Platte River flows into the Missouri River and ends in the Gulf of Mexico (Figure 1.6 A). In this study, the North Platte River drainage system (the area before North Platte City, Nebraska) was chosen as the target fluvial system (Figure 1.6 B). The drainage area of the North Platte River is approximately 90000 km^2. There are two primary sources of the North Platte River, the North Park area and the Medicine Bow Mountains. From the sources, the North Platte River firstly flow north, along the mountain, to Casper, Wyoming, near the north end of the Laramie Range. The whole flowing distance of this part is about 320 km. After Casper, the flowing direction of the North Platte River changes into east-southeast, nearly straightly, until it reaches the North Platte City, Nebraska. The flowing distance of this part is about 560 km. There are three main tributaries of the North Platte, the Sweetwater, Medicine Bow, and Laramie Rivers (Figure 1.6 C and Figure 1.7).

Before Casper, the North Platte River is flowing within the mountain area, while after Casper, the North Platte River reaches the plain area. These two parts of the North Platte River system are divided by Laramin Range. This can be seen obviously from the cross sections in Figure 1.7

According to Dickinson et al. (1988), the sedimentary record of the central Great Plains represents a post-orogenic landscape change from the end of Laramide Orogeny (ca. 55-40 Ma), throughout the Tertiary to the present day. There is a wealth of literature on the geology and geomorphology of this region. Multiple stages of incision and basin-fill have been recognised throughout the central Great Plains. A considerable amount of papers have been published on the causes of the complex sedimentary record within this area (Diffendal, 1982; Dickinson et al., 1988; Heller et al., 2003; McMillan et al., 2006). Until recently, three factors have been identified as potentially crucial causes of these multiple cycles of fluvial incision and aggradation: (1) Tectonic and volcanic activity (due to the Rio Grande Rift in Colorado and the Yellowstone Hotspot in Wyoming) (Heller et al., 2003; McMillan et al., 2006; Duller et al., 2012). (2) Dynamic topography (developing from buoyant mantle underpinning the continental plate in Colorado) (McMillan et al., 2002; Leonard, 2002). (3) Climatic shifts (Pelletier, 2009; Duller et al., 2012).

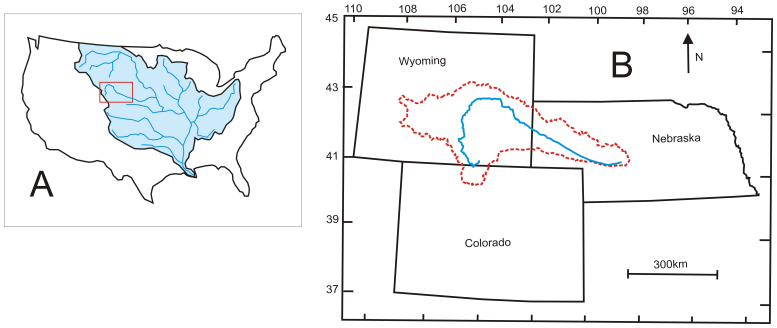

(a)

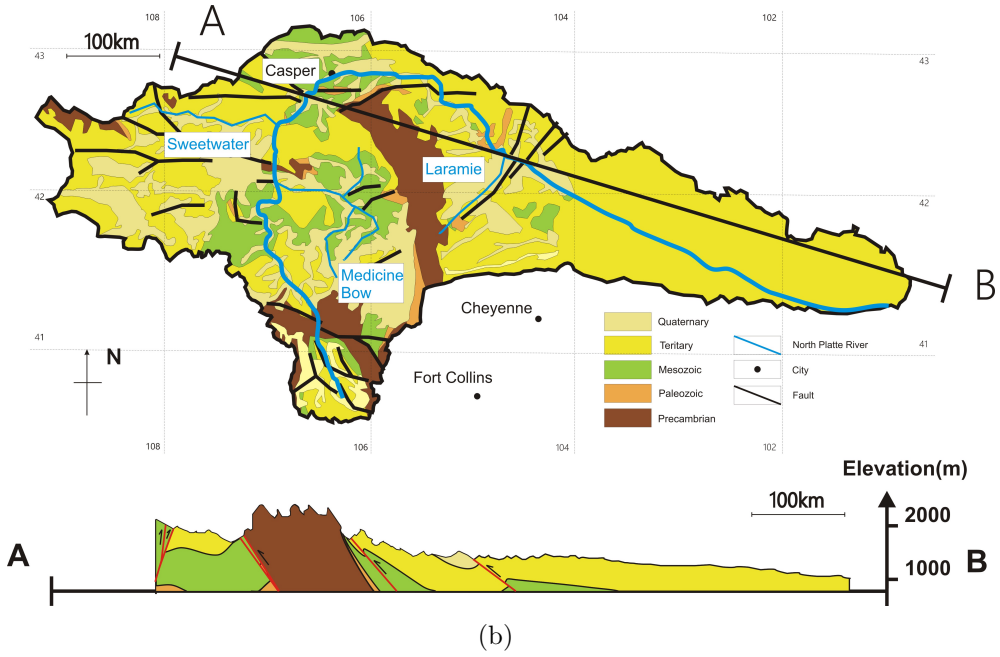

(b)

Figure 1.6: Maps showing location of North Platte River in context of the Mississippi River system (A), its location in context of central USA (B), and its geological context (sorted from USGS). The study area is limited in south-eastern Wyoming, western Nebraska and eastern Colorado, and is the catchment area of the North Platte River.

The following is a detailed review of the literature concerned with the geological setting of the region, including the geological history and the changes of the Platte River network. Also, the literature about tectonic and climatic shifts in the Great Plains is mentioned. This study is mainly on the recycling process that happened throughout the Tertiary to the present day, so that all the literature reviews are focused within this time range.

The methodologies applied here to test for the role of recycling in the evolution of gravels in the plains are described in the following chapters.

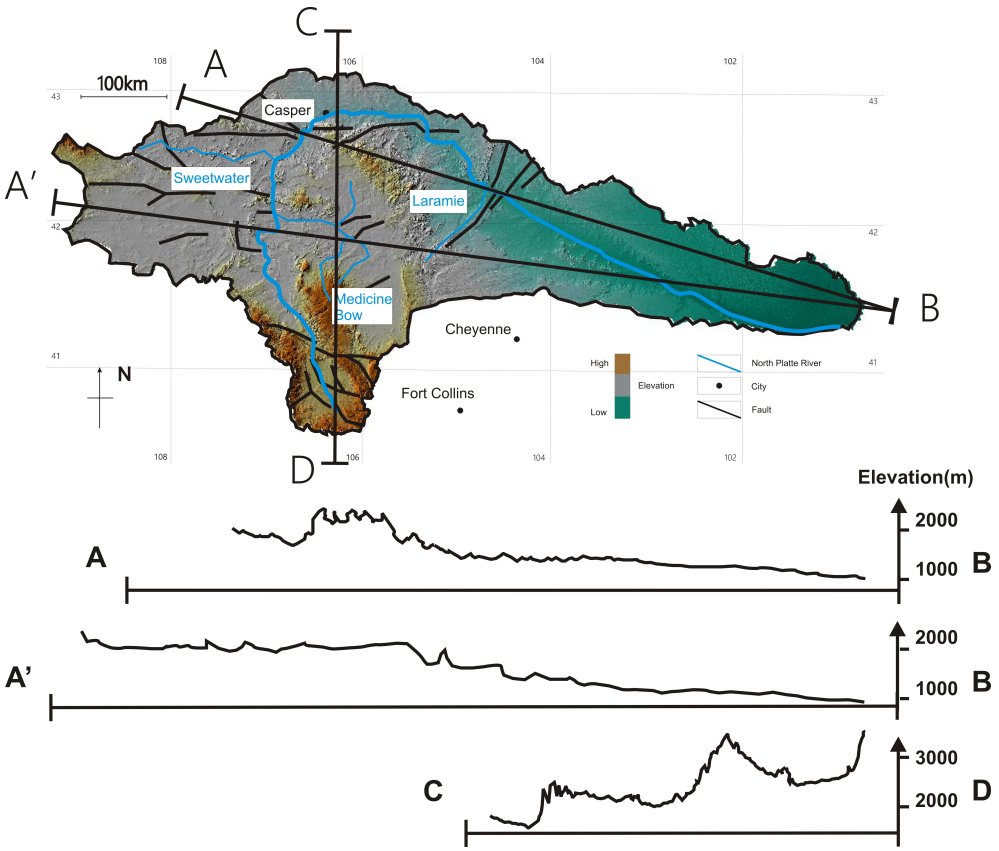

Figure 1.7: Digital elevation map of the catchment area of the North Platte River, with several cross sections of the study area.

1.3.2 Geological Setting

In western North America, from the Late Cretaceous (ca. 80-70 Ma) to the early Tertiary (ca. 55-40 Ma), there was a period of mountain building, which is named the Laramide Orogeny. During that time, the significant characteristics

of these tectonic activities are thick-skinned deformation off the west coast of North America, which contributed to the sliding of the Kula and Farallon Plates under the North American plate (Dumitru et al., 1991). Moreover, sedimentologically isolated nonmarine basins were produced by basement deformation (Dickinson et al., 1988). Following the end of Laramide Orogeny, ca 55-40 Ma (Dickinson et al., 1988), these accumulated sediments formed an unconformity over Cretaceous marine bedrock (Wobus et al., 2010), which is called the Denver Formation. Then during ca 38 - 37 Ma, volcanically derived aeolian siltstone called White River Group formed another unconformity over the paleosediments of the Denver Formation. From the end of the Oligocene to the start of Miocene, the Arikaree Formation (Oligo-Mio 30-18 Ma) can be found throughout this region. From Miocene to Pliocene, Arikaree Formation (Oligo-Mio 30-18 Ma) were unconformably overlain by Ogallala Formation (Miocene 17.5-5 Ma), fluvial cut-and-fill paleoterraces. At the end of Pliocene, all these strata mentioned above were overlain by Broadwater Formation (Pliocene, 4-2.5 Ma), gravelly braided fluvial deposits (Diffendal, 1982). Figure 1.8 is a brief representation of the Tertiary stratigraphy of the Great Plains. There have been several significant periods of incision happened in this region. Figure 1.2 shows the distribution of these Tertiary sedimentary units within the study area; it also briefly illustrates the degree of incision and basin-fill within the sedimentary record of the Great Plains.

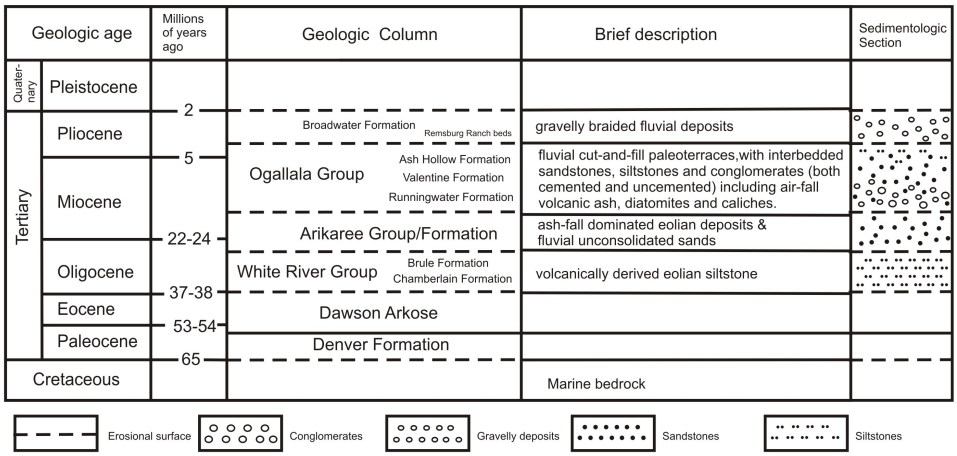

Figure 1.8: A brief geologic column of the Tertiary stratigraphy of the Great Plains.

The following summarises the geologic history of the central Great Plains throughout the Tertiary to the present day, each part includes a detailed description of the formations and the changes of fluvial system within this area.

Miocene

In the central Great Plains, during the transition from the Oligocene to Miocene, the sediments accumulated to form the Arikaree Group (Swinehart et al., 1985;

Swinehart and Diffendal, 1995, 1997). In Nebraska, the oldest formation of Miocene time is called the Harrison Formation, which is included within the Arikaree Group. In contrast to Nebraska, in Colorado and Wyoming, the Arikaree Group is undivided. However, the undivided Arikaree Formation in Colorado was considered Miocene in age (Scott, 1978), whereas the undivided Arikaree Formation in Wyoming was considered Oligo-Mio in age (Flanagan et al., 1993).

Diffendal (1982) characterised the Tertiary stratigraphy of the Great Plains, especially in Nebraska, in great detail. The Oligocene-Miocene Arikaree Group was described as fluvial unconsolidated sands, cemented sandstones, siltstones and conglomerates. According to Scott (1978), the undivided Arikaree Formation (Miocene age) in Colorado was described as conglomerate, sandstone, siltstone, and claystone. On the other hand, Flanagan and Montagne (1993) described the undivided Arikaree Formation (Oligo-Mio age) in Wyoming as small pebbles, sandstones, limestones, and ash beds. In Wyoming, calcareous concretions can always be observed in Arikaree Formation. Despite the differences, a significant aspect of Arikaree in all areas is that the deposits were mixed with volcaniclastic eolian (Condon, 2005).

Sediments accumulated and formed an unconformity over Arikaree Group. And the strata overlying this unconformity are named the Ogallala Group. Some papers have been published to describe the Ogallala Group in Nebraska, dividing it into many formations and members (Swinehart et al., 1985; Swinehart and Diffendal, 1995, 1997). In contrast, subdivisions of the Ogallala Formation in Colorado and Wyoming are informal, which can only partly correspond to the subdivisions in Nebraska (Scott, 1978; Flanagan et al., 1993).

Some papers have been published on the details of the middle to upper Miocene Ogallala Group in Nebraska, especially in western Nebraska. As suggested by these papers, the Ogallala was described as conglomerate, pebbles, sandstones, and siltstones, especially in western Nebraska, which coarsen up into gravels, pebbles and conglomerate (Swinehart and Diffendal, 1995, 1997). According to some other studies, in eastern Nebraska, the lithofacies of Ogallala are coarser than those of western Nebraska while the percentage of finer strata is higher (Swinehart and Diffendal, 1989; Diffendal, 1991; Souders et al., 2000).

In 1978, Scott (1978) divided the Ogallala Group in Colorado into upper and lower parts. In his description, the lower part of the Ogallala are mainly ashy sandstone and siltstone beds, which become coarser up into thin gravels. Haworth (1897) used the term "mortar beds" to stand for the sandstone beds containing calcium carbonate, which is always observed in the upper Ogallala Group. In Scott's paper, he also mentioned that the Ogallala group in Colorado contains a considerable amount of volcanic deposits (Scott, 1978). In Wyoming, Flanagan et al. (1993) described the Ogallala group in detail. In the Laramie Range, the Ogallala is mainly granite-rich conglomerate and metamorphic-rich conglomerate.

The grain sizes decrease eastward, and the Ogallala in eastern Wyoming is composed of sandstone, siltstone, limestone, and ash beds. In the paper of Heller et al. (2003), the Ogallala sandstones and conglomerates unconformably overlied the Arikaree and White River group, and were characterised by episodes of cut-and-fill, braided stream deposition during eastwards sediment transport from the Front Ranges (Diffendal, 1982). In the present-day, the conglomerates of the Ogallala are not exposed in the south of the Plains (e.g. Colorado and New Mexico) but exist in the subsurface (Condon, 2005).

During the end of the Oligocene and the early Miocene, volcanic eruptions were frequent in the central Great Plains. However, these eruptions ceased during the middle Miocene. Renewed intense tectonic activity happened in this area and led to erosion in the mountain area (Scott, 1975; Flanagan et al., 1993), resulting in a large scale unconformity throughout this area (Swinehart et al., 1985). Sediments carried from the mountain area accumulated and deposited on the Great Plains, resulting in the subsidence of the Great Plains. Ogallala Group was formed because of this process (Lugn and Lugn, 1956). The Ogallala spread eastward from the mountain area to the plain area, forming a series of cut and fill sequences. Most of deposits in these sequences represent a fining trend upward. McMillan et al. (2006) characterise the Ogallala as a nearly continuous succession covering most of the basins which were located in the east side of the mountain area, during the time of the Laramide Orogeny. And this succession of Ogallala changed eastward gradually into the low-relief topography of the Great Plains and Colorado Plateau.

After a detailed geological survey, Goodwin and Diffendal (1987) interpreted the depositional environment in Ogallala time as braided streams. Moreover, based on the studies of lithofacies, some other depositional environments have also been recognized, such as alluvial fans, low-relief alluvial plains and lake environments (Diffendal, 1982; Scott, 1982; Flanagan et al., 1993). To conclude, during the Ogallala Group time, large regions of erosion were filled with coarse fluvial sediments, forming an eastward-sloping wedge on the central Great Plains (Blackstone Jr, 1975).

Some data on the paleogeography of the central Great Plains were sorted and compiled by Condon (2005) to reconstruct the distribution of Ogallala Group and paleochannel system existed in that time (shown in Figure 1.9). In this figure, the boundary of the Ogallala Group was from Condon (2005). Three reconstructed paleochannel systems are also shown in this figure. The blue one comes from Swinehart et al. (1985) and Swinehart and Diffendal (1989). As suggested by these papers, in the Ogallala time, the sources of the rivers were located at the northern Front Range, south-eastern Wyoming, north-eastern Colorado and north-western Nebraska, and the drainage was eastward or south-eastward into the central Great Plains. The black onset come from Blackstone (1975). As suggested by this paper, the sources were also set at the northern Front Range.

The red ones come from Steven et al. (1997). In this paper, they suggested a central to southern Front Range source for the Ogallala paleochannels. Also, they suggested the flowing directions to be eastward or north-eastward which is slightly different from the blue one. The green one comes from Pearl (1971).

The later Miocene (ca. 10 -12 m.y.) initiated the present-day drainage system.

In Figure 1.9, the red cross-hatched area on the left represents the uplifts of Miocene age. The red areas represent the distribution of Miocene volcanics. These Miocene volcanics were identified on the west side of the Front Range and Laramie Range (Blackstone Jr, 1975; Stanley, 1976). However, in eastern Wyoming, north-eastern Colorado, and western Nebraska, the same volcanics were also found in other studies (Blackstone Jr, 1975; Flanagan et al., 1993). The most likely reason for this situation might be the filling of Laramie Basin during Miocene time, resulting in the sources of paleochannels being located in the North Park area for some time, thus carrying some clasts from the west side of the Front Range and Laramie Range to the east side (Blackstone Jr, 1975; Flanagan et al., 1993).

Pliocene

It should be noticed here that it is difficult to distinguish the newest part of Pliocene from the oldest part of Pleistocene in the central Great Plains. There are two reasons for this: (1) The lithofacies of upper Pliocene strata and lower Pleistocene strata are similar to each other, the transition from Pliocene to Pleistocene sedimentation is gradual and not noticeable; (2) The standard for distinguishing the ages comes from fossil analysis which cannot be found throughout the central Great Plains (Condon, 2005).

In the middle Miocene, the west part of the Great Plains began to rise (Morrison, 1987; Steven et al., 1997; Condon, 2005). Thus, the mountain areas were stripped away, and most of the stripped sediments accumulated on the east of the mountain area, on top of the Ogallala Group or in the fluvial valleys incised, forming Broadwater Formation, which is composed of gravel-rich channels. The incision in Pliocene times formed deep paleovalleys on the Ogallala Group (Miocene), filled by a further 100 m of sandstones and conglomerates (Swinehart et al., 1985). The uplift in Pliocene times continued and it affected Colorado, and then the amount of stripped sediments increased continually, and they were carried farther away from the mountain area. As suggested by the geological survey, nearly all of the paleosediments of Pliocene-age in Colorado have been stripped and carried eastward (Condon, 2005).

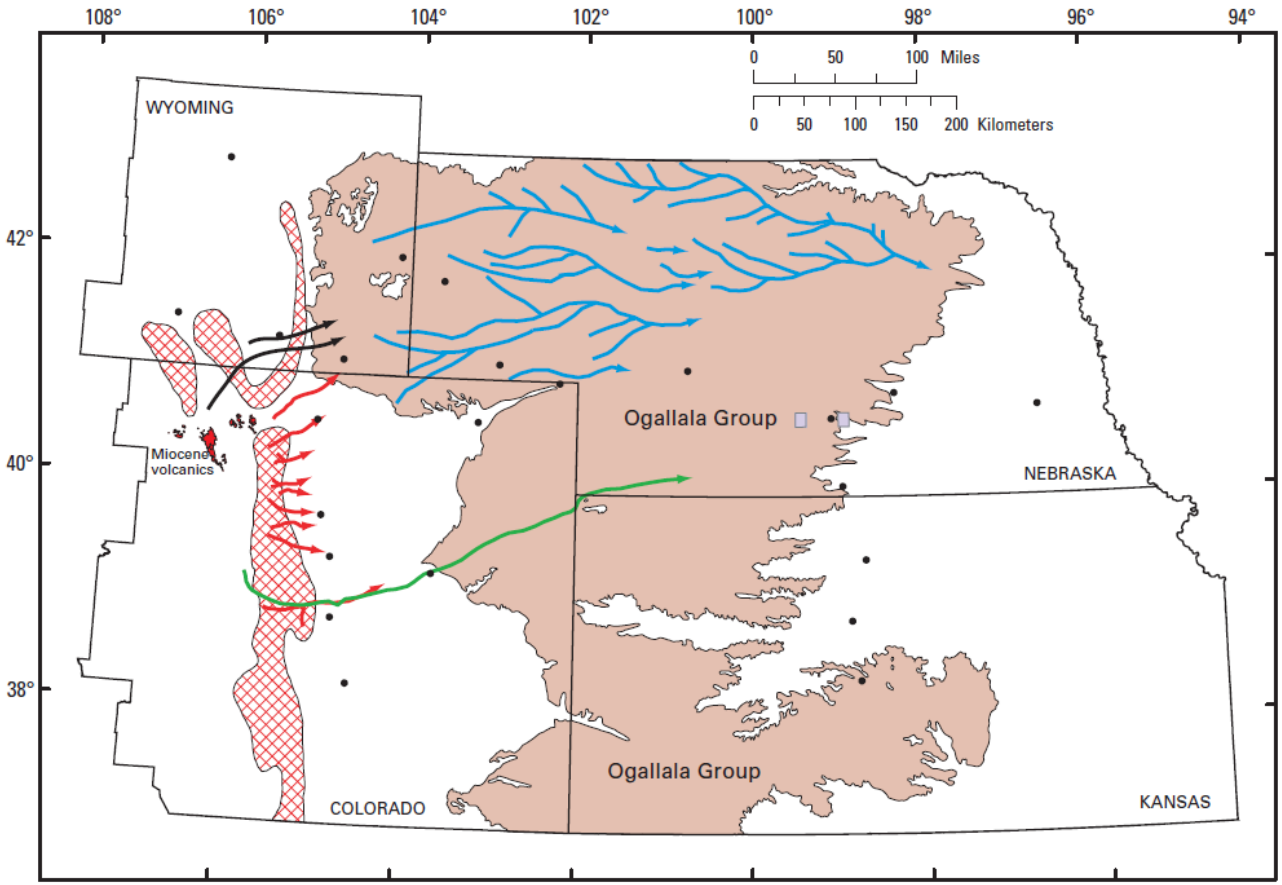

Figure 1.9: Paleogeography in Miocene time (mainly Ogallala Group), cited from Condon (Condon, 2005). The red cross-hatched area represents the distribution of uplifts; the brown area represents the distribution of the Ogallala Group; the lines represent the distribution of channels at that time, with the arrows representing the flowing directions; the red areas represent the distribution of Miocene volcanics.

On the other hand, Nebraska accepted most of the gravel and finer sediments carried from the east mountain area and the Colorado.A study of Steven et al. (1997) suggested that during Pliocene times, the region of Nebraska was tilted to the north-east. During the early Pliocene, the incision paleovalley was filled by 100 m of fluvial sediments, which was recognised and described by Schultz and Stout (1945), and named Broadwater Formation. However, the Broadwater Formation is mainly restricted to the western and northern Nebraska. There have been several studies recognising the equivalent units in other regions. As suggested by Souders et al. (2000), Pliocene-age loess and fluvial sediments were recognised to be equivalent to the Broadwater Formations. In another study of Swinehart (1994), Belleville Formation is recognised along the Republican River in southern Nebraska, considered to be equivalent to the Broadwater Formations. Moreover, some literature (Diffendal, 1991; Swinehart, 1994) have been published on alluvial units in central Nebraska. These units were recognised to be formed at the same time as the Broadwater Formation.

The studies of Pliocene strata in Colorado and Wyoming are limited. As suggested by the summary of Condon (2005), during the Pliocene time, the deposits in these two areas had experienced more erosion processes rather than deposition processes, which contributes to the overall net erosion of the paleosediments of the Pliocene time in these two areas.

In general, the Pliocene Broadwater formation was composed of conglomerate, pebbles, sandstones, siltstones, claystones, and mudstones (Schultz and Stout, 1945). However, there existed slight differences in lithofacies for different parts of the central Great Plains. As suggested by Souder et al. (2000), in south-central Nebraska, the Pliocene can be divided into two units, the base one was mainly composed of gravel and sand, and the component of finer sediments is low. The top unit was mostly composed of silt and clay, while the concentration of coarser components is low. In Colorado, the study of Scott (1982) revealed that the Broadwater and equivalent formations consist of gravel, sand, and minor silt and clay.

Eolian deposition can also be found in the Pliocene sediments. In contrast to the eolian volcaniclastic deposits of Miocene time, these eolian deposits in the Pliocene sediments were probably from overbank material (Condon, 2005).

Also, some data on the paleogeography of central Great Plains from various sources were compiled by Condon (2005) to reconstruct the distribution of uplift areas and paleochannel system existed in Pliocene time (shown in Figure 1.10). The sources of paleochannels in Pliocene times is similar to those of the Miocene time. There are two primary sources of these paleochannels, the Medicine Bow and Laramie Ranges (Wyoming); and the Front Range (Colorado). In this figure, the extent of the Broadwater Formation was modified from Swinehart (1994). Five main different reconstructed paleochannel systems are shown in this figure.

The magenta one comes from Stanley and Wayne (1972), where a distinctive clast suite was identified, indicating a significant channel draining from the Laramie Range, flowing into Nebraska and being divided into two main channels: the north one flowed northward and then eastward, while the south one flowed southward and then eastward. The red one comes from Scott (1975). As suggested by this paper, the uplift happened in the Front Range caused cutting and incision on the west side of the mountain area, setting a north-eastward trend of the South Platte River. Moreover, the complex tectonic activities resulted in the disruption of the fluvial system. The blue one comes from Condon (2005). In this paper, two primary sources for the paleochannels in the Pliocene time were recognised: one is from north-eastern Colorado, while another source is from south and east of Wyoming. These two channels flowed eastward and might join each other in Nebraska. The green one also comes from Condon (2005). The black one comes from Pearl (1971). In this paper, Pearl (1971) drew an ancient Arikaree River which was sourced from the Front Range. Pearl suggested that this river appeared in Ogallala time (Figure 1.9), and had existed until the early Pliocene time. Moreover, during late Pliocene time, this ancient Arikaree River cut off the mountain-sourced channel located in eastern Colorado, forming the early South Platte River system (Condon, 2005).

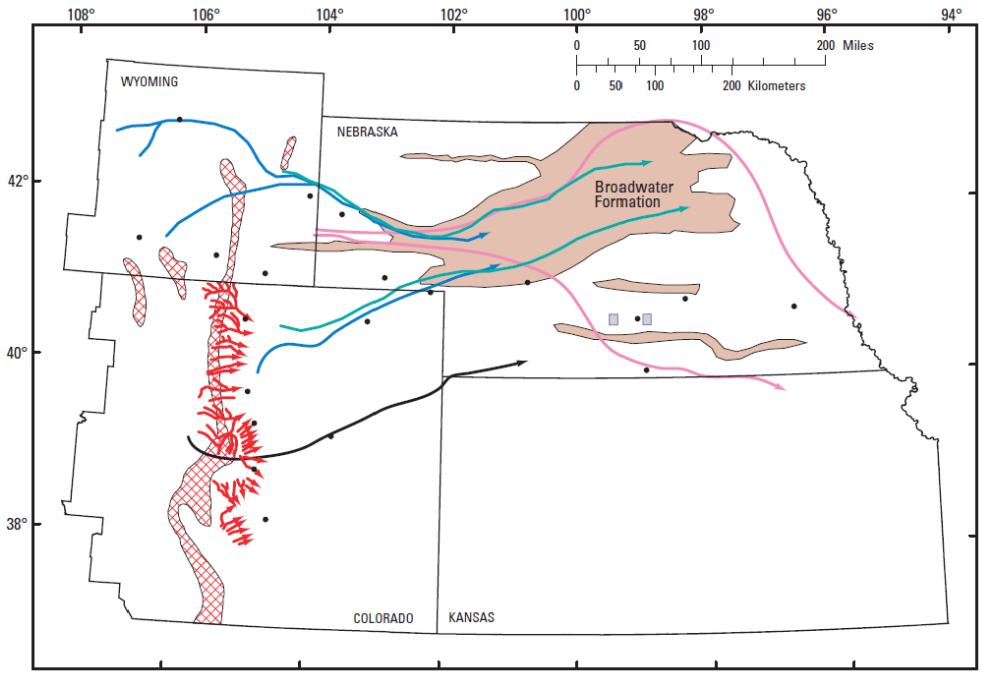

Figure 1.10: Paleogeography in Pliocene time (mainly Broadwater Formation), cited from Condon (Condon, 2005). The red cross-hatched area represents the distribution of uplifts; the brown area represents the distribution of the Ogallala Group; the lines represent the distribution of channels at that time, with the arrows representing the flowing directions.

The basic shape of the drainage system of Platte River was formed in Pliocene time, and this shape did not change a lot until now (Condon, 2005). Moreover, the Pliocene units are exposed widely in the central Great Plain, along the major present-day drainages.

Pleistocene and Holocene

As described on the previous pages, in the central Great Plains, the Miocene sediments mainly formed Ogallala Group, and the Pliocene sediments mainly formed Broadwater Formation. Ogallala Group is incised by 100 m of Broadwater Formation (Swinehart et al., 1985; Wobus et al., 2010). On top of the Ogallala Group and the Broadwater Formation, they were incised by the modern Platte River (Diffendal, 1982), forming a large-scale unconformity (shown in Figure 1.2).

In 1995, May et al. published a paper (May et al., 1995) in which they described the sedimentary units, mainly of Pleistocene times, deposited on the Ogallala Group in Nebraska. As suggested by this paper, there are two sedimentary units at that place. The existence and characteristics of these two gravel units differ from place to place. However, because the lithofacies of these two units are similar (May et al., 1995), and the transition from the lower unit to the upper one is gradual and not noticeable (May et al., 1995), it is hard to distinguish one unit from the other one. The lower unit is composed with coarse clastics, which is recognised by some studies as the Fullerton Formation and be considered Pliocene in age (Condon, 2005). While the upper unit consists of coarse fluvial gravel, interbedded with finer sandstone, silt and clay in some places (Swinehart, 1994; May et al., 1995). As suggested by these studies, some subdivided units can be recognized for the upper unit, those are the Walnut Creek Formation, Sappa Formation, Grafton Loess, Beaver Creek Loess, Loveland Formation, Crete Formation, Gilman Canyon Formation, and Peoria Loess (Swinehart, 1994; May et al., 1995). Several studies (May and Holen, 1985; May, 1989) have found terrace alluviums in Nebraska, which were formed along the paleochannels after Pliocene. The sediments are very coarse in the east side of the mountain area, and becoming finer eastward (Scott, 1982).

At the central Great Plains, the Holocene starts at about 10,000 years B.P. (Condon, 2005), which is composed of fine silt (Pye et al., 1995; Maat and Johnson, 1996). One important feature of the Holocene deposits is the wind and wind- and stream-deposited dune fields, which covers one-quarter of the State of Nebraska (shown in Figure 1.11). Some literature has been published on these dune fields after radiocarbon dates becoming available (Swinehart and Diffendal, 1989; Swinehart and Loope, 1992; Loope et al., 1995; Sweeney et al., 1998; Muhs and Bettis, 2000). As suggested by these studies, there are several stages of the activities of the dune field: 8,000 and 5,000 years B.P., 10,600 years B.P., and 12,000 years B.P. Most studies agreed that the dune field were mainly actived in the middle to late Holocene (from 8,000 to 5,000 years B.P., (Muhs et al.,

1997)). Some other Holocene dunes can also be observed in south of the Platte River, north-eastern Colorado, and south-eastern Wyoming. In 1996, Muhs et al. published a paper (Muhs et al., 1996) in which they described the dunes in Colorado as being mainly from stream channel and floodplain alluvium.

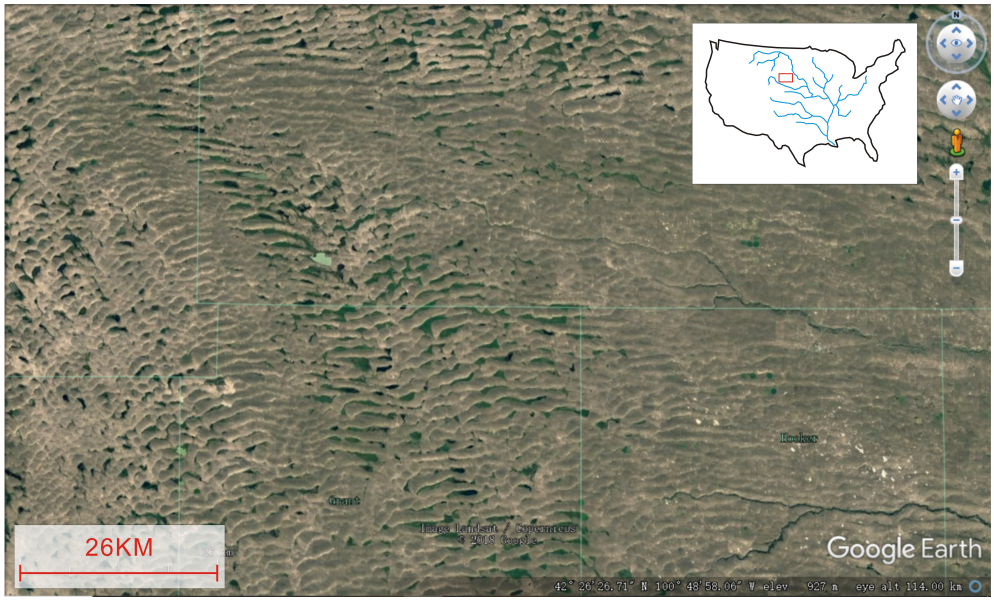

Figure 1.11: Photo of the dune fields in the Great Plains (from Google Earth).

Some dates on the paleogeography of the central Great Plains were also compiled by Condon (2005) to reconstruct the distribution of channel system existed in Pleistocene time (shown in Figure 1.12). In this figure, the red cross-hatched pattern represents metamorphic rocks of Precambrian time, which is based on the studies of Green and Drouillard (1992; 1994). The boundary of the losse-area was modified from Muhs and et al. (1999). The thin blue line represents the modern North, South, and combined Platte Rivers, for reference. It can be demonstrated that paleochannels formed in Pleistocene age were nearly the same as the modern channels. The paleo-North, paleo-South, and combined paleo-Platte Rivers can easily be recognised in the figure. For the reconstructed paleochannels, the black one comes from Stanley and Wayne (1972), who suggested the paleo-Platte River has a source located south of the present North Platte River, while the flow direction of the paleo-Platte River is nearly the same as that of the present one. The green, light blue, and pink streams were reconstructed based on the previous study (Swinehart, 1994). This version of paleo-Platte River system has the closest shape as that of the modern Platte River system. Moreover, the Loup River system which formed and flowed south into the Big Blue River drainage system in the early Pleistocene (Lueninghoener, 1947), is shown as dark blue lines in Figure 1.12.

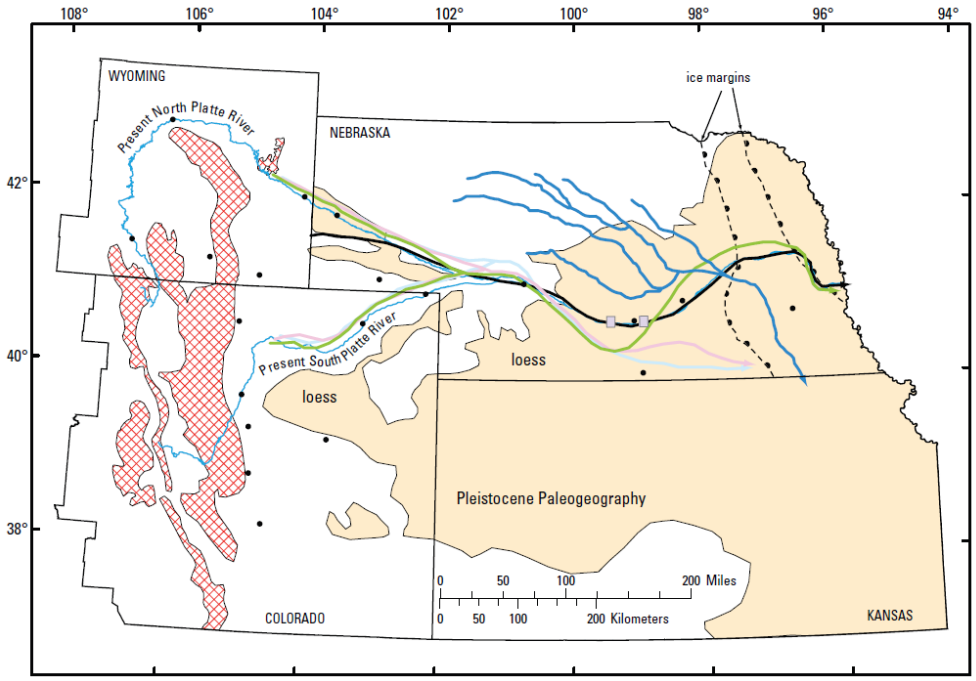

Figure 1.12: Paleogeography in Pleistocene time, cited from Condon (Condon, 2005). The red cross-hatched area represents the distribution of Precambrian granitic or metamorphic rocks; the brown area represents the distribution of the Ogallala Group; the thin blue line represents the modern North, South, and combined Platte Rivers; the thick lines represent the distribution of channels formed at that time, with the arrows representing the flowing directions.

1.3.3 Climate

As fossils are abundant in the Miocene succession, a considerable amount of literature has been published that attempts to reconstruct the climate change in Miocene times in the central Great Plains. There have been several investigations into the diverse mammalian fauna in the Ogallala Group in western Nebraska (Schultz and Stout, 1948; Leite, 1990; Swinehart and Diffendal, 1995, 1997). In the study of Leite (1990), an extinction of some large mammals in Miocene time was revealed; the environment of Nebraska became colder and dryer in the Miocene time, which reduced the amount of vegetation which formed the food for these large mammals, thus resulting in extinction. The study of Flanagan and Montagne (1993) also suggested an increasing aridity and colder climate from the Miocene to the Pliocene in Nebraska. In 1997, Retallack published a paper (Retallack, 1997) in which he divided the climate change in Miocene times into two stages, during the early stage, the precipitation decreased whereas during the later Miocene the precipitation increased.

There have been several studies (Lugn, 1935; Scott, 1982; Swinehart and Diffendal, 1997; Ward and Carter, 1999) investigating the climate change in Pliocene times. Ward and Carter (1999) developed a model based on tectonic activities which points out that, Pliocene uplift in the mountain area caused a rain shadow on the west side of the mountain area, which contributed to the decrease of precipitation and amount of flow in the central Great Plains. However, several studies (Lugn, 1935; Scott, 1982; Swinehart and Diffendal, 1997) have revealed that the Broadwater Formation contains abundant fossils, in which a diverse fauna can be observed. This diverse fauna was regarded as the evidence of a humid climate in Pliocene time. In 1997, Chapin and Kelley (1997) reviewed the previous studies and published a paper in which they demonstrated increased precipitation in Pliocene time and they found four pieces of evidence for this. These are (1) complex drainage systems, (2) Rio Grande Rift and Basin was closed in Miocene timer but reopened in Pliocene time because of expanded channel systems, (3) deep erosion of older strata, (4) stable carbon isotopes of palaeosol carbonates. Another paper (Morrison, 1987) on this topic also provides support for the increased precipitation in the Pliocene, but he also pointed out that significant fluctuations in erosional-depositional cycles can be observed in the paleosediments of the late Pliocene, suggesting that the climate at that time was also fluctuating.

The climate in Pleistocene can be inferred from the lithofacies. (1) Coarse fluvial sediments found at the east side of the mountain area indicate abundant water. (2) Widespread finer deposits in middle and late Pleistocene-age represent a more arid climate. However, the climate of the Pleistocene was complex. As suggested by the studies of Wayne and Aber (1991), and Schultz and Stout (1948), the climate of Pleistocene times was humid because of the diverse fauna fossils found in the paleosediments. The study of Muhs et al. (1999) supported this conclusion based on the analysis of the carbon isotope data. On the other hand, in the

late Pleistocene, in Nebraska, the climate changed a lot (Wayne et al., 1991), resulting in multiple stages of incisions and aggradation (Schultz and Stout, 1948; Morrison, 1987). Moreover, in Haynes's study, most diverse fauna found in the early Pleistocene became extinct in the late Pleistocene and the early Holocene. Which might be resulted from a widespread drought happened at that time (Haynes, 1991). It can be concluded from these studies that throughout the Pleistocene, the climate fluctuated between glacial and interglacial, which arises the possibility that this change could influence the amount of channel flux, resulting in the fluctuation of erosion and deposition of fluvial sediments.

Many studies have been done to investigate the climate in Holocene time (Smith et al., 1997; Xia et al., 1997; Laird et al., 1998). In the late Pleistocene, parts of the central Great Plains were covered by forest. However, during the early Holocene, the glaciers retreated northward, thus changing the coverage area of plants (Wayne et al., 1991). Before 5,000 years B.P., the climate of the central Great Plains persisted as hot and dry conditions while after 4,000 years B.P., the climate changed into cold and moist conditions (Barry, 1983). In the middle Holocene (5,000 years B.P. to 4,000 years B.P.), grassland covered most of central Great Plains, but in the late Holocene (after 4,000 years B.P.) the coverage area of grassland retreated westward (Hoffmann and Jones, 1970). In the paper of Condon (2005), it is noticed that the sediments collected from the flood plain near North Platte City were dated in three different times. The oldest ones were dated as 9,600 years B.P. while the youngest ones were dated as 1,500 years B.P. His interpretation of this situation is that the rivers at this place have been stable throughout this time range (from 9,600 years B.P. to 1,500 years B.P.).

1.3.4 Vertical Motions in the Great Plains

During the Oligocene and early Miocene, volcanic activities dominated in the mountain area. Volcanic sediments can be seen in the central Great Plains, being carried eastward within the channels. However, these volcanic activities ceased in the middle Miocene. During the middle Miocene, some other tectonic activities started in the mountain area, like renewed faulting. These processes led to the uplift of the mountain area and the erosion at the east side of the Rockies (Scott, 1975; Epis et al., 1976; Flanagan et al., 1993; Mears Jr, 1993). This erosion resulted into an unconformity on the older strata (Swinehart et al., 1985) in the central Great Plains. As discussed in the previous pages, some studies have revealed that the middle Miocene erosion caused the planation of some of the mountain area, like Front Range and Medicine Bow (Blackstone Jr, 1975; Mears Jr, 1993; Steven et al., 1997).

The form of the landscape reflects the regional history of the tectonic and climatic processes (Wobus et al., 2010). The Rocky Mountains and Great Plains experienced a spike of an incision around 8-6 Ma, the driver of which has been the

subject of great debate, as both climate change and uplift can induce river incision (McMillan et al., 2002; Wobus et al., 2010). The key to this debate lies in the details of the warping at the base of the Ogallala Group with differential uplift of 600 m at the east of the mountain area and the western edge of the Great Plains, tapering out further east. This warping is thought to have occurred around 8 Ma, preceding Pliocene incision (Swinehart et al., 1985; Leonard, 2002; McMillan et al., 2002).

McMillan and collaborators have dedicated years to the study of this warping and subsequent incision and have produced some seminal papers on this subject matter. One such critical McMillan et.al paper (2002) used the method of reconstructing paleoslopes of coarse-grained fluvial deposits set out by Paola and Mohrig (1996). The result shows that the slope of the Ogallala Group (17.5–5 Ma) represents a value of 10^{-2}, to the east. However, the reconstructed slope based on the collected grain size data indicates a value of 10^{-3} to 10^{-4}, which is the depositional slope during the Ogallala time. The conflict between the modern slope and the reconstructed depositional slope suggests a tilt happened after the Ogallala time. If changes in climate were the main causes, this tilt should been achieved through increased water flux and isostatic rebound due to sediment exhumation. However, the authors argued that these mechanisms cannot fully explain the post-depositional tilt of the Ogallala. Instead, they suggested that the tectonic activities have played a key role in the depositional history of the central Great Plains after the Ogallala time. Furthermore, their study shows that the Yellowstone hotspot related dynamic uplift is only few hundred metres, and this elevation is local and limited nearby. So that the Yellowstone hotspot related dynamic uplift cannot account for the large tilt happened in the western edge of the Great Plains, while the Rio Grande rift is the most likely cause of this uplift.

One of the other studies proposed to explain the Late Cenozoic tilting happened in Colorado is from Leonard (2002). As suggested by the result of his model, the reconstructed deformation closely matches the observed one, but only accounts for half of the magnitude. He then suggested that the other half was attributed to tectonic uplift. In his study, Leonard (2002) also found that the strength of the uplift increased southward across the Colorado, resulting from the Rio Grande Rift in the southern edge of the central Great Plains. This finding matches the conclusion of McMillan's study (2002). Moreover, because of the differential uplift in response to the changing distance from the Rio Grande Rift, this activity in the Rio Grande Rift zone caused the streams of the Arkansas drainage to incise at higher rates at the southern plateau than that at the northern plateau. This differential incision then led to differential isostatic compensation. In addition, this uplift-erosion-isostatic compensation process resulted into an isostatic uplift, the magnitude of which is nearly the same to that of the tectonic uplift.

In 2002, Goes and van der Lee (2002) built an model to simulate the change of the density of the North American upper mantle. The result of this model

suggested an isostatic elevation difference between the southern Rocky Mountains and Kansas of 1 km in the Ogallala time. This elevation difference contributed to a tilt on the order of 10^{-3}. And this tilt is enough for the large pebbles of the mountain area to be carried eastward.

Heller et.al (2003) studied the post-Paleozoic alluvial conglomeratic units (Shinarump Conglomerate, Lower Cretaceous Conglomerates and Ogallala Group) to explore the details of the tilting happened in the Great Plains. Based on the grain size analysis with the pebble data collected along the Platte River, they reconstructed the tilting history of the Great Plains. While acknowledging the influences of the active Rio Grande Rift in the south of the Great Plains, the authors argued that tilting occurred over a higher wavelength could be explained by this activity alone. They took the Neogene uplift of the southern and central Rockies into consideration and pointed out that the tilting of the Ogallala resulted from the low velocity upper mantle beneath the Rio Grande Rift (Figure 1.13).

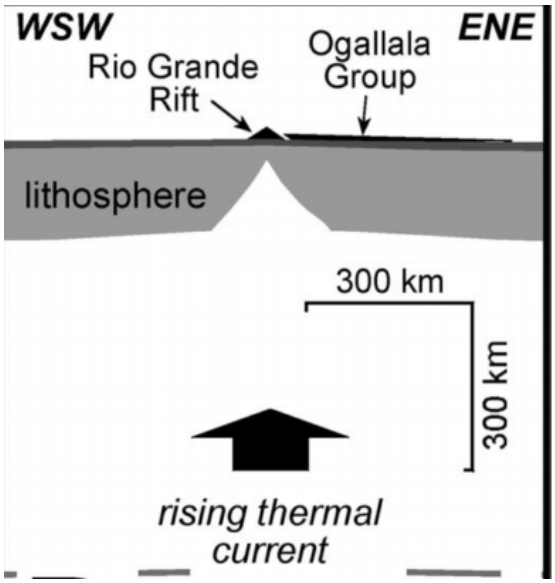

Figure 1.13: Tilting associated with progradation of Ogallala Group is interpreted to relate to regional uplift and active extension associated with evolving Rio Grande Rift in Miocene time (Heller et al., 2003; McMillan et al., 2006)

McMillan and Heller (2006) further proposed another way to support their previous explanation (Heller et al., 2003). Firstly, they calculated the distribution and thickness of the preserved deposits in the Great Plain. Based on these values, they determined the depositional thicknesses and original extent of these deposits. They then subtracted the modern elevation from the reconstructed basin-fill surfaces. These results were regarded as the first-order control of tectonic activities on the tilting history. Secondly, they constrained the timing of incision using volcanic deposits. Their results suggest slow subsidence in the

Great Plains, which started from the end of the Laramide Orogeny and ceased at ca. 6–8 Ma in the mountain area and ca. 3–4 Ma along the eastern edge of the Great Plains. The results of timing of the incision also matches the result of a low velocity upper mantle current happened beneath the Rio Grande Rift (Heller et al., 2003).

However, uncertainties on paleoslope reconstructions have led some authors to solve the problem of incision using another method; Wobus et al. (2010) developed a landscape evolution model based on a stream power approach to reconstruct the incision patterns. In this model, the influences of climatic changes and tectonic activities were both taken into consideration. Also, in this model, the climatic changes were represented by the changes in hydrologic factors while the tectonic activities were represented by changes in tectonic uplift. As suggested by the results, the climate-induced increases in water or decreases in sediments load would result in excess transport capacity of the channels. To adjust for this excess, the river generated a downstream migrating wave of incision and a decrease in channel gradients (Figure 1.14). In contrast, the tectonics-induced drives would result in the increases in channel gradient and upstream migrating incision (Figure 1.15). In this paper, Wobus et al. argued that the uncertainties inherent in the McMillan et al. (2002) method to calculate the paleoslopes of the Ogallala channels are within error of the calculated modern slopes. However, they also pointed out that the gradients of modern channels are lower than those of the Ogallala paleochannels, suggesting that climate changes remain a reliable controls of the fluvial incision across the Great Plains.

Another critical paper advocating the importance of climate change in the evolving landscape of the Great Plains is from Pelletier (2009), concentrating on the impact of snowmelt. Pelletier states that the high erosion from the middle Miocene to the present could be primarily a result of an increase in snowmelt-derived water flux. In the middle Miocene, snowmelt-derived water flux was only locally significant, as runoff was limited to elevations above 3 km. However, with the global cooling event of the late Miocene and Pliocene, the coverage of snow increased significantly. Thus the influence of snowmelt-derived water flux reached further down from 3 km to 1.5 km elevation in the Front Ranges, increasing the magnitude of flooding, the sediment flux, and the fluvial incision within this elevation range. A landscape evolution model was developed by Pelletier to map the spatial distribution of late Cenozoic snowmelt-driven erosion. The result of the model shows that snowmelt-driven erosion had triggered widespread deposition downstream which is consistent with the magnitude, timing and spatial distribution of the Ogallala Formation.

Duller et al. (2012) employed field measurements and DEM analysis of present-day slopes of the modern North Platte and Ogallala and Broadwater paleochannels. The field measurement includes median grain size distributions and channel depths, which are used to calculate the fluvial dynamics of the modern or pale-

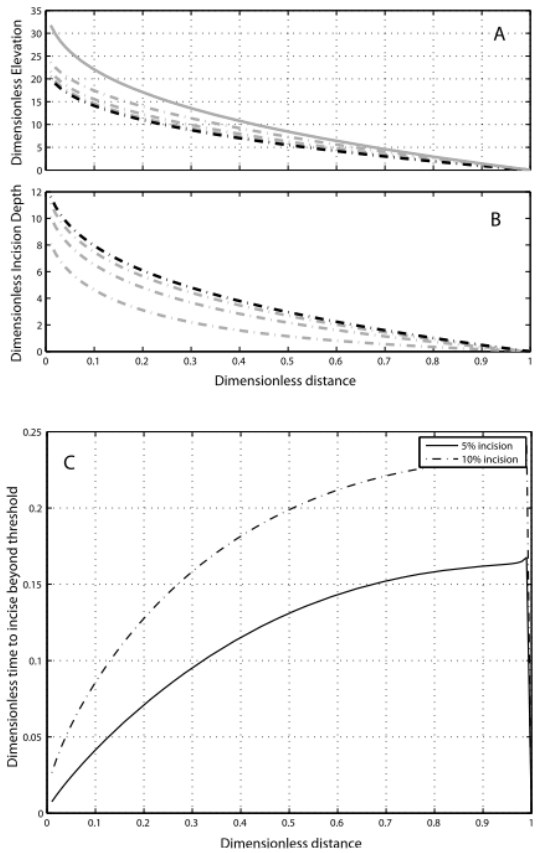

Figure 1.14: Spatial and temporal patterns of incision driven by a decrease in sediments load (Wobus et al., 2010). In a & b, solid gray line represent the initial situation, black dashed line represent the final situation, and the gray dashed line represent the intermediate situation. a shows the changes of the river profile and b is the patterns of incision depth as a function of distance. c shows the temporal progression of incision, expressed as the time required for incision to reach threshold percentages of the initial elevation

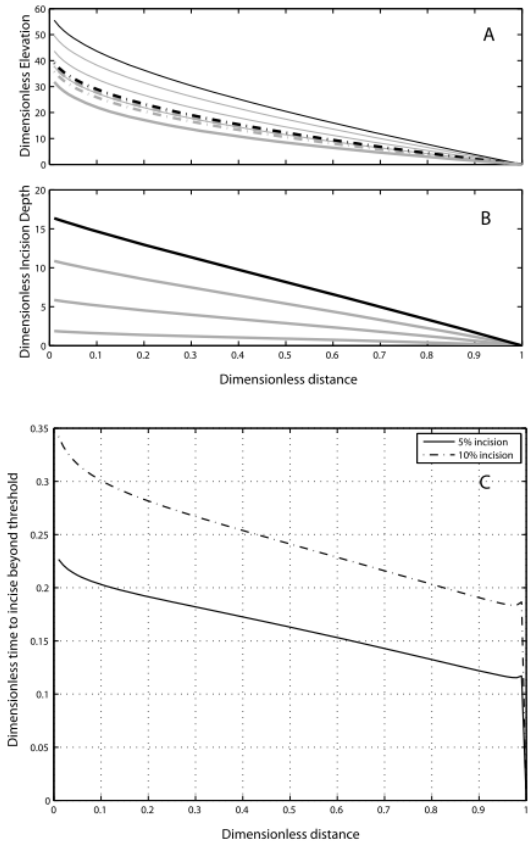

Figure 1.15: Spatial and temporal patterns of incision driven by tectonic uplift (Wobus et al., 2010). In a & b, solid gray line represent the initial situation, black dashed line represent the final situation, and the gray dashed line represent the intermediate situation. a shows the changes of the river profile and b is the patterns of incision depth as a function of distance. Additional thin lines in a represent abandoned paleosurfaces as the channels incise into the uplifted landscape. c shows the temporal progression of incision, expressed as the time required for incision to reach threshold percentages of the initial elevation

ochannels. As suggested by the result, the deposits of the early Miocene have not been tilted. While the deposits of the later Miocene (6-3.7 Ma) have experienced a post-depositional uplift on the order of 100 metres. They argued that this uplift were resulted from the localised tectonic activities happened in the Pliocene. Moreover, they found an increase of water flux and median grain size in the later Miocene, suggesting that an end-Miocene climate cooling which intensified the incision happened at that time. They also stated a warm, wet mid-Pliocene environment which led to a higher sediment supply and resulted in a fluvial aggradation and incision around 3.7-2.5 Ma (deposition of the Broadwater Formation). Furthermore, they pointed out that the modern incision happened from 2.5 Ma was resulted from the start of Northern Hemisphere glaciation.

1.3.5 Summary and Conclusion

Fluvial systems are regarded as a critical tool on geological study as the characteristics of fluvial sediments can reflect the influences of tectonic and climatic processes. To assess the reason of large pebbles near the North Platte River, which are found more than 1400 km away from the sources of the Rockies. A hypothesis was proposed that these pebbles were recycled paleosediments. There are three main steps to test this hypothesis:

(1) Grain sizes analysis

In chapter 2, downstream fining curves were generated, and similarity analysis were done. These tools were used to find the signals of abnormal grain sizes changes, which can be regarded as the signals of probable lateral sediment inputs. The existence of lateral sediment inputs can support the happening of recycling in the Great Plains.

(2) Cosmogenic nuclides analysis

In chapter 3, two models were built to estimate the maximum concentration of cosmogenic ^{21}Ne accumulated from the source to the target location. This is used to explore the influences of recycling process on the fluvial sediments. Also, the age of the oldest paleosediments the modern recycling can affect was estimated based on the result of cosmogenic Ne/Be analysis.

(3) Numerical models

In my study, the result of cosmogenic nuclide analysis introduced an interesting conflict that the cosmogenic ^{21}Ne concentrations contained within the samples collected from the upstream are higher than those from the downstream. To resolve this conflict, in chapter 4, models were built to test the influences of the cosmogenic ^{21}Ne accumulated during recycling. Several geological parameters were evaluated in these models. In addition, this chapter provides a test to assess the impact of introducing recycling on the previous grain-based geological studies.

Chapter 2

Grain Size Analysis

2.1 Introduction

From the geological perspective, the fluvial system is the most important mechanism through which sediments were eroded and transported from the source to the basin. Because the variation in the accumulation and movement of fluvial sediments across space and time is dependent on many external mechanisms, it can be inferred that the characteristics of fluvial successions, grain sizes and texture for example, represent a time-integrated "record" of changing sedimentological processes through time (Hovius and Leeder, 1998; Whittaker et al., 2011). Therefore, it is possible to reconstruct the tectonic and climatic characteristics at the time of deposition by decoding this "record" (Densmore et al., 2007; Whittaker et al., 2010). Characteristics of grains, which formed the fluvial successions, are one of the critical chapters of this "record". Many studies have been done to assess the sedimentary signals contained within the grains (Heller and Paola, 1992; Paola et al., 1992). One vital part of these signals is the distribution of grain size along the river. However, on this topic, the detailed mechanisms that control the transfer of sediments at the Earth's surface to the geological record remains a crucial challenge, because this kind of information cannot be measured directly from sediments (Allen, 2008; Duller et al., 2010; Whittaker et al., 2011).

As shown in Figure 2.1, for the change of grain sizes along the channel, a common observation is the tendency of fining downstream (Heller and Paola, 1992; Paola et al., 1992; Fedele and Paola, 2007; Moussavi-Harami et al., 2004; Frings, 2008). After years of study, it is widely agreed that the downstream fining is produced by two natural processes: selective deposition and abrasion. The selective deposition is a mechanism that can be regarded as a differential transport of grains as a function of grain size (Paola et al., 1992; Ferguson et al., 1996; Paola, 2000; Fedele and Paola, 2007). Abrasion is a process in which large grains are broken

into smaller ones because of fracturing and friction. Many studies have shown that the long-term state of grain-sizes fining is controlled by: (1) the amount and characteristics of the sediment supply; (2) the accommodation which is affected by the distribution of subsidence rate; (3) the influences in the transport and deposition of the sediments (Heller and Paola, 1992; Allen, 2008; Duller et al., 2010; Whittaker et al., 2010).

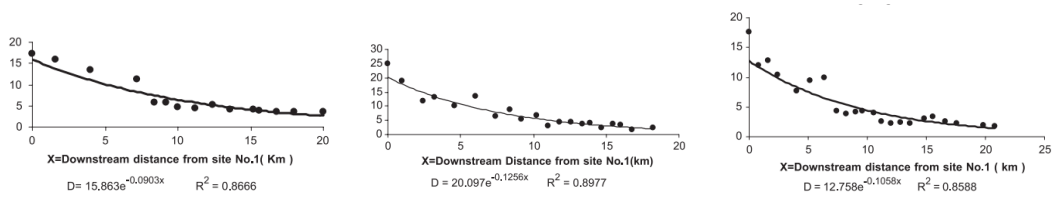

(a) Mayan River (b) Dehbar River (c) Jaghargh River

Figure 2.1: Typical downstream changes in the median diameter in the riverbed material in some rivers (Moussavi-Harami et al., 2004)

The typical downstream fining trend can be characterised using an exponential function as below (Heller and Paola, 1992; Paola et al., 1992; Fedele and Paola, 2007; Whittaker et al., 2011):

$$D_x = D_0 e^{(-ax)} \tag{2.1}$$

Where D_0 is the grain size at the start point (flowing distance = 0), a is the fining exponent, and x is the flowing distance from the start point.

Previous studies suggested it often takes tens of kilometres for a reduction in grain size of one phi (–phi scale, grain size in mm can be transformed into –phi scale using 2^{-phi}). In gravel rivers, a considerable amount of literature has found that there exists a place or an area where the gravel bedload could change into sandy bedload, which is called gravel-sand transition, or gravel front (Sambrook Smith and Ferguson, 1995; Parker and Cui, 1998). The locations of these gravel front are often kilometres to hundreds of kilometres from the sources (Table 1.1).

Sambrook and Ferguson (1995) proposed three causes for the occurrence of the transition: changes in local base-level, lateral input with different grain sizes, and abrasion. They also highlighted that the gravel-sand transition always occurs within a short distance. Moreover, as suggested by their study, the sand and gravel represent different depositional trends. They also pointed out that the gravel-sand transitions occur in more environments and channel types than were suspected in many previous studies.

Parker and Cui (1998) developed a model to test the controls of abrasion and basin subsidence on the location of gravel-sand transitions. In this paper, they

proposed three primary causes of the gravel-sand transition: (1) the abrasion would accelerate the breaking of gravels, thus accelerate the occurrence of gravel-sand transitions; (2) the decrease of water power, at some points the amount of transported gravels would drop to zero, resulting in the occurrence of gravel-sand transitions; (3) the maximum of the transport capacity, at some point the sand transport reaches the maximum capacity thus leads to the occurrence of gravel-sand transitions. It is highlighted in their study that the 3^{rd} mechanism could always be observed if the input rate of sand was raised to a certain level.

In a later paper, Cui and Parker (1998) developed a numerical model to extend their previous theory (Parker and Cui, 1998). This model was revised from an earlier model developed by Paola et al. (1992), taking into consideration the selection process as well as the abrasion. They pointed out that in the three mechanisms they proposed before (Parker and Cui, 1998), only two of them are essential. Those are the breaking of gravels resulted from the abrasion, and the reaching of the maximum transport capacity by sands. They also concluded that in the case of abrasion-induced mechanism, discontinuities could be observed in the channel bed and the water surface in the gravel-sand transitions; whereas these discontinuities can not be observed in the case of capacity-induced mechanism.

However, a simple downstream fining mode may not explain every situation. In many rivers, especially some large-scale channel systems with considerable flowing distances, patterns of the change of grain sizes downstream are more complicated (Rice and Church, 1998; Rice, 1998; Surian, 2002). Due to this complexity, the importance of tributaries on modifying grain size fining rates is widely recognised (Knighton, 1980; Dawson, 1988). Various studies, guided by the milestone set by Miller (1958), have recognised abnormal changes in grain size happened under the influences of tributary (Church and Kellerhals, 1978).

In 1998, Rice and Michael (1998) introduced the concept of “sedimentary links” (Figure 2.2). In the grain size data, there exist some downstream increases in grain size that can be explained by lateral sediment input found nearby. And the area between two adjacent increases in grain size was named ”sedimentary link”. Within each sedimentary link, a normal downstream fining trend can be observed. They also pointed out that even these finning trends within the sediment links represent different strength, these variable trends are insufficient to redefine the fining trend throughout the whole mainstream. For example, in Figure 2.2, some normal downstream fining trends can be observed within these sedimentary links (shown as solid lines), but the main stream still represent a overall trend of downstream fining. Rice (1998) also pointed out that not all tributaries can change the grain size distribution in the mainstream, and it is needed to classify the tributaries based on their influences on the mainstream.

Most previous studies on the downstream change in grain size concentrated on two

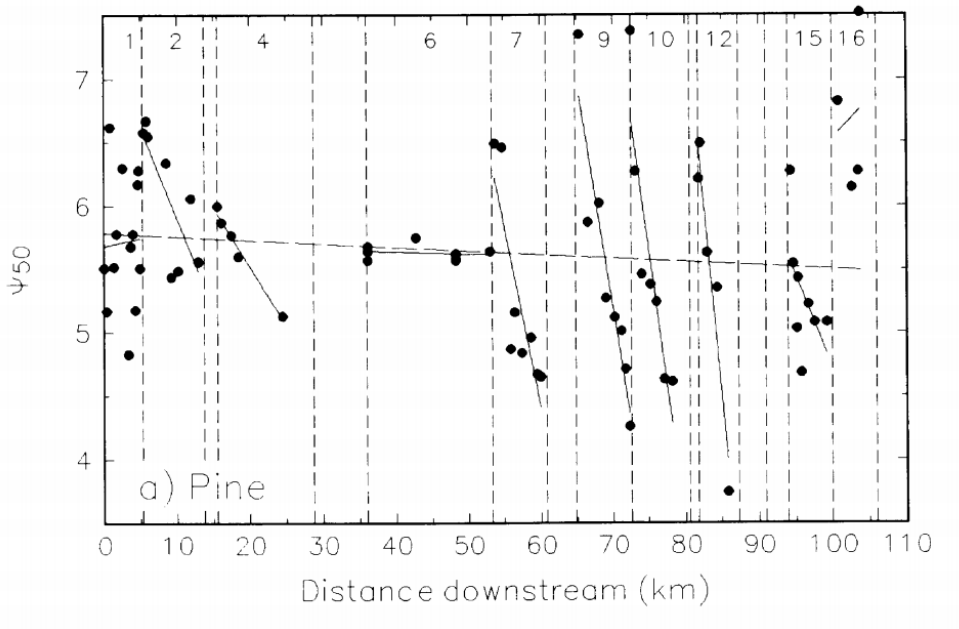

Figure 2.2: A schematic representation showing the downstream increases in grain size, the long dash line represents the exponential regression models fitted to the entire Ψ50 data sets, and the solid lines represent the individual sedimentary links, discontinuities are indicated by dashed vertical lines (Rice and Church, 1998).

main problems: 1. The "sources-changes" problem: the sediments coming from lateral inputs may or may not result in the change of typical downstream fining (Church and Kellerhals, 1978; Rice and Church, 1998); 2. The "details of changes" problem: exploring the characteristics of a typical downstream fining process or an abnormal downstream fining process (Lisle et al., 1993; Robinson and Slingerland, 1998; Rice et al., 2009). However, for the detailed mechanisms that control the transfer of grains, and the quantitative detail of materials contributing to the abnormal change of grain size, the research is far from enough.

Recycling means reworking the buried paleosediments and mixing them with fresh sediments through erosion or incision (Figure 2.3). It is one of the possible processes that could mix the paleosediments with different sizes into the fresh sediments through lateral sediment inputs (Figure 2.4), leading to an increase of the grain sizes collected from the mainstream.

Because information about recycling cannot be acquired directly from the fluvial successions, it remains challenging to reconstruct or quantify recycling. As one of the external mechanisms that affect the sediments accumulation and movement, the recycling process would leave some signals on the sediments, making it possible to decode the detail of recycling by grain size analysis.

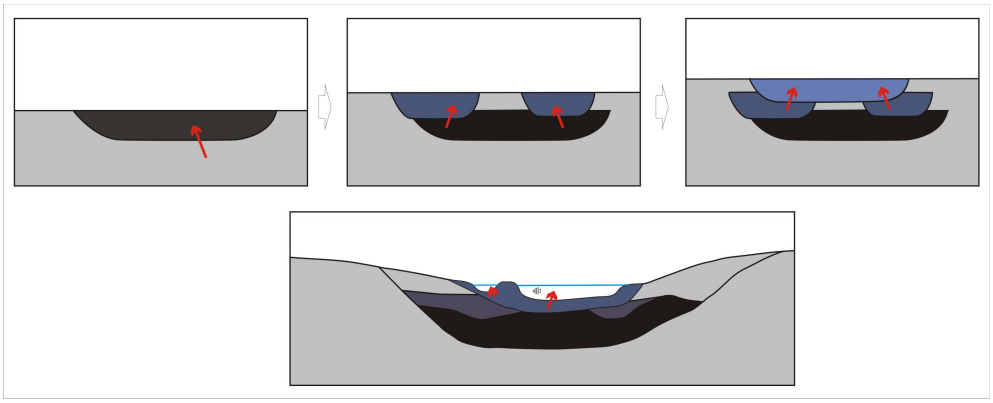

Figure 2.3: A schematic representation showing the recycling processes through incision

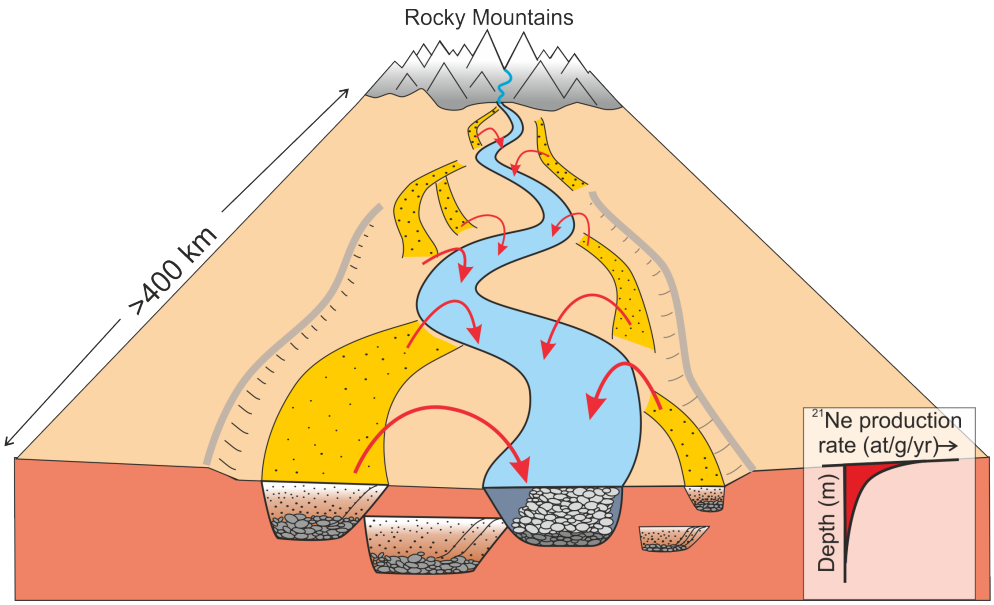

Figure 2.4: A schematic representation showing the recycling processes that could mix the paleosediments into the fresh sediments through lateral sediment inputs

2.2 Previous Work

For the Great Plain, United States, it is widely accepted that several incisions happened throughout the Tertiary to the present day. Some scholars have studied the details of the tilting of the Miocene Ogallala Group and the Pliocene Broadwater Formation (Leonard, 2002; McMillan et al., 2002; Duller et al., 2012).

One such key paper (McMillan et al., 2002) reconstructed the gradients of the paleochannels of Ogallala time. They used the equation from the study of Paola and Mohrig (1996), which describes the relationship between the grain sizes and gradients for gravelly channels, building a reliable basis for the reconstruction of the gradients of paleochannels with grain sizes. In which the shear stress required to carry the largest pebble is calculated using the shear stress on the bed at bankful stage, that's when the water is nearly over the river bank. The equation for slope reconstruction is listed as below:

$$S_{est} = AD_{50}/h \tag{2.2}$$

In which D_{50} is the value of the 50% on the grain sizes distribution, cm, which means half of the grains collected at that site are smaller than this value, h is the depth of the channel, cm, $A = 0.094$ and S_{est} is the reconstructed depositional slope.

The overestimation of the depth of the channel might result in the underestimation the gradients calculated, in contrast, the overestimation of the D_{50} would contribute to the overestimation of the gradients calculated. With an analysis on a collection of about 100 samples each at 10 different sites, the study of McMillan et al. (2002) reveals that in the Great Plains, the gradients of the paleochannels in Ogallala time decrease eastward. The change of paleoslope ranges from 2.1 to 0.8 m/km (10^{-3} to 10^{-4}). However, the eastward decrease of the present slope of the Ogallala base ranges from 10 to 2 m/km (10^{-2} to 10^{-3}), which are much larger than those of the depositional paleoslopes in Ogallala time, implying a tilting on the west. They also pointed out that the amplitude of tilting is about 680m.

Heller et al. (2003) also reconstructed the slope of Ogallala paleochannels based on Paola and Mohrig's method (see equation 5.2, where $A = 0.094$ when D_{50} is used and $A = 0.0238$ when D_{90} is used). Combining the paleoslope with the preserved isopach geometries, it is revealed that aggradation is not enough to develop a sufficient slope for these preserved gravels to be transported. Thus, a post deposition tilting must have occurred to make up the gap.

Some studies assumed that the tilting of the Ogallala strata was resulted from multi-stages of tectonic uplifts. To prove this assumption, Duller et al. (2012) reconstructed the profiles of the paleochannels of Late Miocene Ash Hollow

Formation and Remsburg Ranch beds of Pliocene Broadwater Formation, and compared them with their present-day base. It is pointed out that the timing of Miocene uplift in the Great Plains can be constrained between 6 and 3.7 Ma. And the modern incision occurred from 2.5 Ma. In this paper, the paleoslope is also calculated using the equations developed by Paola and Mohrig (1996). At that paper, the equation was built to describe the fluvial characteristics of pebbles under fully turbulent flow:

$$\tau_c = (H * S)/(\rho_x * D_{50}) \tag{2.3}$$

Where τ_c is the Shields Stress; H is the measured channel depth (cm); S is the gradients of the channel; ρ_x is a factor calculated by $(\rho_s - \rho)/\rho$, in which ρ_s represents the density of the sediments while ρ represents the density of the water. τ_c is 0.045-0.06 based on the previous studies (Paola and Mohrig, 1996; Mueller and Pitlick, 2005). D_{50} is the median grain size, the value of 50% on the grain sizes distribution curve, cm, which means half of the grains collected at that site are smaller than this value. In this equation, the local shear stress is set as 1.2–1.4 times the critical shear stress to be available for the bedload to be retained (Mueller and Pitlick, 2005). Paleoslope S is therefore calculated as:

$$S_{est} = 1.4 * \tau_c * \rho_x * D_{50}/H \tag{2.4}$$

Where $\tau_c = 0.05$, constant with previous workers and $\rho_x = 1.6$.

With all the previous studies it is clear that large scale incisions happened during late Miocene (about 6 Ma) and modern time (from 2.5 M to today). The recycling of older sediments always occurs when incisions happened (shown in Figure 2.5). Moreover, the resulted mixing of ancient and fresh sediments would increase the uncertainties of all the previous grain-size-based studies because the underlying assumption of these grain-size-based reconstructions is that the samples collected in the sediment record can reflect the hydraulic situations at the time of deposition. To solve the contradiction between recycling and grain-size-based reconstructions, exploring the details of recycling happened in the Great Plain is necessary. In the Great Plain, the incision happened in modern time (from 2.5 M to today) makes it possible for us to study recycling using modern samples.

Among the three main tools used in this study, grain size analysis, cosmogenic nuclides analysis, and numerical modelling, the grain size was used in this chapter. To answer three questions: What is the trend of the grain sizes change along the North Platte River? Where are the lateral sediment inputs? What are the effects of lateral sediment inputs on the sediments within the mainstream? Traditional grain sizes analysis and similarity analysis are employed.

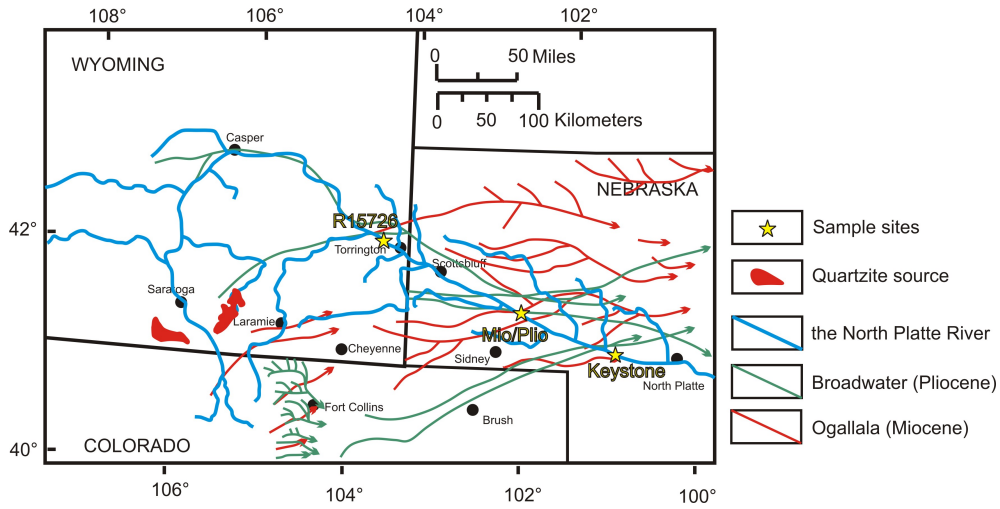

Figure 2.5: Paleochannels and modern channels of the Great Plain. The red lines represent the paleochannels of Ogallala; the green lines represent the paleochannels of Broadwater; the blue lines represent the Platte River of modern time. The arrows represent flowing direction. The red stars and yellow stars represent the localities of the sample sites (revised from (Condon, 2005)). The red areas represent the sources of quartzite pebbles in the Mountain area.

2.3 Methodology

2.3.1 Sampling Methods

Site Selection

In the fluvial system, when the water power is not sufficient to carry the sediments, sediments will deposit, which means the location of deposition depends on the grain size. This situation is easily observed in gravel-bed rivers. To study the variations in grain sizes along the channel, cares must be taken to sampling within a similar environment. In this study, all the gravel data were collected from exposed bars and close to active channels. This choice has several advantages: (1) coarse sediments are easily distinguished on the bar; (2) this place has the most extensive range of grain sizes collected; (3) this place is the closest exposed site to the channel thus has the most reliable relationship with the hydraulic mechanisms (Rice, 1998).

In order to investigate the change of grain sizes along with the $>$ 1000km North Platte River, 15 sites were chosen (shown as stars in Figure 2.6). All the samples were collected in the fall of 2016.

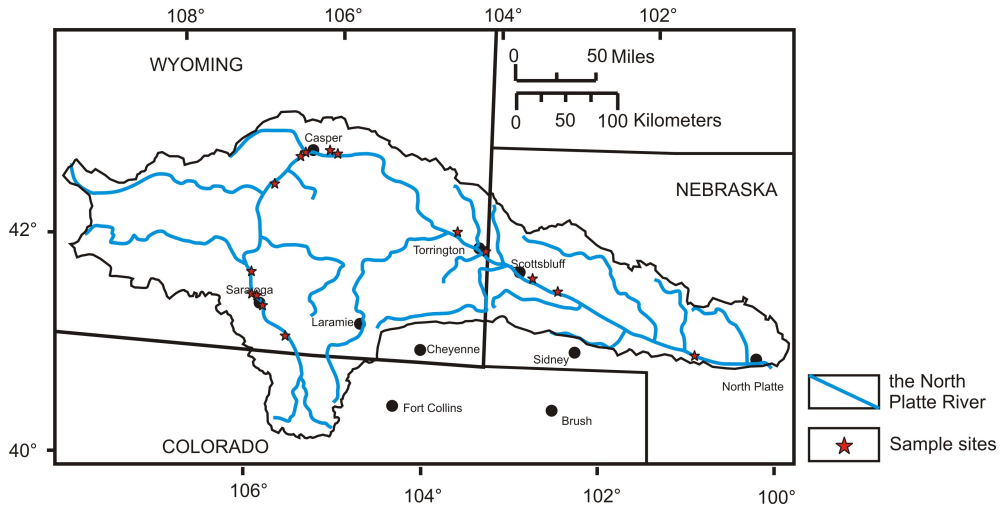

Figure 2.6: Map of the study area and the localities of 15 sampling sites along the North Platte River, USA, shown as stars.

Limitations Associated with this Site Selection

To reflect the real fluvial situation of the river, many samples should be sampled along the river. The more, the better. Also, the samples sites should be chosen with a fixed distance with each other, 50 km for example. However, in the Great Plains, some of the target sampling sites are inaccessible. In the mountain area, these sites are too remote to be accessed, while in the plain areas, some of the sites are belong to private territory which makes sampling illegal. This makes the sampling sites much less than expected. The final sampling sites are shown in Figure 2.6. As shown in this figure, sampling stars are sparse between City Saratoga and City Casper. Similar situations can also be seen between City Casper and City Torrington, and the place between City Scottsbluff and City North Platte.

Recycling processes are resulted from lateral sediment inputs, so that the places, where tributaries exist, might have more possibility to provide signals of recycling. While within the places far from the main tributaries, because of the lack of obvious external influences, the fluvial characteristics would be as normal, and the samples collected at these places might not contain enough information of recycling. As shown in Figure 2.6, most of the samples sites are near the large tributaries of the North Platte River, and most of the inaccessible places are far away from these large tributaries. So that, even the final samples sites didn't cover all the research area, the samples can also be used to do grain sizes analysis to assess the details of recycling happened in the Great Plains.

Surface Material Sampling

To minimise the time of fieldwork while make the resolution of sampling reliable, a photo-based calculation method was used (Rice and Church, 1996; Bunte and Abt, 2001; Attal et al., 2015) in this study to obtain the distribution of the grain sizes along the North Platte River.

To describe the sizes of pebbles, three axis are used: the short one (always marked as "a"), the intermediate one (always marked as "b") and the long one (always be marked as "c"). On a fluvial bar, because of the flowing, the pebbles tend to lie imbricated. This stable position would expose their surfaces which contain the long (a) axis and the intermediate (b) axis. This would, therefore, make the pictures taken perpendicular to the Earth's surface record the information of grain sizes (the a axis and the b axis). Thus, on the photos, the smallest visible axis measured can be regarded as a minimum estimate of the b axis of the pebbles (Attal et al., 2015). A scale should be clear in each photo in order to calculate the b axis of these pebbles. Following Kellerhals and Bray (1971), when measuring grain sizes, a 10*10 grid was imposed on the photos. All the visible clasts lying on each of the grid intersection were measured (shown as Figure 2.7). Clasts covering n grid intersections should be counted n times. As the limit of resolution of the photos, the smallest size that can be calculated with this method is 2 mm (Whittaker et al., 2011), but it does not affect the result because the main object of this study is the recycling of coarse sediments. For each site, D_{50} and D_{84} are estimated. The formal one is the median grain size value, which means half of the sediments collected from this site are smaller than this value, and the later is the 84 percentile grain size value, which means 84% of the sediments collected from this site are smaller than this value.

Limitations Associated with this Method

Using the grid counting method, the number of pebbles counted on the photo is about 100 and lower limit of the size that can be calculated is 2 mm. Ideally, the photos should be chosen that all the pebbles are not obscured by leaves or water, and that no more than one grid intersection falls on one pebble. However, it is impossible to meet all these conditions at all the sampling sites. Also, even at the same place, counting with different photos would provide slightly different results.

To assess the uncertainty resulting from the influence of different photos chosen, two different gravel bars were chosen, one is from the upstream and the other is from the downstream (Figure 2.8), and multiple pictures were taken for each bar. Grain sizes were calculated and the result is shown in Table 2.1. In this table, U1, U2 and U3 are three different photos taken on the upstream bar, while D1, D2 and D3 are those taken on the downstream bar.

As suggested by Table 2.1, for the upstream point, the uncertainty of D_{50} is

Figure 2.7: An example showing the photographic counting technique, the red grid is imposed on the photo, the black solid line represents one marked intermediate axis of a pebble.

11.4%, higher than that of 3.3% for D_{84}; while for the downstream point, the uncertainty of D_{84} is 10.6%, which is higher than that of 2.2% for D_{50}. This situation might result from the different grain size distributions within these two localities. For the upstream area, there is a much larger potion of large pebbles than that of the downstream area. Therefore, for the upstream area, because of the lack of smaller pebbles, a slight change in the amount of smaller pebbles in different photos would affect the calculated D_{50} significantly. In contrast, for the downstream, the lack of larger pebbles would make the calculated D_{84} more sensitive than calculated D_{50}.

Another uncertainty comes from the grid counting method itself. For the calculation of grain sizes for pebbles, Church (1987) suggested the largest grains in a sample should not occupy more than 5% of the total mass of the sample. This is because that if the total amount of the largest grains is low, the adding or reducing of one largest grain would affect the portion of the coarse component, thus distorting the distribution of the grain sizes. In the grid counting method, the largest pebbles always cover multiple grid intersections, and this grain should be counted several times. Bunte and Abt (2001) pointed out that this multiple counting of large pebbles would affect the calculated grain size distribution and make the whole distribution curve migrate to the coarse part. That is to say, the multiple counting would make the estimated value of D_{84} higher than the real value, whereas haven't obvious effect on the estimation of D_{50}. To assess the

(a) the upstream-point

(b) the downstream-point

Figure 2.8: Photos of the two localities chosen to do uncertainty analysis. (a) is the upstream-point which is near Medicine Bow WY, USA, and (b) is the downstream-point which is near Keystone, NE, USA.

Table 2.1: Calculated D_{50}, D_{84} and standard deviation of two localities

	U1 (mm)	U2 (mm)	U3 (mm)	Average	standard deviation	standard deviation/Average
D50	49	48.8	59.2	52.4	6	11.40%
D84	119.6	122.5	114.7	118.9	3.4	3.30%
	D1 (mm)	D2 (mm)	D3 (mm)	Average	standard deviation	standard deviation/Average
D50	11	10.9	11.4	11.1	0.2	2.20%
D84	28.1	22.8	24.9	25.3	2.7	10.60%

uncertainty of the multiple counting method, we used a procedure introduced by Attal et.al (2015). Firstly, the largest grain was removed to count the value of D_{50} and D_{84}, considering that the largest one not been sampled, this step is to calculate the minimum value of D_{50} and D_{84}. Secondly, an extra grain with a same size to the actual largest grain was added to the original data to estimate the value of D_{50} and D_{84}, the number of this added large clast was set as the same as that of the actual largest clast, this step is to calculate the maximum value of D_{50} and D_{84}. This procedure gives a rough estimate of the uncertainty of grid counting method (Attal et al., 2015). The result is shown in Table 2.2, which is also used to generate the error bars in the grain size data next. As suggested by the result, the uncertainties of D_{84} of these sampling sites are more significant than those of D_{50}, which meets the similar results of previous studies (Bunte and Abt, 2001; Attal et al., 2015).

2.3.2 Result of Grain Sizes Data

During the fieldwork in the Great Plain, the erosion of newer channels on the paleosediments can easily be observed (Figure 2.9), the sediments eroded were carried into the newer channels and moved away. This can be regarded as the qualitative evidence of the recycling process. Gaining quantitative information on this dynamics of sediments is more difficult because it is impossible to collect all the sediments and get clear the depositional detail of every pebble. However, it is possible to reconstruct the changes of depositional pebbles under the influence of recycling, based on the real data collected, without incorporating details of recycling on each pebble through time (Whittaker et al., 2011).

Between-site variations of grain sizes were assessed for all the 15 sites along the North Plate River (shown in Figure 2.10). It should be mentioned here that to make a large range of grain sizes to be equally visible in the figure, the grain size is expressed using –phi scale. Grain size in mm can be transformed into –phi scale using 2^{-phi}.

Table 2.2: Result of the uncertainty analysis for the grid counting method

size photo	D50(mm)-(cm)	+(cm)	-(%)	+(%)	D84(mm)-(cm)	+(cm)	-(%)	+(%)
1076	16.8	0.4	0.3	2.40%	1.60%	50.4	2.8	2.7	5.60%	5.40%
1172/1194	12.7	0.3	0.1	2.30%	0.70%	39.9	4.2	5.2	10.50%	13.10%
1235	12.1	0.8	0.4	6.70%	3.00%	46.4	3.4	4.3	7.40%	9.20%
1254	16.6	0.8	0.6	4.60%	3.80%	37.8	2.3	3.2	6.20%	8.40%
1266	11.1	0.4	0.2	3.60%	1.90%	30.1	1.7	1.8	5.80%	5.90%
1291	9.3	0.2	0	2.00%	0.00%	19.3	1.7	0	8.80%	0.00%
1308	10.8	0.1	0	1.00%	0.30%	25.6	2.8	1.1	11.00%	4.20%
1316	14.4	0.3	0.3	2.30%	2.40%	26.6	0.8	0.6	3.00%	2.30%
1366	11.6	0.3	0.2	2.60%	1.60%	21.6	0.5	0.4	2.40%	1.80%
1380	8.7	0.1	0.1	1.20%	0.70%	17.9	0.2	0.7	1.00%	4.20%
1526/1841	11	0.1	0.1	0.70%	0.70%	25.7	0.5	0.8	2.00%	3.30%
1854	18	0.1	0	0.80%	0.10%	28.7	0.1	0.3	0.20%	1.00%
1797	11.3	0.2	0.1	1.60%	1.20%	19.9	0.5	0.4	2.40%	1.80%
14	7.7	0.2	0	2.10%	0.30%	17	0.8	0.9	4.50%	5.10%
1691	12.5	0.1	0.1	0.90%	0.90%	26	0.8	0.3	3.00%	1.00%

Figure 2.9: A photo showing the erosion of newer rivers on the paleosediments (taken in Oct. 2016, near the North Platte River).

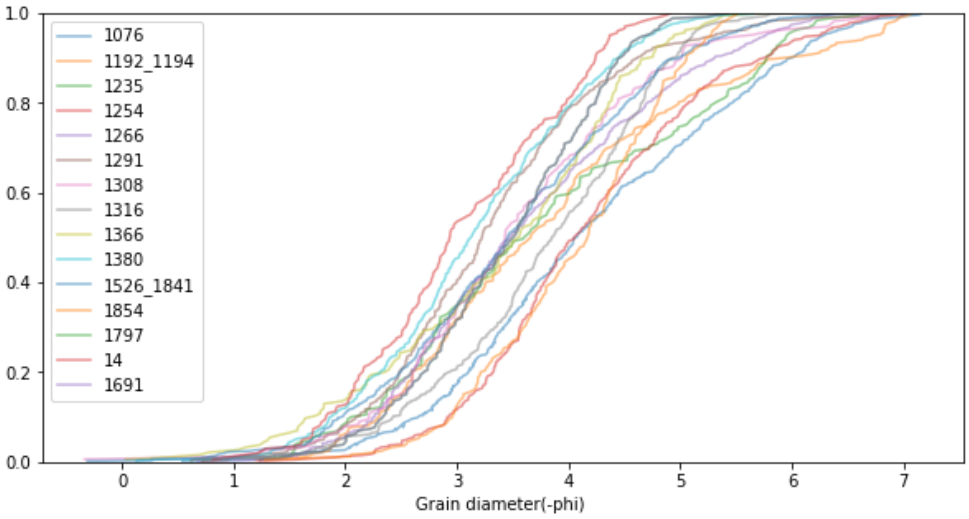

Figure 2.10: Grain sizes distribution curves within all the fifteen sample sites.

As suggested by Figure 2.10, the distributions of grain sizes within all the sample sites meet the typical distribution of river sediments, but they have different ranges from each other.

D_{50} and D_{84} within each site can then be acquired using these grain size distribution curves. The representative values of D_{50} and D_{84} along the river are shown in Figure 2.11 (blue points for D_{50} and orange points for D_{84}). The North Platte River has many sources, so that the distance of any locality along the river would be variable with different source as the start point. To make the quantification of flowing distances along the North Platte River precisely and conveniently, a distance system was developed in this study using the border of Wyoming and Nebraska as the zero point as it is easy to be recognised on the map.

2.4 Grain Sizes Analysis

2.4.1 Basic Analysis

The change of drainage area along the North Platte River and the river profile were extracted using LSDtopo Tools. And these two were put together with the data of grain sizes (shown in Figure 2.12). Each abrupt increase in the value of the drainage area stands for the adding of a new sub-catchment area, representing a tributary nearby. The higher the increase in the drainage area, the larger the catchment area of the tributary. Assuming a constant erosion rate throughout the Great Plain, the larger the catchment area, the more the sediments carried with the tributary into the mainstream.

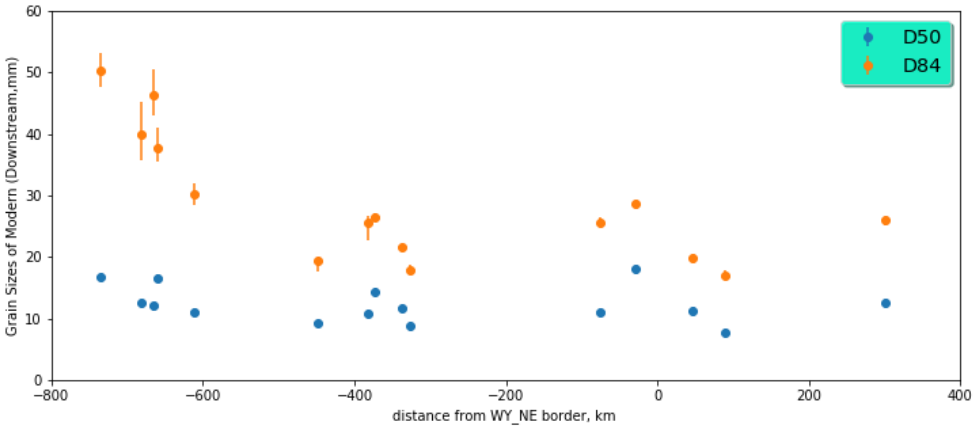

Figure 2.11: Grain sizes data (D_{50} and D_{84}) within each sample site, shown against the distance from the WY-NE border.

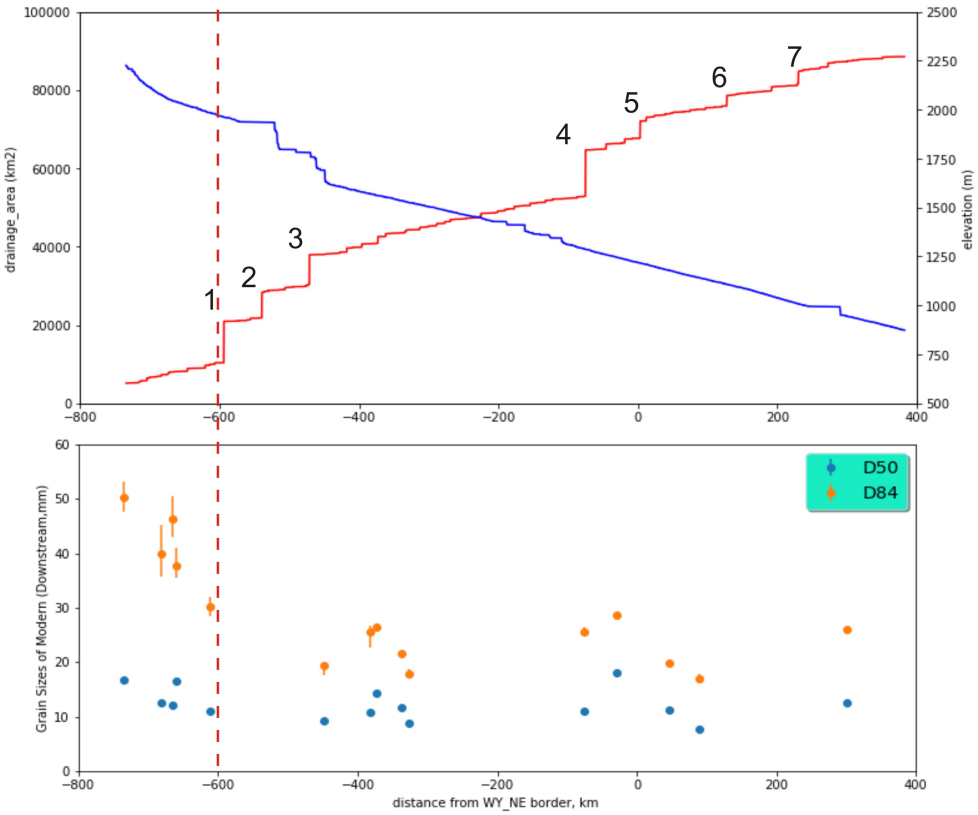

Figure 2.12: A schematic representation showing the longitudinal locations of tributaries and abnormal grain sizes increase. The blue curve is the profile of the North Platte River and the red curve represents the change of drainage area along the North Platte River. There are seven noticeable increases in the drainage area, marked using 1 to 7. The dashed line represents the place where the tributaries start to influence the mainstream of the North Platte River.

There are seven noticeable increases in the drainage area, also tributaries, along the North Platte River, which were mainly located within the area from -450 km to -600 km and the area from -100 km to 250 km). In order to express them easily in the next description, these drainage area increases (tributaries) are marked along the flowing direction, using number 1 to 7 (shown in Figure 2.12).

Firstly, a downstream grain sizes fitting was generated to simulate the natural fining of grain sizes within the mainstream of the North Platte River. This fitting should be generated based on the data without the influence of tributaries. In Figure 2.12, the dashed line represents the place where the tributaries start to influence the mainstream of the North Platte River, therefore, five points on the left of this dashed line were chosen. The downstream grain-size trends for D_{50} and D_{84} were generated using the typical downstream fining equation (Heller and Paola, 1992; Paola et al., 1992; Fedele and Paola, 2007; Whittaker et al., 2011):

$$D_x = D_0 e^{(-ax)} \tag{2.5}$$

Where D_0 is the grain size at the start point (flowing distance = 0), a is the fining exponent, and x is the flowing distance from the start point. Also, the border of Wyoming and Nebraska was used as zero point during the calculation.

The result is shown in Figure 2.13. The reconstructed downstream changes in grain sizes and the real data were put together in Figure 2.14.

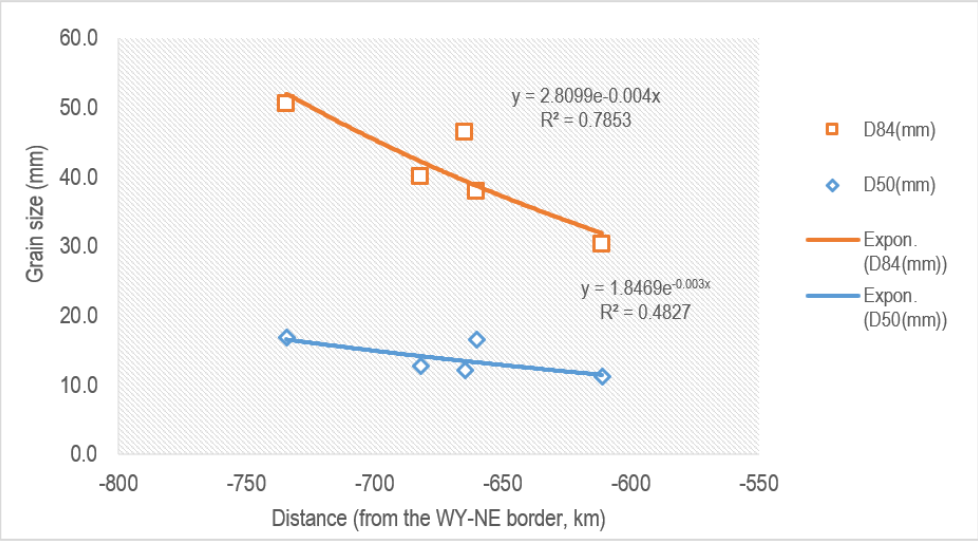

Figure 2.13: The grain sizes fitting using the data without the influences of tributaries.

As suggested by Figure 2.14, except for the points located near -450 km, all the downstream points after -400 km are plotted far above the reconstructed

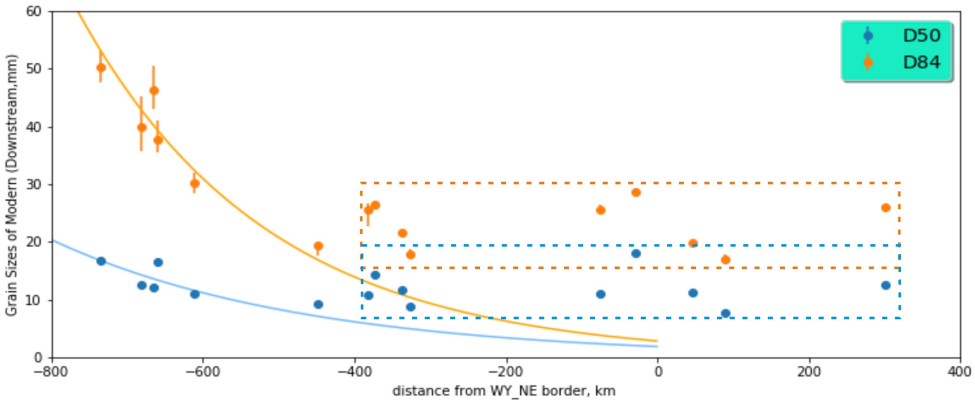

Figure 2.14: The comparison between the reconstructed grain sizes (without tributaries) and the real grain sizes.

downstream fining curve. These points were shown within the boxes in Figure 2.14 (blue one for the D_{50} and orange one for the D_{84}). As described above, this reconstructed downstream fining curve can reflect the natural downstream fining within the mainstream without the influence of the tributaries, thus, it can be presumed that near point -400 km, sediments sourced from lateral input considerably change the grain size distribution of the sediments in the mainstream.

Moreover, to answer the question that if there exists some other lateral sediment inputs far downstream after -400 km, a grain size fitting can also be generated using the points after -400 km, the result is showed in Figure 2.15. As suggested by this figure, the downstream change in grain size is nearly flat within a flowing distance of about 800 km (-400 km to 400 km). If there was no influence of lateral sediment input after -400 km, this abnormal flat of grain sizes means that the hydraulic condition in the mainstream remains the same within such a long distance of 800 km. This is impossible in reality. Therefore, it can be reliably presumed that after -400 km, some other lateral sediment inputs existed and distorted the grain size distribution in the mainstream.

To conclude, it can be presumed that a lateral sediment input existed near -400 km, and some more lateral sediment inputs existed after -400 km.

2.4.2 Similarity Variable

For a row of collapsing data, when it is subject to a stable external changing process, the distribution of this data would change following a statistical rule. That is to say, when the initial distribution of the data and the external changing process are set up, the distribution of this data at any time is dependent only on the time chosen and can be calculated based on the statistical scale effect. Similarity approaches are a way of statistical analysis by removing the statistical

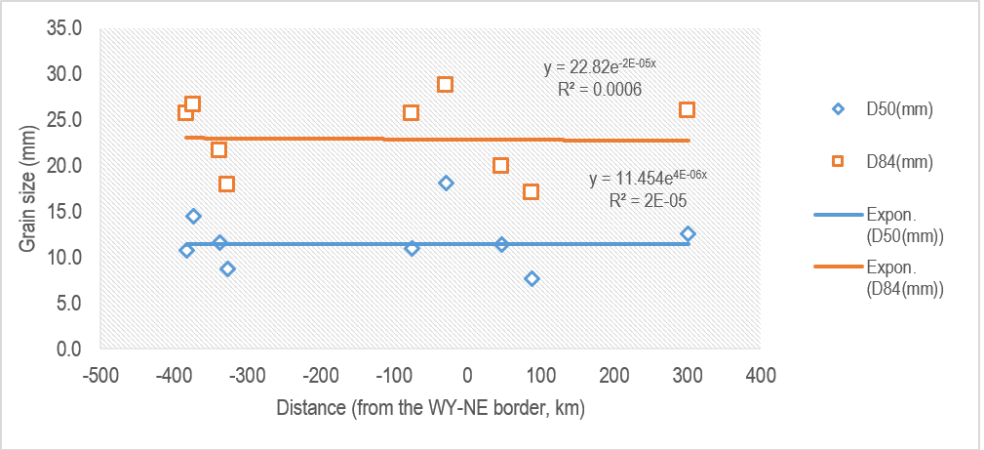

Figure 2.15: The comparison between the fitted downstream fining curve and the data from collected samples.

scale effect. When it is suspected there exists inner connection within a row of collapsing data and these data are only affected by stable external influences, similarity approaches would be used. After removing the scale effect, if there existed inner connection within these collapsing data, the similarity-processed data would represent similar statistical characteristics.

As suggested by the study of Heller (1992), if the river profile and the initial distribution of the grain sizes were set, and there were no other external influences on these sediments, there is a tendency for the distribution of the grain sizes to simply elongate along the river downstream. Based on this conclusion, the study of Fedele and Paola (2007) yielded simplified similarity solutions for the gravel channels under steady-state conditions. In this solution, the distributions of the grain sizes at any location along the channel can be transformed into a uniform shape, regarding the local mean and standard deviation of grain sizes as the local scales to be removed. In that paper, they defined a similarity variable which is called ξ, as

$$\xi = (D - \overline{D}(x_*))/(\phi(x_*)) \tag{2.6}$$

Where x is the flowing distance of one location along the channel, D is the grain size data collected at that location, $\overline{D}(x_*)$ and $\phi(x_*)$ are the local mean and standard deviation at that location, x_* is longitudinal location which is calculated by $x_* = x/L$, and L is the total length of the whole fluvial system. As suggested by the study of Fedele and Paola (2007), for gravel channels, the distribution curves of grain sizes at any locations along the channel represent a same shape when these data were scaled using the similarity variables ξ.

For the data collected along the North Platte River, the similarity variable ξ were

plotted against the frequency density of grain sizes for all the sample-sites, the result is shown in Figure 2.16. In the figure, an internal differentiation can be obviously seen within these sample sites, with a dispersed range of 0.15-0.4 of frequency density.

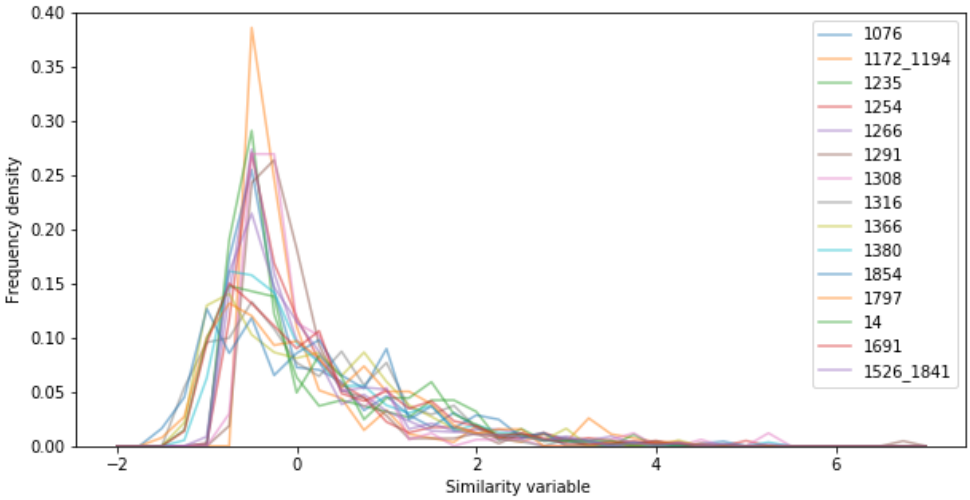

Figure 2.16: Plots showing the self-similar grain size distributions of all the 15 sample-sites.

To classify these confusing curves, another parameter is needed. Fedele and Paola (2007) set the coefficient of variation in Equation 2.7 as C_v, and they found that within one stable fluvial system, this coefficient remains approximately constant in the similarity analysis. This provides a method to classify these grain size data collected from different sample sites.

The way to calculate this coefficient is shown as below:

$$C_v = \frac{\mathrm{d}\phi}{\mathrm{d}x_*} / \frac{\mathrm{d}\overline{D}}{\mathrm{d}x_*} = const. = A \tag{2.7}$$

$$\frac{\mathrm{d}\phi}{\mathrm{d}x_*} = A\frac{\mathrm{d}\overline{D}}{\mathrm{d}x_*} \tag{2.8}$$

$$\int \frac{\mathrm{d}\phi}{\mathrm{d}x_*} = A\int \frac{\mathrm{d}\overline{D}}{\mathrm{d}x_*} \tag{2.9}$$

$$\phi = A\overline{D} \tag{2.10}$$

$$A = \frac{\phi}{\overline{D}} \tag{2.11}$$

And the result of C_v calculated for each sampling site is shown in Table 2.3. The result is also shown against the distance in Figure 2.17.

Table 2.3: Coefficient of variation C_v of all the sample-sites, the data is listed along the flowing direction of the North Platte River. The sample sites with values higher than 0.8 and lower than 0.7 were coloured with red and blue, respectively

	average	standard deviation	distance(border)	Cv	x*
1076	27.05216	25.33401	-734.334	0.936488	0.06925
1172/1194	24.13781	29.38222	-681.784	1.217269	0.113042
1235	21.75659	21.02477	-664.734	0.966363	0.12725
1254	24.39449	21.71096	-660.034	0.889994	0.131167
1266	17.45004	16.16181	-611.114	0.926176	0.171933
1291	13.5094	14.58739	-448.504	1.079796	0.307442
1308	16.69365	18.17192	-382.724	1.088553	0.362258
1316	16.75487	10.20629	-373.994	0.609153	0.369533
1366	13.6142	9.450718	-338.084	0.694181	0.399458
1380	11.08938	7.741885	-327.184	0.698135	0.408542
1526/1841	15.33525	13.65771	-76.174	0.890609	0.617717
1854	19.081	9.939487	-28.524	0.52091	0.657425
1797	12.699	7.145562	46.986	0.562687	0.72035
14	9.9	6.128265	88.646	0.619017	0.755067
1691	15.244	10.64412	300.878	0.69825	0.698945

In Table 2.3, the sample sites with values higher than 0.8 and lower than 0.7 were coloured with red and blue, respectively. As suggested by Table 2.3 and Figure 2.17, all these 15 sample sites can be divided into two groups: the sharp group and flat group.

For the samples within the sharp group, the average C_v is 1.01, which matches the maximum C_v suggested by Fedele and Paola (2007): $0.7 < C_v < 1$.

For the samples within the flat group, the average C_v is 0.66, which matches the minimum C_v in the paper of Fedele and Paola (2007). It should be noted that at point 1526/1841, the value is 0.89, which is higher than the average level of the other downstream points. This suggests that some lateral sediment input might exist near this point.

Based on the division using C_v, the similarity curves can then be divided into two groups, shown as Figure 2.18 and Figure 2.19. In Figure 2.18, the curves in the sharp group represents a similar trend with a similar maximum frequency density of about 0.3. For the flat group (Figure 2.19), all the curves also represent a similar shape, and the maximum frequency density is 0.15. It should be mentioned here that the similarity distribution curve of 1526/1841 is removed in Figure 2.19.

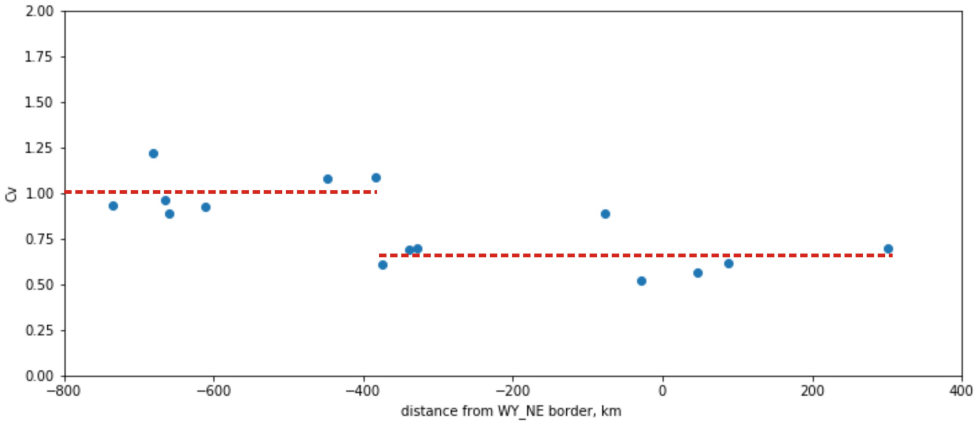

Figure 2.17: Plots showing the C_v against the distance.

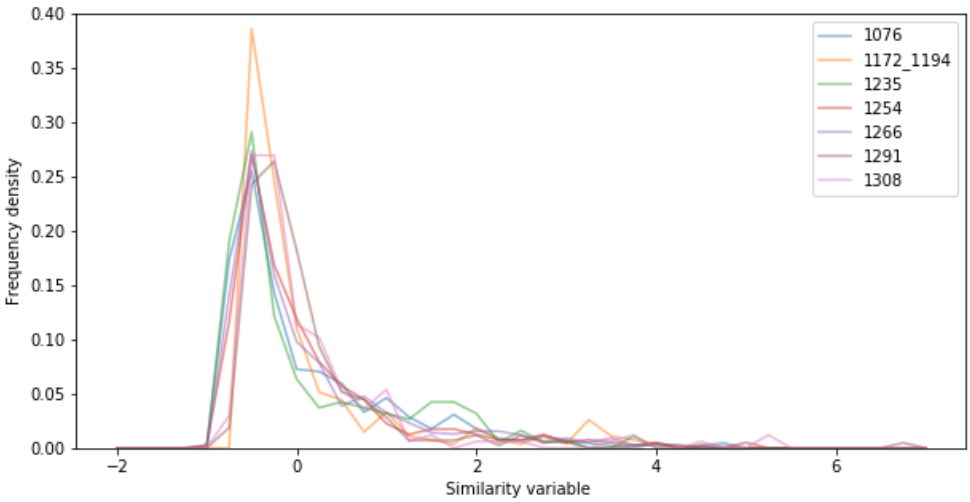

Figure 2.18: Plots showing the self-similar grain size distributions of the upstream group. With the maximum frequency density of about 0.3.

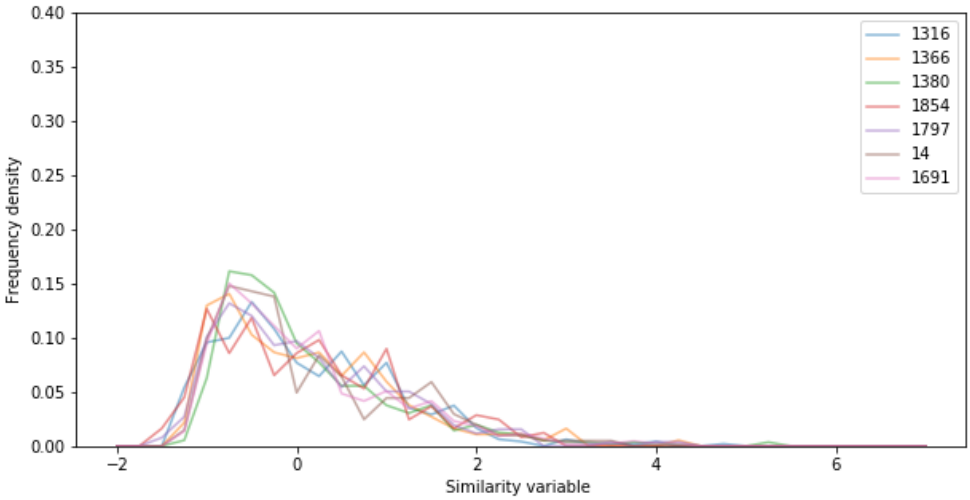

Figure 2.19: Plots showing the self-similar grain size distributions of the downstream group (without 1526/1841). With the maximum frequency density of about 0.15.

This result suggests that the portions of the grains with different sizes changed significantly from the sharp group to the flat group. As the distributions of grain sizes along the channel would remain similar without any lateral influences, the apparent change in the distribution of grain sizes can be explained as the effect of lateral sediment inputs. The boundary between the sharp group and the flat group is located near -380 km. Furthermore, the C_v changes from the level of 0.7 to the level of 0.9 near the point of 1526/1841, suggesting that another lateral sediment input exists nearby. However, more evidence is needed to support this assumption.

2.4.3 Division of the North Platte River System

The results of grain size analysis and similarity analysis are put together in Figure 2.20.

As shown in Figure 2.20, the change of C_v from the level of 1.0 to the level of 0.6 happened near -380 km, which meets the start of the deviation of the real grain size data from the reconstructed downstream fining curve. So it can be concluded that a lateral sediment input exists at this place. And the first target site called Casper was set here.

It was assumed that another lateral sediment input exists near the point of 1526/1841 because of its high C_v of 0.89 compared with the other points around it. Moreover, as suggested by the drainage area curve of Figure 2.20, a large-scale tributary is present near this point (shown as No.4). From the grain size curve, a noticeable increase in grain size can also be seen around this point. The

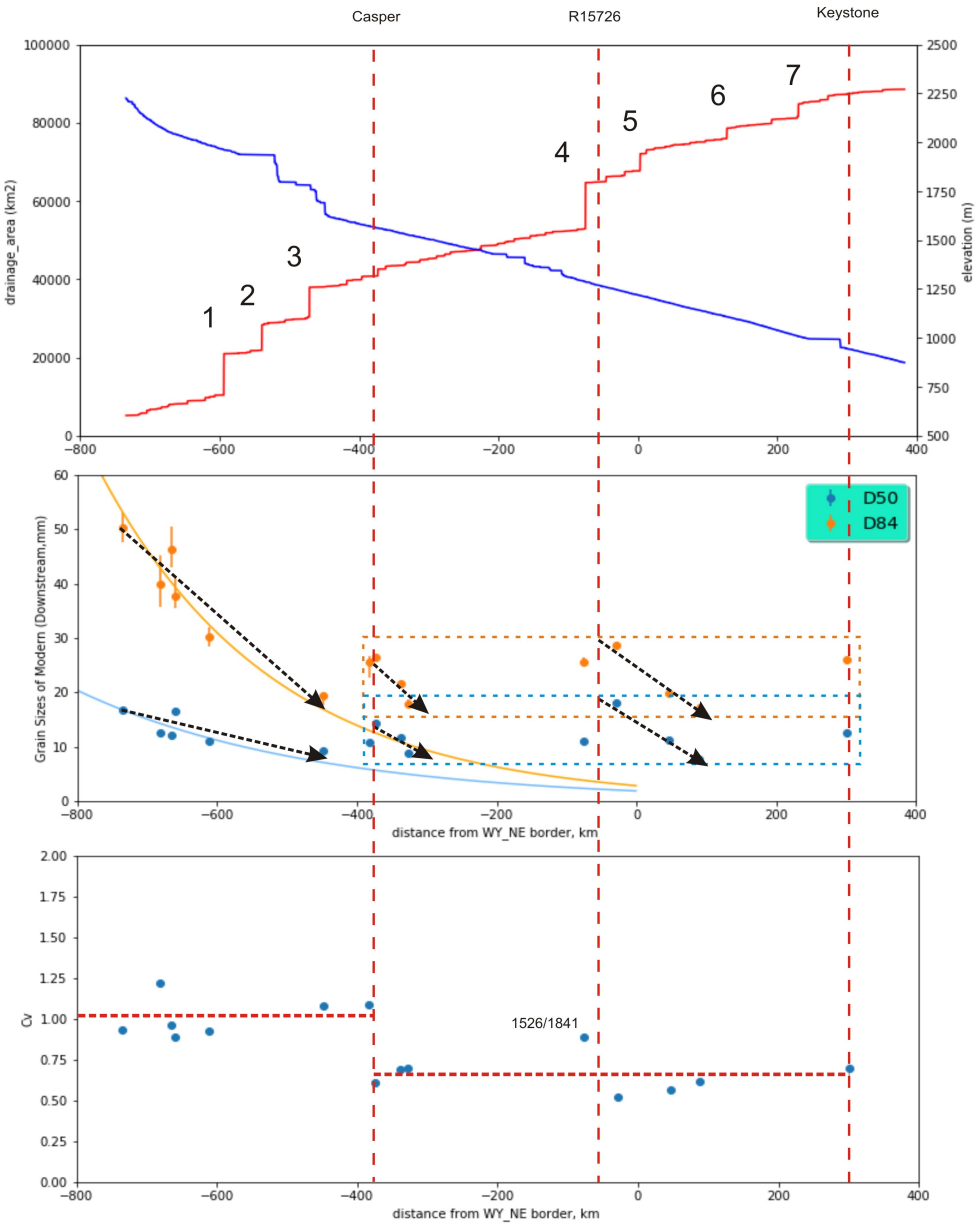

Figure 2.20: Division of the North Platte River System based on the results of the grain size analysis and the similarity analysis.

increase in grain size corresponds to the existence of large tributary provides a reliable support for the assumption that there existed a lateral sediment input near this point. To exploring the detail of grain size resulted from this lateral sediment input, the second target site was chosen as R15726, located after point 1526/1841.

The intersection between the North Platte River and the South Platte River is also the end of the North Platte River system. Keystone was chosen to represent this end. Besides, from the point in front of Keystone (100 km) to the point of Keystone (300 km), an apparent grain size increase and two tributaries (No.6 and No.7) can be recognised. These signals of the existence of tributaries and the change of grain size nearby suggest that a target site can be set here to explore the detail of recycling.

Now the whole North Platte River system is divided, by these three sites, into three main sub-areas: the up-sub-area, the mid-sub-area, and the down-sub-area. The up-sub-area is located before Casper, the mid-sub-area is the area between Casper and R15726, and the down-sub-area is the area between R15726 and Keystone. As is shown with the grain size curve, within each sub-area, the grain sizes exhibit a downstream fining trend (shown in Figure 2.20) and an abrupt downstream increase.

These three sub-areas were also shown in the map (Figure 2.21). The blue line represents the North Platte River and its main tributaries. Red stars represent points with C_v higher than 0.8, and yellow stars represent points with C_v lower than 0.7. Grey stars show the localities of sites representing the lateral sediment inputs.

2.4.4 Grain Sizes Fitting Within Each Sub-Area

As described above, the whole North Platte River system can be divided into three sub-areas: the up one, mid one and down one. Within each sub-area, the grain sizes exhibit a downstream fining trend (shown in Figure 2.22) and an abrupt grain size increase. These abrupt grain size increases represent the mixing of larger grains carried by lateral sediment inputs. However, the fluvial system between two lateral sediment inputs was not influenced by any lateral sediment inputs, and should represent a natural trend of downstream fining within the channel between these two lateral sediment inputs. Therefore, the decreasing grain size data within each sub-area can be used to reconstruct the real depositional features there. Grain size fitting was generated using these data.

Similarity, down-system grain-size trends for D_{50} and D_{84} were calculated using the equation of grain size and flowing distances, which is shown as below:

$$D_x = D_0 e^{(-ax)} \tag{2.12}$$

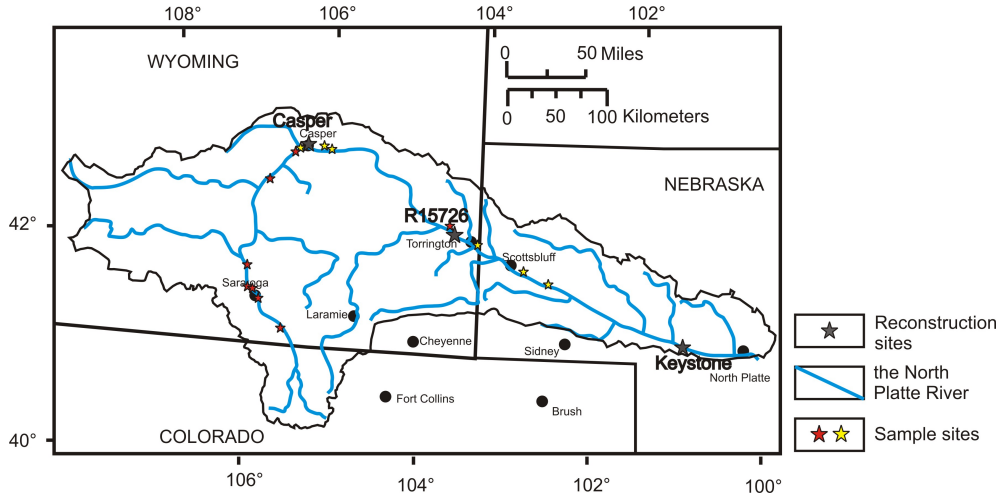

Figure 2.21: Location map, showing samples sites along the main river of the North Plate River. The blue line represents the North Platte River and its main tributaries. Red stars represent points with C_v higher than 0.8 and yellow stars represent points with C_v lower than 0.7. Grey stars represent the localities of sites representing the lateral sediment inputs.

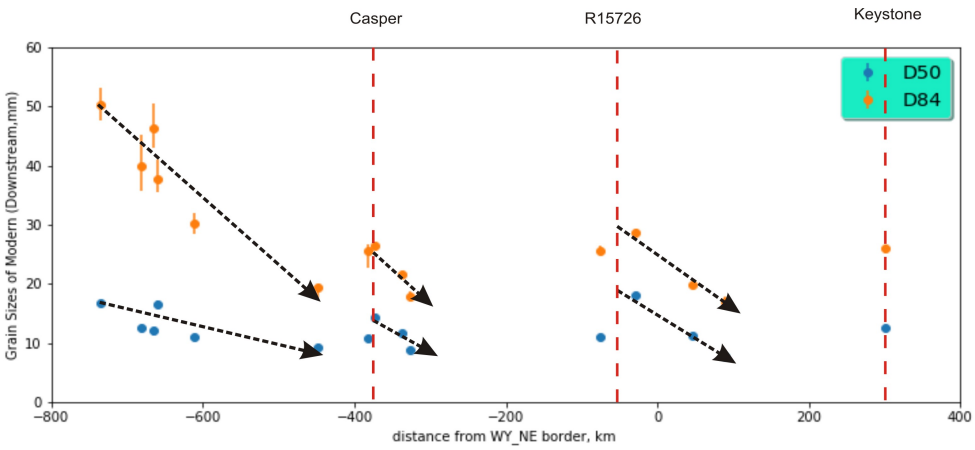

Figure 2.22: Grain size, D, against downstream distance for modern time. D_{50} and D_{84} are shown as dotted blue and orange symbols, respectively. The black dotted lines with arrows represent the downstream fining trend within each sub-area used to reconstruct the fitting curves. Vertical red dashed lines represent three localities standing for the borders of three sub-areas.

Where D_0 is the grain size at the start point (distance = 0), a is the fining exponent, and x is the flowing distance from the start point.

The exponential fitting of these three sub-areas are based on the decreasing grain sizes within each sub-area, and the results are shown in Figure 2.23, 2.24 and 2.25, and the reconstructed parameters are shown in Table 2.4.

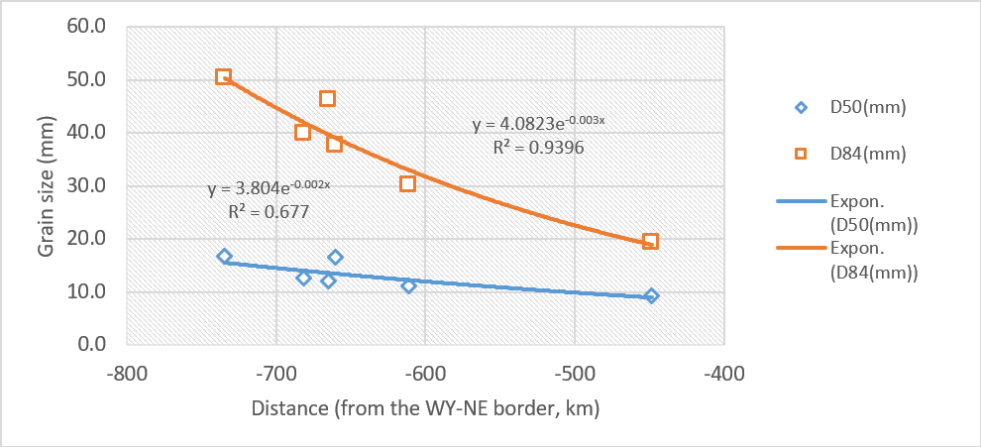

Figure 2.23: Grain size, D against downstream distance for the up-sub-area.

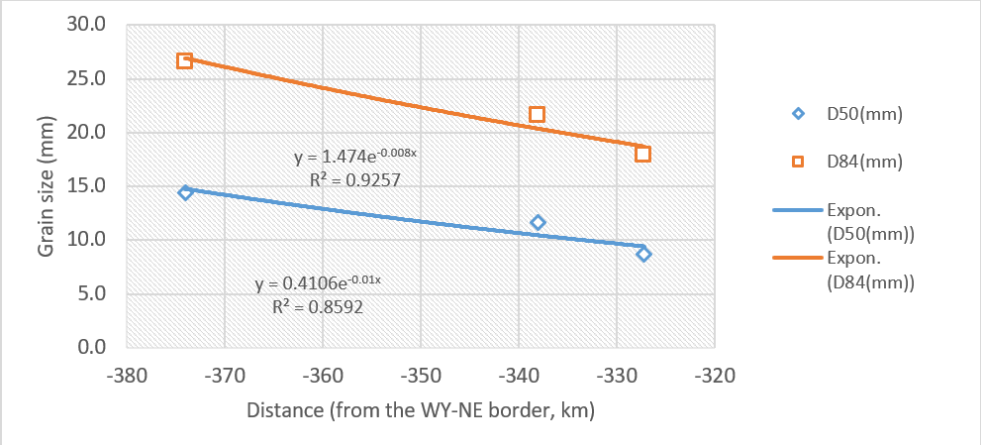

Figure 2.24: Grain size, D against downstream distance for the mid-sub-area.

As is shown in Figure 2.23, for the up sub-area, the reconstructed D_{84} decreases more rapidly than that of D_{50}, with the a of D_{84} smaller than that of D_{50} (-0.003 < -0.002), but nearly the same. Based on the parameters, the D_{50} reconstructed at the place of zero (Wyoming-Nebraska border) is 3.8 mm, and D_{84} of that point is 4.08mm. As the up sub-area is located in the upstream of zero point, these values calculated at the zero point represent the size of the grains from up sub-stream when they reach the WY-NE border.

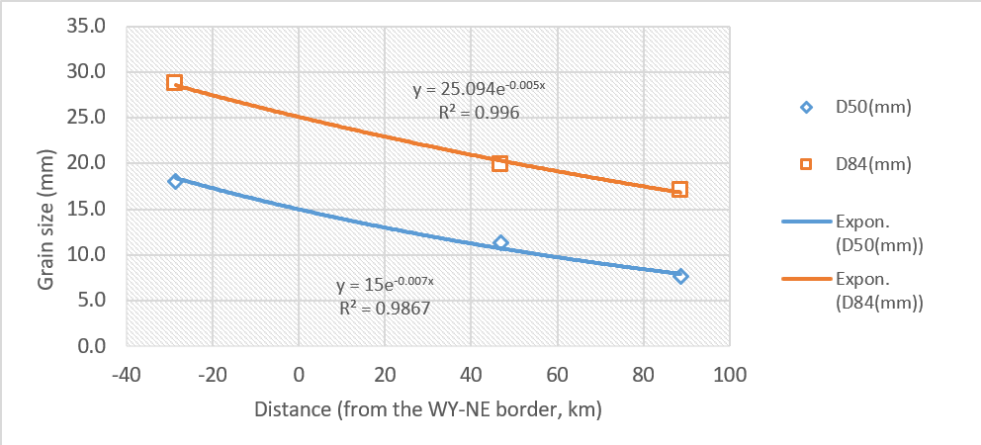

Figure 2.25: Grain size, D against downstream distance for the down-sub-area.

Table 2.4: The parameters of the grain size fitting curves for each sub-area

D50	D0(mm)	a	R2
up_D50	3.8	-0.002	0.677
up_D84	4.08	-0.003	0.9396
mid_D50	0.41	-0.01	0.8592
mid_D84	1.47	-0.008	0.9257
down_D50	15	-0.007	0.9867
down_D84	25.1	-0.005	0.996

As is shown in Figure 2.24, for the mid-sub-area, the reconstructed D_{84} decreases more slowly than that of D_{50} (-0.008 > -0.01), but they also have no discernible difference with each other. With this fitting curve, the D_{50} reconstructed at the place of zero (Wyoming-Nebraska border) is 0.41 mm and D_{84} of that point is 1.47 mm. The mid sub-area is also located in the upstream of zero point, these values calculated at the zero point represent the size of the grains from mid sub-stream when they reach the WY-NE border. It can be found that both the D_{50} and D_{84} calculated with the fitting curve of mid sub-area are less than those of the up sub-area. The sediment coming from the up sub-area can be carried to the mid sub-area, the decrease of predicted grain sizes in the zero point suggests that the downstream fining rate in the mid sub-area is higher than that of the up sub-area. This acceleration in downstream fining rate might be resulted from a weaker fluvial energy of the mid sub-area.

As is shown in Figure 2.25, for the down-sub-area, the reconstructed D_{84} and D_{50} curves also experience similar gradient, with the D_{84} curve a little bit flatter. However, the D_{50} reconstructed at the place of zero (Wyoming-Nebraska border) is 15 mm and D_{84} of that point is 25.1 mm. As the downs-sub-area is located in the downstream of zero point, these values can be regarded as the reconstructed grain sizes of the sediments carried from the zero point to this area.

2.5 The Details of the Lateral Sediment Inputs

An ideal method to explore the influences of lateral sediment inputs on the mainstream is getting details of the grain size data of all the places along the North Platte River. However, obtaining such a big dataset is impossible. Instead, to simplify this method, some representative points can be chosen.

Based on the result of grain size analysis above, three target sites were chosen to represent the localities where lateral sediment inputs exist, including Casper, R15726 and Keystone. The whole North Platte River channel system can then be divided into three sub-areas. As is shown with the grain size curve, within each sub-area, the grain sizes exhibit a downstream fining trend and an abrupt downstream increase (shown in Figure 2.22).

For any point located within the mainstream, if all the sediments from upstream were carried to this point without the influence of lateral sediment inputs on the way, the change of fluvial characteristics would follow the natural trend without interrupt. These fluvial characteristics include the similarity variable ξ and the downstream fining rate. Based on this idea, the detailed grain size distributions - without and with lateral sediment inputs (the predicted one and the real one, respectively) were reconstructed for these three sites. Moreover, the comparison between them will provide insights into the effect of lateral sediment inputs on the grain size distributions of the mainstream.

2.5.1 Casper

Casper is located on the border of up-sub-area and mid-sub-area.

If no lateral sediments inputs existed before Casper, grain size would not increase at this point, but following the downstream fining trend before Casper (as that within the up-sub-area, shown as Figure 2.23). Also, the similarity distribution of the grains in Casper would yield a similar result as that of the upstream part (shown in Figure 2.18).

$$D_{50} = 3.804 \times \ e^{(-0.002x)} \tag{2.13}$$

$$D_{84} = 4.082 \times \ e^{(-0.003x)} \tag{2.14}$$

Under the assumption of no lateral sediment sources, the D_{50} and D_{84} can be predicted using grain sizes downstream fining curve as as Equation 2.13 and 2.14.

The x of Casper is -366.5 km, meaning this point is 366.5 km eastward from the border of Wyoming and Nebraska along the river. The D_{50} calculated is 7.92 mm and D_{84} is 12.26 mm.

In order to get the no-tributary similarity distribution of the grain sizes of the Casper, we calculated the average similarity distribution of all the similarity distributions before Casper (as shown in Figure 2.26), which are all within the sharp group.

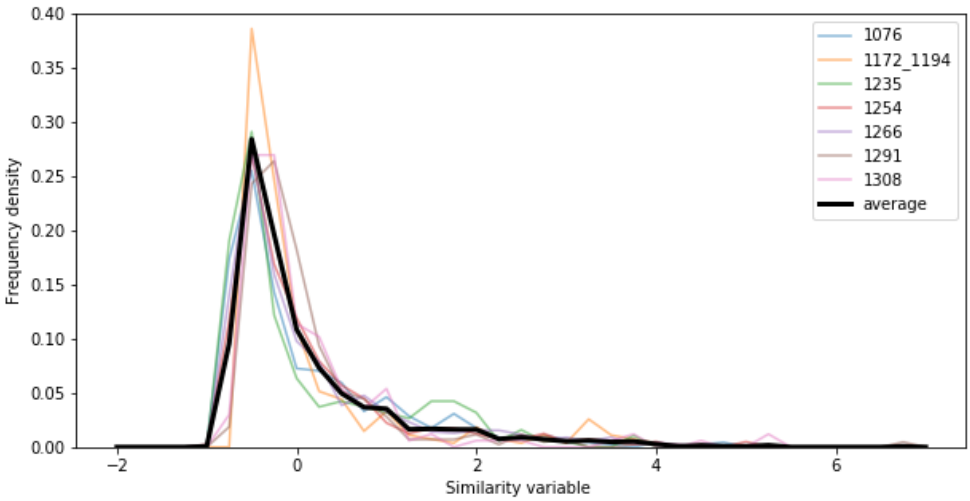

Figure 2.26: The average similarity distribution curve of all the self-similar grain size distributions before Casper (within the sharp group).

The predicted D_{50}, D_{84} can be plotted on the average curve of the frequency density accumulation against the similarity variable, which is shown in Figure

2.27. The corresponding values of the similarity variables for D_{50} and D_{84} were determined in this figure.

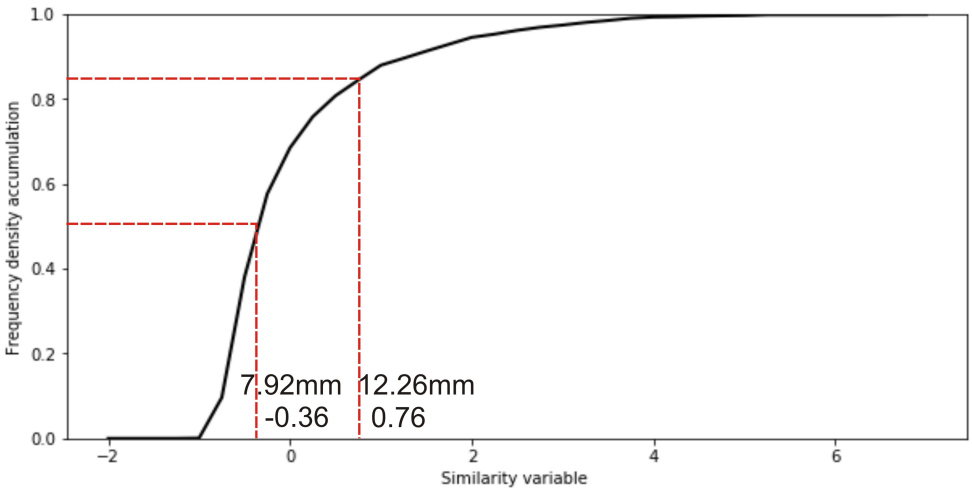

Figure 2.27: The positions of D_{50} and D_{84} on the curve of frequency density accumulation against the similarity variable (no lateral sediment input before Casper).

$$\xi = \frac{D - \bar{D}(x_*)}{\varphi(x_*)} \tag{2.15}$$

Using values from the curve in Figure 2.27 and combining them with the equation of similarity variables (2.15), some calculations can be done as below:

$$-0.36 = \frac{7.92 - \bar{D}(x_*)}{\varphi(x_*)} \tag{2.16}$$

$$0.76 = \frac{12.26 - \bar{D}(x_*)}{\varphi(x_*)} \tag{2.17}$$

Then it can be calculated that $\varphi(x_*)$=3.88 mm, $\bar{D}(x_*)$=9.32 mm.

So if no lateral sediment input existed before Casper, the parameters of grain size distribution of Casper are D_{50}=5.82mm, D_{84}= 8.50mm, $\varphi(x_*)$=3.88 mm, $\bar{D}(x_*)$=9.32 mm; using these parameters the detailed grain sizes distribution curve can be calculated, which is shown in Figure 2.28.

However, the real situation of Casper is different. As suggested by Figure 2.22, the grain size increased before Casper and then decreased after it. This increase of grain size before it is resulted from lateral sediment input, while the decrease of grain size after it represents normal fluvial process without the influences of lateral sediment input. Accordingly, the real D_{50} and D_{84} for point Casper could

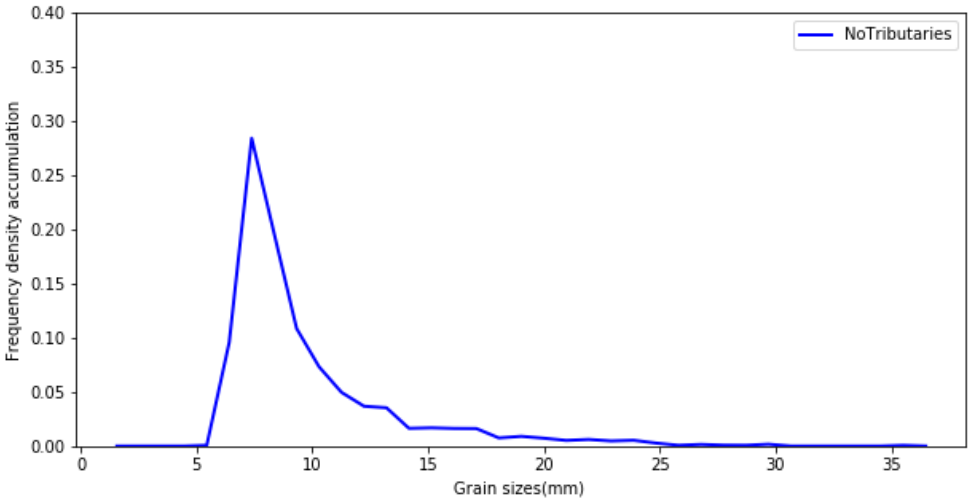

Figure 2.28: Predicted detailed grain sizes distribution in Casper (no lateral sediments input before Casper).

be reconstructed with the decreasing grain sizes data after it, by the grain sizes fitting. The calculations are shown as Equation 2.18 and 2.19.

$$D_{50} = 0.411 \times \ e^{(-0.01x)} \tag{2.18}$$

$$D_{84} = 1.474 \times \ e^{(-0.008x)} \tag{2.19}$$

Using the distance of -366.5 km, the real D_{50} can be calculated as 16.05 mm and the real D_{84} as 27.66 mm.

Also, the real similarity distribution of the sediments in Casper should follow a similar curve as those after Casper. The average curve was calculated and shown in Figure 2.29.

Similarity, D_{50} and D_{84} can be plotted on the curve of frequency density accumulation against similarity variable. The values of corresponding similarity variables for D_{50} and D_{84} can be read, and used in the following calculation (Figure 2.30).

$$-0.25 = \frac{16.05 - \bar{D}(x_*)}{\varphi(x_*)} \tag{2.20}$$

$$0.96 = \frac{27.66 - \bar{D}(x_*)}{\varphi(x_*)} \tag{2.21}$$

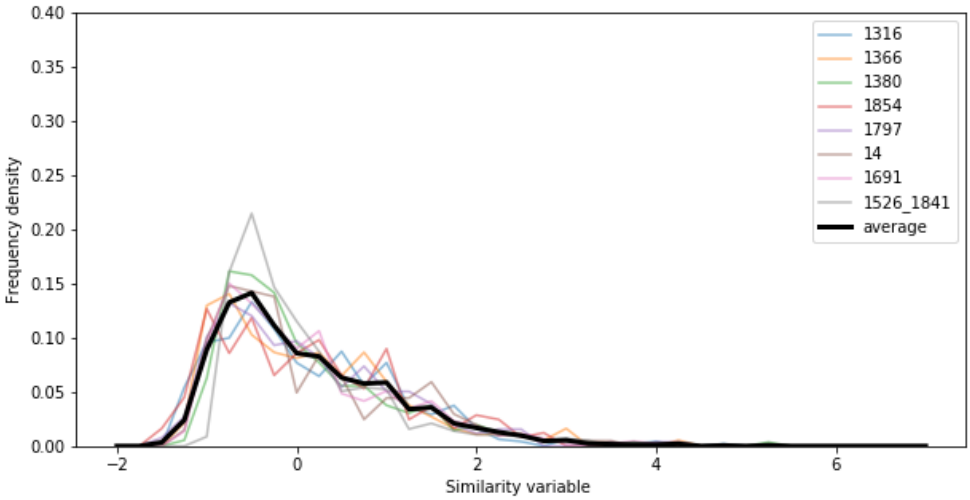

Figure 2.29: The average curve of all the self-similar grain size distributions after Casper (within the flat group).

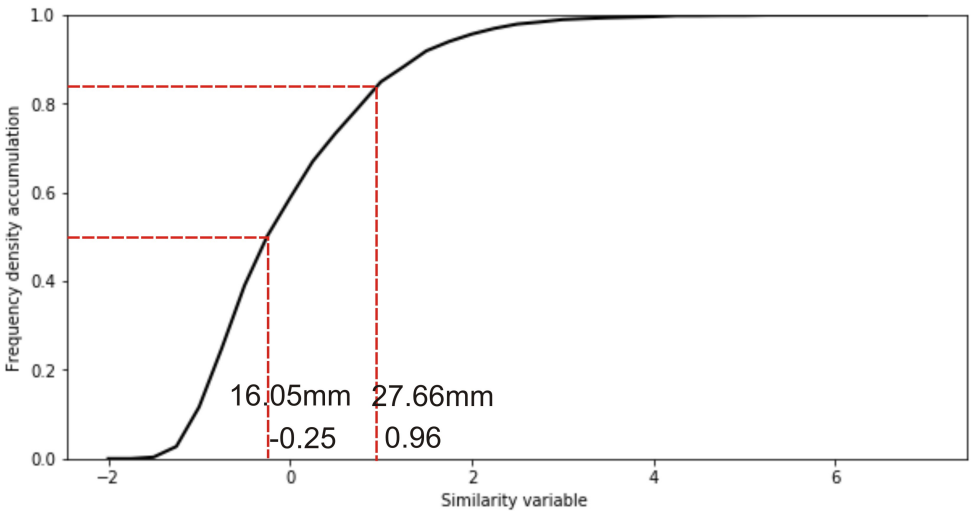

Figure 2.30: The positions of D_{50} and D_{84} on the curve of frequency density accumulation against the similarity variable (real situation).

It then can be calculated that $\varphi(x_*)$=9.60 mm, $\bar{D}(x_*)$=18.45 mm.

The real parameters of the grain size distribution in Casper are D_{50}=16.05 mm, D_{84}= 27.6 6mm, $\varphi(x_*)$=9.6 mm, $\bar{D}(x_*)$=18.45 mm; and the real detailed grain sizes distribution curve can be developed as below (Figure 2.31).

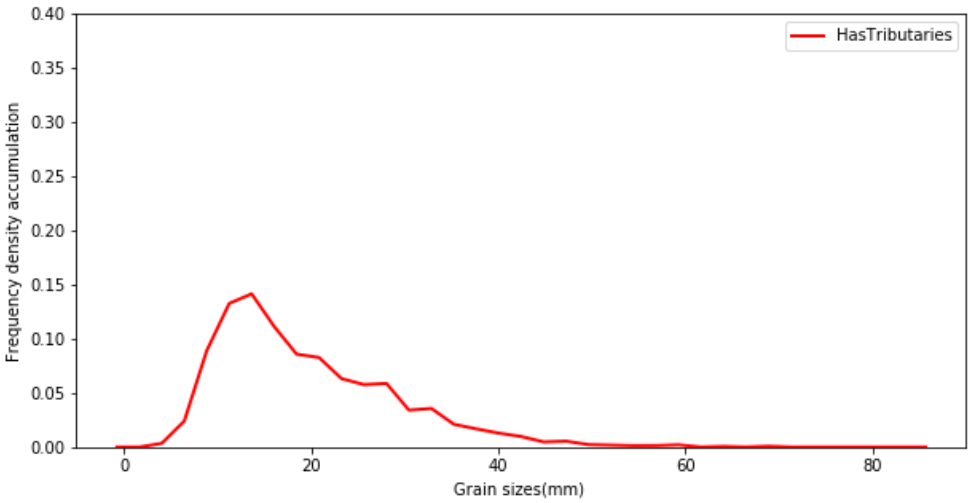

Figure 2.31: Calculated detailed grain sizes distribution in Casper (real situation).

The predicted distribution curve and real distribution curve were shown together (Figure 2.32). This comparison suggests that the lateral sediment input near Casper changes the portion of sediments within the mainstream considerably. If no lateral sediment input existed near Casper, most of the sediments coming from upstream would decrease into smaller than 15 mm (blue line). For the real situation, however, most sediments deposited near Casper are larger than 15 mm (red line). This means that the lateral sediment input has brought a lot of coarse sediments into the mainstream. In other words, most of the coarse sediments collected in Casper were from lateral sediment input.

2.5.2 R15726

For R15726, the calculation is similar. Firstly, it is assumed that no lateral sediment input existed between Casper and R15726. Under this assumption, the D_{50} and D_{84} would follow a typical downstream fining trend between Casper and R15726. Therefore, the downstream grain sizes fittings of this area (2.22 and 2.23) are used.

$$D_{50} = 0.411 \times \ e^{(-0.01x)} \tag{2.22}$$

$$D_{84} = 1.474 \times \ e^{(-0.008x)} \tag{2.23}$$

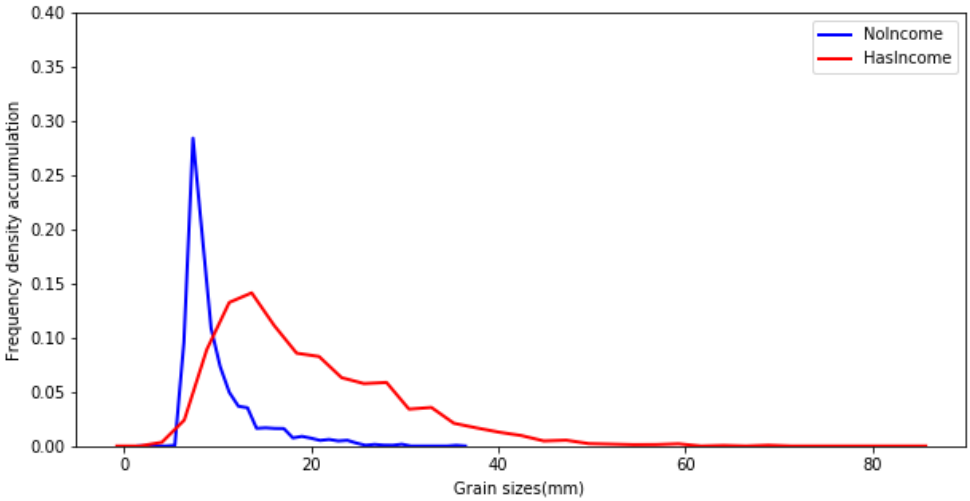

Figure 2.32: The comparison between the predicted distribution of grain sizes (without lateral sediment input) and the real situation (with later sediment input) in Casper.

R15726 is located 62.5km westward from the WY-NE border. Using the distance of -62.5 km, the D_{50} can be calculated as 0.77 mm and D_{84} as 2.43 mm.

If there was no lateral sediment input before R15726, the similarity distribution of the grains in R15726 should be similar to those of the sites before R15726, between Casper and R15726 actually. In addition, the area between Casper and R15726 is within the flat group, so that if these was no lateral sediment input before R15726, the similarity distribution of the grains in R15726 should follow the average similarity distribution within the flat group (shown in Figure 2.33).

Similarity, the position of D_{50} and D_{84} can be plotted on the curve of frequency density accumulation against the similarity variable. Corresponding values of similarity variables were read, and equations were set as below.

$$-0.25 = \frac{0.77 - \bar{D}(x_*)}{\varphi(x_*)} \tag{2.24}$$

$$0.96 = \frac{2.43 - \bar{D}(x_*)}{\varphi(x_*)} \tag{2.25}$$

It can be calculated that $\phi(x_*)$=1.37 mm, $\bar{D}(x_*)$=1.11 mm.

Detailed grain sizes distribution curve can then be calculated and shown in Figure 2.34.

This curve represents the predicted grain size distribution in R15726 without lateral sediment input. It represents the situation of the sediments coming from

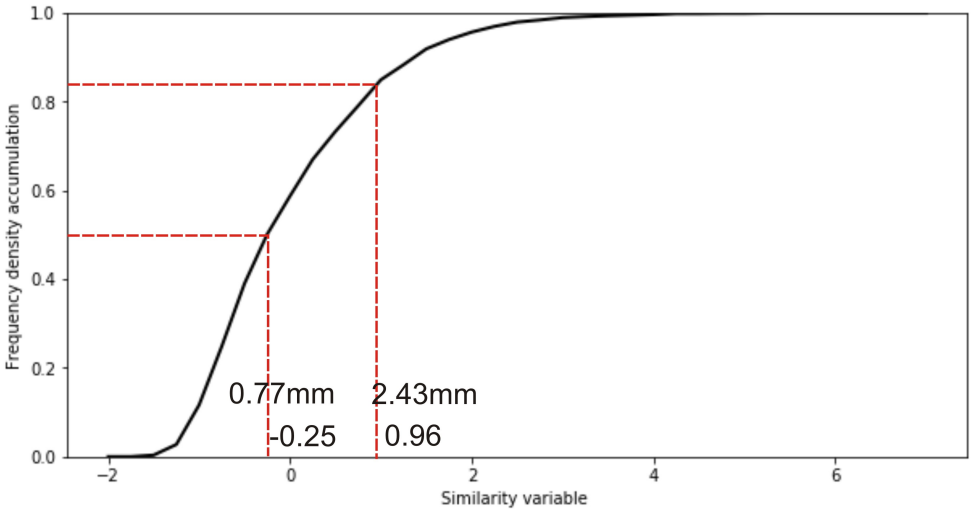

Figure 2.33: The positions of D_{50} and D_{84} on the curve of frequency density accumulation against the similarity variable for R15726 (without lateral sediment input).

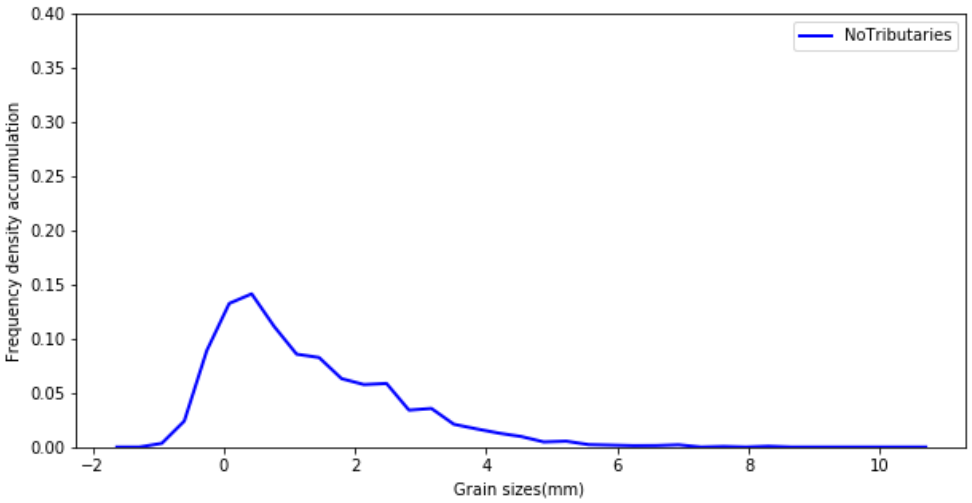

Figure 2.34: Predicted detailed grain sizes distribution in R15726 (without lateral sediment input).

Casper when they reached R15726 if there was no lateral sediment input between Casper and R15726.

The second part of the calculation is for the real situation.

As that used in the previous pages, the real D_{50} and D_{84} can be determined using the decreasing grain sizes data after R15726 (shown as Equation 2.26 and 2.27) because these data represents the normal fluvial situation without the influences of lateral sediment input.

$$D_{50} = 15 \times \ e^{(-0.007x)} \tag{2.26}$$

$$D_{84} = 25.09 \times \ e^{(-0.005x)} \tag{2.27}$$

Using the distance of -62.5 km, the D_{50} can be calculated as 13.0 mm and D_{84} as 26.5 mm.

Then, the real values of D_{50} and D_{84} can be plotted on the frequency density accumulation curve of similarity variables (shown as Figure 2.35). Corresponding values of similarity variables can be read in Figure 2.35, providing the necessary information to develop two equations for the other two essential variables, $\varphi(x_*)$ and $\bar{D}(x_*)$.

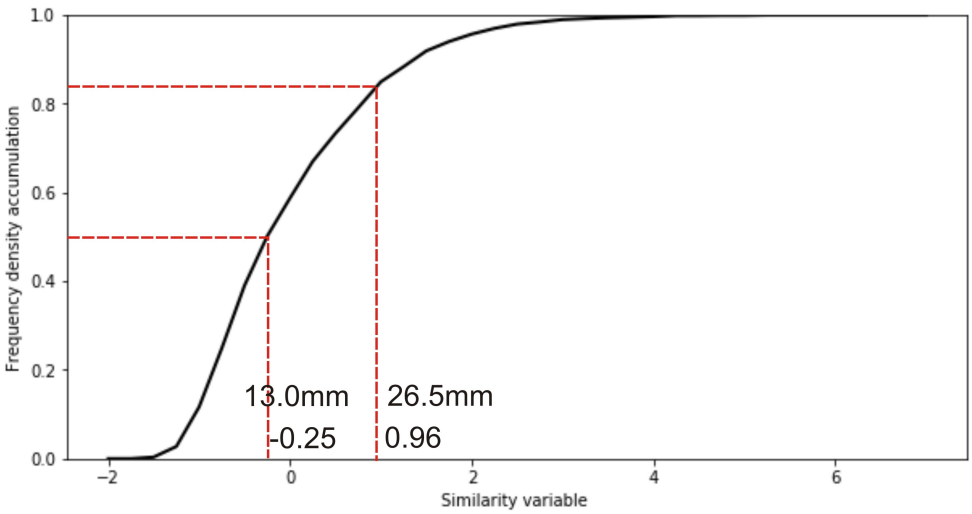

Figure 2.35: The positions of D_{50} and D_{84} on the curve of frequency density accumulation against similarity variable (real situation).

$$0.25 = \frac{13.0 - \bar{D}(x_*)}{\varphi(x_*)} \tag{2.28}$$

$$0.96 = \frac{26.5 - \bar{D}(x_*)}{\varphi(x_*)} \tag{2.29}$$

It can be calculated that $\varphi(x_*)$=11.16 mm,$\bar{D}(x_*)$=15.79 mm.

The real parameters of grain size of R15726 are D_{50}=13.0mm, D_{84}= 26.5mm, $\phi(x_*)$=11.16 mm,$\bar{D}(x_*)$=15.79 mm; and the detailed grain sizes distribution curve is shown in Figure 2.36.

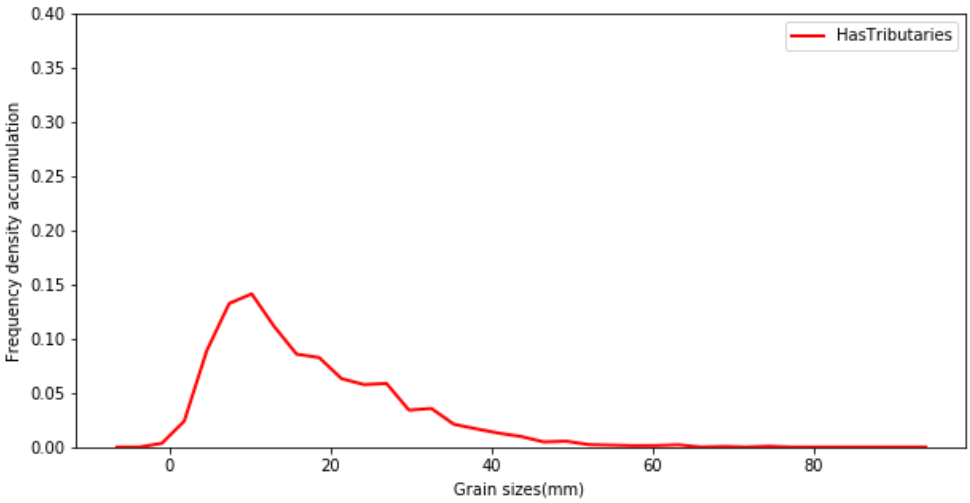

Figure 2.36: Calculated detailed grain sizes distribution curve in R15726 (real situation).

Similar to that of Casper, the comparison between the predicted grain sizes distribution and the real grain sizes distribution can be generated (shown in Figure 2.37). As suggested in this figure, if no lateral sediment input existed near R15726, sediments from Casper would nearly all become sand ($<$ 5 mm, the blue line in Figure 2.37) when they reached R15726. However, for the real samples collected from R15726, a large portion of pebbles can be observed (the red line in Figure 2.37). This suggests that the lateral sediment input near R15726 changed the components of sediments, especially the coarse components, in R15726 considerably. In other words, the pebbles collected in R15726 are mainly from the lateral sediment input.

2.5.3 Keystone

Following the same procedure, some calculations were conducted to get the predicted grain sizes distribution without lateral sediment input for Keystone, which is 300.878 km eastward from the border of Wyoming and Nebraska.

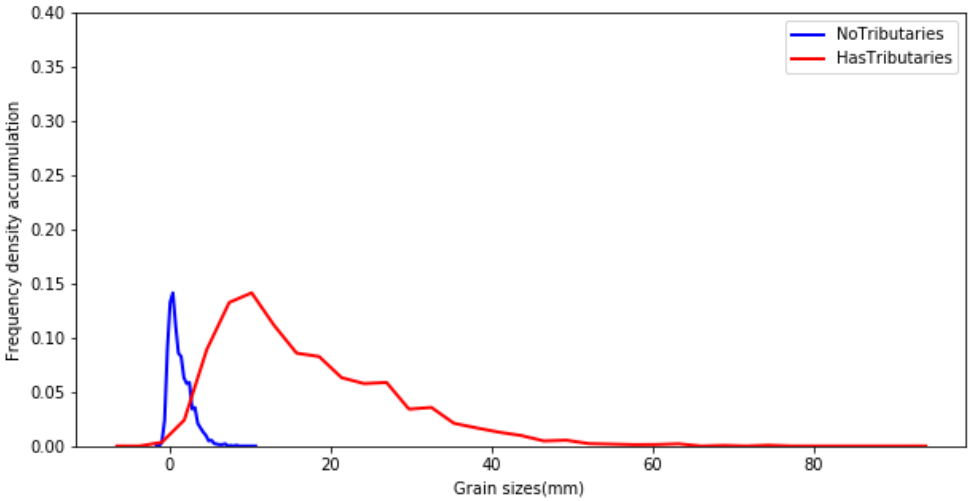

Figure 2.37: The comparison of the predicted distribution of grain sizes (without lateral sediment input) and the real situation (with lateral sediment input) in R15726.

Under the hypothesis that there was no lateral sediment input, the D_{50} and D_{84} can be calculated based on the normal downstream fining trend between R16827 and Keystone.

With these equations of grain sizes fitting (2.30 and 2.31), it can be calculated that D_{50}=1.83 mm and D_{84}=5.57 mm near Keystone. These values represent the situation of pebbles of R15726 when they reached Keystone.

$$D_{50} = 15 \times \ e^{(-0.007x)} \tag{2.30}$$

$$D_{84} = 25.09 \times \ e^{(-0.005x)} \tag{2.31}$$

Because all the points between R15726 and Keystone belong to the downstream part, D_{50} and D_{84} were plotted on the curve of frequency density accumulation against the average similarity distribution of downstream part (Figure 2.38).

Two equations can then be set as below:

$$-0.25 = \frac{1.83 - \bar{D}(x_*)}{\varphi(x_*)} \tag{2.32}$$

$$0.96 = \frac{5.57 - \bar{D}(x_*)}{\varphi(x_*)} \tag{2.33}$$

It can be calculated that $\phi(x_*)$=3.09 mm and $\bar{D}(x_*)$=2.60 mm.

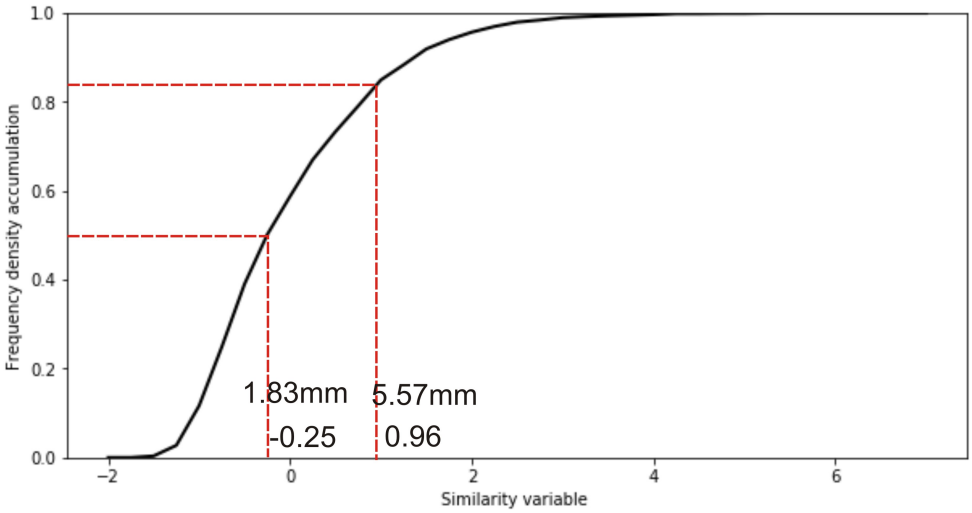

Figure 2.38: The positions of D_{50} and D_{84} on the curve of frequency density accumulation against similarity variable for Keystone (without lateral sediment input).

Using all these parameters, the detailed grain sizes distribution near Keystone can be developed, which is shown in Figure 2.39:

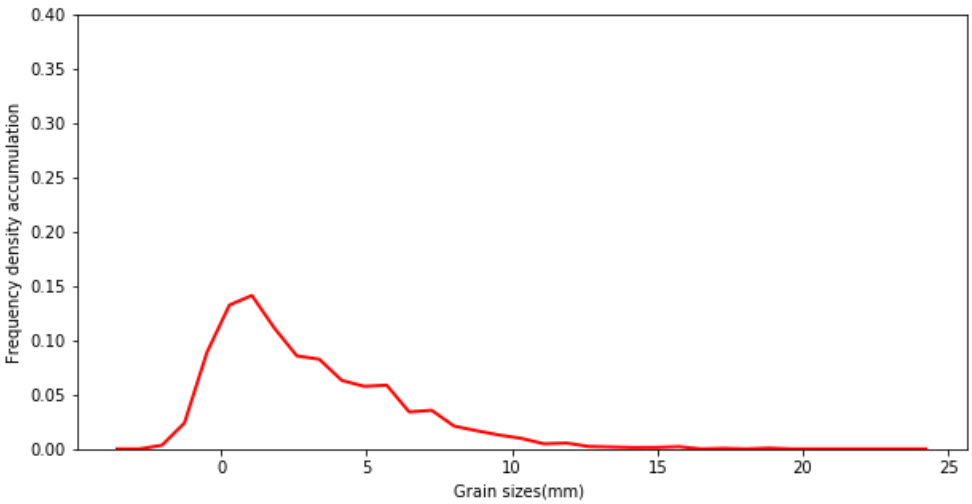

Figure 2.39: The predicted detailed grain sizes distribution curve in Keystone (without lateral sediment input).

For the real parameters of grain size, because the detailed grain size data were collected (1691) in Keystone, there is no need to calculate them. The real data of Keystone are D_{50}=12.5mm, D_{84}= 26.0mm, $\phi(x_*)$=10.64 mm, $\bar{D}(x_*)$ =15.24 mm; and the detailed grain sizes distribution curve is shown in Figure 2.40:

When putting together (Figure 2.41), the conclusion is obvious. As suggested by

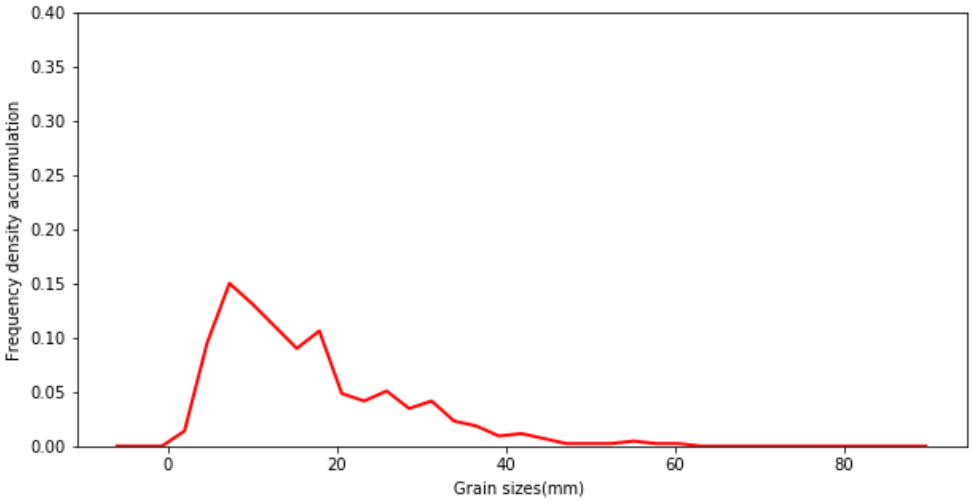

Figure 2.40: Real detailed grain sizes distribution curve in Keystone (same as the sample site of 1691).

the comparison, the pebbles from R15726 nearly disappeared when they reached Keystone, almost all the pebbles of Keystone come from lateral sediment input.

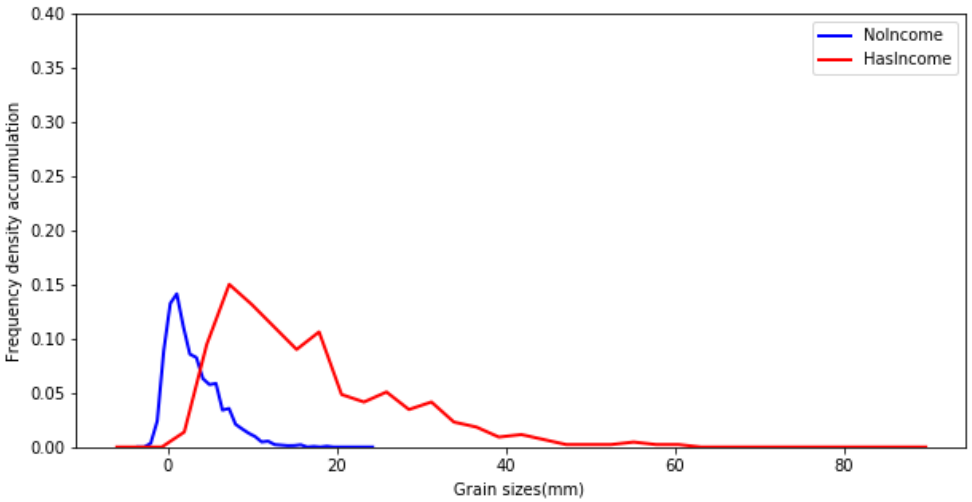

Figure 2.41: Comparison between the predicted distribution of grain sizes (no lateral sediment input) and the real one (1691, with lateral sediment input) in Keystone.

2.6 Summary and Conclusion

Fluvial systems are regarded as a critical component of earth surface processes because they link the sediment source and the basin. The characteristics of fluvial sediments are influenced by tectonic and climatic processes. Thus, sediment

grains, as the basic element of fluvial sediments, are often used to reconstruct changing tectonic and climatic conditions. One common observation of fluvial sediments is a tendency for the bedload to become finer downstream, which is widely used in the geological studies.

In this chapter, downstream fining curves were generated, and similarity statistics were done. Based on the result, three locations of probable lateral sediment inputs were recognised: Casper, R15726 and Keystone. The whole North Platte River system was then divided into three sub-areas based on these three sites. Within each sub-area, the grain sizes exhibit a downstream fining trend and an abrupt downstream increase.

For each of these sites, grain size distributions with and without lateral sediment inputs were generated by combining the grain size fitting curves and the similarity distributions. From the comparisons between the grain size distributions with and without lateral sediment input, it can be concluded that only a small portion of pebbles collected in Casper might come from the mountain area. While for the pebbles collected from R15726 and Keystone, nearly all of them come from lateral sediment input nearby.

Lateral sediment can only be derived from the tributaries or the incision of deposited paleosediments by the mainstream. For tributaries, most sediments carried were also from the incision of the deposited paleosediments. Eroding the paleosediments and mixing them with the fresh sediments is called recycling. The significant influences of lateral sediment inputs on the grain size distributions in the mainstream provides a reliable basis for the existence of recycling in the Great Plains.

From the study in chapter 2, the first question in the introduce that where would recycling take place in the research area, has been answered. Next chapter is on cosmogenic nuclides analysis. Cosmogenic nuclides analysis is mainly used on the calculation of the exposure time of the sediments. As the recycling process is mainly the mixing of paleosediments into fresh sediments. The recycled sediments must be deposited on the surface for a very long time, or buried for a long time and then eroded out. That is to say,the recycled pebbles in the Great Plains must contain the information of a considerably long storage time. In the next chapter, two models were built to estimate the maximum concentration of cosmogenic ^{21}Ne accumulated from the source to the target location. The results of these two models were used to see if the pebbles collected from the research area have experienced long time of storage. Also, based on the result of cosmogenic nuclides analysis, the oldest paleosediments which modern recycling can affect can also be estimated.

Chapter 3

Cosmogenic Nuclides

3.1 Introduction

In the Chapter 2, it has been found there are three main places where recycling happened, those are Casper, R15726 and Keystone. In the normal fluvial system, the grain size would have a downstream fining trend and also, the distribution curves of grain sizes of the grains collected from different places along the channel would represent a statistically similar shape. However, as shown by the result of grain size data (Figure 2.20), the grain sizes have experienced several grain size increases from the mountain area to the plain area. Also, the result of similarity analysis represents that the samples collected along the North Platte River can be divided into two different groups (Figure 2.16,Figure 2.18 and Figure 2.19). These data represents that three are some lateral sediments along the North Platte River. In addition, from the reconstruction of grain sizes distributions with and without the influences of lateral sediments inputs for these target three sites, it can be concluded that almost all of the large pebbles collected from the plain area are from lateral sediment inputs, providing solid evidence of the existence of recycling in the Great Plains.

Knowing the existence of recycling is far more than enough, in the next study, some work have been done on exploring the detail of recycling. In this chapter, the question mainly to answer is that when the recycling take place?

In geological study, cosmogenic nuclide study has been widespread used in the research on the dynamic on the earth surface. In these studies, cosmogenic nuclides are mainly used to extract the information of being exposed and buried contained within the deposits. This tool has proved itself to be reliable in the study of ”age” for the sediments deposited on the earth surface, so that it came into mind that using cosmogenic nuclides to assess the ”age” of recycle pebbles, that is the storage time or burial time of the recycled pebbles in the Great Plains.

In 1934 A.V Grosse (1934) found that when cosmic rays reached the Earth's surface and interacted with the minerals on the surface (or within several meters under the surface), radioactive nuclides were produced. He named them "cosmic radio elements". In 1955 Raymond Davis and Oliver Schaffer (1955) suggested that cosmic radio elements can be used in geological research. In 1967, Lal and Peter (1967) built a theoretical basis for using "cosmic radio elements" to solve geological problems. During the 1970s, the theory of accumulation of this kind of nuclides was clear, and it came into mind that using this to date the exposure time of sediments. However, because the production rate of terrestrial cosmogenic nuclides (TCNs) is much lower than nuclides produced in the atmosphere, the lack of instruments that can precisely measure them limited the development of relevant studies.

In the early 1980s, with the appearance of Accelerator Mass Spectrometer (AMS) and highly sensitive noble gas mass spectrometry, the enormous potential of the cosmogenic nuclides once again got the attention of geologists (Gosse and Phillips, 2001).

Studies on surface processes are essential for geology and geomorphology, especially those on sediments accumulation and transportation in response to the changes of tectonics or climate. Nowadays, the cosmogenic nuclides plays an increasingly important role, being used widely on dating geological events, on quantifying the deposition and erosion processes.

3.1.1 History of the Studies of Cosmogenic Nuclides

According to the summary of J.C. Gosse (2001), the history of the TCN methods can be divided into four stages:

(1) The realisation of the utility of cosmogenic nuclides

As mentioned above, Raymond Davis and Oliver Schaeffer (1955) firstly applied cosmogenic nuclides to the geological problem. Based on the concentration of ^{36}Cl in samples collected in the Rocky Mountains, they calculated the exposure age for a pre-Wisconsinan surface to be 24,000 years based on the estimation of the half-life of ^{36}Cl ($t_{1/2}$ ^{36}Cl $= 3.01 * 10^5$ yr). However, their study did not attract many pursuers because of the noticeable uncertainty in measuring the production rates of the cosmogenic nuclides.

(2) The development of estimating the secondary cosmic-ray flux for different latitudes and elevations

The production rate of the cosmogenic nuclides has a relationship with altitude and latitude, but the scaling factors are difficult to assess. There are three reasons for this: (1) the intensity of cosmic ray become weak when they penetrate the atmosphere, however, the atmosphere is not constant; (2) the weakening rate of

the cosmic ray with the depth of atmosphere is not constant with latitude; (3) the Earth's geomagnetic field is not a geocentric dipole (Gosse and Phillips, 2001). To solve this problem, Lal (1958) built a model, setting the production rate at high elevation at 51°N latitude, which can be used to calculate the production rate with different latitudes or elevations. The model was then verified by one of his subsequent studies (Lal and Peters, 1967). This model (recently presented in (Lal, 1991) was the most widely used one in TCN studies.

(3) The development of relative devices

The appearance of AMS in the 1980s made the accuracy of measurement of the cosmogenic nuclides as low as 10^{-15} atoms per gram, contributing to the rapid development of TCN study. After this milestone, not only ^{36}Cl, some other cosmogenic nuclides were added to the TCN methods. Klein et al. (1986) were the first to apply cosmogenic ^{10}Be to calculate the exposure time of Libyan Desert Glass, which were collected from western Egypt. Graf et al. (1991) found ^{21}Ne is a useful tracer for exposure history, and at the same paper they pointed out that quartz is very well suited for TCN studies because it is simple, stable and allows a straightforward comparison between ^{21}Ne, ^{10}Be and ^{26}Al in the same sample.

(4) The continued development of TCN methods

We are now in the fourth stage of TCN studies. Recently the central development of TCN methods is the updating of production scaling models. Lal (1991) developed a popular method to calculate the production rates of different cosmogenic nuclides based on the scaling factors of different latitude or elevation. Some studies later (Dunai, 2000; Stone, 2000; Desilets and Zreda, 2003; Desilets et al., 2006) developed more models to acquire more accurate scaling factors to calculate the production rates. However, these newer models also have increased sophistication, which to some extent limits their wide application.

3.1.2 Publications On the Nature of Terrestrial Cosmogenic Nuclides (TCN)

In addition to the reviews of TCN methods above, some comprehensive publications focused on the nature of the cosmogenic nuclides. Lal (1988; 1991) provided a fundamental summary of his previous work, including the theory and the application. Granger and Muzikar (2001) provided a summary of the methods to date sediment burial with the cosmogenic nuclides, using ^{10}Be and ^{21}Al as an example. Gosse and Phillips (2001) recently reviewed all the previous TCN studies. This paper sorted out a detailed history of the development of TCN studies, provided a comprehensive view of the theory (estimating the production rate, scaling with altitude and latitude, and the effect of geomagnetic field), and compiled a list of useful information for application (sampling strategies, sample preparation and data interpretation using single or multiple nuclides).

3.2 Glossary

Attenuation length (Λ):

The thickness of sediments needed to attenuate the cosmic ray to a factor of e^{-1}. It is also called 'cosmic ray absorption mean free path'. It has different values for different locality because of the change of the geomagnetic field and atmospheric situation. Units: g cm^{-2}. It has a relationship with an absorption depth scale (z) and density (ρ): $z = \Lambda/\rho$.

Accelerator Mass Spectrometer (AMS):

A device that can accelerates the particles to very high speed before mass analysis. It can separate an isotope from its neighbouring mass (e.g. ^{14}C from ^{12}C). The method can also separate atomic isobars (e.g. ^{14}N from ^{14}C).

Cosmic Rays:

Particles coming from out side of the Earth, which include protons (83%), a-particles (13%), and heavier nuclei (1%) (Gosse and Phillips, 2001). They always have high energy (0.1 to 10^{20} GeV) and are called primary cosmic rays.

When these primary cosmic rays penetrate the atmosphere, the interactions between the primary cosmic rays and the atmospheric particles lead to the decrease of energy and produce secondary cosmic rays with lower energy (0.1 to 500 MeV). Most of them are nucleons (neutrons, protons) and muons.

Denudation Rate:

The rate of the removal of sediments on the Earth's surface. It is resulted from physical or chemical processes. Denudation rate can be recorded by cosmogenic nuclides because they can only accumulate near the Earth's surface. The rate of the removal of sediments due to physical erosion is also called 'erosion rate'.

Muon (μ):

Short-lived nuclear particles with a decay lifetime of about 2.2*10^{-6} s (at rest) and a mass 207 times of an electron.

Muon-induced reactions:

Which are also called muonic reactions. There are two processes of muon-induced reactions:

(1) When the fast muons with high (GeV) energy slow down, they emit Gamma-rays and then release neutrons. These neutrons interacted with the target particles and produced cosmogenic nuclides, this process is called spallation. (Figure 3.1);

(2) Slow negative muons (Stopped muons) might be captured by the nucleus, producing a cosmogenic nuclide (using ^{10}Be as an example, shown as Figure 3.1).

Muonic production dominates at depths >4 m (Figure 3.1).

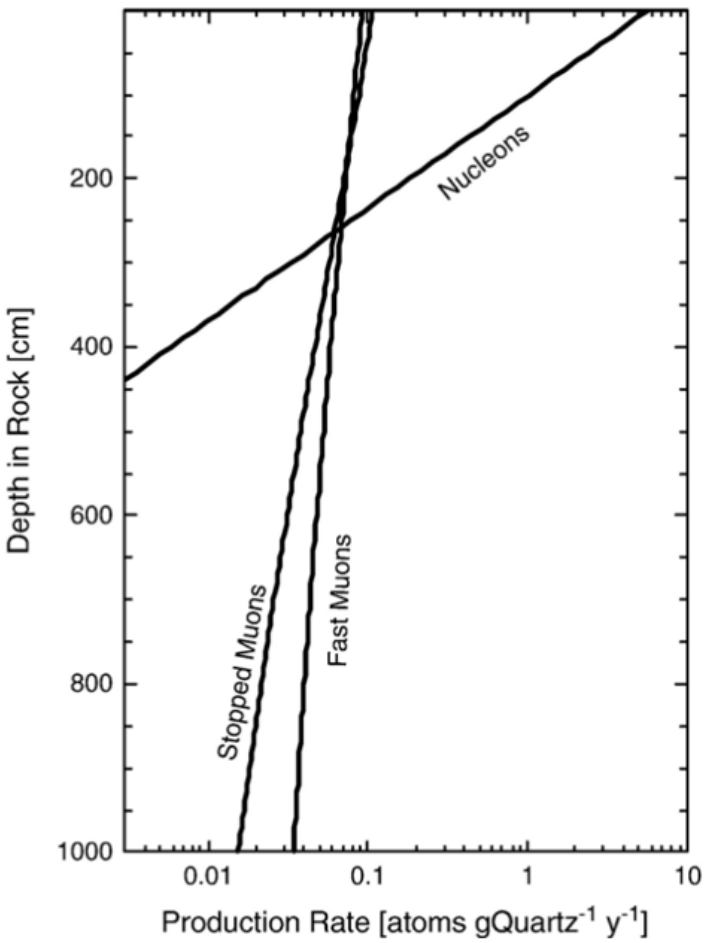

Figure 3.1: The depth-dependency of ^{10}Be production by nucleons (neutrons, protons) and muons (Von Blanckenburg, 2006).

Nucleogenic nuclides:

Radioactive elements in earth materials decay and emit particles which lead to nuclear reactions. The nuclides produced from these reactions are called nucleogenic nuclides.

Nuclide:

A nuclide is any particular atomic nucleus with a combination of unique atomic number and unique neutron number. The families of several different nuclides of the same element are called isotope.

Production rate:

For a sample with a given mass, the concentration of cosmogenic nuclides accumulated in a given time. They are always described as normalised to sea level and high latitude (SLHL). Units: atoms^{-1}yr^{-1}g^{-1}.

Spallation reactions:

A nuclear reaction, it actives when a nucleon with high energy (usually >10 MeV) collides with a target particle. Spallation reactions would release some secondary nuclides (protons and neutrons), these secondary nuclides have less mass than the original particles.

Terrestrial cosmogenic nuclide (TCN):

Terrestrial cosmogenic nuclides (TCNs) are nuclides produced by the reaction (spallation, slow negative muon capture) between the secondary cosmic rays and the exposed materials on the the Earth's surface. They are different from atmospheric cosmogenic nuclides or nucleogenic nuclides. The former ones are produced in the atmosphere and then mixed into sediments, while the later ones are produced in the lithosphere.

3.3 Methodological Principles

3.3.1 Introduction of Terrestrial Cosmogenic Nuclides (TCN)

The galactic cosmic radiation which can produce the cosmogenic nuclides is mostly consisting of high-energy particles (1 GeV to 10^{10} GeV), mostly protons, originating from out side of the Earth. When these high-energy particles reach the upper atmosphere, they cause nuclear reactions, and the energy decreases. After this, the secondary cosmic rays, which are mostly composed with neutrons and muons of MeV energy, are produced. Then these secondary cosmic rays reach the Earth's surface, interact with the minerals in situ and produce terrestrial cosmogenic nuclides (TCN, shown in Figure 1.4).

The cosmogenic nuclides produced are controlled by the details of the arriving cosmic ray particles, including their types and their energy, and the details of the interacted minerals. The production rates of these nuclides are dependent on two factors, the elevation and the latitude (Codilean et al., 2008). Because of the attenuation process, they can only be produced within a limited depth scale (Von Blanckenburg, 2006). That's the foundation of TCN studies to assess bedrock erosion rates and any changes in surface elevation, by determining the exposure duration of the minerals and the amount of pre-detachment cosmogenic nuclides they acquire.

The most widely used cosmogenic nuclides are ^{10}Be ($T_{1/2}$ = 1.5 My), ^{26}Al ($T_{1/2}$

= 0.7 My), ^{36}Cl ($T_{1/2}$ = 300 ky), ^{3}He (stable), ^{21}Ne (stable), and ^{22}Ne (stable) (Von Blanckenburg, 2006). ^{21}Ne and ^{10}Be were mainly used in this study.

Four main mechanisms contribute to the production of radionuclides (Figure 1.4):

(1) Spallation-Nuclear reactions of nucleons (neutrons, protons);

(2) Nuclear reactions of fast muons;

(3) Negative (slow) muon captured by the target nucleus;

(4) Nuclear reactions of neutrons originating from the decay of ^{235}U, ^{238}U, and ^{232}Th.

Among these four mechanisms, only the first three contribute to the generation of the cosmogenic nuclides. On the Earth's surface specifically, TCN produced via spallation processes are much more abundant in number than those produced via muons processes (slow or fast). As a result, at shallow depth up to about 4 m, the production of nucleons from nuclear reactions dominates (as Figure 3.1 shows). However, the reactions between muons and other particles is much less intense, and muons penetrate much more in-depth than nucleons. As the study of (Granger and Muzikar, 2001) shows, for sediments buried about 10 m deep, the cosmogenic nuclides produced by nucleons has nearly disappeared compared to its value on the Earth's surface, while the cosmogenic nuclides produced by muons is still 1/7 compared to its value on the Earth's surface.

3.3.2 Effects of the Geomagnetic Field

Norwegian geophysicist C. Stormer (1934) provided a method to calculate the time needed for a particle to penetrate the geomagnetic dipole field. Although it was found that his calculation is not precise, Stormer's theory provided the basis for all the subsequent studies on this topic.

In 1927, J.Clay (Gosse and Phillips, 2001) found a unnoticeable decrease in the intensity of cosmic-ray around the Suez Canal from Amsterdam to Java, raising the assumption that some cosmic rays might be charged resulted from the influence of the magnetic field. Based on this idea, some measurements were conducted and it was found that the most significant change of cosmic-ray flux happened between 41° and 25° (also be called latitude shift). Then Compton (1933) found that the intensity of cosmic rays was directly controlled by the horizontal thickness (H) of the geomagnetic field.

After that, some subsequent studies had paid attention to the atmospheric distribution of the intensity of cosmic-ray flux world-widely. Simpson et al. (1951) found that the cosmic-ray flux is attenuated rapidly with increasing depth toward the base of the atmosphere because of the interaction between the cosmic-ray and the atmospheric nuclei. It was recognised that below 200

gcm^{-2} the attenuation lengths of fast particles were nearly the same to those of star producing radiations (Simpson et al., 1951). This means that at this situation (below 200 gcm^{-2}), the high energy flux was nearly in equilibrium with the secondary low-to-medium energy flux. This provided the basis for the calculation of atmospheric distribution of the intensity of the cosmic rays e.g. (Lal and Peters, 1967).

Combining the improvement of the understanding of cosmic particles and the measurement of the atmospheric distribution of the cosmic rays, Lemaitre and Vallarta (1933) proposed a means to rebuild the latitudinal variations in cosmic-ray intensity. However, these studies were all based on a geocentric geomagnetic dipole field model. In order to solve the complexities caused by non-dipole components, a refined model of Gall (1960) was employed.

3.3.3 Production Rate of Cosmogenic Nuclides

As mentioned above, when these secondary cosmic rays arrived on the Earth surface, two types of them, nucleons (neutrons and protons) and muons, play essential roles in the generating of cosmogenic nuclides.

When interacting with other matters, the secondary cosmic rays were absorbed. For this absorption happened within several meters below the Earth's surface, Lal (1991) set a law to describe this situation:

$$L_0 = \Lambda/\rho \tag{3.1}$$

in which L_0 is the absorption depth scale; Λ is the absorption mean free path, Λ = 160 gcm^{-2}); ρ is the absorbing materials' density, gcm^{-3}.

Also, the production rate of cosmogenic nuclides by nucleons can be calculated by a simple exponential law as below (Lal, 1991; Brown et al., 1992):

$$P_n(z) = A_0 e^{-z/L_0} \tag{3.2}$$

where P represents the production rate of the cosmogenic nuclide; n represents nucleonic production; A_0 is the production rate for sea level and high latitude (SLHL), in units of atoms per year per gram of samples; z is the absorption depth below the Earth's surface, L represents the nucleon decay length, which has a value of $L_0 = 160/\rho$ (Lauer and Willenbring, 2010), where ρ is the absorbing materials' density, gcm^{-3}.

Then a reasonable expression of production rate can be achieved as below:

$$P_n(z) = A_0 f_1 e^{-z/L_1} + A_0 f_2 e^{-z/L_2} + A_0 f_3 e^{-z/L_3} \tag{3.3}$$

The first term in Equation 3.3 describes the production due to the spallation process, and the second and third terms describe the production due to fast and slow muons, specifically. Also, A_0 is the production rate for sea level and high latitude (SLHL), in units of atoms per year per gram of samples; f is the percent contributions of different mechanisms at SLHL, this value is variable for different nuclides; z is the depth below the Earth's surface; for the decay lengths of these three mechanisms, the values are given by $L_1 = 160/\rho$, $L_2 = 738/\rho$, $L_3 = 2688/\rho$, for ^{21}Ne (Lauer and Willenbring, 2010), where ρ is the absorbing materials' density, gcm^{-3}. This equation can only be applied for the production of cosmogenic nuclides near the Earth's surface.

3.3.4 Estimation of Production Rates

There are three ways to calculate the production rate:

(1) Measure the concentration of the cosmogenic nuclides accumulated in a sample with a known time. In this measurement, this sample should be exposed all the time, and has not been erodes or shielded during this time. A similar way is to do the measurement on the stable surfaces which have been exposed for a very long time, under which condition the concentration of the cosmogenic nuclides would be saturated without the influence of erosion (Brook et al., 1995).

(2) The measurement can also be done by laboratory work: measure the concentration of the cosmogenic nuclides in the slabs of known composition exposure in the cosmic rays (real ones or the accelerated particles with the same energy as the secondary cosmic rays) for a known time (Nishiizumi et al., 1996).

(3) Numerical calculation using models to simulate the interactions contribute to the production of cosmogenic nuclides (Masarik and Reedy, 1995).

Most of the production rates used in modern geological studies come from Lal's paper in 1991 (Lal, 1991), which is based on the first method.

In this thesis, we mainly introduce the production rate of ^{10}Be and ^{21}Ne.

Neon-21

Neon has three stable isotopes- ^{20}Ne, ^{21}Ne, and ^{22}Ne-and their ratios with each other in minerals are commonly plotted on a three-isotope plot (Figure 3.2). Nuclides of cosmogenic neon (^{21}Ne and ^{22}Ne) are produced by neutron spallation at approximately the same rate in quartz (Niedermann et al., 1993), consequently making the concentrations of cosmogenic neon contained by exposed quartz plotted on the spallation line marked in Figure 3.2. The black square in the figure represents atmospheric neon without cosmogenic neon, and the line (spallation line) represents the mixing of atmospheric and cosmogenic neon under spallation process only. Atmospheric neon (The black square, ^{22}Ne/^{20}Ne

= 0.00296: $^{21}Ne/^{20}Ne = 0.102$) is the dominant source of neon in most minerals (Dunai, 2010).

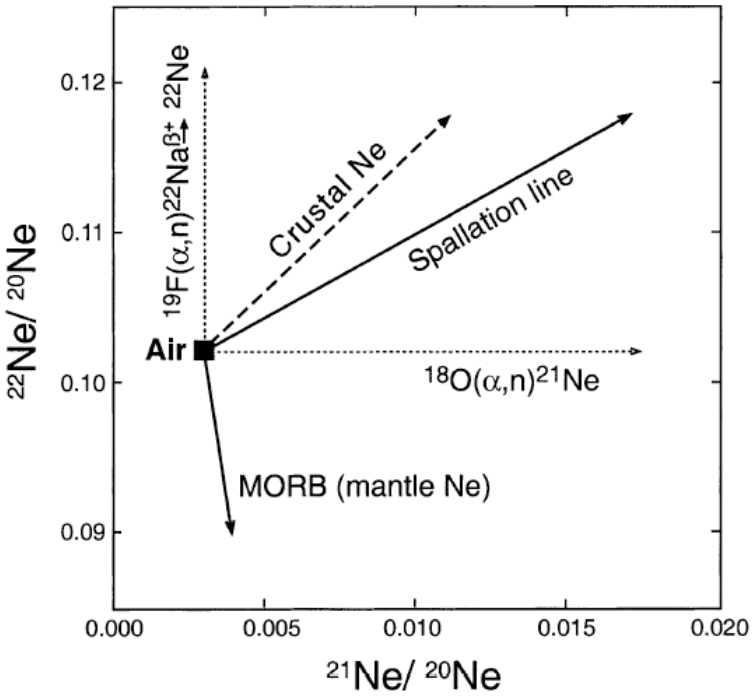

Figure 3.2: Neon three-isotope plot showing the composition of air and various components that can mix with air to alter the chemistry of a sample (Hetzel et al., 2002).

Three mechanisms will contribute to the production of cosmogenic ^{21}Ne in ancient samples: neutron spallation, muon capture, and diffusion. Neutron spallation is the most important mechanism for the generation of cosmogenic ^{21}Ne, from ^{28}Si. A production rate of 20.29 ^{21}Ne atoms g^{-1} $year^{-1}$ is set based on the previous studies (Niedermann et al., 1994; Niedermann, 2000)). For the production rate resulted from muon capture, the maximum ^{21}Ne production rate in quartz is 0.95 ^{21}Ne atoms g^{-1} $year^{-1}$, considerably less than the production rate resulted from neutron spallation (Libarkin et al., 2002). For the production rate resulted from diffusion, researchers have assumed that it is equals to zero in quartz (Von Blanckenburg, 2006).

Nucleogenic Ne: Figure 3.2 also illustrates two critical reactions (vertical and horizontal dotted lines) that produce neon isotopes and complicate this two-types situation, which are named nucleogenic neon. Alpha particles are expelled from the decay of the ^{238}U, ^{235}U- and ^{230}Th- series. When the α-particles are absorbed by the nucleus of ^{18}O or ^{19}F in the quartz (within the lattice or in fluid inclusions), nuclear instability leads to emission of a neutron, producing nucleogenic ^{21}Ne and ^{22}Ne. The amount of in situ nucleogenic neon trapped in the quartz is therefore

dependent on ^{18}O and ^{19}F content, abundance and chemistry of fluid inclusions, and the presence of alpha-generating radiogenic nuclides (Dunai, 2010). The production of nucleogenic ^{21}Ne and nucleogenic ^{22}Ne moves data horizontally and vertically, respectively, thereby moving the plots off the spallation line and complicating the determination of a cosmogenic ^{21}Ne concentration.

A special kind of nucleogenic neon is produced in the crust and can be incorporated during quartz crystallization by trapping fluid inclusions. These fluids tend to be enriched in ^{21}Ne and ^{22}Ne with respect to the air, with concentrations of cosmogenic nuclides following the dotted line outlined in Figure 3.2, with a more substantial component of ^{22}Ne from the relative abundance of ^{19}F in the fluids (Dunai, 2010). The air-crustal neon mixing line has a similar gradient to the spallation line so a crustal neon component may resemble cosmogenic neon. It is crucial to account for crustal Ne as it may either interfere with the cosmogenic age calculation or alter the position of the non-cosmogenic mixing end-member (Dunai, 2010).

Fortunately, at least 80% of the noncosmogenic nuclides are found in the outer 40 μm of the samples collected (Turner, 1993). A preparation was conducted to reduce the noncosmogenic nuclides contained within the samples, that is removing the outer layer of the samples with chemical etching.

Neon has been chosen as a diagnostic isotope for a number of reasons including its nuclear stability (no radioactive decay). When a mineral has decreased into a threshold temperature in which no significant diffusion of the primary or secondary particles out of the mineral, this temperature is defined as the closure temperature of this mineral (Braun et al., 2006). The ^{21}Ne closure temperature for quartz is 94 ± 6 °C and therefore cosmogenic neon is quantitatively retained in a quartz lattice with negligible diffusive loss over periods of time (Shuster and Farley, 2005). This means that the accumulation of cosmogenic ^{21}Ne would start when the sediments were exposed, and would cease (being stable because of no decay) when the sediments were buried. Any new exposure would activate a new round of accumulation. This makes the accumulation of cosmogenic ^{21}Ne behaves like a stopwatch (as Figure 3.3 shows). Furthermore, the previous studies of the production rate of cosmogenic ^{21}Ne show that cosmogenic ^{21}Ne to be well locked in quartz, and neon measurements require only small amounts of quartz, which is relatively quick and simple to prepare.

The most used production rate of ^{21}Ne for sea level and high latitude (SLHL) in quartz is approximately 21 atoms $g^{-1}yr^{-1}$ (Niedermann et al., 1994; Desilets and Zreda, 2001; Niedermann, 2000).

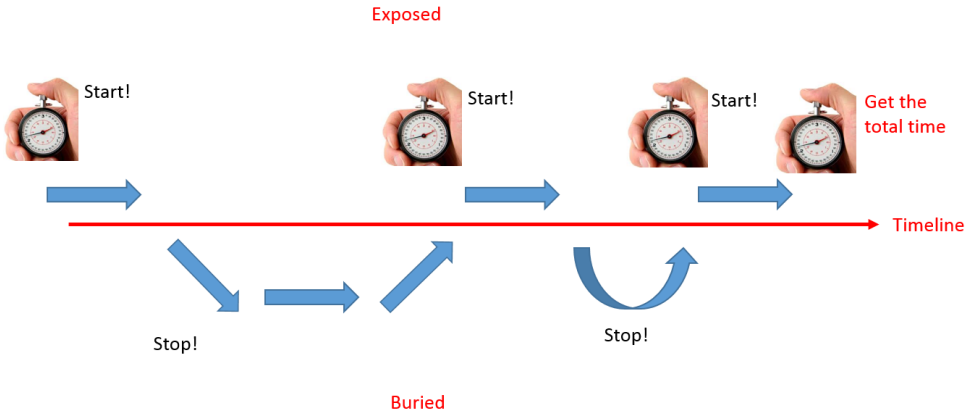

Figure 3.3: A schematic representation showing the accumulation of the cosmogenic ^{21}Ne within the sediments when they were exposed or buried, like a stopwatch.

Beryllium-10

^{10}Be has been the most widely used nuclide, due to its absence in rocks before its exposure into the environment of cosmic ray (Von Blanckenburg, 2006), and its relatively well-constrained production rates (Gosse and Phillips, 2001).

Spallation is also the most critical mechanism for the production of ^{10}Be. In the previous studies on the production rate of ^{10}Be, the range of the calculated production rates remains large. For example, for ^{10}Be in quartz, the production rate ranges from 4.74 atoms g^{-1}yr^{-1} (Clark et al., 1995) to 6.4 atoms g^{-1}yr^{-1} (Brown et al., 1991). These discrepancies may be due to: the uncertainties in the exposure time used to do calculation, the unrecognised shielding matters and magnetic and atmospheric effects (Gosse and Phillips, 2001). After a comparison of all the proposed production rate of ^{10}Be, Stone (1999) found that the production rates calculated from lower elevation sites are lower than those calculated from high elevation sites. He then changed the assumed muonic contribution on the total production at sea level and high latitude (SLHL) to be 3% instead of 15.6% which was used in the previous studies. He suggested the scaled production rates for SLHL as 5.1 $\pm$ 0.3 ^{10}Be atoms g^{-1}yr^{-1} (Stone, 1999).

Atmospheric cosmogenic Be is mainly produced in the atmosphere by the interaction of cosmic rays with oxygen and nitrogen. Then these cosmogenic Be deposited on the Earth's surface (Brown et al., 1992). In the subduction zones, significant levels of ^{10}Be may be found because of the recycling of marine sediment (Morris, 1991). They are also called meteoric ^{10}Be.

Nucleogenic Be is mostly from the interaction between low energy-particles and Li, which is too low to produce significant noise (Brown et al., 1992).

Sample preparation for ^{10}Be: As discussed above, in order to remove the

noncosmogenic Be contained within the outer rim of the samples, the samples must undergo repeated chemical etching (Gosse and Phillips, 2001).

Most studies use quartz for cosmogenic Be analysis. Some studies (Gosse and Phillips, 2001) also tried granites for cosmogenic Be analysis, however, with the whole rock dissolved to more than 35% loss of the original mass, the result still represents much larger concentration of Be than the standard. Even with the whole rock dissolved to more than 90% loss, the result was still not encouraging.

3.3.5 Scaling Factors for the Production Rates of the cosmogenic nuclides

Several factors which would contribute to the correction of the production rates of the cosmogenic nuclides:

(1) The intensities of primary cosmic rays are different in different locations of the geomagnetic field;

(2) The intensity of secondary cosmic rays varies with the air pressure;

(3) TCN samples might be collected on sloping surfaces that are not exposed perpendicularly to the cosmic rays;

(4) A coverage by plants, soils, or snow.

All these can be solved quantitatively through scaling factors.

Scaling of the Geomagnetic Field and Air Pressure

Lal (1958) combined all the previous studies and developed a model to calculate the distribution of the intensity of the cosmic rays flux and then raised a method to calculate the production rate of cosmogenic nuclides all round the world. The most widely used method to calculate the production rate of cosmogenic nuclides now is the updated one by Lal (1991), with the uncertainty of about 10-20%. However, some subsequent studies found that the scaling of elevation has reasonably high uncertainty for sites with high latitude. As discussed above, the production rate of ^{10}Be calculated using the 1991 model may be too large to be the SLHL standard (Stone et al., 1998). To reduce the influence of high elevation, Stone et al. (1998) reduced the muon contribution to the accumulation of cosmogenic ^{10}Be at sea level. Stone's revised model has different result mostly at low altitudes compared with the original model.

Scaling of the Sloping Surfaces

When using the model to calculate the production rate of the cosmogenic nuclides, the most important precondition is that all the production processes happened below a horizontal plan surface. However, the real situation is always that most

samples were collected from sloping surfaces; this kind of circumstance may partially block the cosmic radiation.

Besides, since the cosmic radiation is almost vertical to the Earth surface, the sloping surfaces will decrease the effective surface area perpendicular to the cosmic rays. Also, the change in the angle between the cosmic rays and the surface of the mineral can affect the attenuation length (Gosse and Phillips, 2001).

Scaling of the surface coverage

Sometimes, the sample's surface would be covered throughout its geological history, which will reduce the intensity of the cosmic rays penetrated. Snow is the one of the most common influences. At any time, when the surface is covered by snow, the intensity of the cosmic rays can be described as below:

$$\Phi_{cover}(Z) = \Phi_0 e^{-Z/\Lambda} \tag{3.4}$$

in which the Φ_0 is the intensity of cosmic rays when they penetrate a horizontal surface without surface coverage (particles cm^{-2} yr^{-1}), Φ_{cover} is the cosmic-ray flux when Φ_0 penetrates through the coverage (particles cm^{-2} yr^{-1}), Z is the mass of the surface coverage per unit area (g cm^{-2}), Λ means the attenuation length of the cosmic rays when they penetrate a horizontal surface without surface coverage (g cm^{-2}).

Figure 3.4 represents a most used scaling for the coverage of snow, with different depths or snow densities. It should be mentioned here that in this model, the surface was shielded for 4 months each year (Gosse and Phillips, 2001).

In 1996, Onuchin and Burenina (1996) developed equations to calculate the scaling factors of three other influences on the production rate of cosmogenic nuclides: the thickness of snow coverage, the temperature of air, and the total time of snow coverage, based on the scaling factor of snow density.

3.4 Methodology

In the 2nd chapter, we have demonstrated that recycled sediments were most probably carried into the mainstream through the tributaries or the erosion of paleosediments by the mainstream. Also, it has also been demonstrated that the recycled sediments changed the portion of large pebbles within the mainstream. Based on the result of grain sizes analysis, the pebbles collected from Casper are considered to mainly be derived from lateral sediment inputs; for the samples collected from R15726 and Keystone, all of the large pebbles are thought to come from lateral sediment inputs. Because we have known the places where lateral sediment inputs exist, it is possible to find more information about recycling from

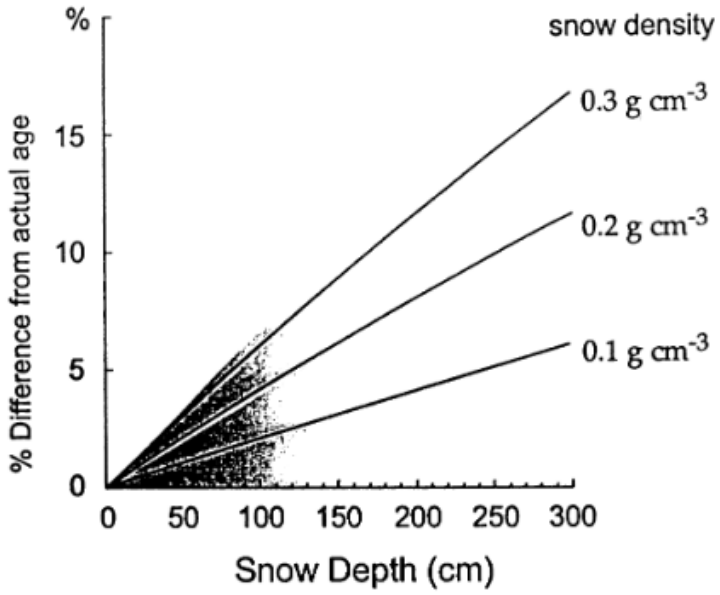

Figure 3.4: Effects of shielding by snow of common densities and thicknesses. In the simulation the surface was shielded instantaneously by snow for 4 months each year (Gosse and Phillips, 2001).

the grain collected from these localities. Using the method of TCN analysis, the duration of being exposed and being burial can be assessed.

3.4.1 Accumulation of Cosmogenic Nuclides in the Great Plain

When calculating concentrations of any cosmogenic nuclides it is vital to account for every source of nuclide accumulation. The concentration of ^{21}Ne will increase when the sediments are retained at and near the surface. The sediments preserved in the Great Plains have had some opportunities to accumulate cosmogenic neon: exposure in the near surface during exhumation, fluvial transport processes, storage in the fluvial network, and final deposition. For the concentration of cosmogenic ^{21}Ne contained within the pebbles collected from the river, short-term exposure process includes exposure during the fluvial transport, which lasted for a time range of 10-10^2 years. Long-term exposure includes storage in the fluvial network and then being recycled by channel switching and reworking, incision, and aggradation, which lasted for a time range of 10-10^7 years (Figure 3.5).

A problem related to the concentrations of the cosmogenic nuclides is that the cosmogenic nuclides within the sediments will evolve downstream as a result of varying histories of transport. For old recycled sediments, the build-up of cosmogenic nuclides might mainly come from a exposure history of several

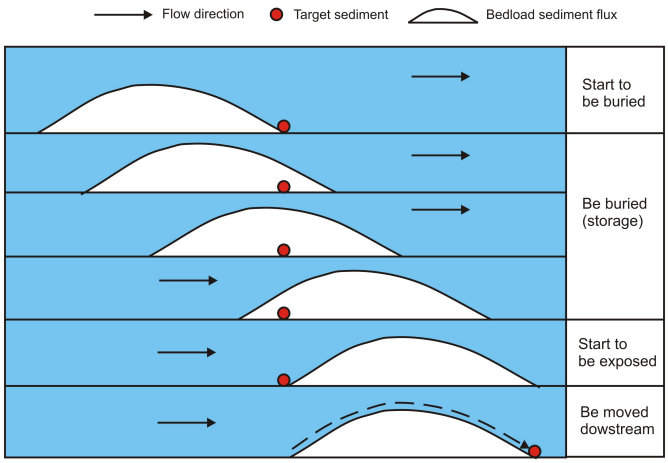

(a) Short-term exposure: exposure during fluvial transport, Time scale: 10-10^2 years

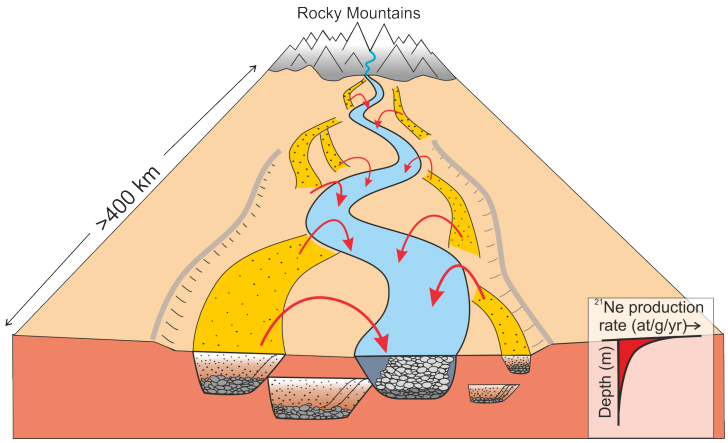

(b) Long-term exposure: storage in the fluvial network and then being recycled (plan view), Time scale: 10-10^7 years

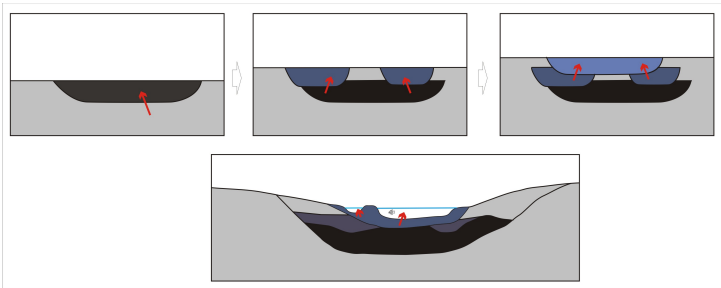

(c) Long-term exposure: storage in the fluvial network and then being recycled (section view), Time scale: 10-10^7 years

Figure 3.5: Schematic representations showing the exposure processes with different time ranges. a. Short-term exposure: exposure during fluvial transport, Time scale: 10-10^2 years; b.& c. Long-term exposure: storage in the fluvial network and then being recycled by channel switching and reworking, incision, and aggradation, Time scale: 10-10^7 years

thousand years, but not the slowly accumulation over millions of years of deep burial. So in this chapter, considering how to distinguish the exposure time from that of burial time is the main problem needed to solve with tools of cosmogenic nuclides.

3.4.2 Sampling and Measurement Strategy

It is vital to get the sampling strategy correct. As mentioned above, quartz has some comparative advantages so that the samples to be collected should be quartz-rich.

The accumulation of the cosmogenic nuclides of modern samples is shown in Figure 3.6. In this figure, the dashed lines, with circles of different colours, represent the accumulation of cosmogenic nuclides in different transport paths. In which the circles represent the concentration of cosmogenic nuclides; the larger the circle, the more the cosmogenic nuclides contained within the grain. The red circles represent the accumulation of ^{21}Ne within the sediments carried directly in the channel. While the green and blue circles represent the accumulation of ^{21}Ne within the sediments which have experienced deposition and recycling. Because the sediments which have experienced recycling have been exposed on the earth's surface for a longer time, they have accumulated more ^{21}Ne than those of the sediments carried directly in the channel. And that's why the green and blue circles are larger than the red circles.

Using cosmogenic Ne as the example, when the quartz-rich rocks were buried deeply at the source, their concentration of ^{21}Ne is non-cosmogenic neon. When they were denuded, eroded downhill from the source, and started to move along the river, cosmogenic neon started to accumulate. In order to extract the real concentration of cosmogenic ^{21}Ne, we have to constrain the content of non-cosmogenic Ne generated. Therefore, two kinds of modern samples need to be collected: shielded samples from the source, for the evaluation of background neon, and standard modern samples, for the calculation of cosmogenic neon.

In order to get the background concentration of non-cosmogenic ^{21}Ne, samples of shielded, two primary quartz-bearing basement lithologies (Medicine Bow Quartzite and the Laramie Range Sherman Granite) were collected.

We have also collected tens of standard modern samples from two different localities downstream (R15726 and Keystone as Figure 2.21), and several samples of shielded Pliocene/Miocene samples. The detail of the samples collected are as follows:

(1) Three Sherman Granite (T = 1.4 Ga) and one granitic gneiss (T = 1.7 Ga) bedrock were taken from the base of road-cuts in the Wyoming Front range in the upper catchment of the North Platte River. (Collected by Louise McCann)

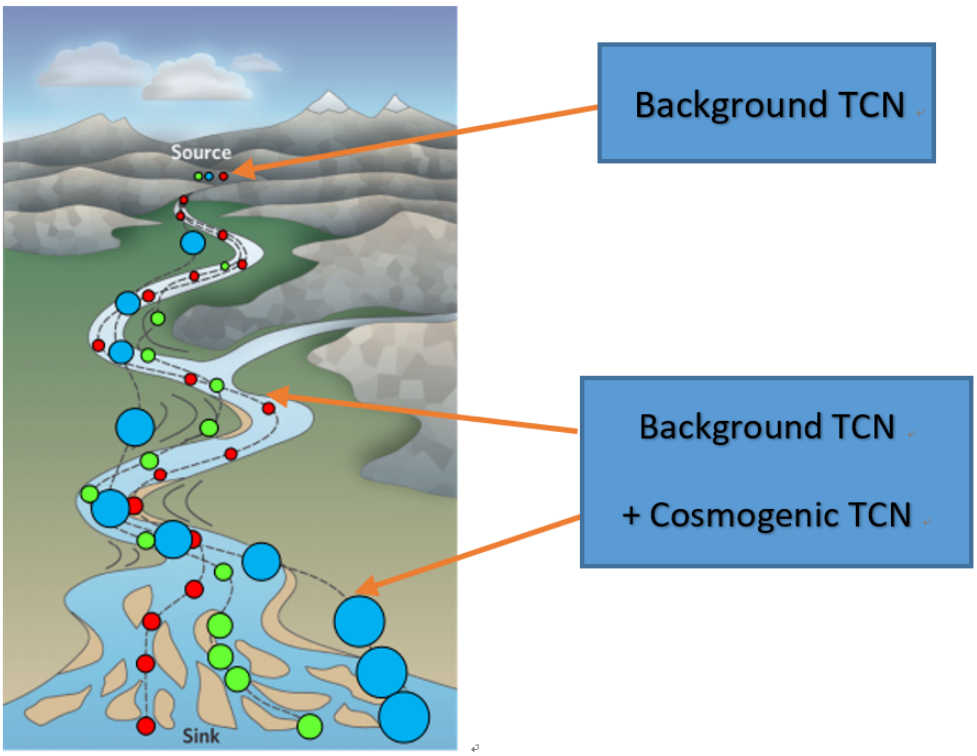

Figure 3.6: The dashed lines, with circles of different colours, represent the accumulation of cosmogenic nuclides in different transport paths. In which the circles represent the concentration of cosmogenic nuclides; the larger the circle, the more the cosmogenic nuclides contained within the grain. The red circles represent the accumulation of ^{21}Ne within the sediments carried directly in the channel. While the green and blue circles represent the accumulation of ^{21}Ne within the sediments which have experienced deposition and recycling.

(2) Five shielded bedrock samples from the Medicine Bow Quartzites. (Collected by Louise McCann)

(3) Twelve exposed pebbles from paleosediments of Pliocene about 200 km away from the border of Wyoming and Nebraska downstream the North Platte River. (Collected by Louise McCann, Zui Tao and Hugh Sinclair)

(4) Eleven exposed pebbles from paleosediments of Miocene about 200 km away from the border of Wyoming and Nebraska downstream the North Platte River. (Collected by Louise McCann, Zui Tao and Hugh Sinclair)

(5) Thirty-two exposed pebbles from Keystone, NE, USA, 1053 km downstream the North Platte River. These samples are all modern. (Collected by Zui Tao and Hugh Sinclair)

(6) Twenty-eight exposed pebbles near the conjunction Road 157 and Road 26 (R15726), the samples are all modern. (Collected by Zui Tao and Hugh Sinclair)

As the first step, the samples were crushed using a jaw crusher and grounded using a pulveriser to obtain grains which are mostly mono-minerallic. The samples were then sieved into a size of 250-710 μm.

Next, the sieved samples were heated in 1:1 HCl with 0.03% of H_2O_2 (about 1g sample per 10ml) to dissolve carbonates and iron oxides. Then the samples were washed with deionised H_2O for several times. The washed samples were kept.

Next, the samples were leached with a dilute HF-HNO_3 mixture to dissolve the outer 40 μm of the target grains in order to reduce the concentration of non-cosmogenic nuclides. Every one gram of samples need about 135 ml of 1% HF-1% HNO_3 mixture. During the leaching process, the sample-acid mixture is being agitated for nine hours in an ultrasonic bath, and the temperature was set as about 95 ℃. Then the samples were washed again with the rinse water for several times. The washed samples were kept. This acid-leaching step can be repeated for two to four times when necessary. The concentration of acid should be reduced as 1/2 to 1/3, for the second to the fourth time of leaching, compared to that of the first time of leaching.

Acid leached samples were then carried to the Scottish Universities Environmental Research Centre (SUERC). The quartz grains are heated in the furnace of the noble gas mass spectrometer to get the real concentration of ^{21}Ne and ^{22}Ne. All the preparation analysis at the SUERC followed established procedures (Codilean et al., 2008). The CREU quartz standard (Vermeesch et al., 2015) was analysed throughout all analytical periods as an internal check on procedures.

3.4.3 Initial Investigation of Inherited ^{21}Ne

The non-atmospheric Ne (Ne*) in detrital quartz is mostly composed of background Ne (Ne_{back}), and depositional cosmogenic Ne (Ne_{cos}). It should be minded that the background Ne contains not only the nucleogenic nuclides generated over the time of the rock but also some cosmogenic Ne generated when it was exposed to the cosmic rays during the formation of the rock. The depositional cosmogenic Ne (Ne_{cos}) can further be divided into those generated during bedrock exhumation (Ne_{cosE}) and those generated during transport and storage in the fluvial system (Ne_{cosTS}). The inherited cosmogenic Ne is the combination of Ne_{back} and Ne_{cosE}.

Calculation of background Ne (Ne_{back})

To determine the Ne_{back} concentration, we can use the shielded rocks from the source. There are two primary quartz-bearing sources with different basement lithologies supplying quartz to the North Platte, namely the Medicine Bow (quartzite) and the Laramie Range Sherman (granite/gneiss). Without knowing the provenance of the quartz, the non-cosmogenic neon from both lithologies has to be accounted for and corrected for. An initial investigation needs to be undertaken to test the feasibility of quartz with different sources.

As shown in Table 3.1 and Table 3.2, the shielded MBq samples from the quartzite have concentrations of inherited nucleogenic ^{21}Ne of 0.22–0.77 $\times$ 10^7 atoms/g. Moreover, for the shielded granite/gneiss collected from the Laramie Range Sherman, the concentrations are higher (3.30 –11.7 $\times$ 10^7 atoms/g).

Table 3.1: Results of background ^{21}Ne of quartzite collected from the Medicine Bow

File	Sample	Weight (mg)	21Ne/20Ne	d	21Ne atoms/g	d	22Ne/20Ne	d
bz057	Qz7 (2) A	115.6	0.00567	0.00028	6.09E+06	1.50E+06	0.1069	0.0018
bz058	Qz8 (a)	174	0.00481	0.00015	7.70E+06	9.70E+05	0.1038	0.0007
bz097	Qz7 (1) B	146.3	0.00654	0.00047	7.29E+06	1.90E+06	0.1058	0.0017
bz098	Qz5 B	131.5	0.00345	0.0001	2.19E+06	1.10E+06	0.1034	0.0006

We can then plot the Ne isotope compositions of two different lithologies on the three-isotope plot (Figure 3.7 and 3.8).

As suggested by Figure 3.7, the Ne isotope compositions within quartzite are plotted near the air-spallation mixing line, and the concentrations of these samples are concentrated within a small plotting area. This means that if the samples collected from the Medicine Bow were used, the result would represent a

Table 3.2: Results of background ^{21}Ne of granite/gneiss collected from the base of road-cuts in the Wyoming Front range

File	Sample	Weight (mg)	21Ne/20Ne	d	21Ne atoms/g	d	22Ne/20Ne	d
bo041	LRGR1 A	94.9	0.0039	0.000047	4.60E+07	1.60E+06	0.10557	0.00039
bp012	LRGR2 A	170.1	0.01274	0.000128	1.17E+08	3.80E+06	0.12745	0.0006
bp022	MBGn A	187.8	0.00956	0.000149	3.30E+07	1.20E+06	0.10996	0.00058
br096	Gr2gB	132.3	0.01495	0.000493	1.37E+08	7.30E+06	0.11584	0.00154

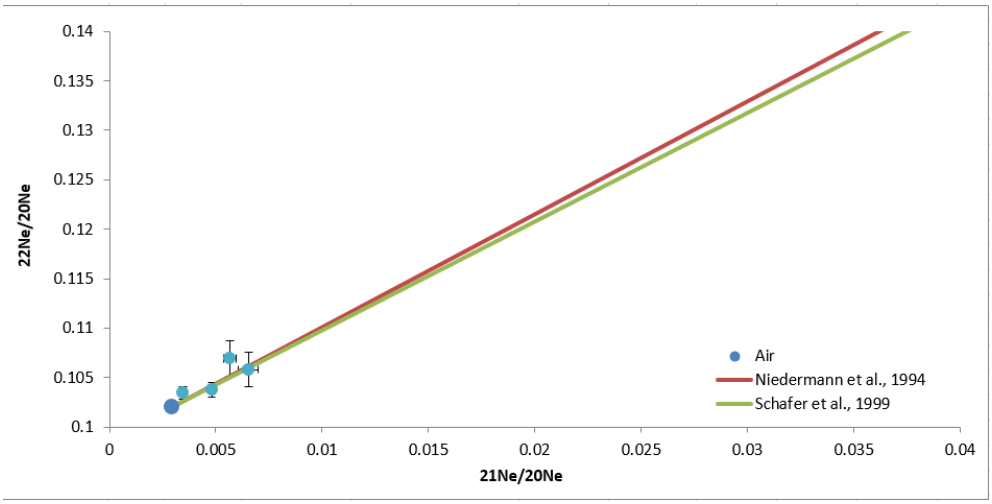

Figure 3.7: Neon ratios with ^{22}Ne/^{20}Ne plotted against ^{21}Ne/^{20}Ne with errors (Basement Quartzite collected from the Medicine Bow).

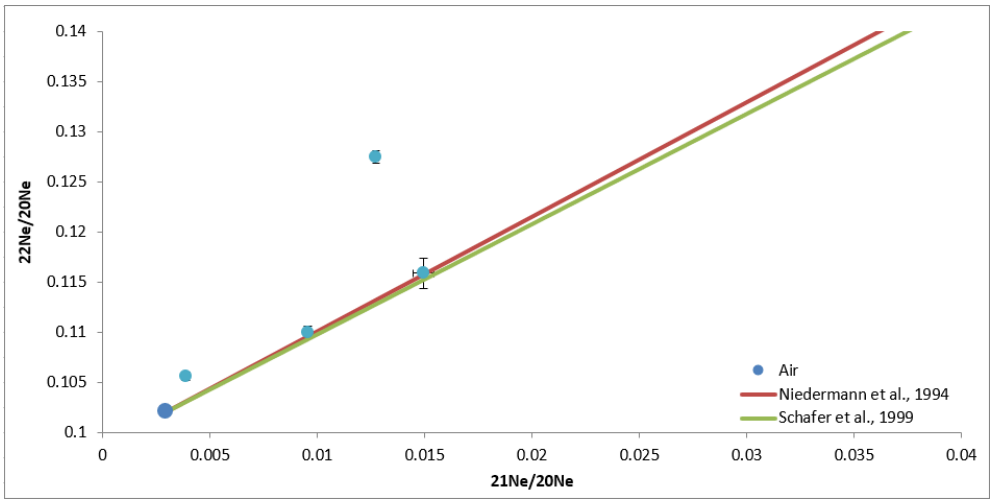

Figure 3.8: Neon ratios with ^{22}Ne/^{20}Ne plotted against ^{21}Ne/^{20}Ne with errors (granite/gneiss collected from the base of roadcuts in the Wyoming Front range).

stable level of ^{21}Ne concentration. Being stable is a good quality for the samples to be regarded as reliable.

In contrast, as suggested by Figure 3.8, the Ne isotope compositions within Granite/Gneiss are not stable; they are far away from each other. One of them is located very far away from the air-spallation mixing line. These make the quartzite of granite/gneiss unreliable as the target sample.

Also, a cosmogenic signal has to be strong enough to overcome the inherited background neon. For these two types of lithologies collected from two different localities, the Laramie Range Sherman Granite background samples yielded a much higher background Ne concentration than those of Medicine Bow Quartzite (Table 3.1 and Table 3.2). Furthermore, granite/gneiss contain some other minerals besides quartzite which will increase complexity and systematic error. Therefore, it was decided to choose the quartzite pebbles collected from the Medicine Bow as the target lithology for detrital cosmogenic nuclides analysis in this chapter.

Calculation of Ne Generated during the Exhumation (Ne_{cosE})

For the inherited cosmogenic neon, another part is generated during the exhumation, called Ne_{cosE}. Before the calculation of ^{21}Ne generated during the exhumation, the exhumation rate of the study area is needed. Detrital sands from streams flowing on the exposed quartzites of the Medicine Bow Mountains have been used to calculate exhumation rates of bedrock. ^{10}Be concentrations contained within these detrital sands is 0.32×10^7 atoms ^{10}Be/g (Dethier et al., 2014), based on which the slowest mean exhumation rate of the southern Rocky Mountains can be calculated as 9 mm/k.y. (Dethier et al., 2014). $^{21}Ne_{cosE}$ concentration of 0.08×10^7 atoms/g can be then calculated with the ^{10}Be/^{21}Ne production rate ratio of Balco and Shuster (2009). Using the upper limits for both $^{21}Ne_{back}$ and $^{21}Ne_{cosE}$, the quartzite pebbles have inherited a maximum of 0.85×10^7 ^{21}Ne atoms/g before downstream transport.

3.4.4 Result of the Analysis on Modern Pebbles

In the 2^{nd} chapter, the result of grain size analysis provides three potential sites for the localities of the lateral sediment inputs along the North Platte River: Casper, R15726 and Keystone. Two sites of these three, R15726 and Keystone were chosen to do cosmogenic nuclides analysis on pebbles in the river.

For each point, tens of standard modern quartzite pebbles were collected. In this study, all the gravels were collected from exposed bars and close to the North Platte River. As mentioned in the 2^{nd} chapter, this choice has several advantages: (1) coarse sediments are easily distinguished on the bar; (2) this place has the most extensive range of grain sizes collected; (3) this place is the

closest exposed site to the channel thus has the most reliable relationship with the hydraulic mechanisms (Rice, 1998). Also, in order to erase the influences of different sources on the lithologies of the samples, quartzite pebbles with the only source of the Medicine Bow Mountain were collected.

These gravel bars are always 100 m^2 or larger. During the sampling, gravels were collected from different localities on a gravel bar to reduce the errors resulted from the variable localities of the bar. Moreover, to avoid the influences of the grain sizes on the accumulation of cosmogenic nuclides, pebbles were collected with sizes within the range of 2 to 2^3 cm evenly. It should be mentioned that because ^{10}Be analysis consume much more on the mass of the samples than that of ^{21}Ne, all the samples prepared for the ^{10}Be analysis are picked out with sizes of about 2^3 cm. Samples were taken to the University of Edinburgh and the Scottish Universities Environmental Research Centre (SUERC) to conduct laboratory analysis. The concentrations of cosmogenic ^{21}Ne were acquired, and the results are shown in Table 3.3 and Table 3.4.

In Table 3.3 and Table 3.4, the corrected ^{21}Ne is calculated by subtracting 0.85 $\times$ 10^7 atoms inherited ^{21}Ne per gram from the absolute concentrations of ^{21}Ne*.

We also plot these data on the three-isotope plot in order to check if these data are all cosmogenic neon. (Shown in Figure 3.9 and 3.10).

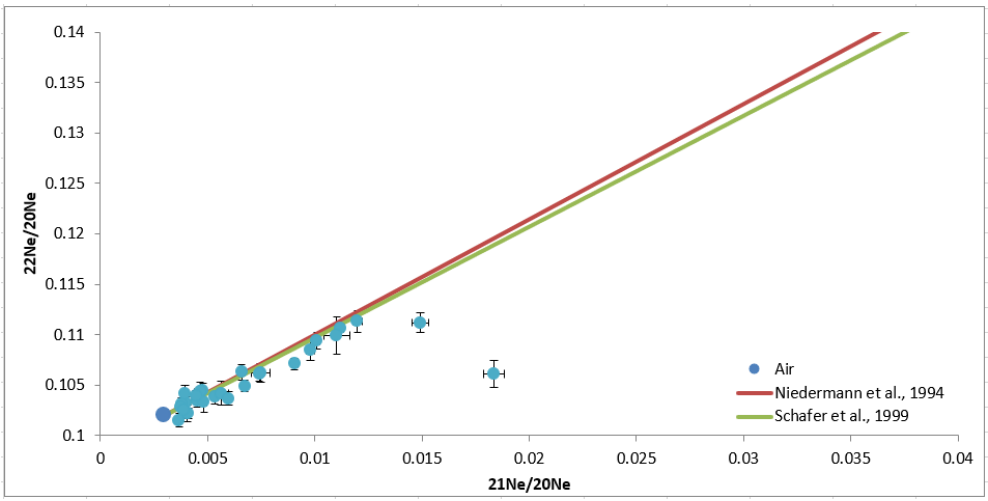

Figure 3.9: Neon ratios with ^{22}Ne/^{20}Ne plotted against ^{21}Ne/^{20}Ne for the samples collected from R15726, with errors

As suggested by Figure 3.10, for the samples collected from Keystone, all the points are plotted on or near the air-spallation line. However, for the samples collected from R15726 (Figure 3.9), two points are too far away from the line. This deviation of points from the air-spallation line means that the ^{21}Ne contained within these two samples are not pure cosmogenic ^{21}Ne. For the calculation of exposure time in the next stage, it should be guaranteed that all the ^{21}Ne are

Table 3.3: Results of pebble study of R15726, with the corrected ^{21}Ne (subtracting background concentration)

File	21/20cor (calibration)	d	22/20 (calibration)	d	21Ne* (atoms/g)	d	Corrected 21Ne (atoms/g)
DK085	0.004	0.00004	0.1033	0.0006	4.28E+07	2.20E+06	3.43E+07
DK091	0.01011	0.00013	0.1094	0.0008	9.59E+07	3.42E+06	8.74E+07
DK092	0.01199	0.00023	0.1113	0.0011	7.63E+07	3.08E+06	6.78E+07
DK094	0.00478	0.00007	0.1044	0.0007	1.04E+08	5.42E+06	9.59E+07
DK096	0.00381	0.00011	0.1031	0.0006	1.71E+07	2.37E+06	8.61E+06
DK097	0.00451	0.00007	0.1034	0.0006	3.62E+07	2.07E+06	2.77E+07
DK108	0.00394	0.00012	0.1042	0.0008	2.41E+07	3.28E+06	1.56E+07
DK109	0.00403	0.00011	0.1022	0.0008	1.63E+07	1.90E+06	7.82E+06
DK110	0.00906	0.00014	0.1071	0.0006	1.12E+08	4.26E+06	1.03E+08
DK111	0.0041	0.00004	0.1022	0.0005	2.82E+07	1.29E+06	1.97E+07
DK113	0.00483	0.00013	0.1033	0.001	2.48E+07	1.97E+06	1.63E+07
DK114	0.00673	0.00007	0.1049	0.0006	1.99E+08	7.12E+06	1.90E+08
DK115	0.00377	0.00008	0.1029	0.0006	1.70E+07	1.92E+06	8.46E+06
DK117	0.00533	0.00014	0.1038	0.0007	3.86E+07	2.68E+06	3.01E+07
DK122	0.00465	0.00028	0.1043	0.0009	1.96E+07	3.47E+06	1.11E+07
DK123	0.00564	0.00032	0.1042	0.0011	2.52E+07	3.24E+06	1.67E+07
DK128	0.00981	0.00021	0.1085	0.001	6.15E+07	2.70E+06	5.30E+07
DK129	0.01118	0.00017	0.1106	0.0007	1.82E+08	6.73E+06	1.73E+08
DK130	0.01102	0.00059	0.1099	0.0018	3.63E+07	3.01E+06	2.78E+07
DK131	0.00748	0.00042	0.1062	0.0009	2.63E+07	2.69E+06	1.78E+07
DK135	0.0074	0.0001	0.1062	0.0007	5.55E+07	2.14E+06	4.70E+07
Dk140	0.00659	0.00014	0.1063	0.0007	1.19E+08	6.07E+06	1.10E+08
Dk141	0.00367	0.00006	0.1015	0.0006	2.27E+07	2.24E+06	1.42E+07
Dk142	0.00448	0.00006	0.1039	0.0006	7.93E+07	4.07E+06	7.08E+07
DK147	0.0039	0.00017	0.1026	0.0007	2.00E+07	3.91E+06	1.15E+07
DK148	0.00597	0.00014	0.1037	0.0007	4.24E+07	2.48E+06	3.39E+07
DK126	0.01492	0.00039	0.1112	0.001	9.06E+07	4.11E+06	8.21E+07
DK124	0.01836	0.00048	0.1061	0.0014	1.27E+08	5.62E+06	1.18E+08

Table 3.4: Results of pebble study of Keystone, with the corrected ^{21}Ne (subtracting background concentration)

File	21/20cor (calibration)	d	22/20 (calibration)	d	21Ne* (atoms/g)	d	Corrected 21Ne (atoms/g)
bz106	0.00457	0.0001	0.1042	0.0004	1.76E+07	1.43E+06	9.13E+06
bz107	0.00321	0.00004	0.1018	0.0002	1.09E+07	2.49E+06	2.44E+06
bz108	0.0093	0.00017	0.1097	0.0008	5.70E+07	2.47E+06	4.85E+07
bz114	0.00626	0.00012	0.1053	0.0008	3.00E+07	1.62E+06	2.15E+07
bz117	0.00466	0.00009	0.1039	0.0005	2.98E+07	1.98E+06	2.13E+07
bz121	0.00465	0.00021	0.1036	0.0008	1.51E+07	2.39E+06	6.58E+06
bz137	0.00624	0.00021	0.1055	0.0015	1.47E+07	1.27E+06	6.19E+06
bz138	0.00549	0.00012	0.1051	0.0006	2.12E+07	1.34E+06	1.27E+07
bz139	0.01063	0.00038	0.1129	0.0041	2.05E+07	1.62E+06	1.20E+07
bz141	0.00382	0.00007	0.1034	0.0005	1.61E+07	1.62E+06	7.56E+06
bz142	0.00611	0.00013	0.1049	0.0007	6.18E+07	3.42E+06	5.33E+07
bz145	0.01015	0.00078	0.1097	0.0008	5.95E+07	7.14E+06	5.10E+07
bz146	0.00572	0.00014	0.105	0.0011	2.81E+07	1.86E+06	1.96E+07
cb074	0.00841	0.00015	0.1096	0.0011	5.37E+07	2.47E+06	4.52E+07
CZ115	0.01052	0.00019	0.1099	0.0012	3.40E+07	1.36E+06	2.55E+07
CZ116	0.00733	0.00019	0.1084	0.001	2.54E+07	1.35E+06	1.69E+07
CZ120	0.01131	0.00029	0.111	0.0011	4.10E+07	1.89E+06	3.25E+07
CZ121	0.00366	0.00006	0.1024	0.0005	2.06E+07	1.95E+06	1.21E+07
CZ124	0.00399	0.00019	0.1024	0.0041	1.03E+07	1.99E+06	1.77E+06
CZ127	0.00561	0.00011	0.1042	0.0009	2.94E+07	1.47E+06	2.09E+07
CZ126	0.0063	0.00008	0.1061	0.0013	2.77E+07	1.09E+06	1.92E+07
CZ132	0.00411	0.00006	0.1009	0.0006	3.86E+07	2.27E+06	3.01E+07
CZ136	0.01585	0.00029	0.116	0.001	8.75E+07	3.29E+06	7.90E+07
CZ137	0.00997	0.00013	0.1085	0.0012	3.11E+07	1.11E+06	2.26E+07
CZ138	0.01505	0.00014	0.1145	0.0008	1.29E+08	4.18E+06	1.20E+08
CZ141	0.01119	0.00028	0.11	0.0013	2.96E+07	1.38E+06	2.11E+07
CZ142	0.00748	0.0001	0.1052	0.0007	7.41E+07	2.78E+06	6.56E+07
Dk143	0.00409	0.00012	0.1049	0.0012	1.05E+07	1.34E+06	1.95E+06
Dk144	0.00522	0.0002	0.104	0.0007	3.61E+07	3.47E+06	2.76E+07
Dk145	0.00414	0.00007	0.1023	0.0005	5.60E+07	3.85E+06	4.75E+07
DK149	0.00396	0.00005	0.1021	0.0006	4.76E+07	3.06E+06	3.91E+07
DK150	0.00496	0.00011	0.103	0.0007	3.93E+07	2.63E+06	3.08E+07

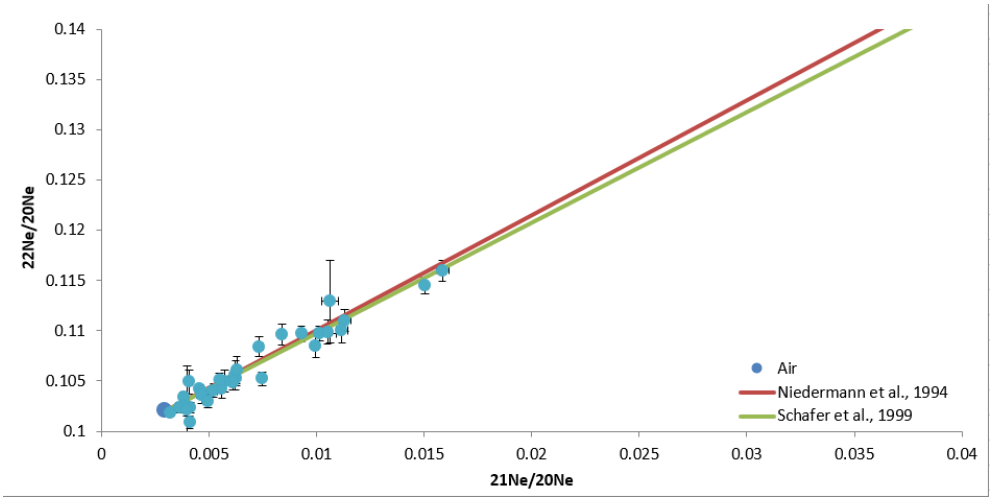

Figure 3.10: Neon ratios with $^{22}Ne/^{20}Ne$ plotted against $^{21}Ne/^{20}Ne$ for the samples collected from Keystone, with errors

cosmogenic ^{21}Ne. So that these two samples with abnormal concentration of ^{21}Ne were abandoned.

3.4.5 Result of the Analysis on Pebbles of Miocene/Pliocene Age

In the previous chapter, the existence of recycling was proved in the Great Plains, but this is the recycling happened during the modern time. Did recycling happen in the Great Plains during the older time? To gain more information and get clear how the fluvial sediments deposited in the Great Plains might change through geological time, analysis on the ancient samples are also needed.

During the Miocene, tectonic activities dominated in the mountain area, like renewed faulting. These activities led to the uplift of the mountain area and the erosion at the east side of the Rockies (Scott, 1975; Epis et al., 1976; Flanagan et al., 1993; Mears Jr, 1993). This erosion resulted into an unconformity on the older strata (Swinehart et al., 1985). Ogallala Group is used to name this group above the erosion. Moreover, in 8-6 Ma, the Rocky Mountains and Great Plains experienced another spike of an incision (McMillan et al., 2002; Wobus et al., 2010). During these time, tectonic activities contributed to changing fluvial systems spreading across the Great Plains (shown in Figure 2.5). Moreover, these channel-induced incisions happened in the Miocene and Pliocene resulted in the potential of recycling sediments happening during the Miocene time and Pliocene time. Accordingly, the samples of Miocene and Pliocene were also collected here, and the sampling site is shown in Figure 3.11.

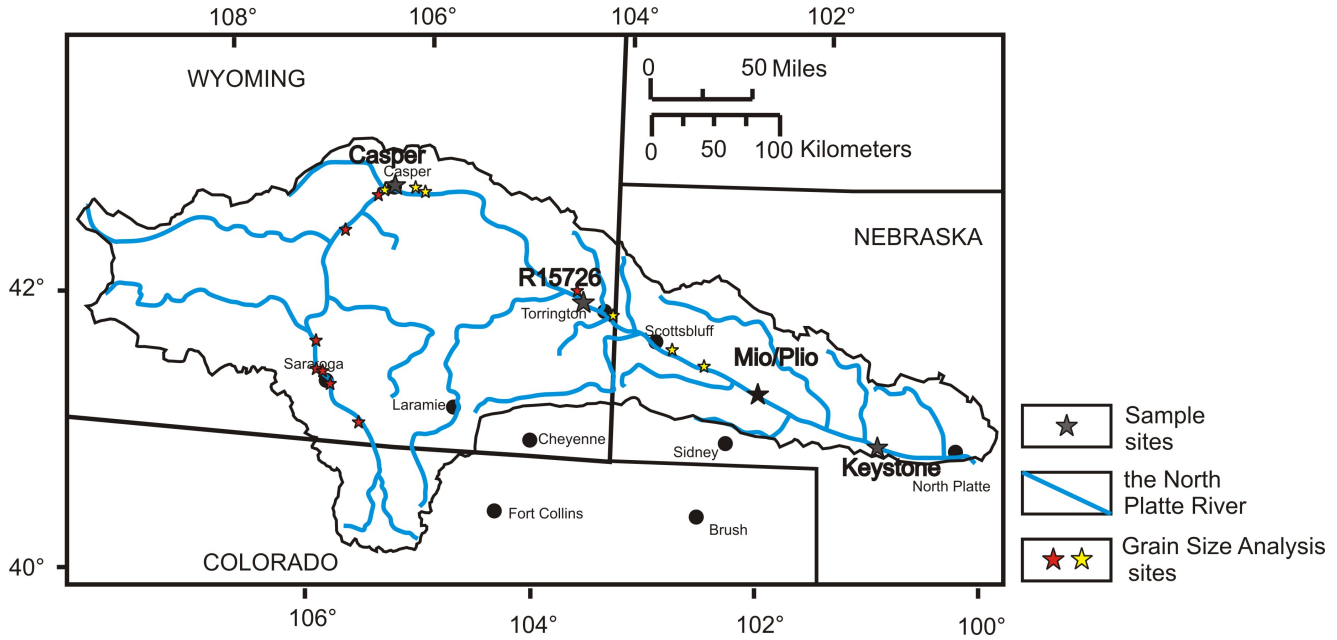

Figure 3.11: Locations of samples collected, for Miocene and Pliocene, marked as a black pentagram.

12 and 11 sheltered samples of Miocene and Pliocene were collected, respectively. Similarity, the concentration of cosmogenic ^{21}Ne contained within these samples were calculated. The results are shown in Table 3.5 and Table 3.6.

Table 3.5: Results of pebble study, Pliocene, with the corrected ^{21}Ne (subtracting background concentration)

File	21/20cor (calibration)	d	22/20 (calibration)	d	21Ne* (atoms/g)	d	Corrected 21Ne (atoms/g)
BZ147	0.0107	0.00021	0.1096	0.0008	4.58E+07	1.99E+06	3.73E+07
bz170	0.00394	0.00015	0.1035	0.0006	9.77E+06	2.13E+06	1.27E+06
bz171	0.01006	0.00026	0.1104	0.0017	3.56E+07	1.87E+06	2.71E+07
BZ172	0.0036	0.00007	0.1039	0.0009	1.45E+07	2.01E+06	6.00E+06
BZ173	0.00659	0.00022	0.1049	0.0018	3.52E+07	2.63E+06	2.67E+07
bz177	0.00974	0.00019	0.1078	0.0007	6.35E+07	2.73E+06	5.50E+07
bz180	0.00637	0.00044	0.1053	0.0009	2.94E+07	4.49E+06	2.09E+07
BZ196	0.0125	0.00023	0.1125	0.0007	6.36E+07	2.59E+06	5.51E+07
cb043	0.01443	0.00019	0.1136	0.0009	6.87E+07	2.47E+06	6.02E+07
cb048	0.00708	0.00007	0.1061	0.0006	6.11E+07	2.22E+06	5.26E+07
cb065	0.00524	0.00003	0.105	0.0005	2.62E+07	9.38E+05	1.77E+07
cb073	0.01907	0.00027	0.1158	0.0009	6.80E+07	2.45E+06	5.95E+07

As suggested by the paleochannels systems in the Figure 3.12, both the paleochannels of the Pliocene time (the Broadwater Formation) and the Miocene time (the Ogallala Group) were sourced from the mountain area and have similar flow path as that of the modern North Platte River. Therefore, the inherited cosmogenic nuclides used in the calculations were set as the same as that for the modern pebbles, which is 0.85×10^7 ^{21}Ne atoms/g.

Also, in order to see whether these data are all cosmogenic neon, these data were plotted on the three-isotope plot (shown in Figure 3.13 and Figure 3.14).

As suggested by Figure 3.13 and 3.14, most of the concentration of ^{21}Ne contained within Pliocene and Miocene samples are plotted on or near the spallation line, indicating that they are reliable for the following analysis.

3.5 Cosmogenic Nuclides Analysis

3.5.1 More Evidence of Recycling

In our research area, quartzite pebbles have been collected 1400 km downstream from the source of the quartzites in the Medicine Bow Mountains (Figure 3.15). In the previous study of Paola et al. (1992), the large pebbles found far away from the source were explained with repeated bed-load transport during bankful

Table 3.6: Results of pebble study, Miocene, with the corrected ^{21}Ne (subtracting background concentration)

File	21/20cor (calibration)	d	22/20 (calibration)	d	21Ne* (atoms/g)	d	Corrected 21Ne (atoms/g)
BZ148	0.00465	0.0001	0.1049	0.0006	1.48E+07	1.20E+06	6.30E+06
BZ150	0.00765	0.00023	0.1089	0.0009	3.61E+07	2.26E+06	2.76E+07
bz166	0.00489	0.0001	0.1033	0.0011	4.42E+07	2.97E+06	3.57E+07
bz169	0.00452	0.00013	0.1041	0.0007	1.08E+07	1.29E+06	2.30E+06
BZ176	0.0043	0.00012	0.1032	0.0004	2.09E+07	2.23E+06	1.24E+07
bz197	0.00336	0.00007	0.1026	0.0004	1.45E+07	2.77E+06	6.00E+06
cb034	0.00355	0.00003	0.1033	0.0006	1.98E+07	1.24E+06	1.13E+07
cb036	0.00443	0.00007	0.1031	0.0017	3.42E+07	2.23E+06	2.57E+07
cb037	0.01428	0.00011	0.1126	0.0007	3.21E+08	1.04E+07	3.13E+08
cb068	0.00414	0.00005	0.1024	0.0006	4.01E+07	2.12E+06	3.16E+07
cb072	0.01147	0.00007	0.1143	0.0008	3.30E+08	1.04E+07	3.22E+08

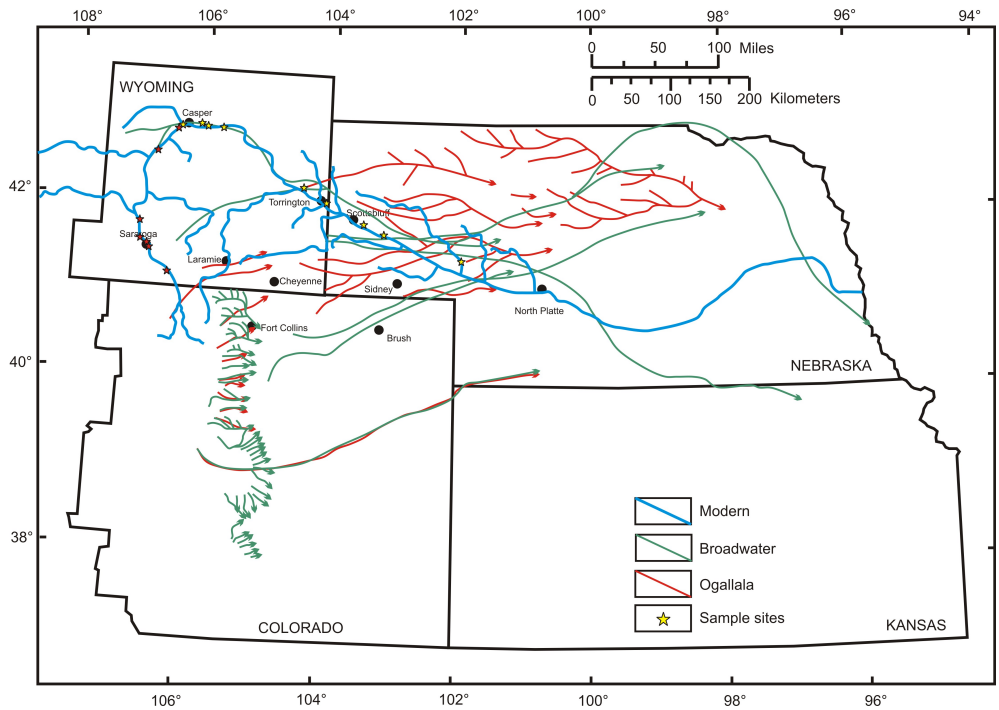

Figure 3.12: Paleochannels and modern channels of the Great Plain. The red lines represent the paleochannels of Ogallala; the green lines represent the paleochannels of Broadwater; the blue lines represent the North Platte River of modern time. The arrows represent flowing direction. The red stars and yellow stars represent the sample sites of the sharp group and the flat group, respectively (Condon, 2005).

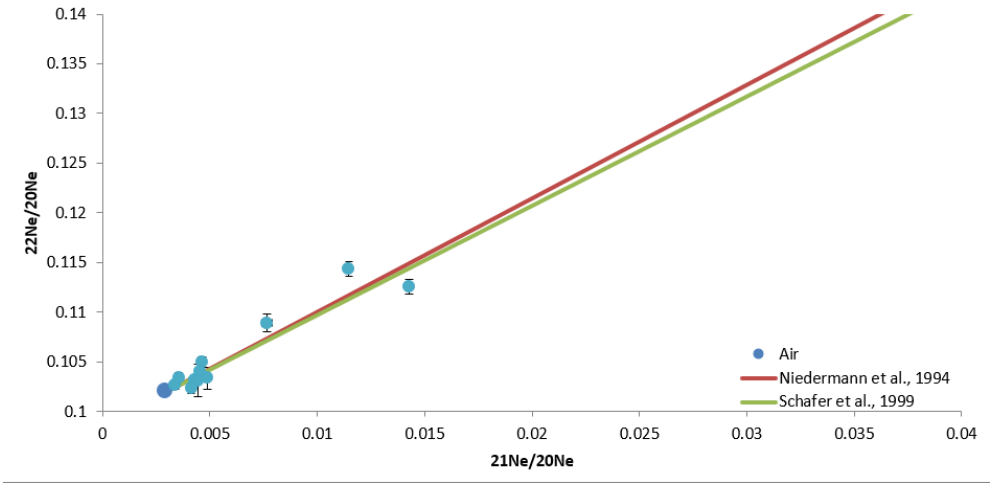

Figure 3.13: Neon ratios with $^{22}Ne/^{20}Ne$ plotted against $^{21}Ne/^{20}Ne$ (Miocene), with errors.

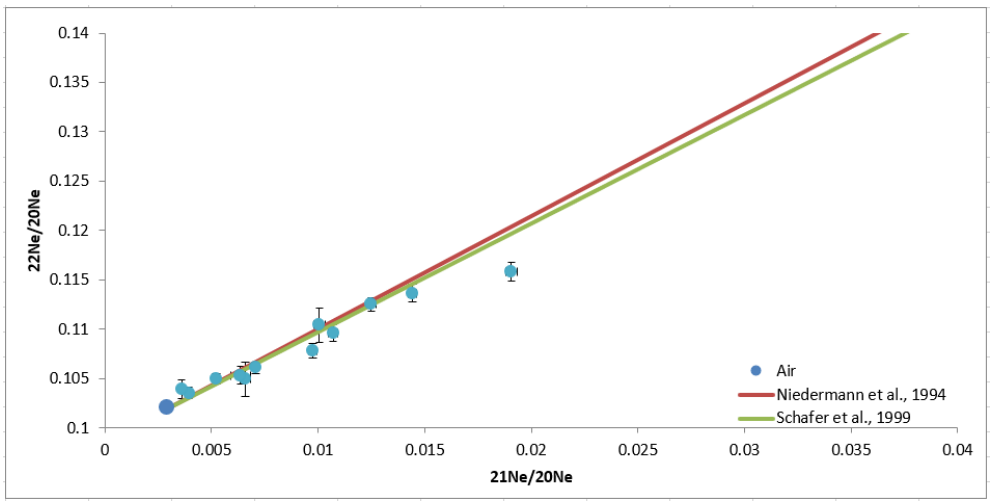

Figure 3.14: Neon ratios with $^{22}Ne/^{20}Ne$ plotted against $^{21}Ne/^{20}Ne$ (Pliocene), with errors.

discharge. However, repeated bed-load transport is not the only explanation to this situation, these abnormal distant pebbles might be resulted from the storage and recycling of the paleosediments. However, the relevant studies on recycling are far more than enough. Recycling is a kind of process that digging out the paleosediments and transforming them from storage to a new round of transportation. The result of the grain size analysis has provided evidence to support the existence of recycling. In the cosmogenic nuclides analysis, more evidence need to be found to support this concept.

Figure 3.15: Pebbles near Keystone which is more than 1400 km downstream from the source of Medicine Bow

Steady-State Model

A simple model called "Steady-State" was built. In this model, the pebbles transported along the river under "steady bed-load situation", which means these pebbles flowed with a constant transport rate and did not experience burial or recycling, and were constantly retained at the surface during the transport. Although in reality most of the pebbles would be buried within the bedform, this assumption provides an end member scenario to calculate the maximum possible cosmogenic neons accumulated during transport, $^{21}Ne_{cosTS}$, with the lowest migration rate downstream, without deposition, burial or recycling. This poses the question as to whether it would be reasonable to generate the measured quantities of $^{21}Ne_{cos}$ by fluvial transport alone.

To calculate the highest concentration of ^{21}Ne, we model with a constant slowest

migration rate. For this, three parameters need to be set: the production rate of ^{21}Ne, the slowest transport rate of coarse sediments and the moving distance.

Since the production rate of cosmogenic nuclides is a function of elevation and latitude. The river profile within the Medicine Bow Mountains and Keystone can be extracted using DEM (Digital Elevation Model). In the DEM, the data are stored in different pixels, and each pixel has its information of elevation and locality. Production rates of each pixel within the North Platte River were calculated using the scaling of Lal (1991). And the result is shown in Figure 3.16.

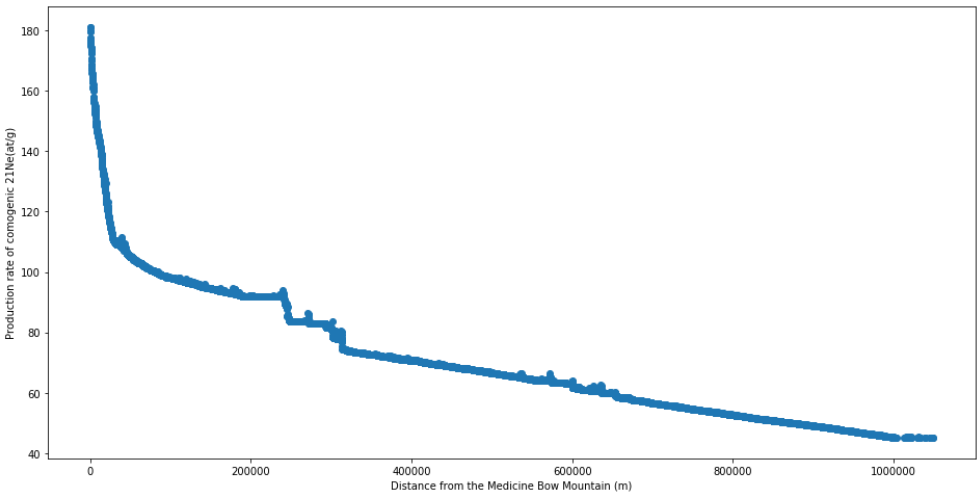

Figure 3.16: Production rates of cosmogenic ^{21}Ne within each pixels extracted using DEM of the North Platte River.

For the lowest transport rate, bedload transport rates in rivers can be estimated using bed shear stress equations for known grain-size populations and channel hydraulics (Meyer-Peter and Müller, 1948). Estimating these for a 1,400 km channel reach over thousands of years is unrealistic, so an alternative approach is presented: Estimating the required rate of sediment transport through the river network needed to discharge all the erosional sediment supply from the upstream catchment on a 10^5 yr timescale. Average erosion rates at this timescale (9-31 mm/kyr) are recorded by ^{10}Be concentrations in river sediments in the region (Dethier et al., 2014). The upstream catchment area of the North Platte River from the mountain front at the town of Douglas is 47336 km^2 based on the digital topography. By multiplying this area by the lowest erosion rate (9 mm/kyr), a conservative estimate of sediment yield from the catchment area of 4.26 *10^5 m^3/yr can be obtained. The bedload proportion can be estimated as between 1 and 10% (Turowski et al., 2010). Again, taking the conservative option of 1% gives a bedload flux of 4.3 * 10^3 m^3/yr. The average width of the North Platte River is 100 m, and the average depth is 1.5m based on documented bedform height (Crowley, 1983b). Therefore, we can get a time-averaged bedload sediment transport rate of 28.4m/yr. Using 31mm and 10% will give us a value of 978m/

yr. Long-term bedform migration rates of about 500 m/yr have been recorded from the Jamuna River, Bangladesh (Ashworth et al., 2000), suggesting that this calculation is not unreasonable.

For the transport distance, we use the point of Keystone which is about 1053 km from the source (Medicine Bow Mountains).

For the calculation of cosmogenic ^{21}Ne accumulated, in the 'Steady-State' model, each pixel extracted with DEM has its own length along the flowing direction, which can be defined using F_n, meter, in which n stands for the number of the pixel along the North Platte River.

In each pixel, the pebbles were transported on the surface of bedload with a constant migration rate of v in meters per year, so the transport time would be $t_n = F_n/v$, and the concentration of cosmogenic ^{21}Ne accumulated when a pebble moved across this pixel would be $M_n = P_n * t_n$, P_n stands for the production rate of cosmogenic ^{21}Ne within this pixel, which can be calculated based on the average elevation and the average latitude of this pixel. And the concentration of cosmogenic ^{21}Ne accumulated in the transport from the Medicine Bow Mountain to Keystone, M_n, can be calculated as below:

$$M = \sum M_n = \sum (P_n * t_n) = \sum (P_n * \frac{F_n}{v}) \tag{3.5}$$

As a result of the analysis above, the v is 28.4m/yr using 9mm of erosion rate and 1% bedload proportion, which represents an ideal slowest transport rate. The rate changes to 978m/ yr if 31mm of erosion rate and 10% bedload proportion are considered, representing the highest possible transport rate in this model. So that we can calculate the concentration of cosmogenic ^{21}Ne with the slowest and highest transport rate.

It can then be calculated that the value of M_n is 2.59*10^6 with a constant migration rate of 28.4m/yr, and the value of M_n is 7.52*10^4 with a constant migration rate of 978m/ yr.

Simplified-Migration Model

However, in reality, the pebbles couldn't be moved on the surface all the time downstream. As the grains moved in the form of dunes in the channels, to evaluate the concentration of cosmogenic ^{21}Ne acquired during the transportation more precisely, the shape of the dunes and the development of the dunes in the channels should be taken into consideration.

As a study of Hein and Walker (1977), the evolution of dunes in the gravelly, braided river can be divided into three stages: in the upstream part, the dunes move in a form called "diffuse gravel sheets" on the floor of the channel. These

sheets are only one to two clast diameters in thickness, which is shown in the up part in Figure 3.17. The forming of "diffuse gravel sheets" is resulted from the large size of pebbles. And during this stage, the movement of pebbles is like what was simulated in the Steady-State Model. By contrast, in the midstream, the dunes are transformed into "longitudinal/diagonal bars". This kind of bars mostly lack foreset slopes at their side facing downstream, which is shown in the middle part in Figure 3.17. And in the downstream, the dunes are transformed into "transverse bars". This kind of bars mostly have a foreset slope which is shown in the down part in Figure 3.17. The transforming from the upstream diffuse gravel sheets to the downstream transverse bars are resulted from the decreasing of grain sizes.

As discussed above, the movement of gravels in the Steady-State Model is like the movement in the form of diffuse gravel sheets. To simulate the concentration of cosmogenic ^{21}Ne acquired during the transportation more precisely, here we need to build another model to simulate the accumulation of cosmogenic ^{21}Ne as the movement of transverse bars. This updated model is called "Simplified-Migration Model" here. In this model, the bedload is migrating as a form of dunes with foreset slope. For a given pebble, when the dune's front end (the end face the flowing direction) reached this pebble, this pebble would be buried, and the dune would move downstream on top of this pebble. This pebble would remain at the same place until the dune passed by. This pebble then moved from the rear end (the end back to the flowing direction) to the front end of the dune, pushed by water; and then start another cycle (Shown in Figure 3.18). In Figure 3.18.a, the blue background represent the water body of the North Platte River, and white sand body represent a sand dune in the channel. The zero point of x-axis represents the source of the North Platte River in the mountain area, and the values of x-axis represent the flowing distance of some points along this channel. The red dot represent the target pebble.When the sand dune move along the channel downstream, this target pebble would experience being buried and recycled. During this process, cosmogenic ^{21}Ne would accumulate. As the production rate of the cosmogenic ^{21}Ne is related to the burial depth and the density of the covered media, in order to calculate the change of the production rate of cosmogenic ^{21}Ne, the relationship between the burial depth and the time was reconstructed, which is shown in the right subfigure of Figure 3.18.b. In this subfigure, z represents the burial depth and s represents the time.

Cosmogenic ^{21}Ne were generated throughout this repeating process. As the lengths of pixels extracted using DEM are much longer than the average length of dune, the way to calculate the accumulation of cosmogenic ^{21}Ne is the same as that used in the "Steady-State Model": the whole accumulation of cosmogenic ^{21}Ne was regarded as the sum of the accumulation of cosmogenic ^{21}Ne in each pixel, and the production rate of cosmogenic ^{21}Ne within each pixel is regarded

consistent, which is calculated based on the average elevation and average latitude of this pixel.

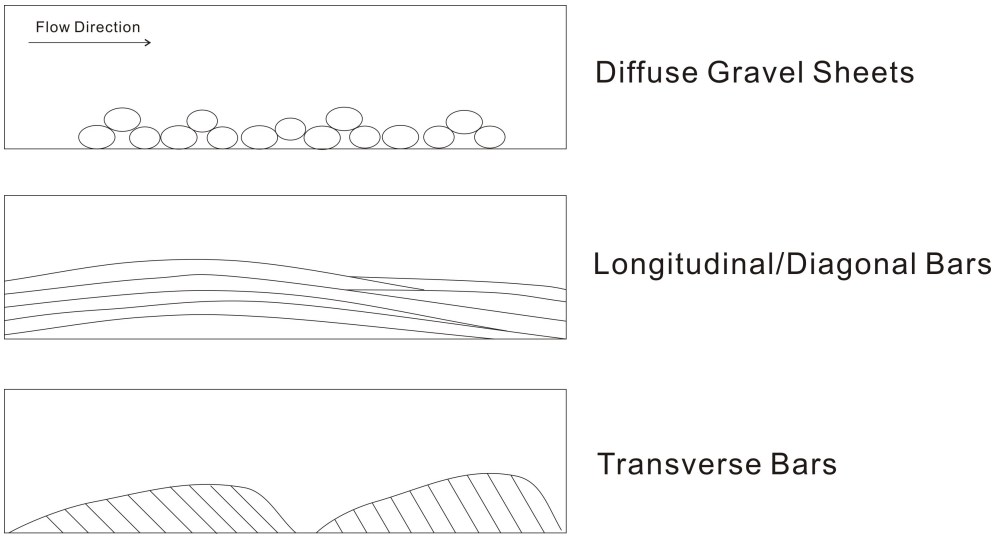

Figure 3.17: A schematic representation showing three typical form of the bars in gravel channels (Hein and Walker, 1977).

The depth-change curve of pebbles was simplified into a sinusoid curve (Figure 3.18 below right). At the point which is x meters away from the source, the burial depth can be shown as equations below:

$$z = f(x) = \frac{H}{2} - \frac{H}{2} * \cos\left(\frac{2\pi x}{L_e}\right) \tag{3.6}$$

$$x = v * t \tag{3.7}$$

z: burial depth, meter; t : time, year; v : velocity of dunes' movement, meter/year; H: average height of dunes, meter; L_e: average length of dunes, meter;

The production rate of ^{21}Ne with shield above can be calculated as below:

$$P = P_0 * e^{(-h*\frac{\rho}{L})} \tag{3.8}$$

L: attenuation length; ρ: density of the shield above; h: height of the shield above;

Because of the shield of the water and the bedload sediment, the production rate of cosmogenic ^{21}Ne within the grain is a little complicated (Figure 3.19 above). Firstly, it can be calculated that the production rate of ^{21}Ne on the surface of the dune underwater:

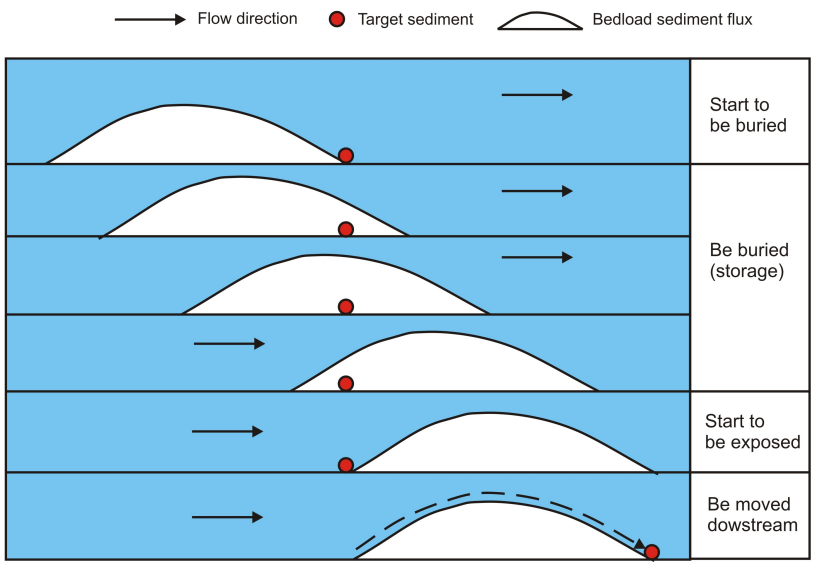

(a) fluvial transport processes in the Simplified-Migration model

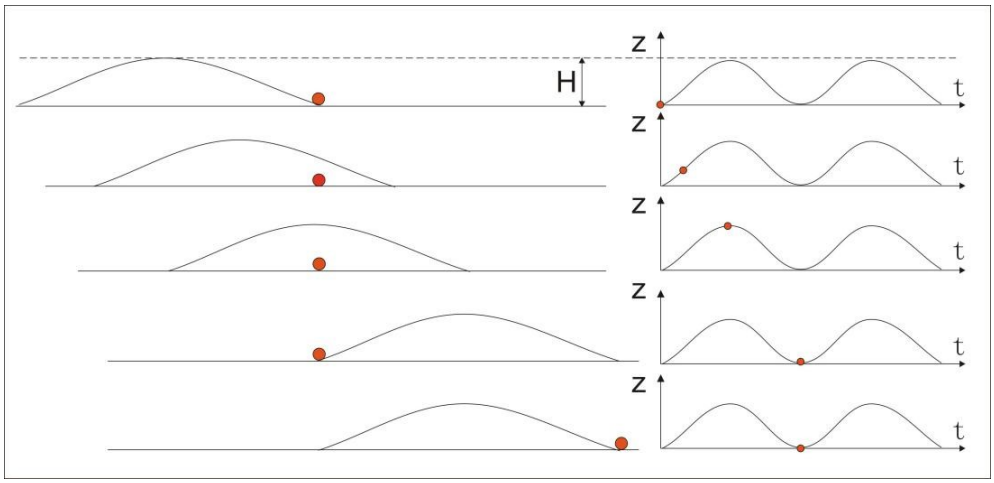

(b) Simplified diagram represents the parameters used in the calculation

Figure 3.18: Schematic representations showing the movement of bedload sediment flux and one pebble. In the above subfigure and the below left subfigure, the red dot represent one pebble; the shape represents the movement of the bedload sediment flux; H stands for the height of the bedload sediment flux. In the below right subfigure, the curve represents the burial depth against the time, z stand for burial depth, t stands for time.

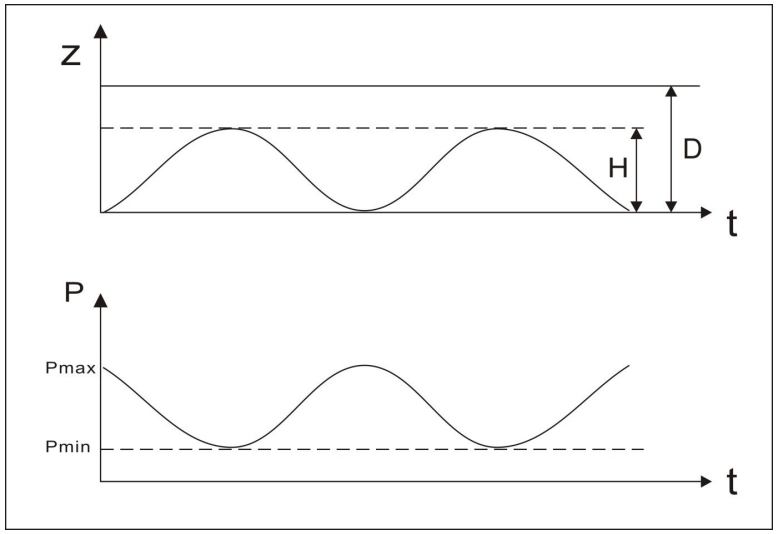

Figure 3.19: A schematic representation showing the calculation in "Simplified-Migration Model", the changes in production rate is calculated by the burial depth of the grain, which is resulted from the movement of the bedload sediment flux. The above subfigure represents the change of burial depth of the pebble with the change of time, and the below subfigure represents the corresponding production rate of the cosmogenic ^{21}Ne within this pebbles, with the change of time.

$$P = P_0 * \ e^{(-h_w * \frac{\rho_w}{L})} \tag{3.9}$$

Then it can be calculated that the production rate under the dune:

$$P_2 = P_1 * \ e^{\left(-h_d * \frac{\rho_d}{L}\right)} = P_0 * \ e^{\left(-h_w * \frac{\rho_w}{L}\right)} * \ e^{\left(-h_d * \frac{\rho_d}{L}\right)} = P_0 * \ e^{((-h_w \rho_w - h_d \rho_d)/L)} \tag{3.10}$$

h_w: height of shielding water, cm; ρ_w: density of water, 1g/cm^3; h_d: height of shielding sediments, the same as burial depth above, cm; ρ_d: density of shielding sediments, 1.6g/cm^3.

As Figure 3.19 above shows,

$$h_d = z \tag{3.11}$$

$$h_w = D - z \tag{3.12}$$

D: depth of the river, cm; so that

$$P_{max} = P_0 * \ e^{\left(-D * \frac{\rho_w}{L}\right)} \tag{3.13}$$

$$P_{min} = P_0 * \ e^{((-(D-H)\rho_w - H\rho_d)/L)} \tag{3.14}$$

For the total amount of ^{21}Ne produced after a period of time (t):

$$M = \int_0^t P_2 \ dt = \frac{(Pmax + Pmin)}{2} * \ t \tag{3.15}$$

M: the amount of ^{21}Ne produced after a period of time (t);

So, when D >= H, the dunes are always under water, the concentration of ^{21}Ne accumulated can be calculated using:

$$M = \frac{P_0 * e^{\left(-D*\frac{\rho_w}{L}\right)} + P_0 * e^{((-(D-H)\rho_w - H\rho_d)/L)}}{2} * \ t \tag{3.16}$$

When D < H, the dunes can sometimes be exposed, the concentration of ^{21}Ne accumulated should be revised:

$$M = \frac{P_0 * e^{\left(-D*\frac{\rho_w}{L}\right)} + P_0 * e^{(-H\rho_d)/L)}}{2} * \ t \tag{3.17}$$

The average height of dunes is set as 1.5 m based on documented bedform height (Crowley, 1983a). As that in the "Steady-State Model", the average depth of river is set as 1.5 m.

As the calculation procedure used in the "Steady-State Model", firstly, the concentration of cosmogenic ^{21}Ne accumulated when a pebble moved across one pixel was calculated using Equation 3.16 and Equation 3.17. And then the concentration of cosmogenic ^{21}Ne accumulated in the transport from the Medicine Bow Mountain to Keystone can be calculated by combining the values of all the pixels (as Equation 3.5).

The results of the "Steady-State Model" and the "Simplified-Migration Model" are shown together in Table 3.7.

Table 3.7: Results of two models with two different migration rates

	28.4m/yr	978m/yr
Steady-State	2.59*10^6	7.52*10^4
Simplified-Migration	2.55*10^6	7.43*10^4

As suggested by Table 3.7, using the model of "Simplified-Migration Model", the amount of cosmogenic neon generated is 2.55 x 10^6 atoms/g with the transport rate of 28.4m/yr. Moreover, the value decreases rapidly to 7.43 x 10^4 with the translate rate of 978m/yr. All of these are lower than those of Steady-State Model (Table 3.7). This is understandable because the Simplified-Migration Model takes the burial process and shielding into consideration which would decrease the production rate of ^{21}Ne during the transport.

The corrected ^{21}Ne concentration of all the samples and the results of two model were put together in Figure 3.20.

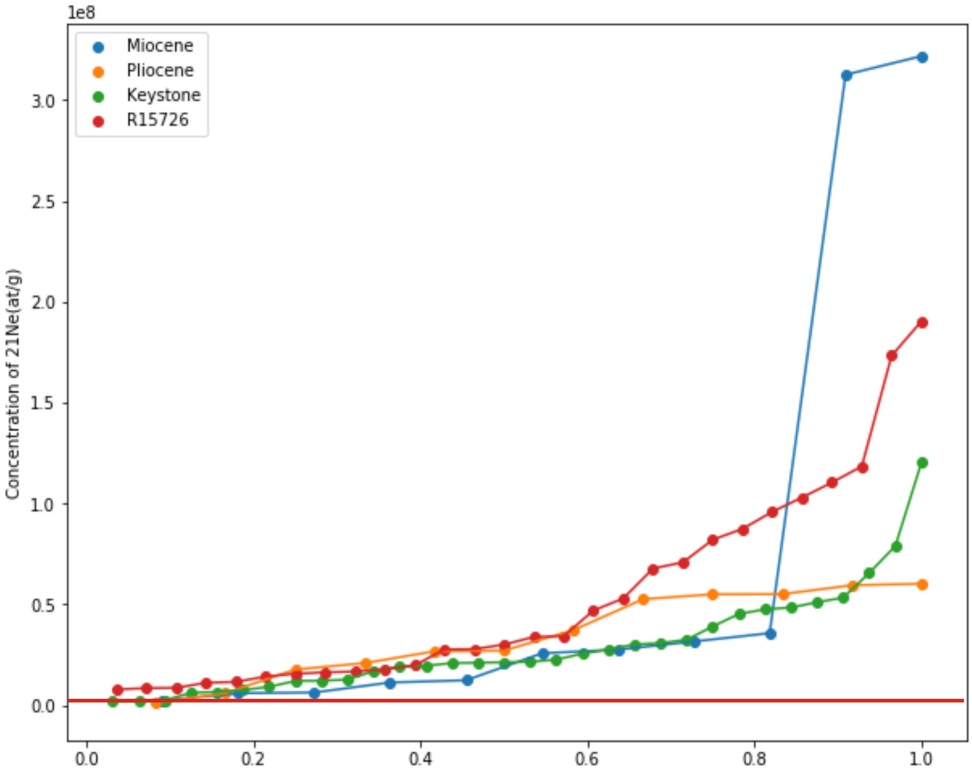

Figure 3.20: The comparison between the concentration of corrected cosmogenic ^{21}Ne contained within the samples and the predicted concentrations of cosmogenic ^{21}Ne in two models. These dotted lines represent the cumulative density curves of the concentration of corrected ^{21}Ne of the two modern localities and two paleosediments. The red solid line represents the results of the Steady-State Model and the Simplified-Migration Model with the transport rate of 28.4m/yr. The results of the Steady-State Model and the Simplified-Migration Model with the transport rate of 978m/yr are too low to be plotted in this figure.

In Figure 3.20, the red line represents the concentration of ^{21}Ne from modern samples collected from R15726; the green one is for Keystone. For comparison, the results of Pliocene/Miocene samples were put together, with the same rule,

from the lowest sample to the highest sample. The yellow and blue lines are for the Pliocene and Miocene data, respectively.

Additionally, in Figure 3.20, the results of these two models were plotted. The red line represents the results of the Steady-State Model and the Simplified-Migration Model with the transport rate of 28.4m/yr (the results are too close to be divided in this figure), the results of the Steady-State Model and the Simplified-Migration Model with the transport rate of 978m/yr are too low to be plotted in this figure.

As shown in Figure 3.20, most parts of the concentrations contained within the samples, not only of the modern time but also of the Miocene/Pliocene ages, are above the results of these two models. For pebbles that flowed downstream with a constant slowest migration rate, the maximum concentration of $^{21}Ne_{cosTS}$ would be accumulated. Even under this ideal condition, the predicted result is still unable to explain the measured $^{21}Ne_{cosTS}$ values in the quartzite pebbles collected. In other words, for the real data, nearly all the sediments need considerable storage time for the accumulation of such a massive amount of $^{21}Ne_{cosTS}$. It can then be concluded that the sediments were not migrating all the time; they must have experienced deposition, being burial and recycling. This result supports the existence of recycling.

3.5.2 The Age of Paleosediments Recycled

It has been proved that all of the sediments collected have experienced long burial and exposure time. If we can get the accurate exposure duration and burial duration of all the samples, the age of paleosediments recycled would be concluded. For these two independent variables, exposure time and burial time, at least two nuclides with different accumulation curves are needed to be measured. This idea of nuclide-pair was first used by Lal (1991). In this paper, Lal used $^{26}Al/^{10}Be$ since both can be measured in single quartz, and both have half-life that differ from each other.

In this thesis, enough data of ^{21}Ne has been generated. ^{21}Ne does not decay, so that it can provide the information about the exposure duration of the samples collected. Another unstable cosmogenic nuclide is needed to provide the information about the burial duration of these samples. ^{10}Be is the most popular cosmogenic nuclide used in geological study, and it has a totally different half life or production curve compared with ^{21}Ne. Moreover, as that in Lal's paper (Lal, 1991), ^{21}Ne and ^{10}Be can be measured in single quartz. In this regard, ^{10}Be is a favourable choice in our study.

The samples for ^{10}Be analysis were collected from the Keystone (41.212, -101.597) which is located near the end of the North Platte River. Keystone is the most distant site within all these three representative sites, the signals of recycling could be apparent as the initial pebbles carried from the mountain area are few

at this place. The ^{10}Be analysis is costly, only five samples did ^{10}Be analysis in this study. Moreover, because of ^{10}Be analysis consume much more of the mass of the samples than that of ^{21}Ne, samples with larger sizes of about 2^3 (-phi scale) cm were picked out to do ^{10}Be analysis. The result is shown in Table 3.8.

Table 3.8: Concentrations of cosmogenic ^{10}Be contained within samples collected from Keystone

Sample ID	Be-10 concentration (atoms/g)	σ Be-10 concentration	% error	size (cm)
ML-2	3.67E+05	6.77E+03	1.84	7.2
ML-8	1.47E+05	3.46E+03	2.35	5
ML-10	1.02E+06	2.20E+04	2.15	5.8
ML-11	5.24E+05	1.15E+04	2.19	5.5
ML-13	5.31E+06	9.48E+04	1.79	5.8

Banana Plot

During the calculation of burial and erosion history, the nuclide with the shorter half-life is always used to calculate the erosion rate (shown in Figure 3.21). For example, after a long time of exposure, under a steady erosion rate, the concentration of the cosmogenic ^{14}C (SLHL, sea level high latitude) would reach a stable level, which is measured as 1.4* 10^5 atoms g^{-1}. Then based on Figure 3.21, the erosion rate can be read as about 10 mm kyr^{-1}. If the erosion rates were lower, such as 1 or 3mm kyr^{-1}, the saturation concentrations of ^{14}C are higher. Once the erosion rate could be estimated using one isotope, another isotope (stable one or the one has longer half-life) could provide more information on the exposure/burial time.

Based on this idea to calculate erosion rate and exposure/burial time using two different nuclides, in Lal's paper (Lal, 1991), the ratio ^{21}Al/^{10}Be is plotted against the log of measured ^{10}Be to evaluate burial time and erosion rate. This kind of figure is called a "banana plot". Other pairs of nuclides with significant half-life difference can also be used with the same plotting method. Here ^{21}Ne (stable) and ^{10}Be ($T_{1/2}$ = 1.5 My) were used because they can be measured from the same quartz.

In Figure 3.22, at the steady-state (constant erosion rate and no burial history), rocks with different erosion rates would be plotted within a fixed zone in the ratio-concentration plot, termed the steady-state erosion island (shown as B in Figure 3.22). This zone is defined with two different curves: zero-erosion (lower one) and infinite-exposure/no-burial line (upper one). However, if the rock surface is shielded from cosmic rays (e.g. being deep buried) after having attained a certain amount of cosmogenic nuclides, the concentration of ^{10}Be would decrease due to decaying while the concentration of ^{21}Ne remains stable, thereby making

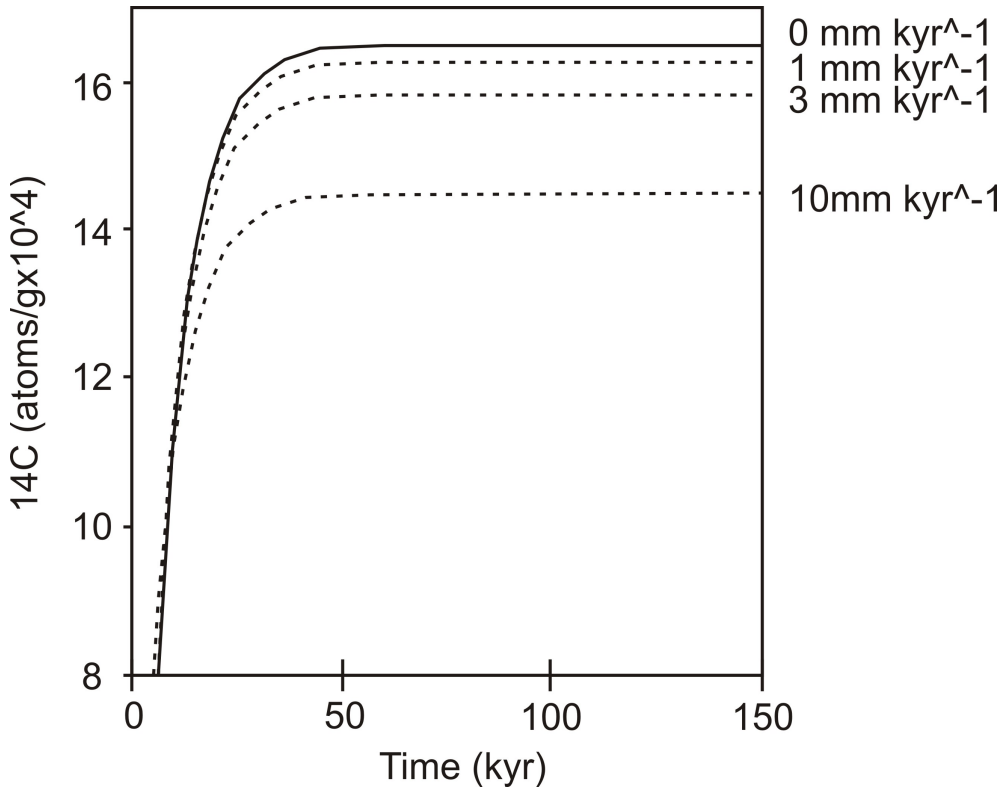

Figure 3.21: How to use one isotope to estimate the erosion rate (revised from (Gosse and Phillips, 2001))

the locations of plotting move along the straight lines up to the left above (parallel straight lines in Figure 3.22). When using the banana plot, the data need to be plotted and then the exposure/erosion history of the samples can be recognised from the locations of the plotting. There are three main fields on the banana plot. Each field provides different information about the history of surface burial of the sample.

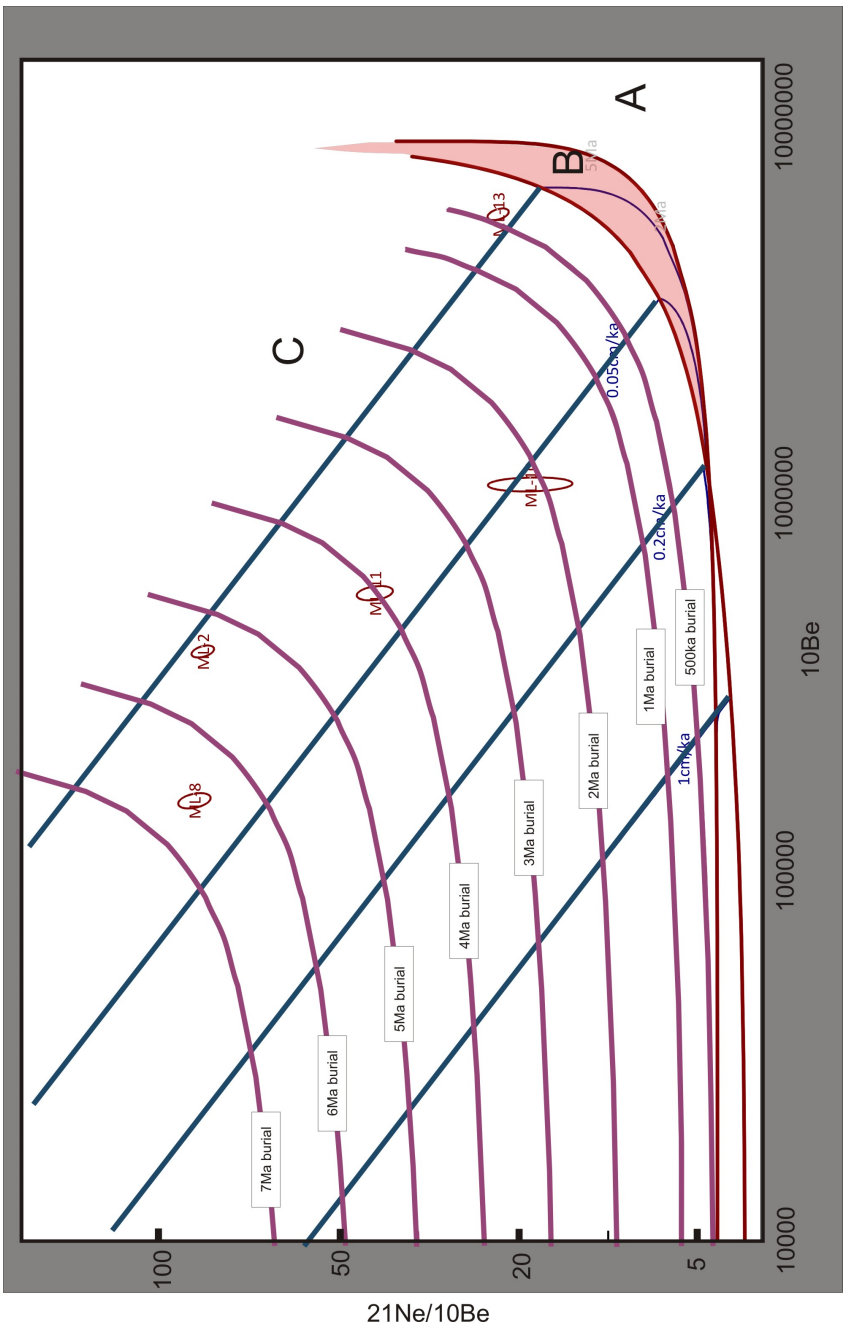

Figure 3.22: Banana plot of ^{21}Ne–^{10}Be

(1) Steady-state erosion island (shown as B in Figure 3.22): The area coloured with the red background, which is limited by zero-erosion (lower one) and infinite exposure line (upper one). Samples plotted within this area can be interpreted to have experienced not only the erosion history but also the exposure history, without burial history.

(2) Under the steady-state erosion island (shown as A in Figure 3.22): Samples plotted within this area cannot be explained by any real situation. The only reason for the samples to be plotted in this area should be preparation or measurement problems.

(3) Above the steady-state erosion island (shown as C in Figure 3.22): Samples plotting within this area can be interpreted to have a history of combined erosion, exposure and burial stage. The erosion rate and burial time can be read directly from the plot.

Time Calculation

The assumptions of the banana plot are: (1) the surface has experienced a constant erosion rate; (2) the samples have experienced continuous periods of being eroded, being exposed or being buried. Based on this assumption, a plot was generated (Figure 3.22) using the ^{21}Ne and ^{10}Be data collected from Keystone. An Excel add-in called CosmoCalc (Vermeesch, 2007) was used in the calculation. The result is also shown in Table 3.9.

Table 3.9: Calculated burial duration if the sediments were eroded continually

Sample ID	Burial Age (ka)	σ	Erosion Rate (cm/ka)	σ
ML-2	5568.7	17931	0.012	0
ML-8	6839.8	25644.1	0.026	0
ML-10	2239.8	3829.2	0.051	0
ML-11	3973.4	5622.6	0.036	0
ML-13	416.2	1575.3	0.008	0

As suggested by Figure 3.22, ML-10 has an erosion rate of 0.05cm/ka, and all the other four samples have lower erosion rates. Moreover, their burial time are different from each other. The longest one (ML-8) is about 6.8Ma. Under the assumption that all the samples were buried all the time and exposed during the modern time, the burial time is within the Ogallala Group (17.5-5 Ma) and matches the vast tilting and incision happened in the Great Plains at that time (McMillan et al., 2002; Wobus et al., 2010). ML-2 represents a burial time of 5.6 Ma which is also within the Ogallala Group. ML-10 and Ml-11 have burial time of 2.2 Ma and 4.0 Ma. These times are located within Broadwater Formation (Pliocene, 4-2.5 Ma).

The assumption can be changed slightly: (1) no erosion process; (2) all the exposure and burial processes happened instantly so that the samples have experienced continuous periods of being exposed (burial depth = 0) or being buried (production rate = 0). Another result can be derived as Table 3.10.

Table 3.10: Calculated burial duration if erosion and burial process happened instantly

Sample ID	Burial Age (ka)	σ	Exposure Age (ka)	σ	Recycling time (ka)	σ	Time involved
ML-2	6062	40.6	4987.8	187.7	11049.8	228.3	Miocene
ML-8	7313.9	67.6	2337.5	107.9	9651.4	175.5	Miocene
ML-10	2571.6	145.4	1177.5	111.3	3749.1	256.7	Pliocene
ML-11	4386	77.8	1673.8	84.1	6059.8	161.9	Miocene-Pliocene
ML-13	840.4	36.3	7346.8	238.4	8187.3	274.6	Miocene

Under this assumption, the exposure duration and burial duration should be added together to get the predicted deposition time of these samples. As shown in the table, ML-13, ML-11, ML-8, and ML-2 are within 17.5-5 Ma and match the deposition time of the Miocene Ogallala Group, during which The Rocky Mountains and Great Plains experienced a spike of the incision. ML-10 is within Pliocene Broadwater Formation (4-2.5 Ma), during which another large scale incision happened in the Great Plains.

The real situation is different from any of these two assumptions, but these two rows of results can provide us with a clear idea that nearly all these samples have experienced very long exposure time and then being recycled into modern sediments. Additionally, these results indicate that the oldest age of recycled sediments in the Great Plains was at least Miocene in age.

3.6 Summary and Conclusion

In the 2^{nd} chapter, it was concluded that the recycled sediments were mostly carried into the mainstream through the tributaries or the incision of paleosediments by the mainstream. Also, almost all of the large pebbles collected from R15726 and Keystone are proposed to come from lateral sediment inputs. From the result of grain size analysis, it has been proved the existence of recycling in the Great Plains. Also, the recycled sediments considerably changed the portion of grains within the mainstream. More information need to be dug from the collected samples in the next study.

Cosmogenic nuclides accumulated when the sediments were exposed so they can provide information about the exposure and burial history of fluvial sediments. As

the recycling process means the incision of burial sediments and mixing of recycled sediments into the fresh sediments, all the recycled sediments have experienced being buried and being exposed. It provides a great tool to evaluate the age of recycling process.

In my study, quartzite was chosen as the target mineral for cosmogenic nuclides analysis. Firstly, two rows of quartzite samples were collected from different sources to investigate the inherited ^{21}Ne contained in the modern samples. After the subtracting of the inherited cosmogenic ^{21}Ne, useful concentration of cosmogenic ^{21}Ne for analysis next can be get.

Next, eighty-two samples (in total) for cosmogenic ^{21}Ne and five samples for ^{10}Be were analysed. A "Steady-State" model and a "Simplified-Migration" model were built to estimate the maximum concentration of cosmogenic ^{21}Ne accumulated from the source to the target location (Keystone) with a constant migration rate. The maximum results of these models represent the maximum concentration of cosmogenic ^{21}Ne which can be accumulated during transportation without recycling. From the comparison between the results of these two models and the real concentrations of cosmogenic ^{21}Ne measured from the pebbles, it can be concluded that most pebbles collected from Keystone have experienced a long time of storage. This provides support for the existence of recycling in the Great Plains.

Next, in order to calculate the exposure duration and the burial duration of the samples collected in the central Great Plains, five samples were chosen in Keystone to do ^{10}Be analysis. Based on the Ne/Be ratio, the duration of exposure and burial of the samples were calculated. Combining the exposure history and the burial history, it was suggested that sediments as old as Miocene-age can be affected by modern recycling.

Now, the time range of recycling happened in the Great Plain is clear. In this chapter, the distributions of cosmogenic ^{21}Ne contained within the samples collected from R15726 and Keystone were developed (shown in Figure 4.1). R15726 is located on upstream of Keystone. Because of inner connection, the concentration of cosmogenic ^{21}Ne contained in the sediments of Keystone should be higher than, or at least the same as those of R15726. However, in Figure 4.1, cosmogenic ^{21}Ne concentrations contained within the samples collected from upstream (R15726) are higher than those from downstream (Keystone). To resolve this conflict and exploring the influences of geological parameters on the recycling, several models were built to reconstruct the recycling processes.

Moreover, in the next chapter, the traditional grain-based method to reconstruct the paleochannel was tested to evaluate the impact of introducing recycling on the geological studies.

Chapter 4

Numerical Models

4.1 Introduction

In Chapter 2, evidences were presented to indicate that recycling has been an important control on the dispersal of conglomerates in the Great Plain, and there are three places where recycling mainly happened (shown in Figure 2.21). In chapter 3, the result of cosmogenic nuclides analysis indicates the duration of exposure of paleosediments during episodes of transport, abandonment, and recycling.

After grain size analysis and cosmogenic nuclide analysis, some questions have been answered, but some new questions arose. In chapter 3, the distributions of cosmogenic ^{21}Ne contained within the samples collected from R15726 and Keystone were developed (shown in Figure 4.1). R15726 is located upstream of Keystone. Because of inner connection, the concentration of cosmogenic ^{21}Ne contained in the sediments of Keystone should be higher than, or at least the same as those of R15726. However, in Figure 4.1, cosmogenic ^{21}Ne concentrations contained within the samples collected from upstream (R15726) are higher than those from downstream (Keystone). To resolve this conflict, more work is needed to obtain the detail about recycling.

In the Great Plains, the recycling did not only happen in the paleosediments, but also in the modern sediments, as the influences of recycling are the same through out the history, what happened in the paleosediments would take place in the modern sediments. In Figure 4.1, cosmogenic ^{21}Ne concentrations contained within the samples collected from upstream (R15726) are higher than those from downstream (Keystone). This conflict is resulted from the different recycled sediments near these two places. That is to say, this conflict contains the secret of modern recycling. In order to know the details of recycling happened in the history, getting clear the influences of this conflict of modern recycling is a good idea.

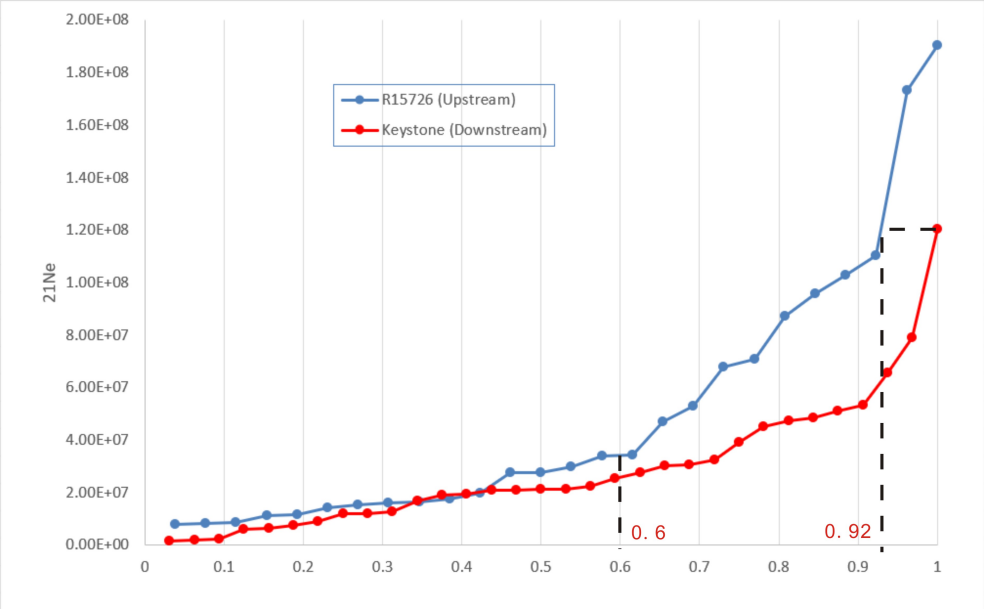

Figure 4.1: Comparison of the distributions of cosmogenic ^{21}Ne of pebbles collected from R15726 and Keystone.

So that, in the first half of this chapter, some geological parameters were chosen to build models, trying to reconstruct this conflict of modern recycling.

As one of the fluvial processes, the recycling is mainly influenced by not only the internal fluvial characteristics, but also the external factors. In this chapter, two factors of internal influences were chosen to be analysed, which are the grain sizes and the age of the sediments recycled. And, one factor of the external influence, elevation was chosen to be analysed.

For the influence of grain sizes, because the coarser pebbles have more opportunities to be stored for longer time, and the finer ones are much easier to be moved away, it is assumed that the grain sizes would have a positive relationship with the concentration of cosmogenic nuclides contained within the samples collected;

For the influence of the age of paleosediments recycled, the older paleosediments have more chances to be exposed for longer time, so that it is assumed that the age of paleosediments would also represents a positive influence on the accumulation of cosmogenic nuclides;

For the influence of elevation, as the increase of elevation would accelerate the production of cosmogenic nuclides, it is assumed that the recycling happened in the area with higher average elevation would contribute to a larger amount of cosmogenic nuclides accumulated in the samples.

Some numerical models were developed in this chapter to test the controls of these factors on the cosmogenic ^{21}Ne accumulated during recycling.

Moreover, the results of chapter 2 & 3 indicate that the recycling is one of dominant factors influencing the distribution of large pebbles collected on the central Great Plains. However, most previous studies in this area have not taken the recycling into consideration. Especially some studies on reconstructing the paleochannels using traditional grainsize-based study, as the recycling strongly change the sources of the grains collected for analysis. In order to evaluate the influence of recycling on the previous studies of paleochannels using grainsize-based tools, a model was built in the last half of this chapter.

As the recycling happened in both the modern channel and the paleochannel, the reconstruction of the modern recycling can reflect the situation of what happened in the past. Therefore, in the model on evaluation the impact of recycling on previous studies, the traditional grainsize-based tool was used to reconstruct the modern channel without the consideration of recycling happened in the modern channel. For the result, if the reconstructed "modern channel" can fit the real channel very well, that means the traditional grainsize-based tool is reliable on the channel which contains dominantly recycled pebbles, in a contrast, if the reconstructed "modern channel" was different from the real one, that means the recycling process should be taken into consideration in the reconstruction of paleochannels.

4.2 The Controls of Recycling

As suggested by the result in chapter 2, almost all the pebbles collected from R15726 and Casper came from recycled paleosediments.

The localities of R15726 and Keystone are shown in Figure 3.11, and the concentrations of cosmogenic ^{21}Ne of all the samples collected from R15726 and Keystone are shown in Figure 4.1. in Figure 4.1, the concentrations of cosmogenic ^{21}Ne are shown as cumulative density curves.

Generally, because of the connection, sediments coming from upstream will accumulate more cosmogenic nuclides during the transport when they were carried downstream, which should contribute to a situation that the concentration of cosmogenic ^{21}Ne of the sediments collected from the downstream point being higher than those of the upstream. In Figure 4.1, nearly half of the concentration of the samples collected from R15726 are overlapped with those of Keystone. However, the concentrations of cosmogenic ^{21}Ne contained within some samples collected from R15726 (upstream) are higher than the highest concentration of cosmogenic ^{21}Ne in Keystone (downstream). For the causes of this conflict, it can be assumed as below:

From the result of grain size analysis (in the 2^{nd} Chapter), it is proposed that most of the pebbles collected in R15726 (upstream) and Keystone (downstream) are sourced from lateral sediment input instead of the upstream part of the North

Platte River. It then can be inferred that the pebbles deposited in R15726 (upstream) are decoupled from the pebbles deposited in Keystone (downstream). The signals carried with the pebbles through the connection is very weak. That is to say, the characteristics of the pebbles collected in these two sites, including the concentration of cosmogenic ^{21}Ne contained within the pebbles, are mostly controlled by the characteristics of the coarse sediments carried by lateral sediment inputs. Thus, the conflict between the pebbles of R15726 and Keystone is actually the conflict between the pebbles carried by the lateral sediment inputs near these two sites.

In Figure 4.1, based on the comparison between these two curves, two important points on the x-axis can be recognised: (1) One is located near the middle of the x-axis, before this point, the concentration of cosmogenic ^{21}Ne contained within the samples collected from these two sites are nearly the same. This point is named "overlap end". In Figure 4.1, the value of "overlap end" can be read as 0.6. (2) The other point is located at the right side of the x-axis. To find this point, firstly, on the curve of R15726, the point which has the same value as the highest one of Keystone can be read, and the corresponding value of this point on the x-axis is the second important point. For all the points on the R15726 curve after this point, they have higher values than those of all the points on the Keystone curve. This point is named "beyond point". In Figure 4.1, the value of "beyond point" can be read as 0.92. In other words, there are about 8% of the pebbles collected from R15726 contain more cosmogenic ^{21}Ne than those of all the pebbles collected from Keystone.

4.2.1 Model to Verify The Effect of Elevation

The production rate of cosmogenic ^{21}Ne has a relationship with altitude and latitude. To investigate the influences of the altitude and latitude on the distribution of the concentrations of the cosmogenic ^{21}Ne contained within the recycled pebbles, a model was developed. As recycling is complex, to simplify the calculation, the model has the following preconditions:

(1) All the sediments recycled have been exposed continually for the same time;

(2) The possibility of old pebbles being recycled into a modern channel is the same throughout the plain area.

As described in chapter 3, the non-atmospheric Ne (Ne*) contained within the recycled pebbles are composed of background Ne (Ne_{back}), and depositional cosmogenic Ne (Ne_{cos}). It should be noted that the background Ne contains not only the nucleogenic nuclides generated over the time of the rock, but also some cosmogenic Ne generated when it was exposed to the cosmic rays during the formation of the rock. Moreover, the depositional cosmogenic Ne (Ne_{cos}) can further be divided into those generated during bedrock exhumation (Ne_{cosE}) and

those generated during transport and storage in the fluvial system (Ne_{cosTS}). The inherited cosmogenic Ne is the combination of Ne_{back} and Ne_{cosE}.

Based on the result of chapter 3, in the Great Plains, the quartzite pebbles have inherited a maximum of 0.85×10^7 atoms ^{21}Ne/g before downstream transport.

Then in the model, the concentration of cosmogenic ^{21}Ne contained within all the sediments recycled can be calculated as below:

$$N = Ne_{back} + Ne_{cosE} + Ne_{cosTS} \tag{4.1}$$

$$Ne_{back} + Ne_{cosE} = 0.85 * 10^7 \tag{4.2}$$

$$Ne_{cosTS} = P * T \tag{4.3}$$

$$N = 0.85 * 10^7 + P * T \tag{4.4}$$

Within these equations, N represents the concentration of cosmogenic ^{21}Ne contained within one of the grains recycled; P represents the production rate within this grain, which is related to the elevation and latitude of this grain. For the calculation of the production rate for each elevation and latitude, a tool called CosmoCalc, an Excel add-in for cosmogenic nuclide calculations and generated by Vermeesch (2007) was used; T means the exposure time. In the first calculation of this model, the time range from the end of Pliocene to now (2.58Ma) is used.

In this model, as the possibility for each grain deposited on the Great Plains to be recycled into the channel is the same, and all the recycled grains are modelled as having experienced the same period of exposure time. The distribution of the cosmogenic ^{21}Ne contained within the sediments of any site along the river, should be the same as the distribution of the cosmogenic ^{21}Ne contained within all the surface-sediments (sediments exposed on the Earth's surface) within the catchment area of that site.

Thus, the distributions of the cosmogenic ^{21}Ne contained within the sediments of R15726 and Keystone can be represented using the distributions of the cosmogenic ^{21}Ne accumulated in the surface-sediments all across their catchment areas, respectively.

However, in the real calculation based on equation 4.4, calculating the production rate of each grain deposited on the surface of the Great Plains is a challenge. Moreover, after the calculation of the production rate of each grain and the concentration of the cosmogenic ^{21}Ne accumulated in each grain, how to do mathematical statistics for this big data is another challenge.

To simplify the calculation, the catchment areas of R15726 and Keystone can be extracted using the DEM (Digital Elevation Model). In the DEM, the data are stored in different pixels, and each pixel has its information of elevation and locality. In the simplified calculation, each pixel can be regarded as a collection of grains and the grains within one pixel have similar localities and fluvial characteristics, therefore the statistical characteristics of all the grains can be represented using the statistical characteristics of all the pixels. This thinning of data also makes the calculation easier to be processed. The production rates of each pixel can be calculated based on the average latitude and altitude of this pixel, using the scaling of Lal (1991). Moreover, statistical analysis on the pixels is much easier to conduct comparing to the statistical analysis on all the deposited grains.

Model for R15726

As suggested by the result of chapter 2, the pebbles coming from Casper nearly disappeared when they reached R15726, thus the pebbles collected in R15726 were mostly from the lateral sediment input nearby. So that it can be inferred the source of these recycled pebbles are mainly from the catchment area between Casper and R15726. The catchment area between Casper and R15726 was extracted (shown as a yellow area in Figure 4.2). This place represents where the possible recycled sediments of R15726 came from.

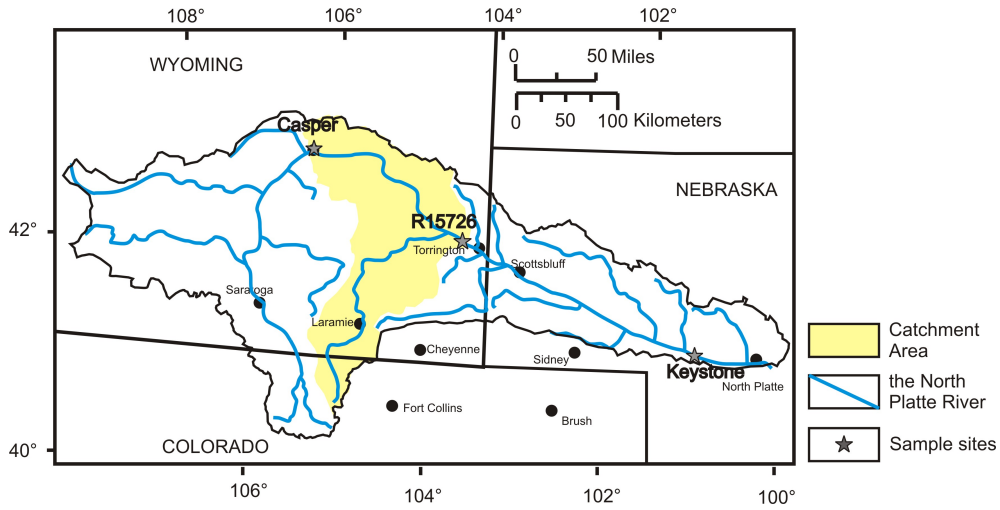

Figure 4.2: The location of the catchment area between Casper and R15726.

The production rate of cosmogenic ^{21}Ne within each pixel was scaled based on the average latitude and altitude of this pixel. Then the cosmogenic ^{21}Ne accumulated from the end of Pliocene to now (2.58Ma) for each pixel was calculated based on Equation 4.4.

With the concentrations of cosmogenic ^{21}Ne accumulated in each pixel, the

predicted distribution of cosmogenic ^{21}Ne contained within all of the sediments in R15726 can be plotted as Figure 4.3.

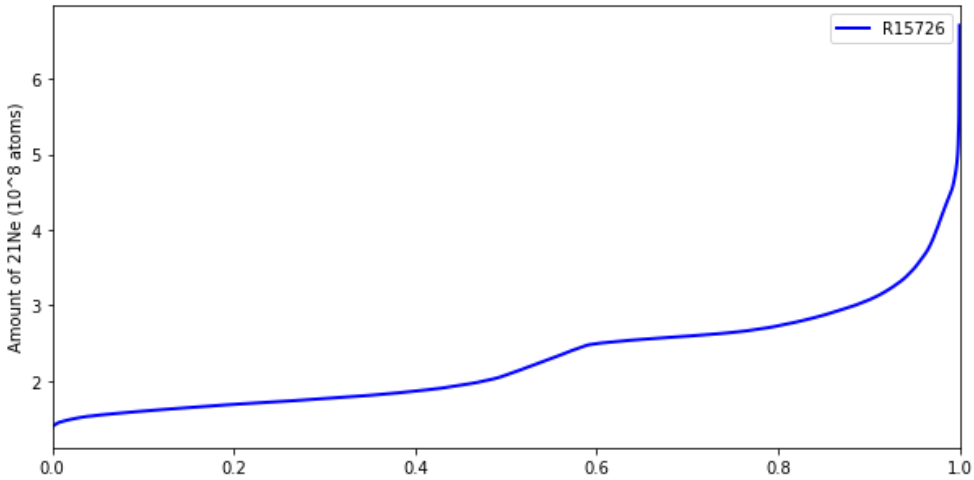

Figure 4.3: The predicted distribution curve of the cosmogenic ^{21}Ne contained within all the pebbles in R15726.

Model For Keystone

The same procedure was followed to extract the catchment area between R15726 and Keystone (shown as a yellow area in Figure 4.4.). This place is where the recycled sediments of Keystone are proposed to have been sourced based on the result of grain-size analysis.

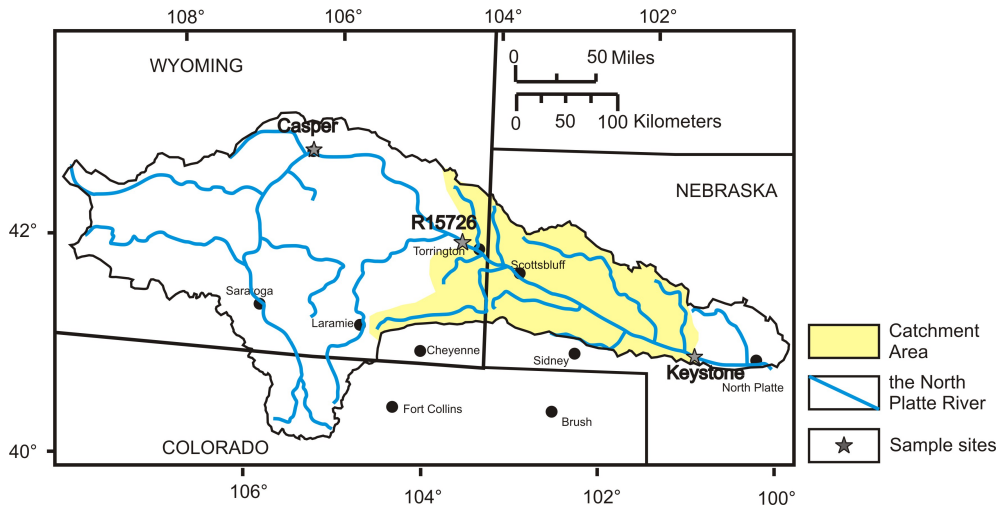

Figure 4.4: the location of the catchment area between R15726 and Keystone.

The production rate of cosmogenic ^{21}Ne within each pixel can be scaled based on the average latitude and altitude of this pixel. Moreover, using equation 4.4, the

predicted distribution curve of all the sediments in Keystone can be calculated and plotted in Figure 4.5.

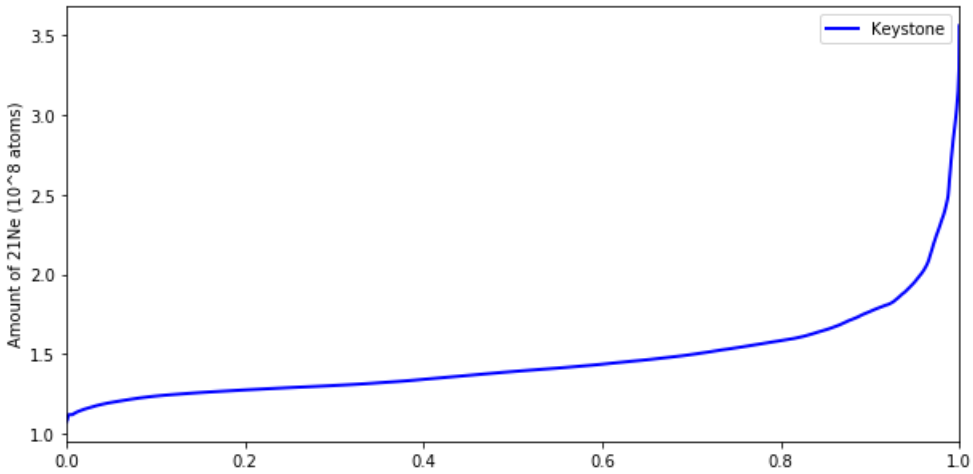

Figure 4.5: The predicted distribution curve of the cosmogenic ^{21}Ne contained within all the pebbles in Keystone

Comparison and Analysis of the Result

The predicted cosmogenic nuclides ^{21}Ne distributions of all the sediments in R15726 and Keystone were plotted together, comparing with the real cosmogenic nuclides ^{21}Ne distributions within the samples collected from these two localities (shown in Figure 4.6).

In Figure 4.6, the fluctuation in the predicted concentration curves was due to the difference of elevation and latitude within each pixel. However, at the study location, the change of latitude is very slight and can not affect the production considerably. The elevation, therefore, mainly influences the fluctuation of the amount of cosmogenic ^{21}Ne contained within the sediments.

As suggested by Figure 4.6, the predicted concentration distribution curves matches very well, in the shape, with the measured ones. Following the same procedure, in Figure 4.6 two important points on the x-axis can also be recognised. The value of "overlap end" can be read as 0.5. Before this point, the concentration of cosmogenic ^{21}Ne contained within the samples collected from these two sites are very close to each other. And the value of "beyond point" can be read as 0.95. For the area between the "overlap end" and the "beyond point", the gap between these two curves becomes wider. And all the points on the R15726 curve after "beyond point" have higher concentrations of cosmogenic ^{21}Ne than all those on the Casper curve. In other words, there are about 5% of the pebbles collected from R15726 contain more cosmogenic ^{21}Ne than all the pebbles collected from

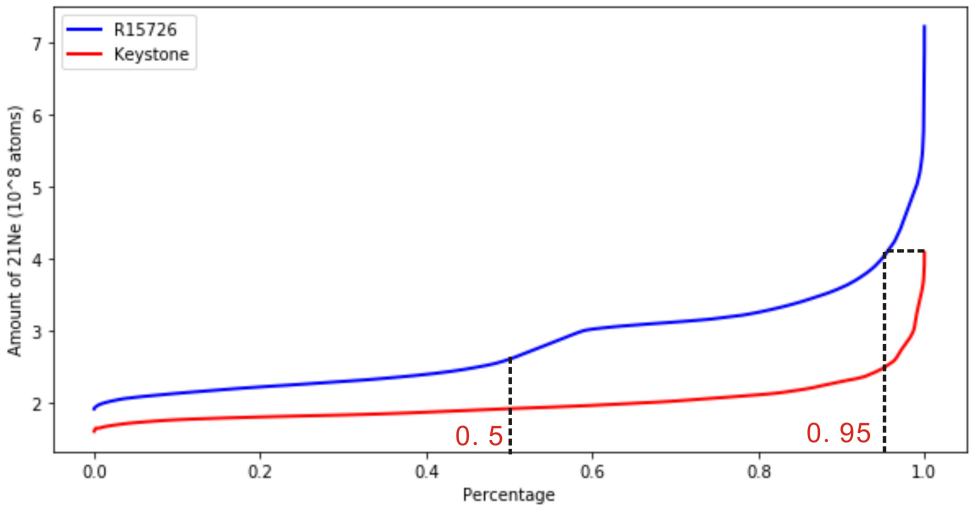

(a) a

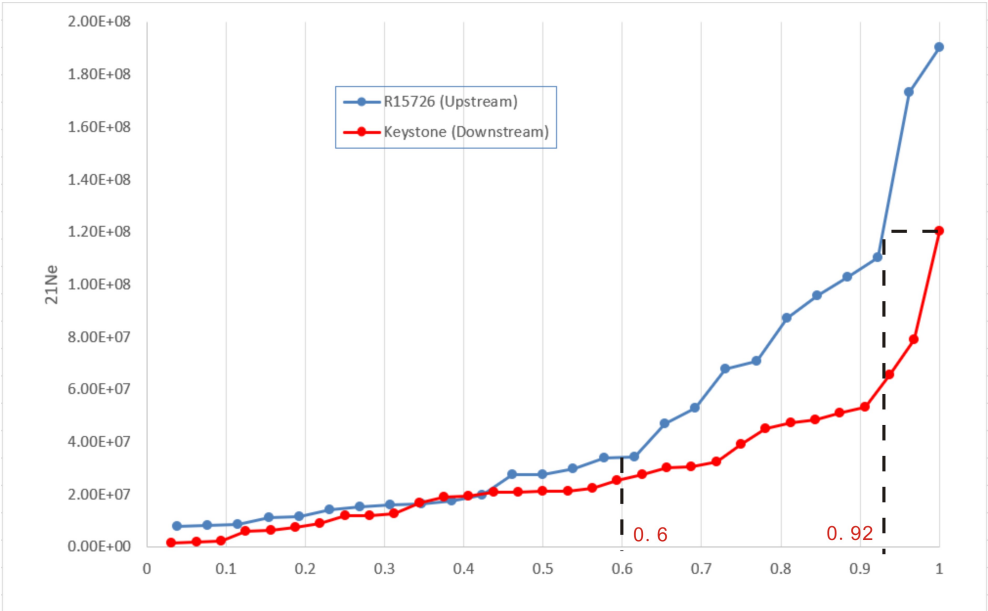

(b) b

Figure 4.6: The comparison between the predicted distribution curves of cosmogenic ^{21}Ne and the real ones at R15726 and Keystone ($T = 2.58$Ma)

Keystone. The values of "overlap end" and "beyond point" on the predicted curves are very close to those of the measured curves.

However, there is an obvious difference of the shape between the predicted curves and the real curves: For the points before "overlap end", the real curves are very close to each other while the predicted curves are slightly different from each other. This difference might be the result of the preconditions of the numerical model. Following the preconditions, the production rates of the cosmogenic ^{21}Ne contained within the pixels are mainly controlled by the elevation. Moreover, the elevations of the upstream catchment area are always higher than those of the downstream catchment area because of the overall eastward tilting in the Great Plains. Therefore, the pixels within the catchment area of R15726 have higher elevations than those within the catchment area of Keystone. So that the predicted curve of R15726 before "overlap end" can be always higher than that of Keystone.

To conclude, based on the Figure 4.6, the predicted distributions of the cosmogenic ^{21}Ne contained within these two sites matches the measured ones very well in shape. This gives a possible explanation of the abnormal higher concentration of ^{21}Ne in the upstream point comparing to that of the downstream point.

However, even the shapes of these two row of curves look similar to each other, the predicted concentration of cosmogenic ^{21}Ne is much higher than that of the real situation, not only the lowest concentration but also the highest one. This might be resulted from the abnormal high value of T during the calculation. For our first calculation, T as 2.58Ma was used, which is based on the assumption that all the sediments remain exposed from the end of Pliocene to now.

The exposure time can be adjusted to get different concentration curves. When using 0.8 Ma as the exposure duration T, a distribution curve with a similar range of concentration as the real one (shown in Figure 4.7) can be developed.

However, from the result of ^{21}Ne-^{10}Be analysis (shown in Table 3.9 and Table 3.10), it is clear that most of the exposure duration calculated is higher than the 0.8 Ma used in the numerical model.

This conflict might be also resulted from the preconditions of this model. In the first precondition, all the sediments recycled have been exposed continually for the same time. However, in the previous chapters, it has been demonstrated that the recycled sediments in the Great Plains have experienced varying degrees of burial and recycling during their transport from the source area.

In addition, the revised result of the model (shown in Figure 4.7) means that if these recycled sediments were exposed continually, it would take only 0.8 Ma for them to accumulate such a number of cosmogenic ^{21}Ne. In the Chapter 3, the result of ^{21}Ne-^{10}Be analysis has proved that these sediments had experienced much longer time of being exposed. These sediments have experienced not only being

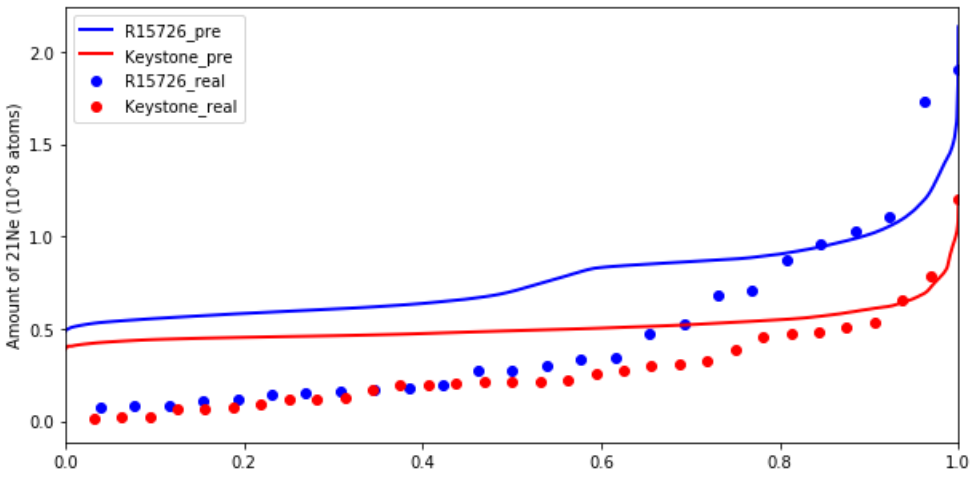

Figure 4.7: The comparison between the predicted distribution curves of cosmogenic ^{21}Ne and the real ones at R15726 and Keystone (T= 0.8Ma)

exposed, but also being buried and recycled. This over-simplified precondition might result in the underestimation of exposure time.

In Figure 4.7, with a changed T of 0.8 Ma, the highest points of the predicted concentration curves are very closed to those of the measured concentration curves. However, There exists variation of the shapes between the predicted concentration curves and the measured one. As suggested by this figure, these curves matches well for the pixels with high concentrations of ^{21}Ne while have significant variation for the pixels with low concentrations of ^{21}Ne.

Because the production rate of ^{21}Ne within each pixel has a strong relationship with the elevation of this pixel, the distribution curves of the elevation (as Figure 4.8) of all the pixels within these two catchments could mirror the distribution curves of the concentrations of ^{21}Ne contained within these pixels. In other words, every point on the curve of predicted concentrations of ^{21}Ne has a corresponding point on the curve of elevation. As suggested by Figure 4.8,the predicted curve matches well with the measured one for the pixels with high elevation, while the variation between the predicted and the real curves is significant for the pixels with low elevation.

This variation in Figure 4.7 is also resulted from the idealised preconditions. In the second precondition, the possibility of old pebbles being recycled into a modern channel is at the same rate throughout the Great Plains. This situation is highly improbable. The reality is, the landscape is in non-steady state topographically, the possibility of old pebbles being recycled is strongly dependent on the erosion rate at that location, and the erosion rate is controlled by the slope because the areas with higher gradients erode more quickly and produce a greater volume of materials.

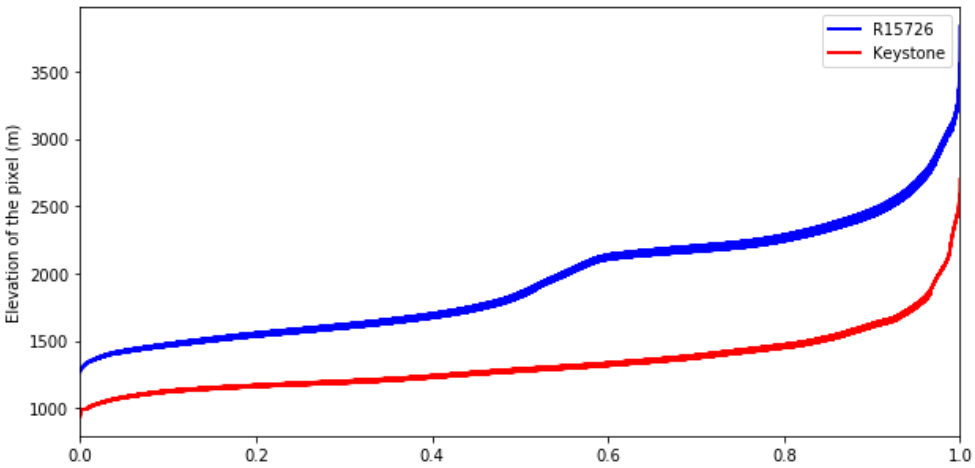

Figure 4.8: The distribution of elevation of the two catchment areas of R15726 and Keystone.

To find more information of the variation in Figure 4.7, the comparison between the predicted concentrations and the measured concentrations was put together with the distribution curves of the elevation within these two catchment areas (shown in Figure 4.9). As suggested from this figure, the change points of elevation, under which the variation in the comparison mainly happened, can be read. For R15726, the change point is 2300 m while for Keystone, the change point is 1500 m. For the pixels with higher elevations than the change point, the predicted concentrations of cosmogenic ^{21}Ne match well with the real one, while for the pixels with lower elevations than the change points, the variation between the predicted result and the real data is obvious.

To explore the cause of this situation, the average slope of each pixel was extracted using the DEM. With these data, the accumulation distribution curves of the elevations of each catchment area were generated. At the same time, the pixels of each catchment area were divided into two groups based on the change points read from Figure 4.9. Also, the accumulation distribution curves of the elevations within each group were developed. The results are shown in Figure 4.10 and Figure 4.11, for R15726 and Keystone, respectively.

For R15726, as suggested by the Figure 4.10, the red line is located to the left of the green line, which means the pixels with elevation lower than 2300 m (red line) are mostly distributed in a range of smaller gradients, compared with those pixels with elevation higher than 2300 m (green line). Therefore for the pixels, there exists a trend that the higher the elevation, the higher the gradients. As described above, the areas with higher gradients erode more quickly and produce greater volume of materials. And then these eroded sediments from the higher-elevation place would be carried to the lower-elevation place. This process would influence the shape of the distribution curve of cosmogenic ^{21}Ne in two ways: (1)

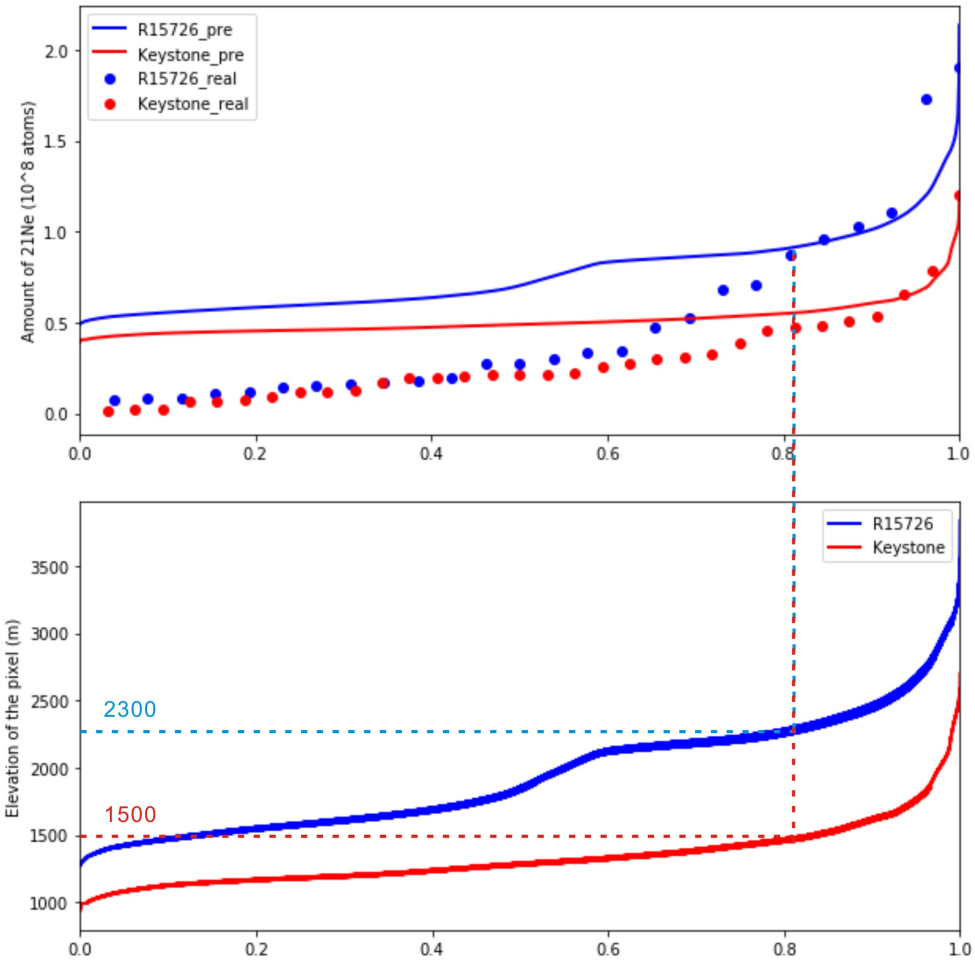

Figure 4.9: A schematic representation showing the change point of the elevation under which the variation in the concentration of ^{21}Ne happened.

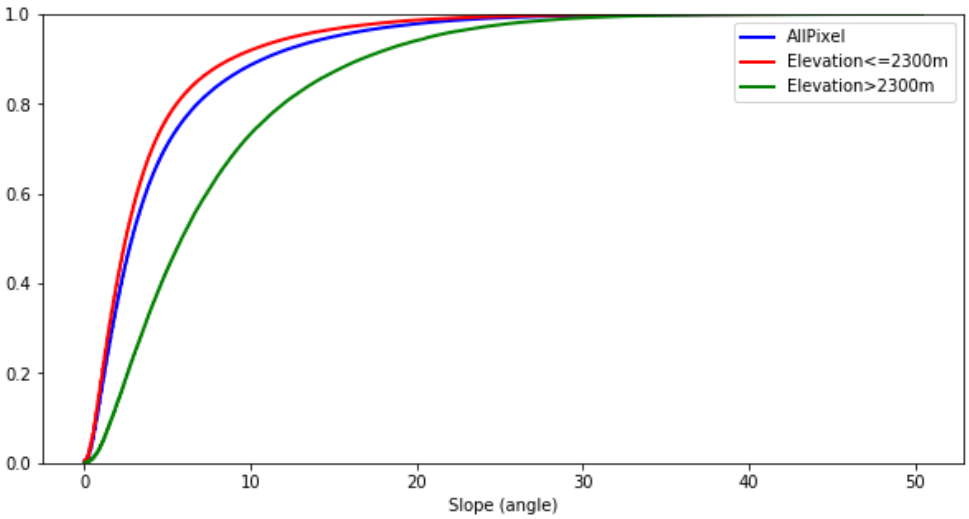

Figure 4.10: The accumulation distribution curve of the elevation in the catchment area of R15726 (blue line); the pixels were divided into to groups with the change point of 2300m, the accumulation distribution curves for these two groups are shown as red line and green line, respectively.

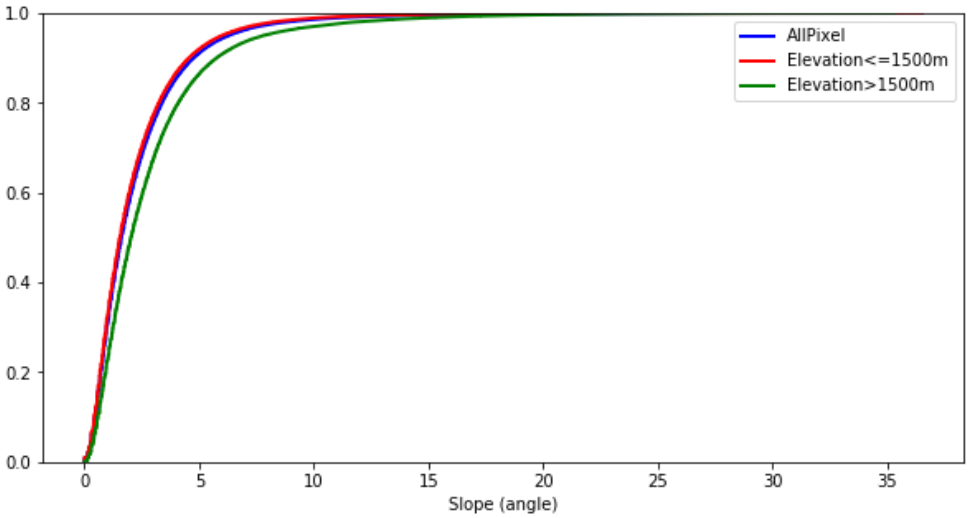

Figure 4.11: The accumulation distribution curve of the elevation in the catchment area of Keystone (blue line); the pixels were divided into to groups with the change point of 1500m, the accumulation distribution curves for these two groups are shown as red line and green line, respectively.

The sediments which were eroded from the high-elevation place and then carried to the low-elevation place would experience more time in the lower-elevation area, thus increasing the portion of the sediments with low concentrations of cosmogenic ^{21}Ne. This would make the "overlap end" of the measured curve migrate rightward, representing as from 0.5 to 0.6 in Figure 4.6; (2) The sediments which were eroded from the high-elevation place and then carried to the low-elevation place would bury the original sediments in situ. When being buried, the production rate of cosmogenic ^{21}Ne within the initial sediments of lower-elevation area decreases because of shielding, so that the the total cosmogenic ^{21}Ne accumulated would decrease. This would make the measured concentrations of cosmogenic ^{21}Ne in the low-elevation place considerably lower than the predicted concentrations with the numerical model. This is represented as the significant variation in Figure 4.7.

For Keystone, in Figure 4.11, a similar situation can be observed: the red line is located to the left of the green line, which means the pixels with elevation lower than 1500 m (red line) are mostly distributed in a range of smaller gradients, compared with those pixels with elevation higher than 1500 m (green line). However, the gap between the red line and the green line in Keystone (Figure 4.11) is smaller than that in R15726 (Figure 4.10). This means the variation of the high-elevation place and the low-elevation is less in Keystone, contributing to a smaller variation between the solid and the dotted red curves in Figure 4.7.

To conclude, although there is variation between the predicted curve and the measured data for the low elevation samples, the broad match between the predicted result and the measured data suggests that recycling from contrasting elevations is a key process in the long transport distances of gravels in these rivers.

4.2.2 Model to Verify the Effect of Source Sediments

The result of cosmogenic nuclides analysis (shown as Table 3.9, Table 3.10 and Figure 3.22) suggest that the recycled sediments are mainly from the Pliocene and Miocene time. This raises a question regarding the control of recycling: Does the source of paleosediments (Pliocene or Miocene) affect the concentrations of the cosmogenic ^{21}Ne contained within the recycled grains, thus contributing to the higher concentrations of the cosmogenic ^{21}Ne in the upstream pebbles?

To find the information about the influence of paleosediments on the accumulated cosmogenic ^{21}Ne, the distribution of paleochannels throughout the study area was firstly examined. Condon (2005) compiled all the previous studies and drew a map of the possible distribution of paleochannels of Pliocene time (mainly Broadwater Formation) and Miocene time (mainly Ogallala Group), which is shown in Figure 2.5.

As suggested by Figure 2.5, from Casper to R15726, the channel system mainly

recycled the Pliocene paleosediments, while after R15726, especially the plain area between R15726 and Keystone, the channel system cross-cuts Pliocene and Miocene paleochannels. A numerical model was developed to test if this difference in source paleosediments contribute to the higher concentrations of cosmogenic ^{21}Ne contained within the upstream pebbles (the conflict shown in Figure 4.1).

Numerical Model

The concentrations of cosmogenic ^{21}Ne within the samples collected from Miocene and Pliocene are shown in Figure 4.12. Except for two sample of the Miocene age which contains an abnormal higher concentration of ^{21}Ne than those of the Pliocene age, most Pliocene samples contain more cosmogenic ^{21}Ne than those of Miocene age.

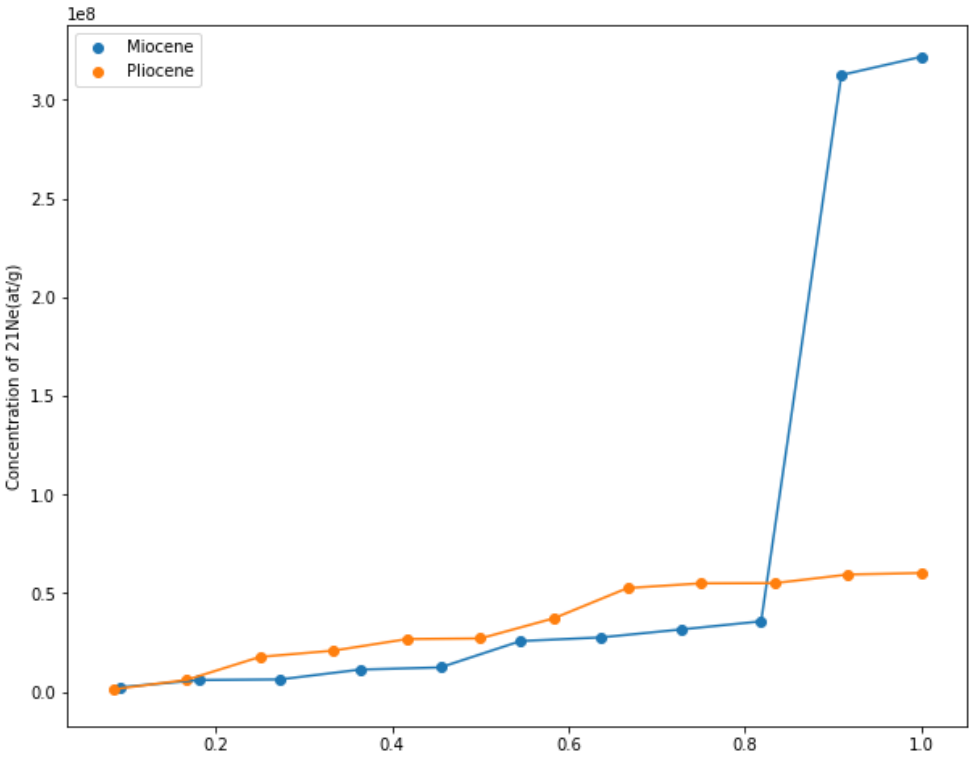

Figure 4.12: Distribution curves of ^{21}Ne of Miocene and Pliocene (background Ne)

To test the influences of the sources of the recycled paleosediments, a model was developed. In this model, the distributions of the concentrations of the cosmogenic ^{21}Ne contained within the Pliocene sediments and Miocene sediments were simplified based on the fitting curves of the measured data (shown in Figure 4.13).

Next, the pebbles collected from R15726 were assumed to be from lateral sediment sources which contain mostly recycled Pliocene paleosediments. While

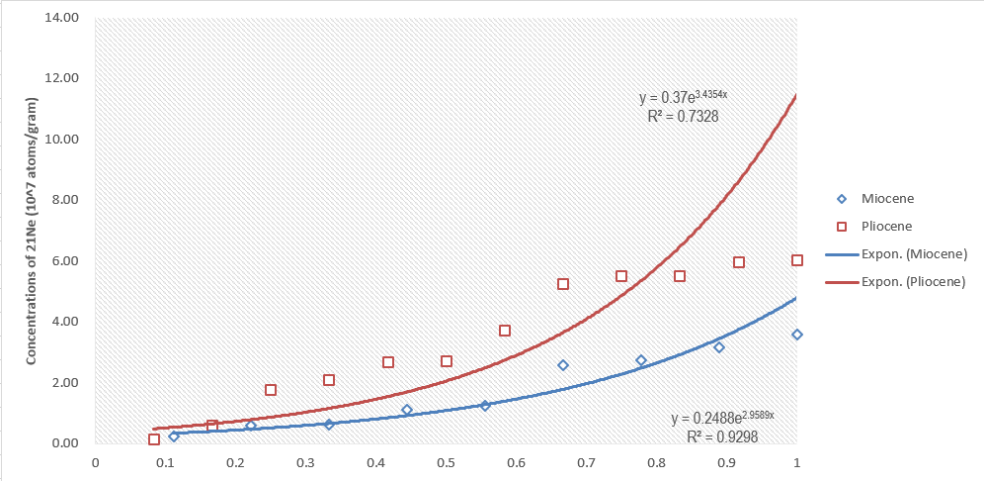

Figure 4.13: Predicted concentrations of the cosmogenic ^{21}Ne contained within the Pliocene sediments and Miocene sediments based on the fitting curves.

for Keystone, the recycled pebbles are assumed to be from not only the Pliocene paleosediments but also the Miocene paleosediments. Firstly, the portion of different paleosediments recycled into Keystone was assumed as 1:1, which means 50% of the recycled sediments in Keystone were Pliocene paleosediments and 50% were Miocene paleosediments. The result is put together with the measured data of these two sites, showing in Figure 4.14.

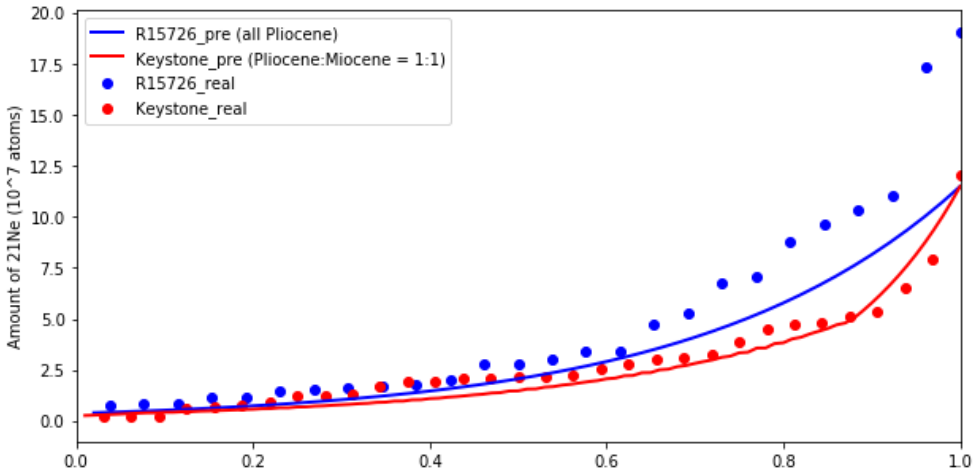

Figure 4.14: Predicted distribution curves of ^{21}Ne of R15726 (pure Pliocene) and Keystone (Miocene mixed with Pliocene), the ratio of Pliocene paleosediments to Miocene paleosediments is 1:1. The measured concentrations of ^{21}Ne in these two sites are also plotted.

As suggested by this figure, the predicted distribution of the concentrations of cosmogenic ^{21}Ne in Keystone (red solid curve) matches very well with the

measured one (red dotted curve). So that it can be concluded that the pebbles collected from the Keystone are mostly from the recycling, in addition, these pebbles were not only recycled from the Pliocene paleosediments, but also the Miocene paleosediments, the ratio of the recycled pebbles from two sources are nearly 1:1.

However, it can also be observed that the predicted concentrations of cosmogenic ^{21}Ne in R15726 (blue solid curve) are lower than the measured one, especially for the high-elevation place. Because the predicted concentrations are all based on the measured data of the paleosediments collected from the shielding strata, the result of the model can mirror the situations that the pebbles experienced recycling shortly before being collected. Thus, the higher concentrations of the measured data than the predicted results suggests that the pebbles collected from the R15726 have experienced a considerable period of exposure time before being collected. Moreover, this phenomenon is more apparent for the pebbles with higher elevation because of the higher production rate of the cosmogenic nuclides at that place.

At last, in the model, the portion of different paleosediments recycled was adjusted to see the corresponding changes in the curves of distribution. Here, three different portions as 1:1, 1:2 and 2:1 were set. Results are shown in Figure 4.15.

As suggested by Figure 4.15, the change of the portion of different paleosediments recycled only has a slight influence on the distribution curve.

Analysis of the Result

Figure 4.15 indicates that the concentration of ^{21}Ne from pure Pliocene sediments (R15726, the upstream point) are higher than those from the mixed sediments (Keystone, the downstream point). This agrees the result of the concentration distribution of some pebbles collected from R15726 are higher than those of Keystone. Moreover, as suggested by the result (Figure 4.14), for the pebbles collected in Keystone, half of them were from Pliocene paleosediments and half from Miocene paleosediments. In addition, the pebbles collected from R15726 have experienced a considerable exposure history before being collected. However, changing the portion of paleosediments from different ages has a modest effect on altering the curves (Figure 4.15).

To conclude, the result of this part suggests that paleosediments of Pliocene/Miocene are the main sources of the recycled pebbles in the Great Plains, but the portion of them plays a minor role in the distributions of cosmogenic ^{21}Ne contained within the pebbles along the North Platte River.

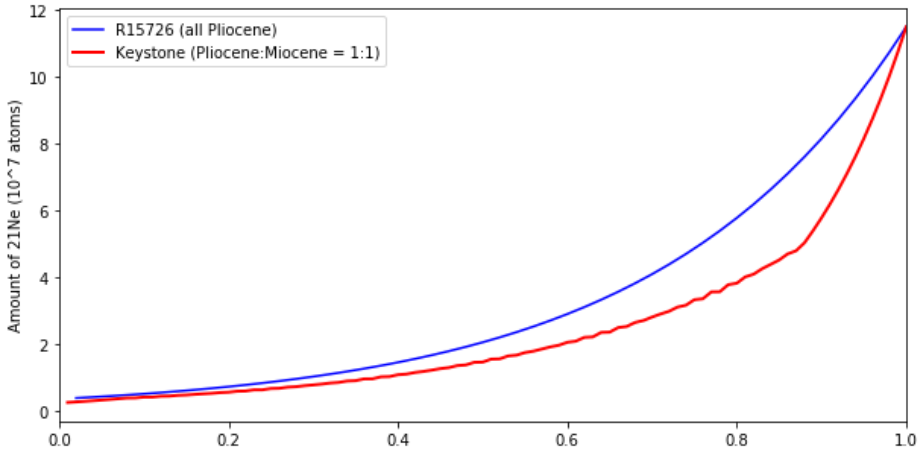

(a) Upstream point all Pliocene; Downstream: Pliocene sediments: Miocene sediments = 1:1

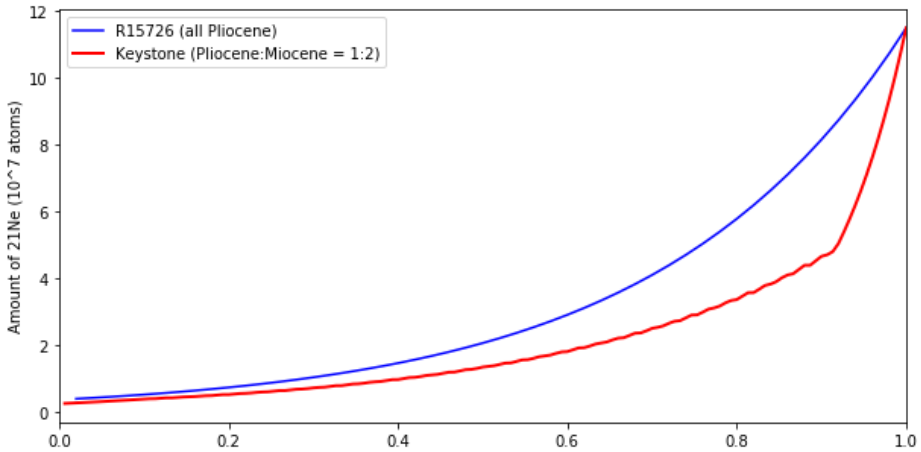

(b) Upstream point: all Pliocene; Downstream: Pliocene sediments: Miocene sediments = 1:2

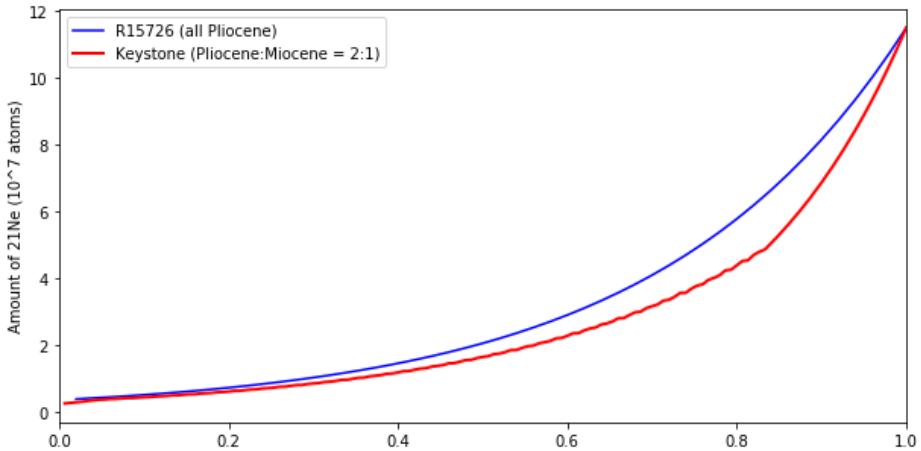

(c) Upstream point: all Pliocene; Downstream: Pliocene sediments: Miocene sediments = 2:1

Figure 4.15: Predicted distribution curves of ^{21}Ne of R15726 (pure Pliocene) and Keystone (Miocene mixed with Pliocene), with different ratios of the recycled Pliocene sediments and the recycled Miocene sediments.

4.2.3 The Effect of Grain Sizes

The concentration of ^{21}Ne contained within the collected samples can be plotted against the grain sizes of these samples (shown in Figure 4.16, the data is shown in Table 4.1 and Table 4.2). Here, the intermediate axis of these pebbles was used.

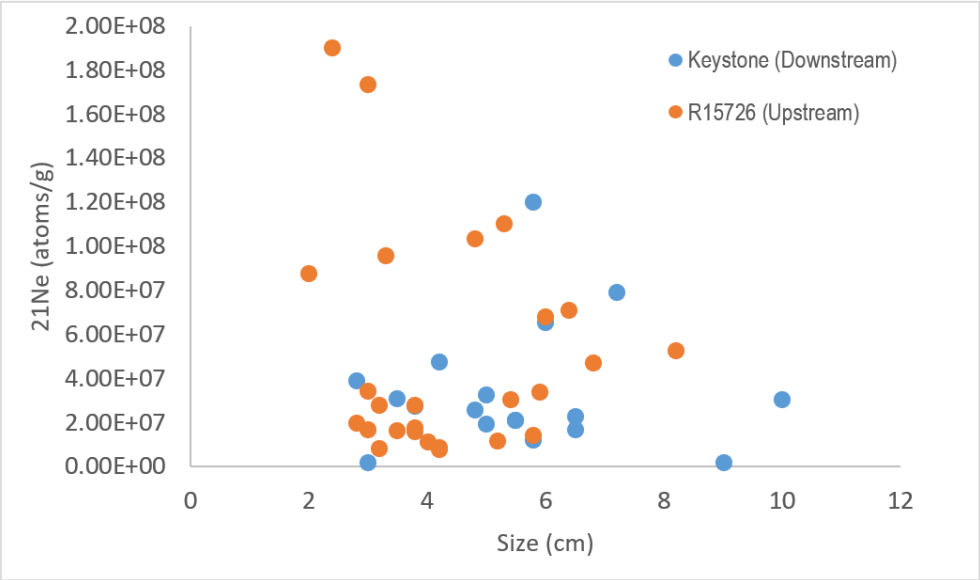

Figure 4.16: The concentration of ^{21}Ne contained within the samples against the grain sizes

Among the samples collected from R15726, the highest concentration of ^{21}Ne appears in the small sample (about 2 mm), but for the samples collected from R15726, the highest concentration of ^{21}Ne appears in the sample with an intermediate axis of about 6mm. For both the sampling localities, no apparent relationship between the concentration of ^{21}Ne and the grain sizes was recognised, suggesting the control of grain sizes on the recycling is weak.

4.2.4 Summary of the Controls of Recycling

The result of cosmogenic nuclides introduced an interesting apparent contradiction conflict that cosmogenic ^{21}Ne concentrations contained within the samples collected from upstream are higher than those from downstream. To resolve this conflict, numerical models were built to test the controls of cosmogenic ^{21}Ne accumulated during recycling. Two geological parameters, elevation and age of paleosediments, were tested in these models. As suggested by the results, elevation plays a dominant role in the accumulation of cosmogenic ^{21}Ne during recycling. And, paleosediments of Miocene/Pliocene age are the main source of recycled pebbles. For Keystone, the ratio of the paleosediments from these two sources is

Table 4.1: Data of ^{21}Ne contained within the collected samples from R15726 (upstream) and the intermediate axis of these samples

	File	Size (cm)	21Ne*at/g	d	%	subtract inherited 21Ne
R15726 (Upstream)	DK109	4.2	1.63E+07	1.90E+06	11.70%	7.82E+06
R15726 (Upstream)	DK115	3.2	1.70E+07	1.92E+06	11.30%	8.46E+06
R15726 (Upstream)	DK096	4.2	1.71E+07	2.37E+06	13.80%	8.61E+06
R15726 (Upstream)	DK122	4	1.96E+07	3.47E+06	17.70%	1.11E+07
R15726 (Upstream)	DK147	5.2	2.00E+07	3.91E+06	19.50%	1.15E+07
R15726 (Upstream)	Dk141	5.8	2.27E+07	2.24E+06	9.90%	1.42E+07
R15726 (Upstream)	DK108	3.8	2.41E+07	3.28E+06	13.60%	1.56E+07
R15726 (Upstream)	DK113	3.5	2.48E+07	1.97E+06	7.90%	1.63E+07
R15726 (Upstream)	DK123	3	2.52E+07	3.24E+06	12.90%	1.67E+07
R15726 (Upstream)	DK131	3.8	2.63E+07	2.69E+06	10.20%	1.78E+07
R15726 (Upstream)	DK111	2.8	2.82E+07	1.29E+06	4.60%	1.97E+07
R15726 (Upstream)	DK097	3.8	3.62E+07	2.07E+06	5.70%	2.77E+07
R15726 (Upstream)	DK130	3.2	3.63E+07	3.01E+06	8.30%	2.78E+07
R15726 (Upstream)	DK117	5.4	3.86E+07	2.68E+06	7.00%	3.01E+07
R15726 (Upstream)	DK148	5.9	4.24E+07	2.48E+06	5.90%	3.39E+07
R15726 (Upstream)	DK085	3	4.28E+07	2.20E+06	5.10%	3.43E+07
R15726 (Upstream)	DK135	6.8	5.55E+07	2.14E+06	3.90%	4.70E+07
R15726 (Upstream)	DK128	8.2	6.15E+07	2.70E+06	4.40%	5.30E+07
R15726 (Upstream)	DK092	6	7.63E+07	3.08E+06	4.00%	6.78E+07
R15726 (Upstream)	Dk142	6.4	7.93E+07	4.07E+06	5.10%	7.08E+07
R15726 (Upstream)	DK091	2	9.59E+07	3.42E+06	3.60%	8.74E+07
R15726 (Upstream)	DK094	3.3	1.04E+08	5.42E+06	5.20%	9.59E+07
R15726 (Upstream)	DK110	4.8	1.12E+08	4.26E+06	3.80%	1.03E+08
R15726 (Upstream)	Dk140	5.3	1.19E+08	6.07E+06	5.10%	1.10E+08
R15726 (Upstream)	DK129	3	1.82E+08	6.73E+06	3.70%	1.73E+08
R15726 (Upstream)	DK114	2.4	1.99E+08	7.12E+06	3.60%	1.90E+08

Table 4.2: Data of ^{21}Ne contained within the collected samples from Keystone (downstream) and the intermediate axis of these samples

	File	Size (cm)	21Ne*at/g	d	%	subtract inherited 21Ne
Keystone (Downstream)	CZ124	9	1.03E+07	1.99E+06	19.40%	1.77E+06
Keystone (Downstream)	Dk143	3	1.05E+07	1.34E+06	12.80%	1.95E+06
Keystone (Downstream)	CZ121	5.8	2.06E+07	1.95E+06	9.50%	1.21E+07
Keystone (Downstream)	CZ116	6.5	2.54E+07	1.35E+06	5.30%	1.69E+07
Keystone (Downstream)	CZ126	5	2.77E+07	1.09E+06	3.90%	1.92E+07
Keystone (Downstream)	CZ127	5.5	2.94E+07	1.47E+06	5.00%	2.09E+07
Keystone (Downstream)	CZ141	5.5	2.96E+07	1.38E+06	4.70%	2.11E+07
Keystone (Downstream)	CZ137	6.5	3.11E+07	1.11E+06	3.60%	2.26E+07
Keystone (Downstream)	CZ115	4.8	3.40E+07	1.36E+06	4.00%	2.55E+07
Keystone (Downstream)	Dk144	3.8	3.61E+07	3.47E+06	9.60%	2.76E+07
Keystone (Downstream)	CZ132	10	3.86E+07	2.27E+06	5.90%	3.01E+07
Keystone (Downstream)	DK150	3.5	3.93E+07	2.63E+06	6.70%	3.08E+07
Keystone (Downstream)	CZ120	5	4.10E+07	1.89E+06	4.60%	3.25E+07
Keystone (Downstream)	DK149	2.8	4.76E+07	3.06E+06	6.40%	3.91E+07
Keystone (Downstream)	Dk145	4.2	5.60E+07	3.85E+06	6.90%	4.75E+07
Keystone (Downstream)	CZ142	6	7.41E+07	2.78E+06	3.80%	6.56E+07
Keystone (Downstream)	CZ136	7.2	8.75E+07	3.29E+06	3.80%	7.90E+07
Keystone (Downstream)	CZ138	5.8	1.29E+08	4.18E+06	3.20%	1.20E+08

about 1:1. However, changes in the ratio of the paleosediments from these two sources plays a minor role in the measured concentrations of cosmogenic ^{21}Ne. For the influence of grain size, the data shows no obvious relationship between the grain sizes and the measured concentrations of cosmogenic ^{21}Ne contained within the R15726 and Keystone.

4.3 Application of Recycling in Previous Studies

In chapter 3 the real concentration of cosmogenic ^{21}Ne and the predicted concentration of cosmogenic ^{21}Ne in the two models are put together (shown in Figure 3.20). As suggested by the comparison between the real data (solid lines) and the predicted data (dotted lines), almost all the real data have higher concentrations than the predicted data. This means that even the grains sourced from the mountain area moved downstream with a considerably low migration rate, the cosmogenic ^{21}Ne accumulated are still not enough to reach the level of the measured one. In other words, all the sediments have stayed exposed on the Great Plain for a very long time and then been recycled into the fluvial sediments. This conclusion is not only suitable for the modern sediments, but also for the paleosediments. Most of the paleosediments were not migrating all the time during their transport; they must have experienced deposition, being burial and recycling.

Paleosediments are widely applied in the studies of reconstructing the fluvial characteristics, gradients for example, of the paleochannels because the paleosediments are assumed to reflect the real fluvial situation when these paleosediments deposited. However, recycling might happen during the transport and the deposition of the paleosediments, thus mixing the fresh paleosediments with even older ones, and distorting the relationship between the characteristics of the sediments and the fluvial environment. In this part, a grain size-based study of the Great Plain was re-done, taking the recycling into consideration, to examine the effects of recycling on reconstructing paleochannel systems.

4.3.1 Previous Studies

According to the study of Duller et al. (2012), the gradient of Miocene and Pliocene is reconstructed using the sediments collected from the Miocene and Pliocene.

In that paper, paleoslopes can be estimated from D_{50} (the value at the 50% point in the grain sizes distribution curve) and H (the depth of the paleochannels measured), based on the famous equation developed by Paola and Mohrig (1996):

$$\tau_c^* = \frac{HS}{(\rho_s - \rho)/\rho * D_{50}} \tag{4.5}$$

S is the gradients of the channel; ρ_s represents the density of the sediments while ρ represents the density of the water. τ_c^* is 0.045-0.06 based on the previous studies (Paola and Mohrig, 1996; Mueller and Pitlick, 2005). D_{50} is the value at the 50% point in the grain sizes distribution curve, cm, which means half of the grains collected at that point are smaller than this value. In this equation, the local shear stress is set as 1.2 – 1.4 times the critical shear stress which is suitable for the bedload to be retained (Mueller and Pitlick, 2005). Paleoslope S is therefore calculated as:

$$S_{(x)} = \frac{1.2 * \tau_c^* * \rho_s * D_{50}}{H} = \frac{1.4 * 0.05 * 1.6 * D_{50}}{H} = \frac{0.112 * D_{50}}{H} \tag{4.6}$$

Where

$$\rho_s = {}^{(\rho_s - \rho)}/_{\rho} \tag{4.7}$$

In Duller's paper (2012), D_{50} for estimating the paleoslopes came from a field data collected from sites within Remsburg Ranch beds (RRB) and Ash Hollow Formation (AHF). For the depth of the paleochannels, 1m< H< 2m is used in Miocene calculations and 1.5m< H< 2m is used in Pliocene calculations.

The basis for this kind of study is that the samples collected from the old strata can reflect the depositional environment of the channel. However, as suggested by the results in the previous chapters, the paleosediments in the Great Plains had also experienced recycling. Recycling has changed the distribution of the grain sizes considerably. That is to say, the paleosediments collected from the strata cannot be used to reflect the depositional environment of the channel because they might come from the recycling through the lateral sediment inputs.

Because the modern river has experienced recycling, to simulate the reconstruction of channel profile using grain size data which have experienced recycling, a model was developed to reconstruct the modern North Platte River using the modern grain sizes collected. If the recycling couldn't affect the relationship between the grain sizes and the fluvial environment, the reconstructed river profile would be very closed to the real one. In contrast, if the reconstructed river profile cannot mirror the characteristics of the real one, it means the recycling happening in the Great Plains has a unignorable impact on the well-believed idea that collected samples can be used on reconstructing the fluvial situation.

Here, we also used the same method in Duller's paper (2012). For modern North Platte River, the data of D_{50} were collected using the photo counting method (shown in Chapter 2) along the modern river. The depth of modern North Platte River can be estimated in two steps: (1) the river depth near Grand Island, Nebraska, is 1.2 ± 0.4m, based on the previous study (Crowley, 1983a), which is located about 500km downstream from the Wyoming-Nebraska border; (2) There

is an equation used to calculate the change of river depth along the river, shown as below:

$$H = k_1 x^b + H_0 \tag{4.8}$$

in this equation, k_1 equals to 0.02 and b equals to 0.4 (Duller et al., 2012). With the distance x of 500km and the corresponding value of 1.2m for H, the depth of other localities can be calculated. Within the study area, the calculated depth of river is shown in Figure 4.17). As suggested by this figure, the values of $H_1 = 1$ m and $H_2 = 1.5$ m were used.

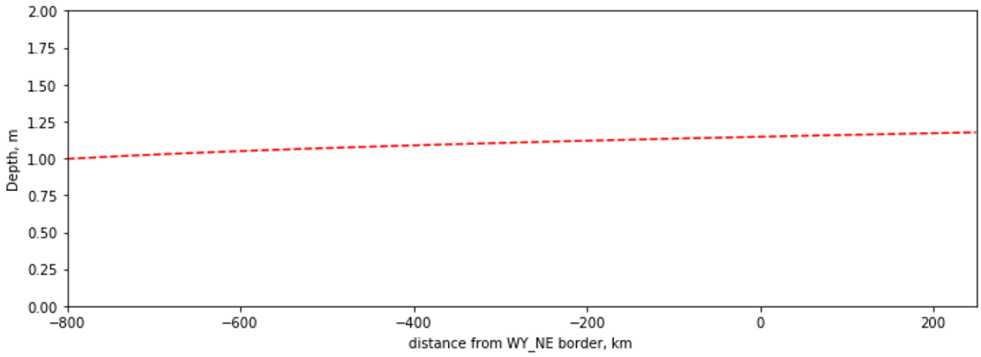

Figure 4.17: Depth of the river, against downstream distance for the North Platte River.

In this part, the model was developed to test the influence of recycling on the reconstruction method, so that we used the same method as that in Duller's paper (2012). Moreover, in order to be consistent with the study in that paper, the data collected from the same area (shown in the black dotted square in Figure 4.18) was used in the calculation.

The results of slope reconstruction are shown in Figure 4.19, with the detailed value shown in Table 4.3.

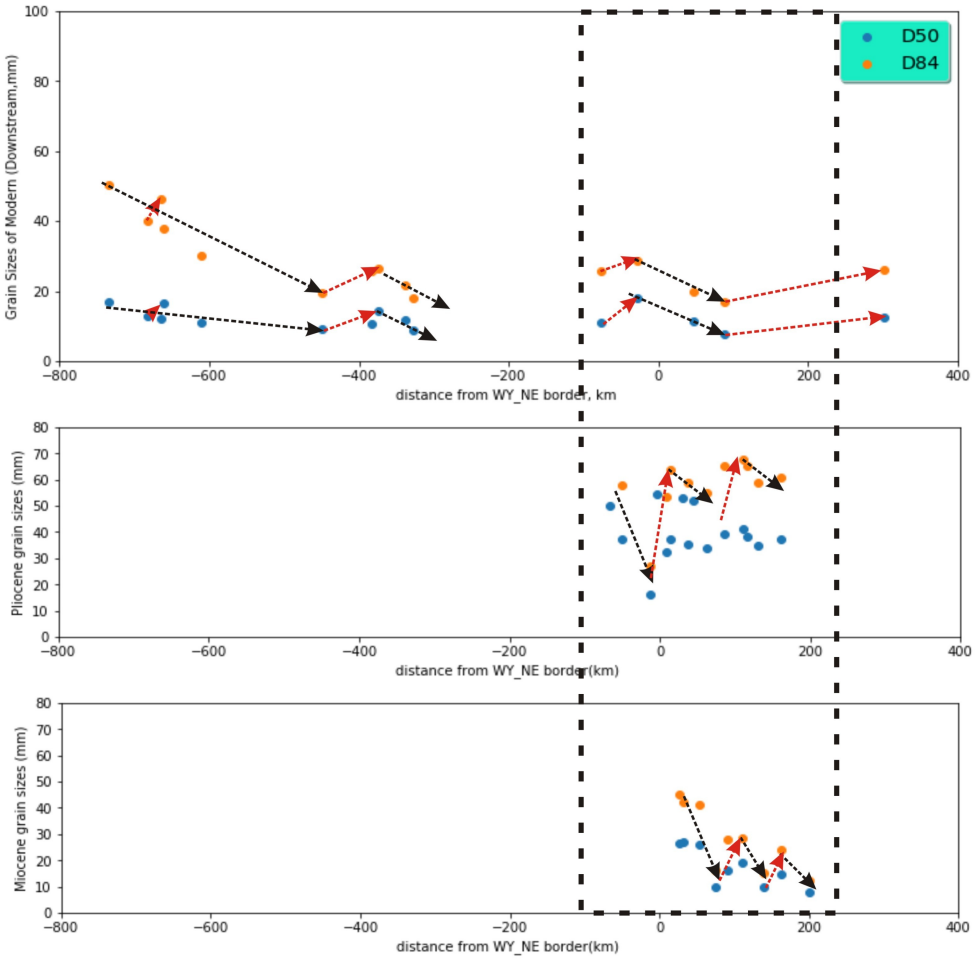

Figure 4.18: Sedimentary sinks. D_{50} and D_{84} are shown as dotted blue and orange symbols, respectively. The red dotted lines with an arrow represent the abnormal increase of grain size; while the black dotted lines with an arrow represent the normal downstream fining used to reconstruct the fitting curves. Data of the modern samples comes from this study, and the data of the Pliocene/Miocene samples are from the previous study (Duller et al., 2012).

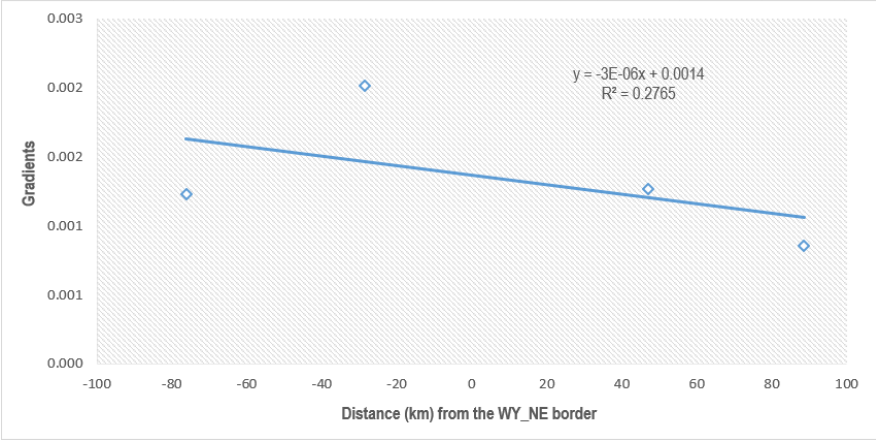

(a) H = 1m

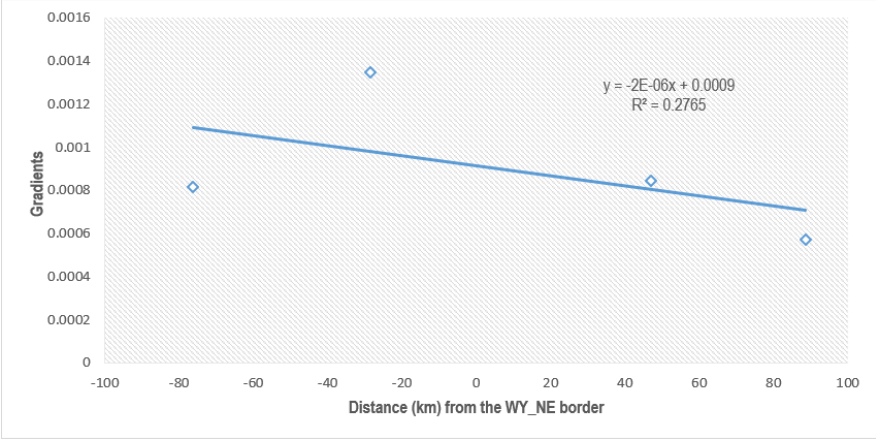

(b) H = 1.5m

Figure 4.19: Results of slope reconstruction using different river depth.

Table 4.3: Results of slope reconstruction of four groups

	longitude	latitude	D50(mm)	Distance E of WY-NE border	Slope(1m)	Slope(1.5m)
Modern	-104.533	42.211	11	-76.174	0.001	0.000818
Modern	-104.183	42.054	18	-28.524	0.002	0.001346
Modern	-103.636	41.839	11.3	46.986	0.001	0.000846
Modern	-103.315	41.733	7.7	88.646	0.001	0.000573

$$S_1 = -\frac{dE_1}{dx} = -0.000003x + 0.0014 \tag{4.9}$$

$$S_{1.5} = -\frac{dE_{1.5}}{dx} = -0.000002x + 0.0009 \tag{4.10}$$

Within the equation, S represents the slope, dE represents the change of elevation between two points, dx represents the change of the distance between two points.

Integral calculation can be done to assess the changes of the elevations against the flowing distances, which is also the river profile. And the results of the river-profile reconstruction is shown as below:

$$E_1 = (0.0000015x^2 - 0.0014x) * 1000 + C_1 \tag{4.11}$$

$$E_{1.5} = (0.000001x^2 - 0.0009x) * 1000 + C_{1.5} \tag{4.12}$$

In these equations, C represents the constants generated during the integration and C_1 is for the situation with 1 m depth, and $C_{1.5}$ represents that with 1.5m depth. The constants do not matter because they only affect average elevation of these river profiles, but not the gradient of them. The comparison between the reconstructed river profile and the real one were put together, showing in Figure 4.20.

As suggested by Figure 4.20, the matching of the reconstructed river profile and the real profile is poor: The reconstructed profile matches well with the real profile within the area samples collected. However, for both the upstream and the downstream parts, a considerable variation can be recognised. In Duller's paper (Duller et al., 2012), the reconstructed paleochannel profile was used to infer the strength of the tilting happened in the mountain area. However, the result shown in Figure 4.20 suggest that, in the places where recycling dominants, the reconstructed river profile using a limited area of grain size data cannot be used to reconstruct the whole picture of the channel system as it would contribute to a great deviation between the reconstructed profile and the real one.

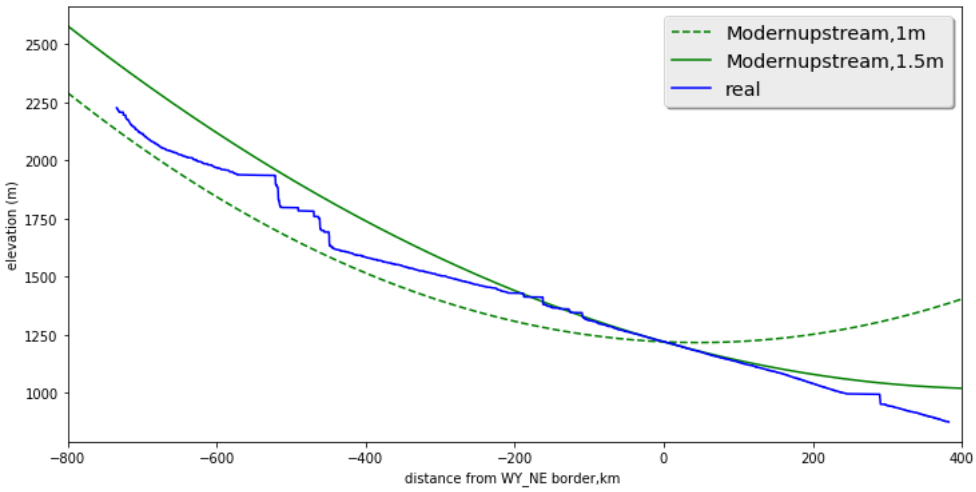

Figure 4.20: Comparison between the reconstructed profile and the real profile.

4.3.2 Updated Method Reconstructing the River Profile

From Figure 4.20, the good news is that the grain sizes data collected can be used to reconstruct the regional fluvial situation. So that, a further test was done to explore how to update this method to reconstruct the whole picture of the river profile using grain size data.

Based on the result in chapter 2, the North Platte River system can be divided into three sub-areas. Moreover, within each sub-area, the grain sizes exhibit a downstream fining trend and an abrupt downstream increase (shown in Figure 2.20). These abrupt downstream increases represent the mixing of larger grains from lateral sediment inputs, while these downstream fining trends represent the normal flowing process between two lateral sediment inputs. So that, the grain size data within these downstream decreasing stages can reflect the real fluvial environment without the influences of lateral sediment inputs. That is to say, using these data to reconstruct the regional river profile is feasible (shown in Figure 4.21).

Firstly, the regional gradients of these stages with normal downstream grain size fining trend was reconstructed (shown in Figure 4.23). The data was shown in Table 4.4.

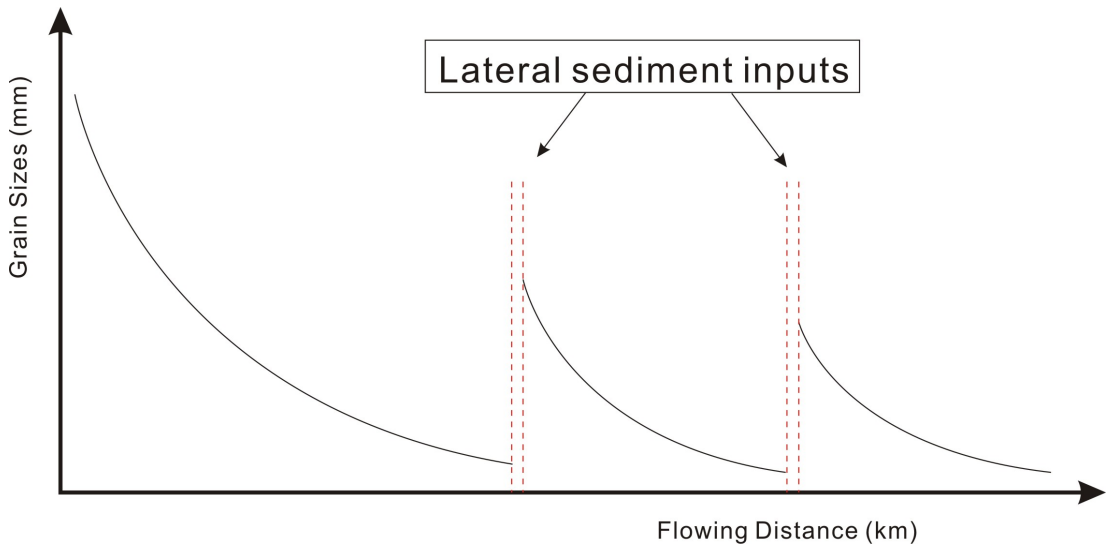

Figure 4.21: Reconstruct the whole channel using grain sizes data within different parts, which are divided based on the localities of lateral sediment inputs.

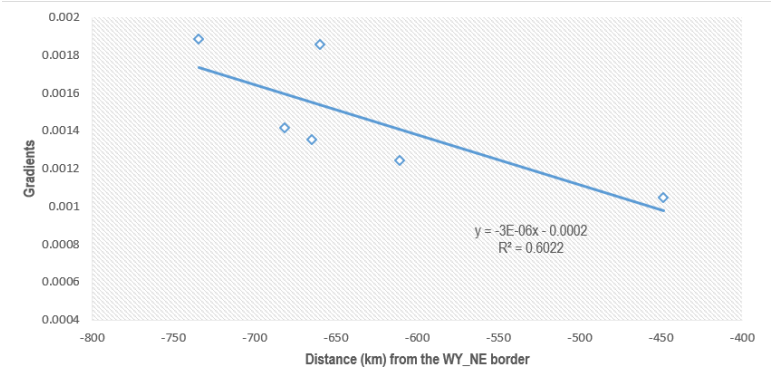

(a) the 1st downstream fining stage, when H = 1m

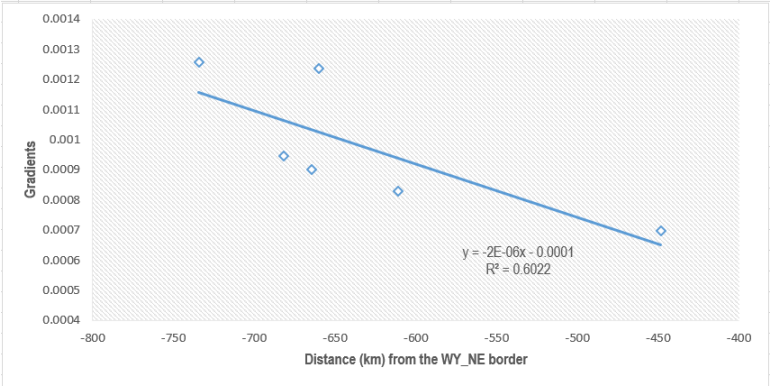

(b) the 1st downstream fining stage, when H = 1.5m

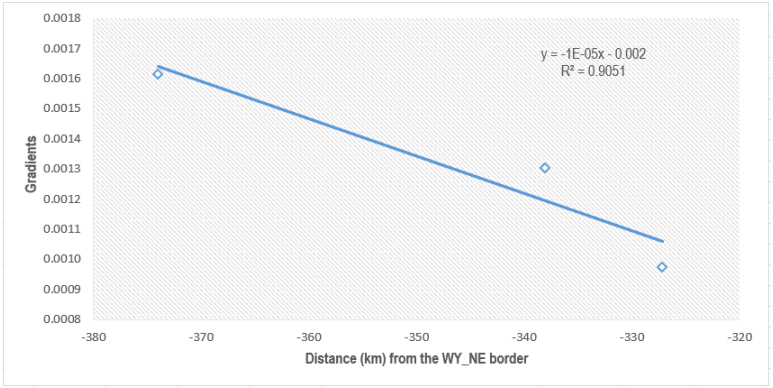

(c) the 2nd downstream fining stage, when H = 1m

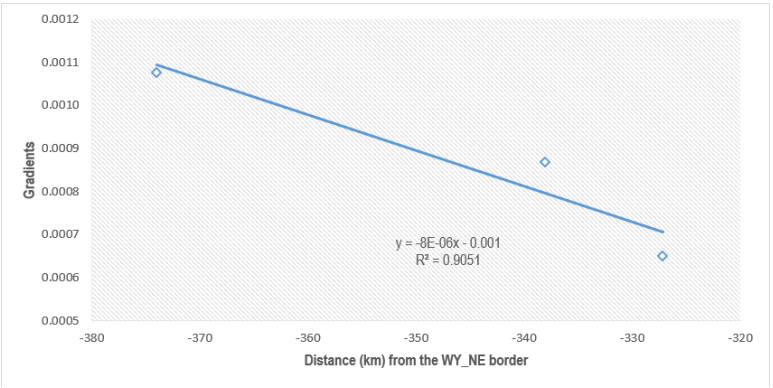

(d) the 2nd downstream fining stage, when H = 1.5m

Figure 4.22: Results of slope reconstruction using different river depth for the three downstream fining stages(1/2).

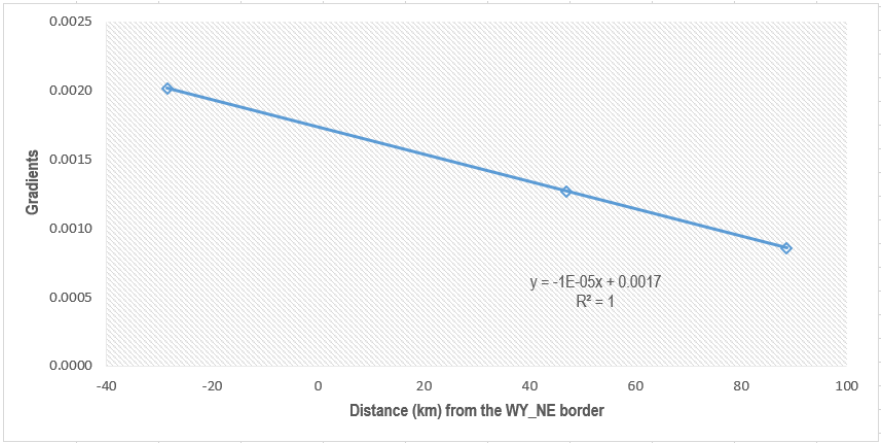

(a) the 3rd downstream fining stage, when H = 1m

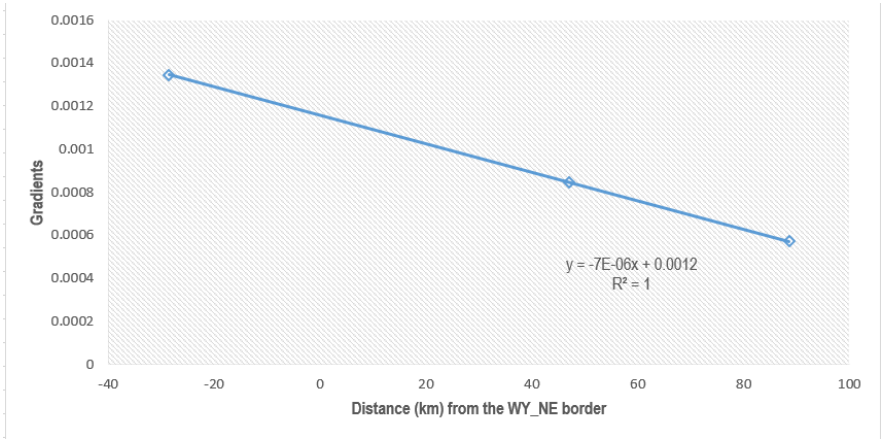

(b) the 3rd downstream fining stage, when H = 1.5m

Figure 4.23: Results of slope reconstruction using different river depth for the three downstream fining stages(2/2).

Table 4.4: Results of slope reconstruction using different river depth for the three downstream fining stages

	longitude	latitude	D50(mm)	Distance E of WY-NE border	Slope(1m)	Slope(1.5m)
Modern	-106.716	42.55	9.3	-448.504	0.001046	0.000697
Modern	-106.945	41.749	11.1	-611.114	0.001244	0.000829
Modern	-106.919	41.556	16.6	-660.034	0.001857	0.001238
Modern	-106.88	41.54	12.1	-664.734	0.001353	0.000902
Modern	-106.806	41.453	12.7	-681.784	0.001417	0.000945
Modern	-106.543	41.192	16.8	-734.334	0.001887	0.001258

	longitude	latitude	D50(mm)	Distance E of WY-NE border	Slope(1m)	Slope(1.5m)
Modern	-106.368	42.838	14.4	-373.994	0.002	0.001
Modern	-106.074	42.863	11.6	-338.084	0.001	0.001
Modern	-105.981	42.851	8.7	-327.184	0.001	0.001

	longitude	latitude	D50(mm)	Distance E of WY-NE border	Slope(1m)	Slope(1.5m)
Modern	-104.183	42.054	18	-28.524	0.002	0.001346
Modern	-103.636	41.839	11.3	46.986	0.001	0.000846
Modern	-103.315	41.733	7.7	88.646	0.001	0.000573

Similarity, the regional river profiles for these stages were reconstructed.

For the downstream fining stage within the up-sub-area, the reconstructed regional river profile is as below:

$$E_1 = (0.0000015x^2 + 0.0002x) * 1000 + C_1 \tag{4.13}$$

$$E_{1.5} = (0.000001x^2 + 0.0001x) * 1000 + C_{1.5} \tag{4.14}$$

For the downstream fining stage within mid-sub-area, the reconstructed regional river profile is as below:

$$E_1 = (0.000005x^2 + 0.002x) * 1000 + C_1 \tag{4.15}$$

$$E_{1.5} = (0.000004x^2 + 0.001x) * 1000 + C_{1.5} \tag{4.16}$$

For the downstream fining stage within down-sub-area, the reconstructed regional river profile is as below:

$$E_1 = (0.000005x^2 - 0.0017x) * 1000 + C_1 \tag{4.17}$$

$$E_{1.5} = (0.0000035x^2 - 0.0012x) * 1000 + C_{1.5} \tag{4.18}$$

Now, all the reconstructed regional profiles and the modern profiles can be plotted together (shown in Figure 4.24). Also, the constants of all these reconstructed regional profiles are adjusted to make them plotted near the real profile.

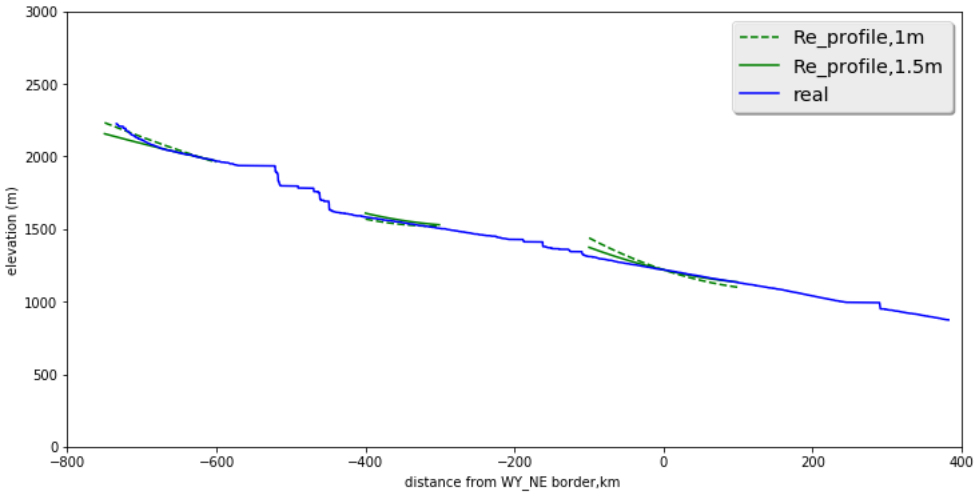

Figure 4.24: Comparison between the reconstructed profile and the real profile.

As Figure 4.24 shows, the reconstructed profiles match well with the real one. However, on this figure, all the reconstructed profiles are limited within the area where the samples were collected.

These fragments of the reconstructed profile can then be extended to get a combined reconstructed profile. There are two ways to extend the fragments to get the combined profile: the first is to elongate each fragment following its own reconstructed equation (shown in Figure 4.25), and the second is to connect these fragments with straight lines (shown in Figure 4.26).

As suggested by these two figures, the combined reconstructed profile, connected with simple straight lines, matches the real profile better than the other one. The imperfect match between profiles near -200 can be explained with the intense changes of channel profile nearby.

To conclude, in the area where recycling existed, the grain sizes should be checked to be used to reconstruct the fluvial environment. The normal downstream fining trend between two lateral sediment inputs can reflect the real fluvial situation because that place had not been influenced by the lateral sediment inputs. However, they can only reflect the regional fluvial environment. The

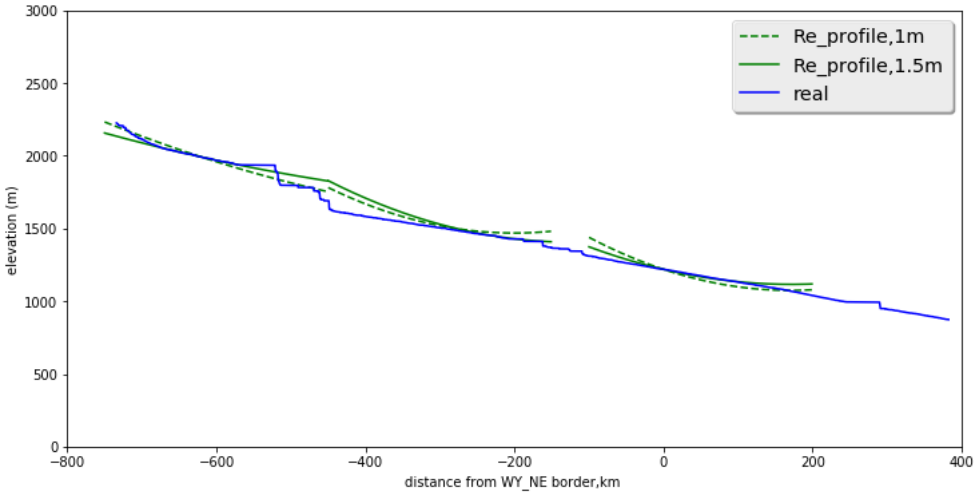

Figure 4.25: Comparison between the combined reconstructed profile (elongation) and the real profile.

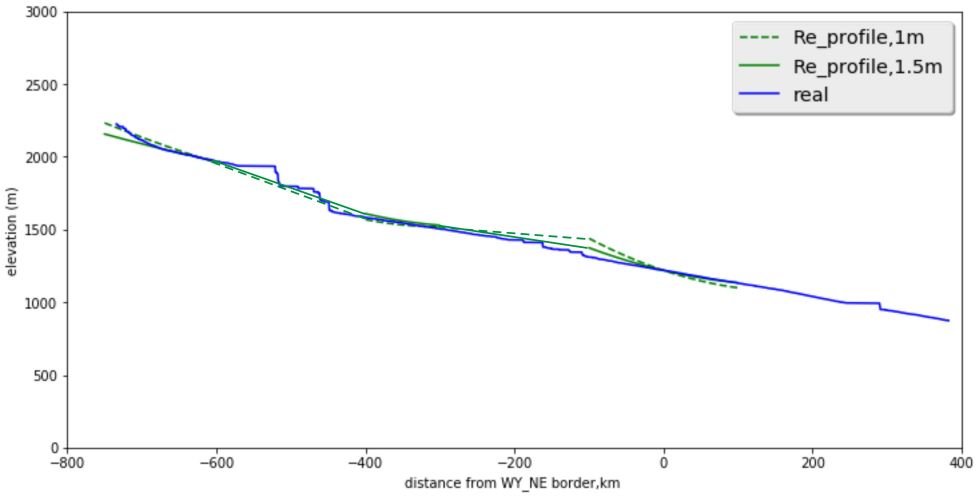

Figure 4.26: Comparison between the combined reconstructed profile (connection) and the real profile.

reconstruction results with these data can be regarded as the fragments of the whole channel. And then these fragments can be put together to get the whole picture of the the mainstream.

For the grain sizes used to reconstruct the profile of the paleochannel in the paper (Duller et al., 2012), there exists not only downstream fining, but also downstream coarsening (shown in Figure 4.18). They are the signals of lateral sediment inputs and recycling. Failing to consider the recycling process would contribute to an unignorable error in the last result.

4.3.3 Summary of the Influences of Recycling on the Previous Study

Lastly, a previous study which used grain size to reconstruct paleochannel profile was tested to evaluate the impact of introducing recycling on the previous interpretations. As the result suggests, the method of reconstructing the profile using grain size data is reliable. However, regional grain sizes with downstream fining trend cannot be used directly to reconstruct the gradient of whole channels, when recycling is dominant. In the reconstruction, the profile can only be reliably reconstructed using data with a normal downstream fining trend which always exist between two lateral sediment inputs.

For the area recycling happened, it was recommended to reconstruct the whole river profile in four steps: (1) recognise the lateral sediment inputs based on the grain size analysis or other tools; (2) recognise the normal downstream fining trends without obvious influence of lateral sediment inputs, which are always between two lateral sediment inputs; (3) reconstruct the regional river profile; (4) The fragments of regional profile reconstructed can be connected with straight lines to get a combined whole picture of the mainstream.

4.4 Conclusion

There are two main parts in this chapter.

In the first half of this chapter, numerical models were built to test the controls of cosmogenic ^{21}Ne accumulated during recycling. Several parameters were evaluated by reconstruct the conflict that upstream pebble contains more cosmogenic ^{21}Ne than the downstream one. As suggested by the results, elevation plays a dominant role in the accumulation of cosmogenic ^{21}Ne during recycling. And, paleosediments of Miocene/Pliocene age are the main source of recycled pebbles. In addition, the data shows no obvious relationship between the grain sizes and the measured concentrations of cosmogenic ^{21}Ne contained within the R15726 and Keystone.

In the other half of this chapter, traditional grainsize-based tool was used to

reconstruct the modern river profile without the consideration of recycling. As both the modern sediments and paleosediments have experienced recycling in the Great Plains, using traditional grainsize-based method to reconstruct the modern channel without the consideration of recycling can give us a idea of the impact of recycling on previous studies. As the result suggests, the grainsize-based tool is reliable, however, in the river with dominant recycled pebbles, this tool should be updated to do reconstruction. So that in the Great Plains, as the existence of recycling, some previous studies should be revised a little to reconstruct a reliable profile of the paleochannel.

In chapter 2 and 3, grain size analysis and cosmogenic nuclides analysis were completed. And it is clear that recycling happened in the Great Plains. Moreover, the oldest sediments recycled were from Miocene age. In this chapter, the study of recycling step further. Some geological influences of recycling were found. In addition, the effect of recycling on traditional grainsize-based tool was evaluated and the updated method of reconstruction taking recycling into consideration was recommended. So that, in the next chapter, three parts of this study of recycling would be put together to give a whole picture of the recycling happened in the Great Plains. And, some previous studies on the paleochannels using grain sizes data, not only in the Great Plains but also in some other places all around the world, would be sorted together to shed a light on the significance of recycling on geological studies. Furthermore, the concept of recycling would be clearly built and some assumption of recycling would be listed.

Chapter 5

Discussion

5.1 Summary

This chapter brings together all the results of previous chapters to show how they are related to each other and to construct our final interpretations.

The main goal of this study is exploring the details of recycling happened in the central Great Plains. However, gaining first-hand information on recycling is impossible because we cannot collect every pebble and check the history of each of them. So that indirect tools are needed to be applied to solve this problem. In this study, grain sizes analysis, cosmogenic nuclides analysis and numerical modelling were employed.

5.1.1 Grain Sizes Analysis

In the 2^{nd} chapter of grain size analysis, fifteen samples sites were selected along the North Plate River to do grain size analysis. As there are several large tributaries in the study area, in order to erase the effect of them on the grain size in the mainstream, an simulated curve fitting was done with the grain size data before the first large tributary. With the comparison between this simulated grain size downstream fitting curve and the real data collected, it was found that all the real grain sizes after point -400 km are much larger than the simulated values, suggesting that lateral sediment inputs contribute a lot of coarse sediments into the mainstream which distort the grain size distribution of the sediments in the mainstream.

However, this simple reconstruction can only provide limited information on the effect of lateral sediment inputs, more details are needed. In order to find the localities where grain size changes took place, similarity analysis was employed.

When it is suspected that there exists inner connection within a row of collapsing

data and these data are only affected by stable external influences, similarity approaches would be used by removing the statistical scale effect. After removing the scale effect, if there existed inner connection within these collapsing data, the similarity-processed data would represent similar statistical characteristics. For the fluvial system, if all the sediments had the same source and there were no lateral influences, the distribution curves of the grain sizes for each point along the river would represent a similar shape under similarity analysis. Also, the C_v, defined by Fedele and Paola (2007), would remain constant along the channel.

In this study, by plotting together the distribution curves of the grain sizes for all the 15 sites, it is evident that there exists inner difference among them, suggesting the existence of the influences of lateral sediments input. Based on the values of C_v, these 15 sites can be divided into two groups, which were named the sharp group and the flat group.

By putting grain size analysis and similarity analysis together, the boundary of the sharp group and the flat group (change of C_v from the level of 1.0 to the level of 0.6) is near -380 km, which also meets the start of the deviation of the real grain size data from the simulated downstream fining curve. So it can be concluded that a lateral sediment input exists at this place. A point named Casper was set at this place.

An abnormal grain size increase and an abrupt drainage area increase can be seen near the point of 1526/1841. The increase in grain size corresponds to the existence of large tributary, providing a reliable support for the assumption that there existed a lateral sediment input near this point. In addition, with the support from the regionally high C_v of 0.89 compared with the other points near it, another point called R15726, was set at this place to represent the locality of a possible lateral sediment input.

The intersection between the North Platte River and the South Platte River is also the end of the North Platte River system. Keystone was chosen to represent this end. Besides, from the point in front of Keystone (100 km) to the point of Keystone (300 km), an apparent grain size increase and two tributaries (No.6 and No.7 in Figure 2.12) can be recognised. The existence of tributaries and the change of grain size nearby suggest that a target site can be set here for the study of recycling.

As shown in Figure 2.20, the whole North Platte River system was divided into three sub-areas based on these three points, which were the up one, middle one and the down one.

Then for each of these localities, grain size distributions with and without the influences of lateral sediment inputs were generated by combining the grain size fitting curves and the similarity distributions. From the comparison between the grain size distributions with and without the influences of lateral sediment inputs,

it can be concluded that most of the pebbles found near Casper came from lateral sediment inputs, and nearly all the pebbles collected from R15726 and Keystone are from lateral sediment inputs.

Tributaries and the modern valley incised deeply on the deposited paleosediments, carrying many pebbles and mixing them into the mainstream. This recycling process is the source of the lateral sediment inputs, so that the apparent effects of lateral sediment inputs on the grain size distribution of the mainstream provide substantial evidence of the existence of recycling in the central Great Plains.

5.1.2 Cosmogenic Nuclides

The concentration of cosmogenic nuclides will increase when the sediments are retained at and near the surface. A problem related to the concentrations of cosmogenic nuclides contained within the fluvial sediments is that these concentrations will evolve downstream as a result of varying histories of transport (Figure 3.5). Even the pebbles collected from the same locality contain different amount of cosmogenic nuclides because their varying exposure duration and burial duration. So in the 3^{rd} chapter, the main goal is how to distinguish the exposure duration from that of burial duration for the collected pebbles, by using cosmogenic nuclides analysis. As the previous studies (for example, (Lal, 1991)) show, two or more cosmogenic nuclide are needed to provide enough information on both the exposure duration and burial duration. So that in this study, eight-two samples (in total) for cosmogenic ^{21}Ne and five samples for cosmogenic ^{10}Be were analysed, providing reliable information of the exposure duration and burial duration of the pebbles collected in the Great Plains.

Before the use of cosmogenic nuclides data, it is vital to extract the concentrations of useful cosmogenic nuclides from the background noises for these collected samples. In this study, only the cosmogenic nuclides accumulated during the transportation and storage processes are useful, which is called "inherited cosmogenic nuclides". By the calculation of background Ne (Ne_{back}) and those cosmogenic nuclides generated during bedrock exhumation (Ne_{cosE}), the inherited cosmogenic nuclides ^{21}Ne contained within the samples can be accessed.

A "steady-state" model and a "simplified migration" model were then built to estimate the maximum concentration of cosmogenic ^{21}Ne accumulated from the source to the target location (Keystone) with a constant migration rate. In the first model, an assumption was set that all the pebbles were carried downstream with a constant moving rate, and they were all exposed during the moving process. In the second model, a simplified migration process was set, but all the sediments were still experienced an unstoppable moving downstream with a constant speed. In these two models, the concentrations of cosmogenic ^{21}Ne were calculated with the lowest rate. Under these assumptions, the results would tell us the highest concentration of cosmogenic ^{21}Ne accumulated during transportation

without storage. No storage, no recycling, this result also represents the highest concentration of cosmogenic ^{21}Ne accumulated during transportation without recycling. However, as suggested by the result, the predicted concentration in these two models are much lower than the concentration of cosmogenic ^{21}Ne measured within the collected samples. It can then be concluded that most pebbles collected from Keystone must have experienced long time of storage (being burial) and then been recycled into the fresh sediments. This result can be regarded as more solid evidence of the existence of recycling in the central Great Plains.

In addition, through the comparison between the predicted concentration of cosmogenic nuclides and the real value measured, it can be concluded that the recycling not only existed in the modern time, but also in the Pliocene and Miocene ages. Almost all the pebbles collected on the plain area have experienced recycling.

Combining the data of cosmogenic ^{21}Ne and ^{10}Be within the samples collected from Keystone, the banana plot was generated to represent the exposure duration and burial duration of all these collected samples. The precondition for the generation of banana plots is that all the sediments have experienced erosion process with a constant rate. The result of banana plot suggested that all the five pebbles collected from Keystone have experienced a considerable history of storage (being buried), the start of which can be backtracked to Miocene. The precondition was then revised a little: for the recycled sediments, both the burial and exposed process happened instantly. In this revised calculation, the earliest time recycling could affect was generated by putting the burial and exposure time together. As suggested by the result of the revised calculation, all the recycled pebbles collected from modern river are as old as Pliocene-, Miocene-ages, or even older.

5.1.3 Numerical Modelling

The result of cosmogenic nuclides introduced an interesting apparent contradiction conflict that cosmogenic ^{21}Ne concentrations contained within the samples collected from the upstream (R15726) are higher than those from the downstream (Keystone). To resolve this conflict, in the 4^{th} chapter, numerical models were built to test the controls of cosmogenic ^{21}Ne accumulated during recycling, by reconstructing this “conflict”.

Three controls were assumed to have influences on the recycling, elevation, the age of sediments recycled and grain sizes. As suggested by the results, elevation plays a dominant role in the accumulation of cosmogenic ^{21}Ne during recycling. And, paleosediments of Miocene/Pliocene age are the main source of recycled pebbles. For Keystone, the ratio of the paleosediments from these two sources is about 1:1.

For the influence of grain size, the data show no relationship between the grain size and the concentration of cosmogenic ^{21}Ne within these grains.

Grain sizes were always used to reconstruct the characteristics of paleochannels because it is believed that the grains collected can reflect the fluvial characteristics at the time of deposition. However, the existence of recycling attributes more uncertainties into this well-believed method. A previous study which used grain size to reconstruct paleo-river profile was tested to evaluate the impact of introducing recycling on the previous interpretations.

In the Great Plains, because of the large scales of erosion, not only the paleosediments of Miocene and Pliocene, the modern sediments (from 2.5 Ma to today) also have experienced recycling. This makes it possible for us to use the recycling happened in the modern sediments to simulate what happened on the paleosediments experienced recycling. A model was developed to reconstruct the modern North Platte River using the modern grain sizes collected. This is to mirror the method used on the paleosediments in the previous studies. If the recycling couldn't affect the grain sizes, the reconstructed river profile would be very closed to the real one. That is to say, if the reconstructed river profile cannot mirror the real one, it means the recycling happened in the Great Plains has a unignorable impact on the well-believed idea that collected samples can be used to reconstruct the fluvial characteristics.

As suggested by the result, only the downstream fining trend without the influence of lateral sediment inputs can be used to reconstruct the regional characteristics of the mainstream. In order to reconstruct the whole picture of the channel, especially for the study area where recycling existed, firstly, lateral sediment inputs are needed to be recognized, secondly, regional fragments between two lateral sediment inputs can be reconstructed using the data which has natural downstream fining trend; thirdly, the fragments should be put together to reconstruct the whole picture of the river.

5.2 Recycling Happened in the Central Great Plains

We can now answer all the questions asked in the 1^{st} chapter:

1. Where would recycling take place in the catchments?

From the comparison between the grain size distributions with and without lateral sediment input, it can be concluded that most of the pebbles found in the chosen sites are from lateral sediment inputs. Which is regarded as the signal of the existence of recycling in the study area. Also, as suggested by the comparison between the concentrations of the corrected cosmogenic ^{21}Ne contained within the samples and the predicted concentrations of cosmogenic ^{21}Ne in the models,

the pebbles collected in the central Great Plains have experienced a long storage history, providing substantial evidence for the existence of recycling in the study area.

A conclusion can be made here that almost all the pebbles collected in the plain area have experienced recycling. Also, three main localities (near Casper, R15726 and Keystone) where the lateral sediment inputs exist along the North Platte River (before North Platte City) were recognised.

2. What is the age of the paleosediments that could be recycled, and hence how long might they have been preserved in the basin prior to recycling?

In the central Great Plains, the primary sources of sediments recycled into the modern mainstream are the paleosediments of Pliocene and Miocene ages. The timing of recycling matches the time when huge incision happened in the study area. As suggested from the result of cosmogenic nuclides analysis (^{21}Ne and ^{10}Be), the oldest paleosediments which recycling can affect are at least from early Miocene (>10 Ma old).

3. What are the main controls of the cosmogenic ^{21}Ne contained within the sediments recycled?

Two geological parameters, elevation and age of paleosediments, were tested using numerical models. As suggested by the results, elevation plays a dominant role in the accumulation of cosmogenic ^{21}Ne during recycling. And, paleosediments of Miocene/Pliocene age are the main source of recycled pebbles. For Keystone, the ratio of the paleosediments from these two sources is about 1:1. Furthermore, the data of the samples collected from R15726 and Keystone shows no relationship between the grain size and the concentration of cosmogenic ^{21}Ne .

5.3 Application of Recycling on Previous Study

Because the variation in the accumulation and movement of fluvial sediments is dependent on many external mechanisms, it can be inferred that the characteristics of fluvial successions represent a time-integrated "record" of changing sedimentological processes through time (Hovius and Leeder, 1998; Whittaker et al., 2011). Therefore, it is possible to reconstruct the tectonic and climatic characteristics at the time of deposition by decoding this "record" (Densmore et al., 2007; Whittaker et al., 2010). Characteristics of grains, which formed the fluvial successions, are one of the critical chapters of this "record". Many studies have been done to access the sedimentary signals contained within the grains (Heller and Paola, 1992; Paola et al., 1992).

As shown in Figure 2.1, for the change of grain sizes along the channel, a common observation is the tendency of fining downstream (Heller and Paola, 1992; Paola et al., 1992; Fedele and Paola, 2007; Moussavi-Harami et al., 2004; Frings, 2008).

The typical downstream fining trend can be characterised using an exponential function as below (Heller and Paola, 1992; Paola et al., 1992; Fedele and Paola, 2007; Whittaker et al., 2011):

$$D_x = D_0 e^{(-ax)} \tag{5.1}$$

Where D_0 is the grain size at the start point (flowing distance = 0), a is the fining exponent, and x is the flowing distance from the start point.

Another important paper is from the study of Paola and Mohrig (1996), which describes the relationship between the grain sizes and the gradients for gravelly channels, building a reliable basis for the reconstruction of the gradients of paleochannels with the data of grain sizes. In this paper, the shear stress required to carry the largest pebble is calculated using the shear stress on the bed at bankful stage, that's when the water is nearly over the river bank. The equation for reconstruction the gradients is listed as below:

$$S_{est} = AD_{50}/h \tag{5.2}$$

In which D_{50} is the value of the 50% on the grain sizes distribution, cm, which means half of the grains collected at that site are smaller than this value, h is the depth of the channel, cm, $A = 0.094$ and S_{est} is the reconstructed depositional slope.

For the Great Plain, United States, it is widely accepted that several incisions happened throughout the Tertiary to the present day. Some scholars have studied the details of the tilting of the Miocene Ogallala Group and the Pliocene Broadwater Formation (Leonard, 2002; McMillan et al., 2002; Duller et al., 2012).

One such key paper (McMillan et al., 2002) reconstructed the gradients of the paleochannels of Ogallala time. They used the equation from the study of Paola and Mohrig (1996). With an analysis on a collection of about 100 samples each at 10 different sites, the study of McMillan et al. (2002) reveals that in the Great Plains, the gradients of the paleochannels in Ogallala time decrease eastward. The change of paleoslope ranges from 2.1 to 0.8 m/km (10^{-3} to 10^{-4}). However, the eastward decrease of the present slope of the Ogallala base ranges from 10 to 2 m/km (10^{-2} to 10^{-3}), which are much larger than those of the depositional paleoslopes in Ogallala time, implying a tilting on the west. The amplitude of tilting is about 680m based on the result of their study.

The underlying assumption of these grain-size-based reconstructions is that the samples collected in the sediment record of the Ogallala time can reflect the hydraulic situations during the Ogallala time. However, as suggested by the results in the previous chapters, in the Great Plains, the paleosediments of the Ogallala time had experienced recycling. Most of the large grains collected in

the plain area are from recycling, which means these collected grains are much larger than the natural flowing grains which can truly reflect the real hydraulic situation. This error would make the calculated paleo-gradients of the Ogallala time much higher than the real ones. That is to say, the amplitude of tilting in the conclusion of this paper (McMillan et al., 2002) would be highly overestimated.

Heller et al. (2003) also reconstructed the slope of Ogallala paleochannels based on Paola and Mohrig's method (see equation 5.2, where $A = 0.094$ when D_{50} is used and $A = 0.0238$ when D_{90} is used). Combining the paleoslope with the preserved isopach geometries, it is revealed that aggradation is not enough to develop a sufficient slope for these preserved gravels to be transported. Thus, a post deposition tilting must have occurred to make up the gap.

With all the previous studies it is clear that large scale erosion and recycling happened during late Miocene to early Pliocene (about 6 Ma). The resulted mixing of ancient and fresh sediments would increase the uncertainties of this grain-size-based study. In Heller's conclusion (Heller et al., 2003), these preserved gravels are the strongest evidence of titling because the calculated slope is not enough to transport these large gravels. However, in the plain area, almost all of the gravels were recycled, even they were collected from the fluvial sediments of the Ogallala strata, they had no relationship with the real channel gradients during the Ogallala time. That is to say, the making up of post deposition titling might be unnecessary.

According to the study of Duller et al. (2012), the gradient of Miocene and Pliocene is reconstructed using the sediments collected from the Miocene and Pliocene.

In that paper, paleoslopes can be estimated from D_{50} (the value at the 50% point in the grain sizes distribution curve) and H (the depth of the paleochannels measured), based on the famous equation developed by Paola and Mohrig (1996):

$$\tau_c^* = \frac{HS}{(\rho_s - \rho)/\rho * D_{50}} \tag{5.3}$$

S is the gradients of the channel; ρ_s represents the density of the sediments while ρ represents the density of the water. τ_c^* is 0.045-0.06 based on the previous studies (Paola and Mohrig, 1996; Mueller and Pitlick, 2005). D_{50} is the value at the 50% point in the grain sizes distribution curve, cm, which means half of the grains collected at that point are smaller than this value. In this equation, the local shear stress is set as 1.2 – 1.4 times the critical shear stress which is suitable for the bedload to be retained (Mueller and Pitlick, 2005). Paleoslope S is therefore calculated as:

$$S_{(x)} = \frac{1.2 * \tau_c^* * \rho_s * D_{50}}{H} = \frac{1.4 * 0.05 * 1.6 * D_{50}}{H} = \frac{0.112 * D_{50}}{H} \tag{5.4}$$

Where

$$\rho_s = {}^{(\rho_s - \rho)}/_{\rho} \tag{5.5}$$

In Duller's paper (2012), D_{50} for estimating the paleoslopes came from a field data collected from sites within Remsburg Ranch beds (RRB) and Ash Hollow Formation (AHF). For the depth of the paleochannels, 1m< H< 2m is used in Miocene calculations and 1.5m< H< 2m is used in Pliocene calculations.

However, Duller's paper (2012) has the similar deficiencies. The recycling happens in the central Great Plains can not only affect the modern sediments, but also the paleosediments of Pliocene and Miocene time. Which means that the grains, especially the pebbles collected from the paleo-bedload on the plain area might from recycling of sediments which were even older, rather than being carried from the source of that time. Furthermore, in my study, Duller's study was redone on the modern North Platte River to represent the impact of introducing recycling on the previous grain-based geological studies. In Duller's paper (2012), the reconstructed paleochannel profile was used to infer the strength of the tilting happened in the mountain area. However, as suggested by Figure 4.20 in chapter 4, for the modern channel, the matching of the reconstructed river profile and the real profile is poor. Which suggests that, in the places where recycling dominants, grain size data within a limited area cannot be used to reconstruct the whole picture of the channel system.

5.4 Assumption of Recycling

After the study, now we can have some basic conclusions of the recycling process happened in the Great Plains, USA. We can also make some assumptions of the recycling process.

1. Recycling happened when erosion happened, especially when large scale erosion happened.

2. The localities of recycling matches the localities of tributaries well. However, some of the tributaries might induce recycling, some might not.

3. For the area where recycling happened, only the data of grain sizes without the influence of recycling can be used to reconstruct the fluvial characteristics of the mainstream, which is limited within the area between two lateral sediment inputs.

1. Recycling happened when erosion happened, especially when large scale erosion happened.

Recycling means reworking the buried paleosediments and mixing them with fresh sediments through erosion or incision (Figure 2.3). It could mix the

paleosediments into the fresh sediments, which have different sizes with each other, through lateral sediment inputs (Figure 2.4), leading to an increase of the grain sizes in the mainstream. There are two main sources of lateral sediment inputs: the tributaries and the incision of the mainstream on the deposited paleosediments in the mainstream. For tributaries, most sediments carried were also from the incision on the deposited paleosediments.

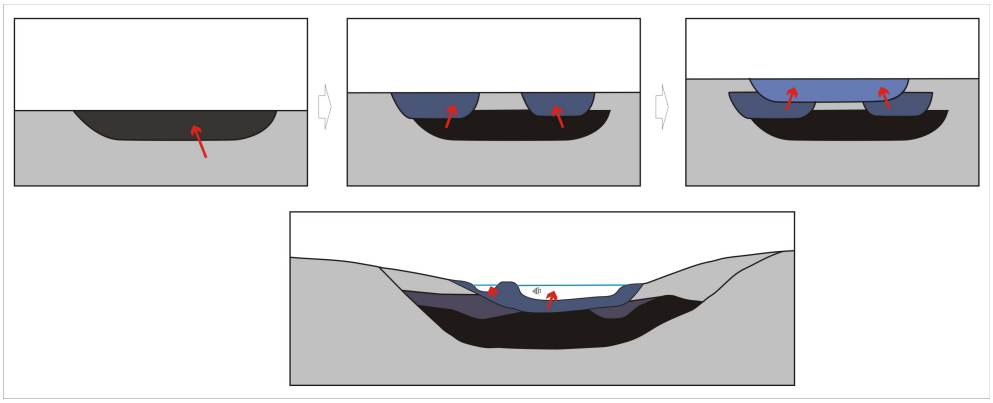

Figure 5.1: A schematic representation showing the recycling processes through incision.

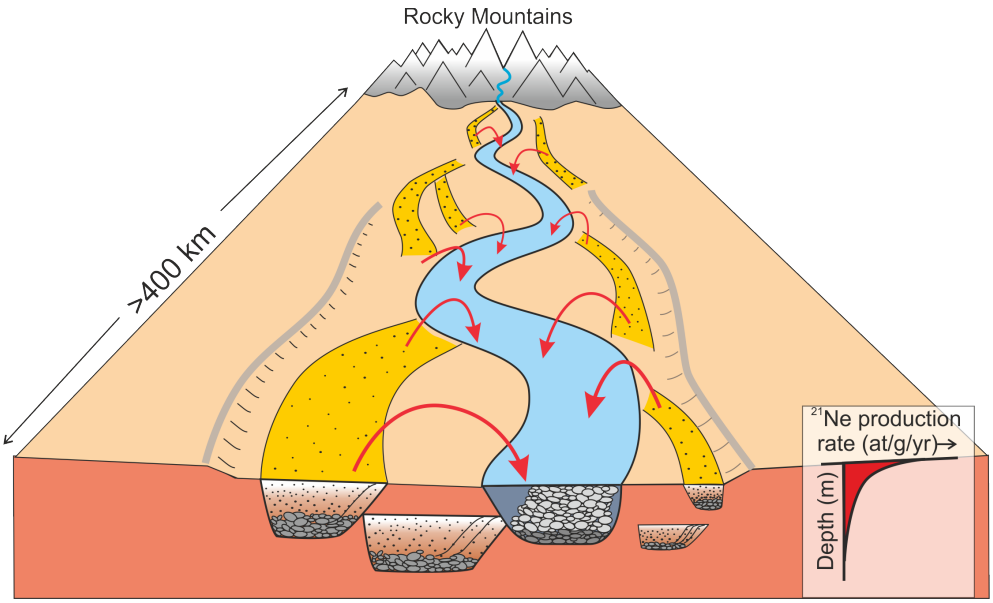

Figure 5.2: A schematic representation showing the recycling processes that could mix the paleosediments into the fresh sediments through lateral sediment inputs.

When the upper part of older strata is removed through subsequent erosion (or avulsion), recycling happened. In 1977,Leeder (1977) build a quantitative model based on random channel avulsions and residence intervals to simulate the concentrations of fluvial deposits. The result of Leeder's study represents that

the concentrations of deposits within the channels were mainly influenced by the frequency of avulsion of the channel belt, the ratio of floodplain width to the width of fluvial sandbody, and vertical aggradation rate of the floodplain.

However, this original model was too simple which ignored some important geological influences on avulsing channels. So that in a later study of Bridge and Leeder (1979), they built a updated model to evaluate more influences of the distribution of channel-belt sand and gravel bodies. Those are (1) vertical aggradation rate of the floodplain, (2) effects of compaction, (3) vertically tectonic movement, and (4) channel avulsion. As shown by the result, the interconnectedness and stacking density of fluvial deposits decrease with increasing mean avulsion period, ratio of floodplain width to the width of fluvial sandbody, and vertical aggradation rate of the floodplain. The result also shown that the influence of tectonic movements on the stacking density is insignificant.

For the stacking density, Bristow et al. (1993) pay more attention on braided fluvial deposits. They (Bristow and Best, 1993) pointed out that it is possible that the fluvial sediments should be preserved after the migration, or avulsion, of the channel, but in many cases the preserved deposits are mostly the older fluvial sediments. This conclusion matches the impact of recycling on the recycled pebbles of the mainstream in my study. The result of their paper (Bristow and Best, 1993) is shown in a schematic diagram (Figure 5.3) which represents the influences of avulsion, migration and aggradation rate upon braided alluvial architecture. As shown by this figure, the structure of the channel deposits may not change obviously with the change of aggradation rate. However, an increase in either the avulsion frequency or the migration rate may considerably increase the stacking density, thus the possibility of the happening of recycling. This conclusion is similar to that of Bridge and Leeder's study (Bridge and Leeder, 1979). In addition, it can be seen in this figure that the preservation morphology of isolated channel sandbodies requires both a high avulsion frequency and a high aggradation. That is to say, any imperfect situations would contribute to the erosion of fresh fluvial deposition on the paleosediments, thus the happening of recycling.

In Bristow et al.'s study (Bristow and Best, 1993), they also considered the contrast between the short-term depositional process and the long-term basin subsidence/aggradation rate, especially in some situations the fluvial sedimentary sequences represent long periods of non-deposition or erosion, but be punctuated by rapid increasing of sediments induced by geological events. This high rate of sediment inputs induced by rapid geological events would contribute to more avulsion and more recycling. In his study, Bristow et al.pointed out that even this kind of instantaneous avulsion should result in complete form preservation, a combination of migration and aggradation would contribute to the reworking of these complete fluvial sandbodies, forming multi-storey sandbodies.

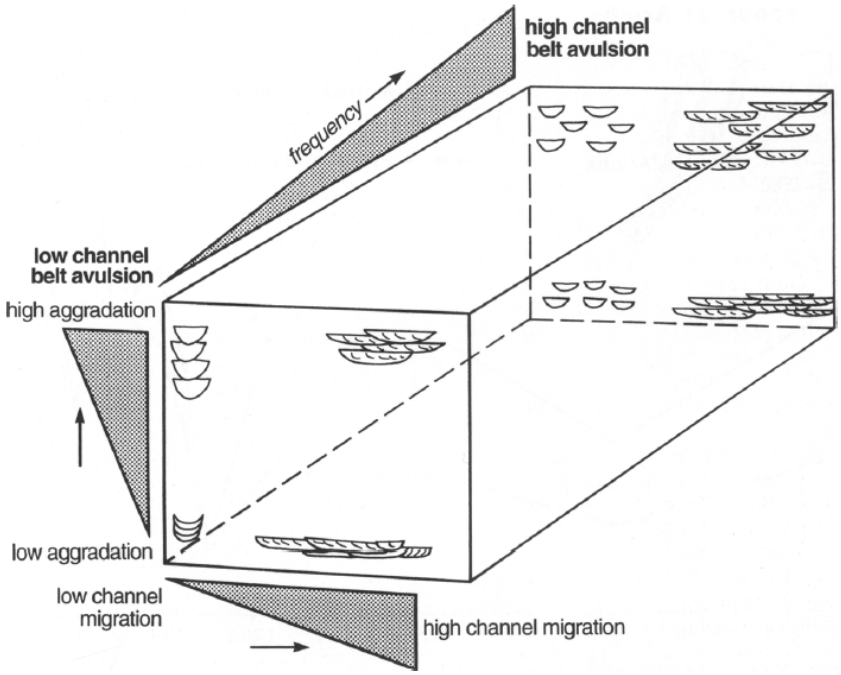

Figure 5.3: A schematic diagram illustrating the structures of braided fluvial deposits which are controlled by aggradation rate, channel migration rate and channel avulsion (Bristow and Best, 1993).

However, Heller and Paola (1996) doubted Leeder et al.'s model (Leeder, 1977; Bridge and Leeder, 1979) which decouple avulsion frequency from sedimentation rates. Heller and Paola pointed out that it was likely that there existed a relationship between the avulsion frequency and the sedimentation rates, within the active channel belt. In their study (Heller and Paola, 1996), Heller and Paola built a simple model whereby avulsion takes place only when a considerably minimum relief is formed between the river bank and the flood plain. The result shows that if avulsion frequency increases at rates slower than the increase in sedimentation rate, the Leeder et al.'s prediction is right, which is that decreasing sedimentation rate could lead to the increasing of stacking density. However, if avulsion frequency increases at the same rate with the sedimentation rate, then the stacking density would have no relationship with the sedimentation rate. In addition, if avulsion frequency increases faster than the sedimentation rates, the result would be totally different from that of Leeder et al.'s model, which is that increasing sedimentation rate could lead to the increasing of stacking density.

Heller and Paola (1996) also built a revised model, in which some controls are taken into consideration, including changes of subsidence rate, the geometry of subsidence, locality of avulsion taking place within the basin, sedimentation rate, flow depth, and the relationship between the avulsion frequency and the sedimentation rate which were used in the original model above. As shown by the result of this revised model, subsidence rate considerably affects how the alluvial architecture changes downstream, while the other parameters affect the stacking density in the downstream direction. So that in the conclusion, Heller and Paola suggested subsidence to be an important control on stacking density, but should be recorded in three dimensions, not vertical sections.

2. The localities of recycling matches the localities of tributaries well. However, some of the tributaries might induce recycling, some might not.

Even for the lateral sediment input carried through tributaries, these sediments were also from the incision of the fresh valley on the deposited paleosediments. There are several tributaries of the North Platte River, there are only two of them have obvious signal of recycling. Here list some simple assumptions for the reason of this strange situation.

In the previous studies of downstream fining process, many studies had found that a simple downstream fining mode may not explain every situation. In many rivers, especially some large-scale channel systems with considerable flowing distances, patterns of the change of grain sizes downstream are more complicated (Rice and Church, 1998; Rice, 1998; Surian, 2002). Due to this complexity, the importance of tributaries on modifying grain size fining rates is widely recognised (Knighton, 1980; Dawson, 1988). Various studies, guided by the milestone set by Miller (1958), have recognised abnormal changes in grain size happened under the influences of tributary (Church and Kellerhals, 1978).

In 1998, Rice and Michael (1998) introduced the concept of "sedimentary links" (Figure 5.4). In the grain size data, there exist some downstream increases in grain size that can be explained by lateral sediment input found nearby. And the area between two adjacent increases in grain size was named "sedimentary link". Within each sedimentary link, a normal downstream fining trend can be observed. They also pointed out that even these finning trends within the sediment links represent different strength, these variable trends are insufficient to redefine the fining trend throughout the whole mainstream. For example, in Figure 5.4, some normal downstream fining trends can be observed within these sedimentary links (shown as solid lines), but the main stream still represent a overall trend of downstream fining. Rice (1998) also pointed out that not all tributaries can change the grain size distribution in the mainstream, and it is needed to classify the tributaries based on their influences on the mainstream.

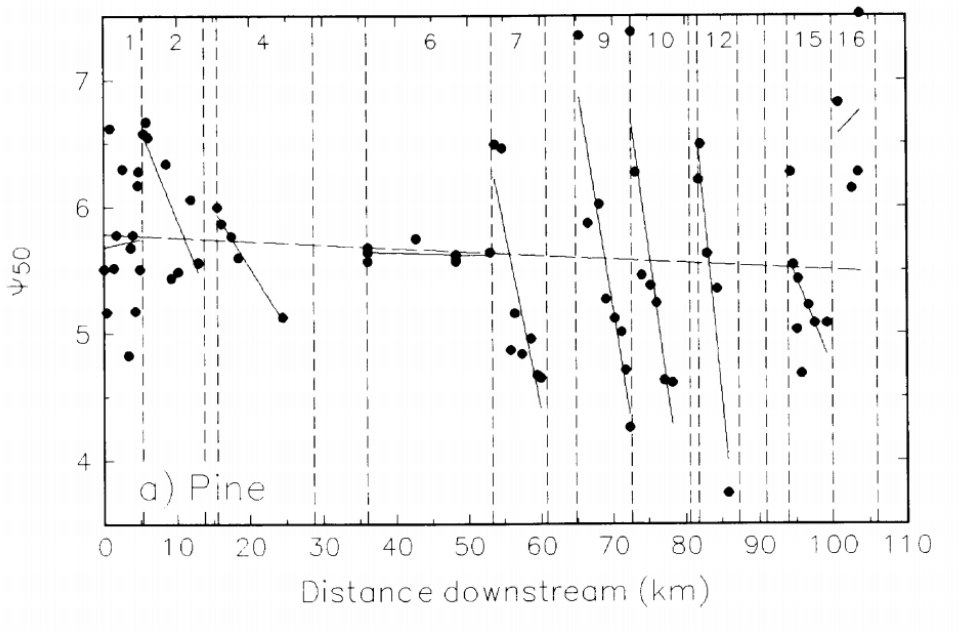

Figure 5.4: A schematic representation showing the downstream increases in grain size, the long dash line represents the exponential regression models fitted to the entire Ψ50 data sets, and the solid lines represent the individual sedimentary links, discontinuities are indicated by dashed vertical lines (Rice and Church, 1998).

Most previous studies on the abnormal downstream change in grain size concentrated on two main problems: 1. The "sources-changes" problem: the sediments coming from lateral inputs may or may not result in the change of typical downstream fining (Church and Kellerhals, 1978; Rice and Church, 1998); 2. The "details of changes" problem: exploring the characteristics of the abnormal downstream fining process (Lisle et al., 1993; Robinson and Slingerland, 1998; Rice et al., 2009). However, for the detailed mechanisms that could contribute to

the abnormal changes of grain sizes, the research is far from enough. Also, they haven't pointed out why some of the tributaries can change the grain sizes of the deposits in the mainstream, some can not.

Based on the sizes of the grains carried by the tributaries and the mainstream, the influences of the tributaries on the mainstream can be divided into two situation (Figure 5.5).

(1) The tributaries have smaller water power than that of the mainstream, which means all the pebbles carried by the tributaries can also be carried by the mainstream (Figure 5.5 A.). In this situation, the pebbles carried by the tributaries would be flowed further downstream by the mainstream, leaving no signal of the "lateral sediment inputs". In other words, this kind of lateral sediment inputs cannot affect the grain size distribution of the mainstream at the place where the tributary exists.

(2) The tributaries have larger water power than that of the mainstream, which means that the largest pebbles carried by the tributaries cannot be carried by the mainstream (Figure 5.5 B.). Because the abrupt decrease of water power resulted from the mixing of the tributaries and the mainstream, these largest pebbles carried by the tributaries cannot be carried any longer, they have to deposit nearby. In this situation, an obvious increase of grain size can be seen from the samples collected near the river junction. In addition, as the pebbles carried by the tributaries have a range of sizes, even the largest ones couldn't be carried any further by the mainstream, those smaller ones could be carried continually. These smaller grains would deposit as the decreasing of water power in the mainstream, leaving a normal downstream fining trend afterwards. That's why this downstream fining trend between two lateral sediment inputs can reflect the regional flowing situation of the mainstream, which is a part of conclusion in chapter 4.

These two situations are not only suitable for the lateral sediment inputs through tributaries, but also for the recycled sediments through the incision of the mainstream on the deposited paleosediments. If the recycled sediments are too large to be carried downstream, they would be just exposed nearby. In contrast, if the recycled sediments were small enough to be carried by the the mainstream, they would be mixed into the fresh fluvial sediments and flowed away.

The "water power" used here is a concept to describe the ability of the channel to carry the sediments, or erode the sediments. It is known that steeper channels should erode more rapidly (Davis, 1899). It raises the possibility of using channel gradients to infer erosion rates.

Howard and Kerby (1983) proposed that in channels, stream power had positive relationship with the flux of water in the river, which is a function of drainage area, and the slope. Thus, if the lithology and climate was uniform, a equation

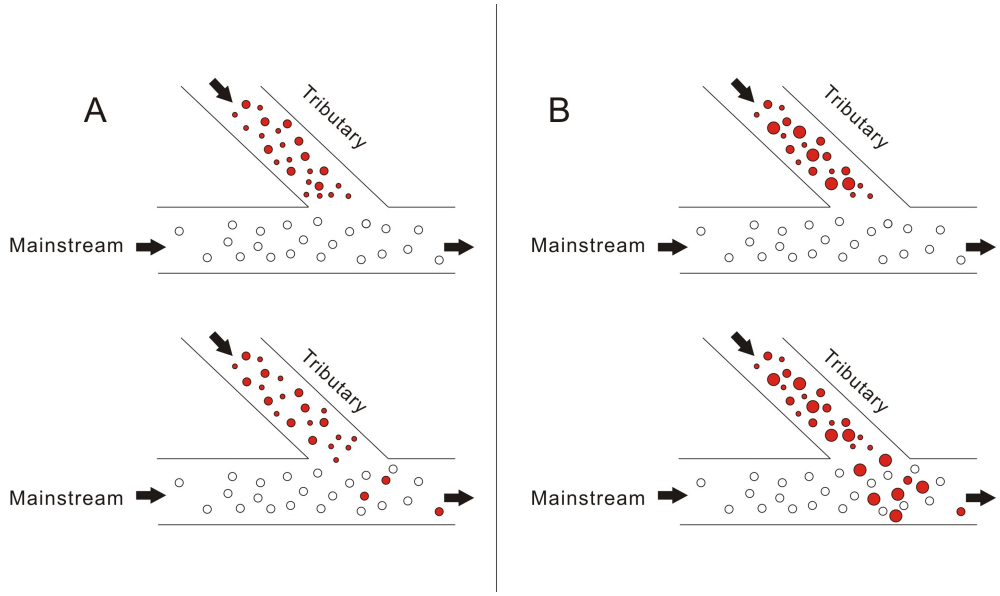

Figure 5.5: A schematic representation showing the influences of the sizes of the pebbles within the tributary on the grain size distribution within the mainstream. The size of the circles represent the size of the pebbles, and the red circles represent the pebbles carried through the tributaries.

linking the gradient and drainage area can be built for a given erosion rate. However, as the uncertainties in the collection process and natural heterogeneity, the data of gradients collected directly are always noisy.

To solve this problem, Perron and Royden (2013) offered a method to transform the channel profile's horizontal coordinate into a variable value, called chi, which has units of distance but accounts for longitudinal variations in drainage area. For a normal channel profile, it always obeys the stream power law, defined as $E = KA^mS^n$ where E represents erosion rate, K represents the erodibility, A represents the drainage area, S represents the channel gradient, and m and n are constants. In the conclusion of their study (Perron and Royden, 2013; Mudd et al., 2014), for each point of this normal channel, the plots of channel elevations against the values of chi, can be used to reflect the ratio of erosion rate to channel erodibility raised to a power 1/n. The gradients of the transformed profile in chi-elevation plots are called mchi, which is often used to reflect the channel steepness (Perron and Royden, 2013; Mudd et al., 2014).

In my study, using DEM, each pixel of the North Platter River and its tributaries was extracted to calculate its chi and mchi. The calculation tools here were also LSDtopo Tools. The results was shown in Figure 5.6.

In the mchi figure (Figure 5.6), the red dots represent high mchi, or high channel steepness, which also represents high possibility to erode larger pebbles. As shown by this figure, for the tributaries of the North Platte River. All of the No.1,

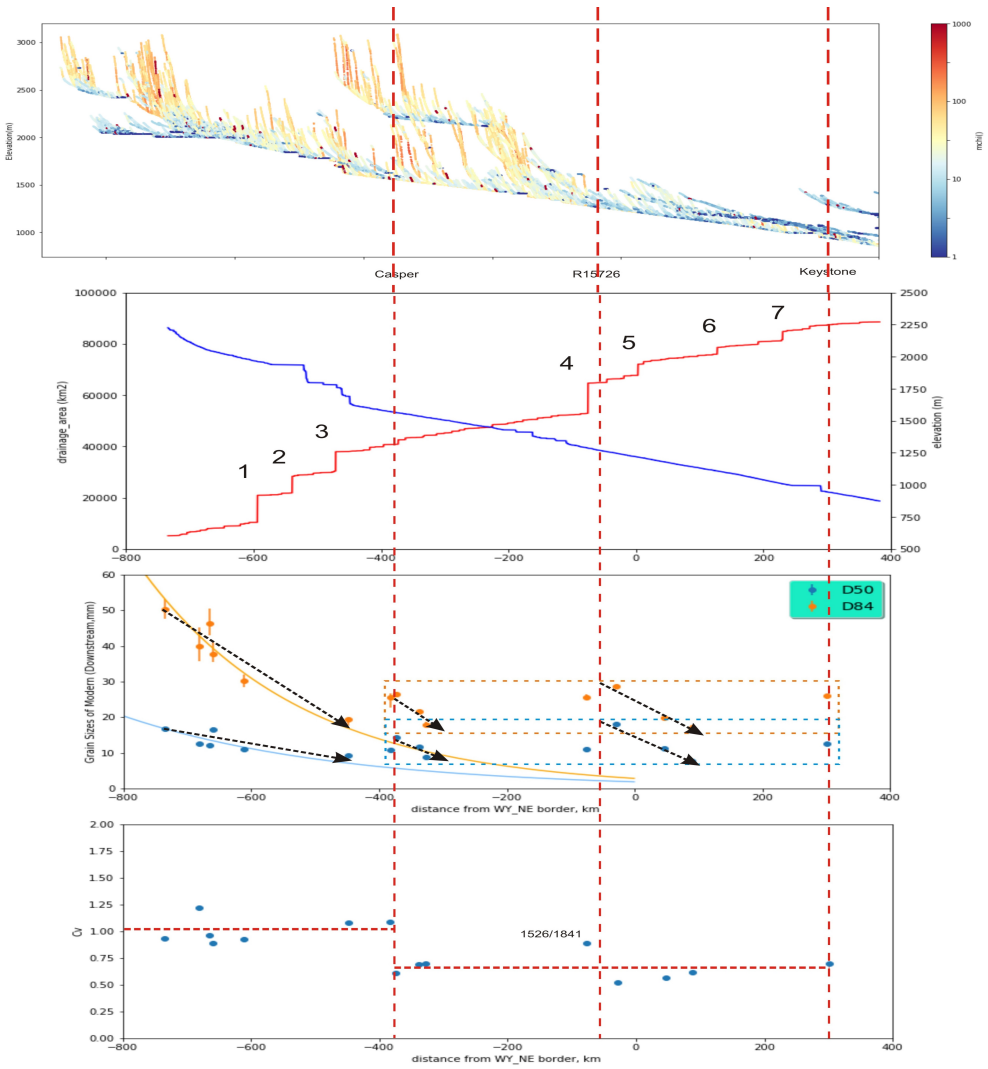

Figure 5.6: Division of the North Platte River System based on the results of the grain size analysis and the similarity analysis and Distribution of Mchi (above) along the rivers (red represents high and blue represent low).

No.2 and No.3 tributaries have more red dots than those near the junctions in the mainstream. Which means they have higher possibilities to introduce larger pebbles into the mainstream, thus contributing to the deposition of abnormal large recycled grains near the junctions. However, as the lacking of data near No.1 and No.2, only an abnormal increase of grain sizes was observed near the junction of No.3.

For the No.4 tributary, a lot of sub-tributaries with high mchi (red dots) can be seen. So it can also have high possibility to contribute larger recycled grains into the mainstream than the fresh grains in the mainstream. And as shown by the result of grain size analysis, an signal of "lateral sediment inputs" can be found nearby. In addition, the values of mchi of No.4 tributary are similar to them of the No.3 tributary, so that the largest recycled pebbles collected near the junctions of these two tributaries represent similar distributions (similar D_{50} and D_{84}).

For the No.5 and No.6 tributaries, their values of mchi are similar to those of the mainstream (blue dots), as discussed above, in this situation, the largest recycled grains carried by the tributary can be flowed away by the mainstream. So that near the junctions of No.5 and No.6 tributaries, the signals of "lateral sediment inputs" are very weak, that is also the reason for a normal downstream fining curve .

For the No.7 tributary, some points of high mchi can be seen nearby, it might be the reason of the abnormal increase of grain size near the junction of No.7 tributary.

As shown by this figure (Figure 5.6), the localities of possible "lateral sediment inputs" matches the junctions of tributaries with high mchi (red dots) very well. So that it can be concluded that mchi analysis can be a good tool to evaluate the impact of the recycled grains of the tributaries on the mainstream.

5.5 Future Directions

From the aspect of grain size analysis, there is still much to be done as there are many tributaries for the North Platte River system. More fieldwork for collecting the samples are needs to be started along the North Platte River and its tributaries, to access enough grain size data. The distant areas in the mountain area is another top target for fieldwork. More research is required to acquire the first-hand information on the lateral sediment inputs. As mentioned before, there is a kind of tributaries which only carried smaller recycled pebbles into the mainstream, thus leaving no signal of "lateral sediment inputs". More samples are needed to collect to explore this kind of "lateral sediment inputs".

For the aspect of cosmogenic nuclides analysis, it has been proved by this

study that using cosmogenic nuclides to infer the deposition process of channel sediments is a good idea. Future studies would do well to combine more kinds of cosmogenic nuclides to access the detail of recycling. Also, more samples collected from more sites are needed, especially the sites near the large tributaries. It could be better to have samples collected before/after the tributaries and make comparison, to get the details of the influence of the lateral sediment inputs on the concentrations of cosmogenic nuclides near the junctions. More ^{10}Be analysis needs to be started to access the detailed burial duration and exposure duration of the pebbles collected along the North Platte River.

For the aspect of numerical models, more controls need to be taken into consideration, including changes of subsidence rate, the geometry of subsidence, sedimentation rate and some other potential parameters, to evaluate the possibilities of the happening of recycling, and the impacts of recycling on the grain size distribution of the sediments within the mainstream. Moreover, it has been proved in my study that the mchi analysis is a good tool to evaluate the impact of tributary on the grain sizes in the mainstream. More work need to be done to find some other useful index to quantify the impact of recycling.

In addition, based on the existence of recycling, many previous studies should be updated with the consideration of this concept. Studies on recycling is an infusion of new blood for not only the geological studies using cosmogenic nuclides but also traditional fluvial studies using grain size data as the main tool. The other places which have experienced slow subsidence and huge incision would be also suitable for the study of recycling, such as Himalaya.

Bibliography

Allen, P. A. (2008). Time scales of tectonic landscapes and their sediment routing systems. *Geological Society, London, Special Publications*, 296(1):7–28.

Ashworth, P. J., Best, J. L., Roden, J. E., Bristow, C. S., and Klaassen, G. J. (2000). Morphological evolution and dynamics of a large, sand braid-bar, jamuna river, bangladesh. *Sedimentology*, 47(3):533–555.

Attal, M., Mudd, S., Hurst, M., Weinman, B., Yoo, K., and Naylor, M. (2015). Impact of change in erosion rate and landscape steepness on hillslope and fluvial sediments grain size in the feather river basin (sierra nevada, california). *Earth Surface Dynamics*, 3(1):201–222.

Balco, G. and Shuster, D. L. (2009). Production rate of cosmogenic 21ne in quartz estimated from 10be, 26al, and 21ne concentrations in slowly eroding antarctic bedrock surfaces. *Earth and Planetary Science Letters*, 281(1-2):48–58.

Ballantyne, C. (1978). Variations in the size of coarse clastic particles over the surface of a small sandur, ellesmere island, nwt, canada. *Sedimentology*, 25(1):141–147.

Barry, R. G. (1983). Climatic environment of the great plains, past and present. *Transactions Nebraska Academy of Sciences*.

Blackstone Jr, D. (1975). Late cretaceous and cenozoic history of laramie basin region, southeast wyoming. *Geol. Soc. Am. Mem*, 144:249–279.

Braun, J., Van Der Beek, P., and Batt, G. (2006). *Quantitative thermochronology: numerical methods for the interpretation of thermochronological data*. Cambridge University Press.

Bridge, J. S. and Leeder, M. R. (1979). A simulation model of alluvial stratigraphy. *Sedimentology*, 26(5):617–644.

Bristow, C. and Best, J. L. (1993). Braided rivers: perspectives and problems. *Geological society, London, special publications*, 75(1):1–11.

Brook, E. J., Brown, E. T., Kurz, M. D., Ackert Jr, R. P., Raisbeck, G. M., and Yiou, F. (1995). Constraints on age, erosion, and uplift of neogene glacial deposits in the transantarctic mountains determined from in situ cosmogenic 10be and 26al. *Geology*, 23(12):1063–1066.

Brown, E. T., Brook, E. J., Raisbeck, G. M., Yiou, F., and Kurz, M. D. (1992). Effective attenuation lengths of cosmic rays producing 10be and 26al in quartz: Implications for exposure age dating. *Geophysical Research Letters*, 19(4):369–372.

Brown, E. T., Edmond, J. M., Raisbeck, G. M., Yiou, F., Kurz, M. D., and Brook, E. J. (1991). Examination of surface exposure ages of antarctic moraines using in situ produced 10be and 26al. *Geochimica et Cosmochimica Acta*, 55(8):2269–2283.

Bunte, K. and Abt, S. R. (2001). Sampling surface and subsurface particle-size distributions in wadable gravel-and cobble-bed streams for analyses in sediment transport, hydraulics, and streambed monitoring. *Gen. Tech. Rep. RMRS-GTR-74. Fort Collins, CO: US Department of Agriculture, Forest Service, Rocky Mountain Research Station. 428 p.*, 74.

Chapin, C. E. and Kelley, S. A. (1997). The rocky mountain erosion surface in the front range of colorado.

Church, M. (1987). River bed gravels: sampling and analysis. *Sediment transport in gravel-bed rivers*, pages 43–78.

Church, M. and Kellerhals, R. (1978). On the statistics of grain size variation along a gravel river. *Canadian Journal of Earth Sciences*, 15(7):1151–1160.

Clark, D. H., Bierman, P. R., and Larsen, P. (1995). Improving in situ cosmogenic chronometers. *Quaternary research*, 44(3):367–377.

Codilean, A. T., Bishop, P., Stuart, F. M., Hoey, T. B., Fabel, D., and Freeman, S. P. (2008). Single-grain cosmogenic 21ne concentrations in fluvial sediments reveal spatially variable erosion rates. *Geology*, 36(2):159–162.

Compton, A. H. (1933). A geographic study of cosmic rays. *Physical Review*, 43(6):387.

Condon, S. M. (2005). Geologic studies of the platte river, south-central nebraska and adjacent areas¡[a]geologic maps, subsurface study, and geologic history.

Crowley, K. (1983a). Large-scale bed configurations (macroforms), platte river basin, colorado and nebraska: Primary structures and formative processes. *Geological Society of America Bulletin*, 94(1):117–133.

Crowley, T. J. (1983b). Depth-dependent carbonate dissolution changes in the eastern north atlantic during the last 170,000 years. *Marine Geology*, 54(1-2):M25–M31.

Cui, Y. and Parker, G. (1998). The arrested gravel front: stable gravel-sand transitions in rivers part 2: General numerical solution. *Journal of Hydraulic Research*, 36(2):159–182.

Davis, W. M. (1899). The geographical cycle. *The Geographical Journal*, 14(5):481–504.

Davis Jr, R. and Schaeffer, O. A. (1955). Chlorine-36 in nature. *Annals of the New York Academy of Sciences*, 62(5):107–121.

Dawson, M. (1988). Sediment size variation in a braided reach of the sunwapta river, alberta, canada. *Earth surface processes and landforms*, 13(7):599–618.

Densmore, A. L., Allen, P. A., and Simpson, G. (2007). Development and response of a coupled catchment fan system under changing tectonic and climatic forcing. *Journal of Geophysical Research: Earth Surface*, 112(F1).

Desilets, D. and Zreda, M. (2001). On scaling cosmogenic nuclide production rates for altitude and latitude using cosmic-ray measurements. *Earth and Planetary Science Letters*, 193(1-2):213–225.

Desilets, D. and Zreda, M. (2003). Spatial and temporal distribution of secondary cosmic-ray nucleon intensities and applications to in situ cosmogenic dating. *Earth and Planetary Science Letters*, 206(1-2):21–42.

Desilets, D., Zreda, M., and Prabu, T. (2006). Extended scaling factors for in situ cosmogenic nuclides: new measurements at low latitude. *Earth and Planetary Science Letters*, 246(3-4):265–276.

Dethier, D. P., Ouimet, W., Bierman, P. R., Rood, D. H., and Balco, G. (2014). Basins and bedrock: Spatial variation in 10be erosion rates and increasing relief in the southern rocky mountains, usa. *Geology*, 42(2):167–170.

Dickinson, W. R., Klute, M. A., Hayes, M. J., Janecke, S. U., Lundin, E. R., McKITTRICK, M. A., and Olivares, M. D. (1988). Paleogeographic and paleotectonic setting of laramide sedimentary basins in the central rocky mountain region. *Geological Society of America Bulletin*, 100(7):1023–1039.

Diffendal, R. F. (1982). Regional implications of the geology of the ogallala group (upper tertiary) of southwestern morrill county, nebraska, and adjacent areas. *Geological Society of America Bulletin*, 93(10):964–976.

Diffendal, R. F. (1991). Geologic map showing configuration of the bedrock surface, north platte, 1 degree x 2 degrees quadrangle, nebraska.

Duller, R., Whittaker, A., Fedele, J., Whitchurch, A., Springett, J., Smithells, R., Fordyce, S., and Allen, P. (2010). From grain size to tectonics. *Journal of Geophysical Research: Earth Surface*, 115(F3).

Duller, R. A., Whittaker, A. C., Swinehart, J. B., Armitage, J. J., Sinclair, H. D., Bair, A., and Allen, P. A. (2012). Abrupt landscape change post–6 ma on the central great plains, usa. *Geology*, 40(10):871–874.

Dumitru, T. A., Gans, P. B., Foster, D. A., and Miller, E. L. (1991). Refrigeration of the western cordilleran lithosphere during laramide shallow-angle subduction. *Geology*, 19(11):1145–1148.

Dunai, T. J. (2000). Scaling factors for production rates of in situ produced cosmogenic nuclides: a critical reevaluation. *Earth and Planetary Science Letters*, 176(1):157–169.

Dunai, T. J. (2010). *Cosmogenic Nuclides: Principles, concepts and applications in the Earth surface sciences*. Cambridge University Press.

Dunai, T. J. and Lifton, N. A. (2014). The nuts and bolts of cosmogenic nuclide production. *Elements*, 10(5):347–350.

Epis, R., Scott, G., Taylor, R., and Chapin, C. (1976). Cenozoic volcanic, tectonic, and geomorphic features of central colorado. *Studies in Colorado field geology: Professional Contributions of Colorado School of Mines*, (8):323–338.

Fedele, J. J. and Paola, C. (2007). Similarity solutions for fluvial sediment fining by selective deposition. *Journal of Geophysical Research: Earth Surface*, 112(F2).

Ferguson, R. and Ashworth, P. (1991). Slope-induced changes in channel character along a gravel-bed stream: The allt dubhaig, scotland. *Earth surface processes and landforms*, 16(1):65–82.

Ferguson, R., Hoey, T., Wathen, S., and Werritty, A. (1996). Field evidence for rapid downstream fining of river gravels through selective transport. *Geology*, 24(2):179–182.

Flanagan, K. M., Montagne, J., Snoke, A., Steidtmann, J., and Roberts, S. (1993). Neogene stratigraphy and tectonics of wyoming. *Geology of Wyoming: Laramie, Geological Survey of Wyoming Memoir*, 5:572–607.

Frings, R. M. (2008). Downstream fining in large sand-bed rivers. *Earth-Science Reviews*, 87(1-2):39–60.

Gall, R. (1960). The secular variation and the geomagnetic theory of cosmic radiation. *Journal of Geophysical Research*, 65(11):3545–3558.

Goes, S. and van der Lee, S. (2002). Thermal structure of the north american uppermost mantle inferred from seismic tomography. *Journal of Geophysical Research: Solid Earth*, 107(B3):ETG–2.

Goodwin, R. and Diffendal, R. (1987). Paleohydrology of some ogallala (neogene) streams in the southern panhandle of nebraska.

Gosse, J. C. and Phillips, F. M. (2001). Terrestrial in situ cosmogenic nuclides: theory and application. *Quaternary Science Reviews*, 20(14):1475–1560.

Graf, T., Kohl, C., Marti, K., and Nishiizumi, K. (1991). Cosmic-ray produced neon in antarctic rocks. *Geophysical Research Letters*, 18(2):203–206.

Granger, D. E. and Muzikar, P. F. (2001). Dating sediment burial with in situ-produced cosmogenic nuclides: theory, techniques, and limitations. *Earth and Planetary Science Letters*, 188(1-2):269–281.

Green, G. N. (1992). The digital geologic map of colorado in arc/info format.

Green, G. N. and Drouillard, P. H. (1994). The digital geologic map of wyoming in arc/info format. Technical report, US Dept. of the Interior, US Geological Survey,.

Grosse, A. (1934). Metallic element 91. *Journal of the American Chemical Society*, 56(10):2200–2201.

Haworth, E. (1897). Physical properties of the tertiary: Kansas univ. *Geol. Survey*, 2:247–284.

Haynes, C. V. (1991). Geoarchaeological and paleohydrological evidence for a clovis-age drought in north america and its bearing on extinction. *Quaternary Research*, 35(3-Part1):438–450.

Hein, F. J. and Walker, R. G. (1977). Bar evolution and development of stratification in the gravelly, braided, kicking horse river, british columbia. *Canadian Journal of Earth Sciences*, 14(4):562–570.

Heller, P. L., Dueker, K., and McMillan, M. E. (2003). Post-paleozoic alluvial gravel transport as evidence of continental tilting in the us cordillera. *Geological Society of America Bulletin*, 115(9):1122–1132.

Heller, P. L. and Paola, C. (1992). The large-scale dynamics of grain-size variation in alluvial basins, 2: Application to syntectonic conglomerate. *Basin Research*, 4(2):91–102.

Heller, P. L. and Paola, C. (1996). Downstream changes in alluvial architecture; an exploration of controls on channel-stacking patterns. *Journal of Sedimentary Research*, 66(2):297–306.

Hetzel, R., Niedermann, S., Ivy-Ochs, S., Kubik, P. W., Tao, M., and Gao, B. (2002). 21ne versus 10be and 26al exposure ages of fluvial terraces: the influence of crustal ne in quartz. *Earth and Planetary Science Letters*, 201(3-4):575–591.

Hoffmann, R. S. and Jones, J. K. (1970). Influence of late-glacial and post-glacial events on the distribution of recent mammals on the northern great plains. *Pleistocene and Recent environments of the central Great Plains*, pages 355–394.

Hovius, N. and Leeder, M. (1998). Clastic sediment supply to basins. *Basin Research*, 10(1):1–5.

Howard, A. D. and Kerby, G. (1983). Channel changes in badlands. *Geological Society of America Bulletin*, 94(6):739–752.

Kellerhals, R. and Bray, D. I. (1971). Sampling procedures for coarse fluvial sediments. *Journal of the Hydraulics Division*, 97(8):1165–1180.

Klein, J., Giegengack, R., Middleton, R., Sharma, P., Underwood, J., and Weeks, R. (1986). Revealing histories of exposure using in situ produced 26 al and 10 be in libyan desert glass. *Radiocarbon*, 28(2A):547–555.

Knighton, A. (1980). Longitudinal changes in size and sorting of stream-bed material in four english rivers. *Geological Society of America Bulletin*, 91(1):55–62.

Laird, K. R., Fritz, S. C., Cumming, B. F., and Grimm, E. C. (1998). Early-holocene limnological and climatic variability in the northern great plains. *The Holocene*, 8(3):275–285.

Lal, D. (1958). *Investigations of nuclear interactions produced by cosmic rays*. Tata Institute of Fundamental Research.

Lal, D. (1988). In situ-produced cosmogenic isotopes in terrestrial rocks. *Annual Review of Earth and Planetary Sciences*, 16(1):355–388.

Lal, D. (1991). Cosmic ray labeling of erosion surfaces: in situ nuclide production rates and erosion models. *Earth and Planetary Science Letters*, 104(2-4):424–439.

Lal, D. and Peters, B. (1967). Cosmic ray produced radioactivity on the earth. In *Kosmische Strahlung II/Cosmic Rays II*, pages 551–612. Springer.

Lauer, J. W. and Willenbring, J. (2010). Steady state reach-scale theory for radioactive tracer concentration in a simple channel/floodplain system. *Journal of Geophysical Research: Earth Surface*, 115(F4).

Leeder, M. (1977). A quantitative stratigraphic model for alluvium, with special reference to channel deposit density and interconnectedness.

Leite, M. B. (1990). Stratigraphy and mammalian paleontology of the ash hollow formation (upper miocene) on the north shore of lake mcconaughy, keith county, nebraska. *Rocky Mountain Geology*, 28(1):1–29.

Lemaître, G. and Vallarta, M. S. (1933). On compton's latitude effect of cosmic radiation. *Physical Review*, 43(2):87.

Leonard, E. M. (2002). Geomorphic and tectonic forcing of late cenozoic warping of the colorado piedmont. *Geology*, 30(7):595–598.

Libarkin, J., Quade, J., Chase, C., Poths, J., and McIntosh, W. (2002). Measurement of ancient cosmogenic 21ne in quartz from the 28 ma fish canyon tuff, colorado. *Chemical Geology*, 186(3-4):199–213.

Lisle, T. E., Iseya, F., and Ikeda, H. (1993). Response of a channel with alternate bars to a decrease in supply of mixed-size bed load: A flume experiment. *Water Resources Research*, 29(11):3623–3629.

Loope, D. B., Swinehart, J. B., and Mason, J. P. (1995). Dune-dammed paleovalleys of the nebraska sand hills: intrinsic versus climatic controls on the accumulation of lake and marsh sediments. *Geological Society of America Bulletin*, 107(4):396–406.

Lueninghoener, G. C. (1947). The post-kansan geologic history of the lower platte valley area.

Lugn, A. and Lugn, R. (1956). The general tertiary geomorphology and sedimentation in nebraska and the northern great plains: Compass, v. 33.

Lugn, A. L. (1935). The pleistocene geology of nebraska.

Maat, P. B. and Johnson, W. C. (1996). Thermoluminescence and new 14c age estimates for late quaternary loesses in southwestern nebraska. *Geomorphology*, 17(1-3):115–128.

Masarik, J. and Reedy, R. C. (1995). Terrestrial cosmogenic-nuclide production systematics calculated from numerical simulations. *Earth and Planetary Science Letters*, 136(3-4):381–395.

May, D. and Holen, S. (1985). A chronology of holocene erosion and sedimentation in the south loup valley, nebraska. *Geographical Perspectives*, 56:8–12.

May, D. W. (1989). Holocene alluvial fills in the south loup valley, nebraska. *Quaternary Research*, 32(1):117–120.

May, D. W., Swinehart, J. B., Loope, D., and Souders, V. (1995). Late quaternary fluvial and eolian sediments: Loup river basin and the nebraska sand hills. *Geologic Field Trips in Nebraska and Adjacent Parts of Kansas and South Dakota¡±(CA Flowerday, Ed.)*, pages 13–31.

McMillan, M. E., Angevine, C. L., and Heller, P. L. (2002). Postdepositional tilt of the miocene-pliocene ogallala group on the western great plains: Evidence of late cenozoic uplift of the rocky mountains. *Geology*, 30(1):63–66.

McMillan, M. E., Heller, P. L., and Wing, S. L. (2006). History and causes of post-laramide relief in the rocky mountain orogenic plateau. *Geological Society of America Bulletin*, 118(3-4):393–405.

Mears Jr, B. (1993). Geomorphic history of wyoming and high-level erosion surfaces. *Geology of Wyoming: Laramie, Geological Survey of Wyoming Memoir*, 5:608–626.

Menting, F., Langston, A. L., and Temme, A. J. (2015). Downstream fining, selective transport, and hillslope influence on channel bed sediment in mountain streams, colorado front range, usa. *Geomorphology*, 239:91–105.

Meyer-Peter, E. and Müller, R. (1948). Formulas for bed-load transport. In *IAHSR 2nd meeting, Stockholm, appendix 2*. IAHR.

Miller, J. P. (1958). High mountain streams: effects of geology on channel characteristics and bed material.

Morris, J. D. (1991). Applications of cosmogenic 10be to problems in the earth sciences. *Annual Review of Earth and Planetary Sciences*, 19(1):313–350.

Morrison, R. (1987). Long-term perspective: changing rates and types of quaternary surficial processes: erosion-depositionstability cycles. *Geomorphic systems of North America: Geological Society of America Centennial Special*, 2:163–210.

Moussavi-Harami, R., Mahboubi, A., and Khanehbad, M. (2004). Analysis of controls on downstream fining along three gravel-bed rivers in the band-e-golestan drainage basin ne iran. *Geomorphology*, 61(1-2):143–153.

Mudd, S. M., Attal, M., Milodowski, D. T., Grieve, S. W., and Valters, D. A. (2014). A statistical framework to quantify spatial variation in channel gradients using the integral method of channel profile analysis. *Journal of Geophysical Research: Earth Surface*, 119(2):138–152.

Mueller, E. R. and Pitlick, J. (2005). Morphologically based model of bed load transport capacity in a headwater stream. *Journal of Geophysical Research: Earth Surface*, 110(F2).

Muhs, D. R., Aleinikoff, J. N., Stafford Jr, T. W., Kihl, R., Been, J., Mahan, S. A., and Cowherd, S. (1999). Late quaternary loess in northeastern colorado: Part i¡^{a}age and paleoclimatic significance. *Geological Society of America Bulletin*, 111(12):1861–1875.

Muhs, D. R. and Bettis, E. A. (2000). Geochemical variations in peoria loess of western iowa indicate paleowinds of midcontinental north america during last glaciation. *Quaternary Research*, 53(1):49–61.

Muhs, D. R., Stafford, T. W., Cowherd, S. D., Mahan, S. A., Kihl, R., Maat, P. B., Bush, C. A., and Nehring, J. (1996). Origin of the late quaternary dune fields of northeastern colorado. *Geomorphology*, 17(1-3):129–149.

Muhs, D. R., Stafford, T. W., Swinehart, J. B., Cowherd, S. D., Mahan, S. A., Bush, C. A., Madole, R. F., and Maat, P. B. (1997). Late holocene eolian activity in the mineralogically mature nebraska sand hills. *Quaternary Research*, 48(2):162–176.

Niedermann, S. (2000). The 21ne production rate in quartz revisited. *Earth and Planetary Science Letters*, 183(3-4):361–364.

Niedermann, S., Graf, T., Kim, J., Kohl, C., Marti, K., and Nishiizumi, K. (1994). Cosmic-ray-produced 21ne in terrestrial quartz: the neon inventory of sierra nevada quartz separates. *Earth and Planetary Science Letters*, 125(1-4):341–355.

Niedermann, S., Graf, T., and Marti, K. (1993). Mass spectrometric identification of cosmic-ray-produced neon in terrestrial rocks with multiple neon components. *Earth and Planetary Science Letters*, 118(1-4):65–73.

Nishiizumi, K., Finkel, R., Klein, J., and Kohl, C. (1996). Cosmogenic production of 7be and 10be in water targets. *Journal of Geophysical Research: Solid Earth*, 101(B10):22225–22232.

Onuchin, A. and Burenina, T. (1996). Climatic and geographic patterns in snow density dynamics, northern eurasia. *Arctic and Alpine Research*, 28(1):99–103.

Paola, C. (2000). Quantitative models of sedimentary basin filling. *Sedimentology*, 47:121–178.

Paola, C., Heller, P. L., and Angevine, C. L. (1992). The large-scale dynamics of grain-size variation in alluvial basins, 1: Theory. *Basin research*, 4(2):73–90.

Paola, C. and Mohrig, D. (1996). Palaeohydraulics revisited: Palaeoslope estimation in coarse-grained braided rivers. *Basin Research*, 8(3):243–254.

Parker, G. and Cui, Y. (1998). The arrested gravel front: Stable gravel-sand transitions in rivers part 1: Simplified analytical solution. *Journal of hydraulic research*, 36(1):75–100.

Passega, R. (1964). Grain size representation by cm patterns as a geologic tool. *Journal of Sedimentary Research*, 34(4):830–847.

Pearl, R. H. (1971). Pliocene drainage of east-central colorado and northwestern kansas. *The Mountain Geologist*.

Pelletier, J. D. (2009). The impact of snowmelt on the late cenozoic landscape of the southern rocky mountains, usa. *GSA today*, 19(7):4–11.

Perron, J. T. and Royden, L. (2013). An integral approach to bedrock river profile analysis. *Earth Surface Processes and Landforms*, 38(6):570–576.

Pye, K., Winspear, N., and Zhou, L. (1995). Thermoluminescence ages of loess and associated sediments in central nebraska, usa. *Palaeogeography, Palaeoclimatology, Palaeoecology*, 118(1-2):73–87.

Retallack, G. J. (1997). Neogene expansion of the north american prairie. *Palaios*, 12(4):380–390.

Rice, S. (1998). Which tributaries disrupt downstream fining along gravel-bed rivers? *Geomorphology*, 22(1):39–56.

Rice, S. (1999). The nature and controls on downstream fining within sedimentary links. *Journal of Sedimentary Research*, 69(1):32–39.

Rice, S. and Church, M. (1996). Sampling surficial fluvial gravels; the precision of size distribution percentile sediments. *Journal of Sedimentary Research*, 66(3):654–665.

Rice, S. and Church, M. (1998). Grain size along two gravel-bed rivers: statistical variation, spatial pattern and sedimentary links. *Earth Surface Processes and Landforms: The Journal of the British Geomorphological Group*, 23(4):345–363.

Rice, S. P., Church, M., Wooldridge, C. L., and Hickin, E. J. (2009). Morphology and evolution of bars in a wandering gravel-bed river; lower fraser river, british columbia, canada. *Sedimentology*, 56(3):709–736.

Robinson, R. A. and Slingerland, R. L. (1998). Grain-size trends, basin subsidence and sediment supply in the campanian castlegate sandstone and equivalent conglomerates of central utah. *Basin Research*, 10(1):109–127.

Sambrook Smith, G. H. and Ferguson, R. I. (1995). The gravel-sand transition along river channels. *Journal of Sedimentary Research*, 65(2a):423–430.

Schultz, C. B. and Stout, T. M. (1945). Pleistocene loess deposits of nebraska. *American Journal of Science*, 243(5):231–244.

Schultz, C. B. and Stout, T. M. (1948). Pleistocene mammals and terraces in the great plains. *Geological Society of America Bulletin*, 59(6):553–587.

Scott, G. R. (1975). Cenozoic surfaces and deposits in the southern rocky mountains. *Geol. Soc. Am. Mem*, 144:227–248.

Scott, G. R. (1978). Map showing geology, structure, and oil and gas fields in the sterling 1 x 2 quadrangle, colorado, nebraska, and kansas. Technical report.

Scott, G. R. (1982). *Paleovalley and geologic map of northeastern Colorado*. US Geological Survey.

Seal, R., Paola, C., Parker, G., Southard, J. B., and Wilcock, P. R. (1997). Experiments on downstream fining of gravel: I. narrow-channel runs. *Journal of hydraulic engineering*, 123(10):874–884.

Shuster, D. L. and Farley, K. A. (2005). Diffusion kinetics of proton-induced 21ne, 3he, and 4he in quartz. *Geochimica et Cosmochimica Acta*, 69(9):2349–2359.

Simpson, J., Baldwin, H., and Uretz, R. (1951). Nuclear bursts produced in the low energy nucleonic component of the cosmic radiations. *Physical Review*, 84(2):332.

Smith, A. J., Donovan, J. J., Ito, E., and Engstrom, D. R. (1997). Groundwater processes controlling a prairie lake's response to middle holocene drought. *Geology*, 25(5):391–394.

Souders, V. L. et al. (2000). Geologic maps and cross sections showing configurations of bedrock surfaces, broken bow 1x2 degree quadrangle, east-central nebraska.

Stanley, K. (1976). Sandstone petrofacies in the cenozoic high plains sequence, eastern wyoming and nebraska. *Geological Society of America Bulletin*, 87(2):297–309.

Stanley, K. and Wayne, W. J. (1972). Epeirogenic and climatic controls of early pleistocene fluvial sediment dispersal in nebraska. *Geological Society of America Bulletin*, 83(12):3675–3690.

Steven, T. A., Evanoff, E., and Yuhas, R. H. (1997). Middle and late cenozoic tectonic and geomorphic development of the front range of colorado.

Stone, J. (1999). A consistent be-10 production rate in quartz¡^{a}muons and altitude scaling. *AMS-8 Proceedings Abstract Volume, Vienna, Austria.*

Stone, J. O. (2000). Air pressure and cosmogenic isotope production. *Journal of Geophysical Research: Solid Earth*, 105(B10):23753–23759.

Stone, J. O., Ballantyne, C. K., and Keith Fifield, L. (1998). Exposure dating and validation of periglacial weathering limits, northwest scotland. *Geology*, 26(7):587–590.

Størmer, C. (1934). On the trajectories of electric particles in the field of a magnetic dipole with applications to the theory of cosmic radiation. third communication. with 3 figures in the text. *Astrophysica Norvegica*, 1:1.

Surian, N. (2002). Downstream variation in grain size along an alpine river: analysis of controls and processes. *Geomorphology*, 43(1-2):137–149.

Sweeney, M., Swinehart, J., and Loope, D. (1998). Testing the hypothesis for latest wisconsin blockage of streams at the west margin of the nebraska sand hills (abs.). In *Proceedings of the Nebraska Academy of Sciences, 118th Annual Meeting, Lincoln, NE*, page 50.

Swinehart, J. (1994). *Quaternary geologic map of the Platte River 4¡ x 6¡ quadrangle, United States*. The Survey.

Swinehart, J. and Loope, D. (1992). A giant dune-dammed lake on the north platte river, nebraska. *Geological Society of America, Abstracts with Programs;(United States)*, 24(CONF-921058–).

Swinehart, J. B. and Diffendal, R. (1995). Geologic map of morrill county, nebraska.

Swinehart, J. B. and Diffendal, R. (1997). Geologic map of the scottsbluff 1 degree x 2 degrees quadrangle, nebraska and colorado.

Swinehart, J. B. and Diffendal, R. F. (1989). Geology of the pre-dune strata.

Swinehart, J. B., Souders, V. L., DeGraw, H. M., and Diffendal, R. F. (1985). Cenozoic paleogeography of western nebraska. Rocky Mountain Section (SEPM).

Turner, J. (1993). Location of uranium and thorium in granites¡[a]radiogenic influence on cosmogenic isotope abundance. In *Geol. Soc. Am. Abstr. Programs*, volume 25, pages A–89.

Turowski, J. M., Rickenmann, D., and Dadson, S. J. (2010). The partitioning of the total sediment load of a river into suspended load and bedload: a review of empirical data. *Sedimentology*, 57(4):1126–1146.

Vermeesch, P. (2007). Cosmocalc: An excel add-in for cosmogenic nuclide calculations. *Geochemistry, Geophysics, Geosystems*, 8(8).

Vermeesch, P., Balco, G., Blard, P.-H., Dunai, T. J., Kober, F., Niedermann, S., Shuster, D. L., Strasky, S., Stuart, F. M., Wieler, R., et al. (2015). Interlaboratory comparison of cosmogenic 21ne in quartz. *Quaternary Geochronology*, 26:20–28.

Visher, G. S. (1969). Grain size distributions and depositional processes. *Journal of Sedimentary Research*, 39(3).

Von Blanckenburg, F. (2006). The control mechanisms of erosion and weathering at basin scale from cosmogenic nuclides in river sediment. *Earth and Planetary Science Letters*, 242(3-4):224–239.

Ward, P. A. and Carter, B. J. (1999). Rates of stream incision in the middle part of the arkansas river basin based on late tertiary to mid-pleistocene volcanic ash. *Geomorphology*, 27(3-4):205–228.

Wayne, W. J., Aber, J., Agard, S., Bergantino, R., Bluemle, J., Coates, D., Cooley, M., Madole, R., Martin, J., Mears Jr, B., et al. (1991). Quaternary geology of the northern great plains. *Quaternary nonglacial geology of the conterminous US: Boulder, Colorado, Geological Society of America, The Geology of North America*, 2:441–476.

Whittaker, A. C., Attal, M., and Allen, P. A. (2010). Characterising the origin, nature and fate of sediment exported from catchments perturbed by active tectonics. *Basin Research*, 22(6):809–828.

Whittaker, A. C., Duller, R. A., Springett, J., Smithells, R. A., Whitchurch, A. L., and Allen, P. A. (2011). Decoding downstream trends in stratigraphic grain size as a function of tectonic subsidence and sediment supply. *Bulletin*, 123(7-8):1363–1382.

Wobus, C. W., Tucker, G. E., and Anderson, R. S. (2010). Does climate change create distinctive patterns of landscape incision? *Journal of Geophysical Research: Earth Surface*, 115(F4).

Xia, J., Haskell, B. J., Engstrom, D. R., and Ito, E. (1997). Holocene climate reconstructions from tandem trace-element and stable-isotope composition of ostracodes from coldwater lake, north dakota, usa. *Journal of Paleolimnology*, 17(1):85–100.